Chair of Designing Plastics and Composite Materials

Doctoral Thesis

Simultaneous Structural and Material Optimization

Dipl.-Ing. Margit Christa Lang

January 2021

MONTANUNIVERSITÄT LEOBEN
www.unileoben.ac.at

EIDESSTATTLICHE ERKLÄRUNG

I declare on oath that I wrote this thesis independently, did not use other than the specified sources and aids, and did not otherwise use any unauthorized aids.

I declare that I have read, understood, and complied with the guidelines of the senate of the Montanuniversität Leoben for "Good Scientific Practice".

Furthermore, I declare that the electronic and printed version of the submitted thesis are identical, both, formally and with regard to content.

Datum 02.01.2021

Signature Author
Margit Christa Lang

Abstract

Innovative and resource-efficient products are of great importance for a number of industries including automotive and aerospace. As a consequence, increased usage of lightweight materials in highly optimized structural designs is of highest priority. Structural optimization, in particular topology optimization, has seen accelerated deployment throughout all industries in the past decade, mainly due to the fact that significant efficiency gain can be achieved at the concept design level. In terms of extremely lightweight structures, composite structures are a key-player as they offer the possibility of tailoring the material to a specific application. Hence, the purpose of introducing composite materials as part of the design formulation for structural optimization requires both, to determine the optimal spatial distribution as well as the optimal local choice of material properties, i.e., the orientation and the anisotropy of the local material tensor which is controlled by the composite microstructure. Since a change in topology affects the local stress situation, it also affects the adjustment of material parameters (orientation, degree of anisotropy) and vice versa. As a consequence, it is essential to address the aspects of topology optimization and local material optimization simultaneously, which is contrary to the present design practice.

The current work presents a new method for optimization of structural layout and material that simultaneously addresses the design of the global geometry (topology) and the more or less detailed design of the material itself in terms of orientation and anisotropy of the local material tensor. The concept, which is implemented for three-dimensional structures, is evaluated on simple pseudo two dimensional (academic) test cases. The global design objective is to minimize the compliance of a structure, subject to a volume constraint. The developed method is implemented in Python. The Python code takes advantage of the advanced FEM capacities of the Abaqus software and employs the Abaqus Scripting Interface (ASI) to communicate with Abaqus. The global geometry (topology) is determined using the Bi-Evolutionary Structural Optimization Algorithm (BESO), based on the use of sensitivity analysis and mathematical programming. Material optimization is achieved by adjusting the material orientation, based on the local loading conditions (i.e., principal stress directions). Furthermore, the optimized local anisotropy is determined by adjusting the respective volume fractions of continuous cylindrical inclusions, based on the relation of the absolute values of the principal stresses. The homogenized stiffness tensor is determined using a micromechanics mean field approach. Therefore, the method yields physically realistic material configurations and is based on a reasonable amount of design variables without adding unnecessary restrictions to the design space. The developed method is applicable to single as well as multiple loadcases.

The numerical application of the method on simple pseudo two dimensional (academic) test cases shows its effectiveness and robustness. The material determined with this method goes beyond topology optimized quasi-isotropic and orientation optimized unidirectional material as it can be directly optimized for the functional needs at the structural scale. Therefore, the compliance is significantly reduced compared to a standard topology optimization with quasi-isotropic material. It is observed that the method is very robust, i.e. shows good convergence and little sensitivity to the startdesign and control parameters. Therefore, the proposed method opens up a wide range of interesting perspectives. Next steps include the generalization of the concept to three dimensional topologies as well as including manufacturing constraints such that the practical feasibility of the optimized design can be taken into account in the optimization process.

Kurzfassung

Die Entwicklung innovativer und ressourceneffizienter Produkte ist von großer Bedeutung für eine Reihe von Industriesektoren, unter anderem Automobilindustrie sowie Luft- und Raumfahrt. Infolgedessen hat der verstärkte Einsatz von Leichtbaumaterialien in hochoptimierten Strukturen höchste Priorität. Der Einsatz von Strukturoptimierung, insbesondere Topologieoptimierung, hat in den letzten Jahren an Bedeutung gewonnen. Topologieoptimierung bietet die Möglichkeit eine optimale Materialverteilung für ein Design unter bestimmten funktionalen Nutzungsbedingungen zu erreichen, mit dem Ziel bereits auf der Ebene des Konzeptdesigns eine signifikante Effizienzsteigerung zu erreichen. Im Hinblick auf Leichtbau ist die Verwendung von Verbundwerkstoffen ein Schlüsselfaktor, da sie die Möglichkeit bieten die mechanischen Eigenschaften des Bauteils gezielt an die Belastungssituation anzupassen. Bei der Optimierung von Verbundwerkstoffen werden daher zwei Ziele verfolgt: die optimale Materialverteilung sowie die Ermittlung optimaler lokaler Materialeigenschaften, definiert über die Orientierung und den Anisotropiegrad des lokalen Steifigkeitstensors. Eine Änderung der Topologie beeinflusst die lokale Spannungssituation und damit auch die optimalen Materialparameter. Dies gilt natürlich auch im umgekehrten Fall. Daher ist es, im Gegensatz zur derzeitigen Auslegungspraxis notwendig, die Aspekte der Topologieoptimierung und der lokalen Materialoptimierung gleichzeitig zu berücksichtigen.

Die vorliegende Arbeit stellt eine neue Methode zur Optimierung von Struktur und Material vor. Dabei werden der Entwurf der globalen Geometrie und der Entwurf des Materials, in Bezug auf Orientierung und Anisotropie des lokalen Steifigkeitstensors, gleichzeitig berücksichtigt. Das Konzept, das für dreidimensionale Strukturen entwickelt wurde, wird an pseudozweidimensionalen Testbeispielen demonstriert und evaluiert. Ziel der Optimierung ist die Minimierung der Gesamtnachgiebigkeit der Konstruktion unter Berücksichtigung einer Volumenrestriktion. Die hier vorgestellte Methode ist mit Python in Verbindung mit Abaqus FEM implementiert. Die Ermittlung der Topologie basiert auf dem Algorithmus der Bi-Evolutionären Strukturoptimierung (BESO). Die Optimierung des Materials erfolgt einerseits durch Anpassung der Materialorientierung, basierend auf den lokalen Belastungsbedingungen (Hauptspannungsrichtungen) und andererseits durch die Anpassung der jeweiligen Volumenanteile kontinuierlicher zylindrischer Einschlüsse (Fasern), basierend auf dem Verhältnis der Absolutwerte der Hauptspannungen. Der homogenisierte Steifigkeitstensor wird mit einem mikromechanischem Mean-Field Ansatz bestimmt. Die Methode liefert physikalisch realistische Materialkonfigurationen basierend auf einer angemessenen Anzahl von Entwurfsvariablen, ohne dabei den Designraum unnötig einzuschränken. Die entwickelte Methode ist gleichermaßen für den Einzellastfall als auch für mehrere Lastfälle anwendbar.

Die Robustheit und Effizienz des vorgestellten Konzepts wird anhand von Standard Testbeispielen evaluiert. Das optimierte Material geht dabei über quasi-isotropes und unidirektional verstärkter Material hinaus, da die Materialeigenschaften direkt an die funktionalen Anforderungen auf Strukturebene angepasst werden. Die Simulationsergebnisse zeigen eine deutliche Reduktion der Gesamtnachgiebigkeit der Struktur. Des Weiteren zeigt die Methode eine gute Konvergenz und eine geringe Empfindlichkeit gegenüber dem Ausgangsdesign und für den Topologieoptimierungsalgorithmus notwendigen Eingabeparametern. Dies verdeutlicht das Potenzial der Methode, eine Vielzahl von interessanten Perspektiven für die Entwicklung innovativer Bauteile zu eröffnen. Weitere Schritte beinhalten die Erweiterung des Konzepts auf dreidimensionale Strukturen sowie die Berücksichtigung von Fertigungsrestriktionen hinsichtlich der praktische Umsetzbarkeit des optimierten Designs.

Acknowledgments

This thesis is the result of a challenging journey. Therefore, it does not only give me the opportunity to present the interesting work I have done, but also to thank those that have contributed and gave me guidance and support.

A special thanks goes out to:

Univ.-Prof. Dipl.-Ing. Dr.techn. Clara Schuecker for the continuous support of my Ph.D. study and related research, for her patience, motivation and constructive criticism which was very helpful towards the successful completion of this thesis. Claras insight and knowledgement steered me through this research and helped me realize the power of critical reasoning. Our meetings and conversations were vital in inspiring me to think outside the box, from multiple perspectives to form a comprehensive and objective critique.

My colleagues at the Chair of Designing Plastics and Composite Materials, in particular Siegfried Frankl, for the pleasant working atmosphere and interesting discussions. I really enjoyed being part of the team!

Univ.-Prof. Dr. Stefanie Elgeti for her friendly support advice.

My mother Helga, my father Manfred, and my brother Martin for their encouragement and moral support. I am glad to have a wonderful family that will always stay by my side, believe in me, support me, listen to my problems, and give advice. A special thanks goes out to my brother Martin for hours of proof reading through my work at several stages of the writing process. Thank you for everything!

My girls, Marion and Julia. Your love, patience and encouragement kept me focused through the thick and the thin of my journey.

Some special words of gratitude to my friend Carmen who has always been a major source of support when things would get a bit discouraging. Thank you for being part of my success story.

Contents

List of Symbols and Abbrevations

List of Greek Symbols

α^*	Step length
α_i	Element sensitivity number
α_j	Nodal sensitivity number
ε	Convergence tolerance value
ν	Poisson ratio
$\boldsymbol{\nabla}$	Gradient of a function
ρ	Density
σ^{vM}	Von Mises stress
$\sigma_{11}, \sigma_{22}, \sigma_{33}$	Principal stresses
θ_i	Fiber (inclusion) angle
ξ_i	Volume fraction

List of Latin Symbols

C^{global}	Global Mean Compliance
c_{ER}	Evolutionary ratio
c_{rr}	Rejection rate
E	Elastic modulus
ER	Evolution Rate
$f(\boldsymbol{x})$	Objective function
$\boldsymbol{f}$	Global load vector
G	Shear Modulus
g_j	Inequality constraint
$\boldsymbol{H}$	Hessian matrix
h_k	Equality constraint
$\boldsymbol{K}$	Stiffness matrix
m_{size}	Mesh size
n	Total number of design variables
N	Total number of elements in the discretized design domain
$\boldsymbol{p}$	Search direction
p	Penalty exponent
r_{min}	Scale Parameter (Filter Radius)
$\boldsymbol{u}$	Global displacement vector
V^*	Prescribed target volume of the structure
V_i	Volume of one element
w_i	Weight Factor
$\boldsymbol{x}$	Vector of the design variables $x_i,\ i = 1, \ldots, n$
x_i	Design variable
x_{min}	Minimum value for design variable

List of Abbrevations

A	Anisotropic
ABC	Artificial Bee Colony Algorithm
ACO	Ant Colony Optimization
AESO	Additive Evolutionary Structural Optimization
ALLWK	External Work (Abaqus)
AO	Anisotropic-Orient
AOM	Anisotropic-Orient-Material
BESO	Bi-Evolutionary Structural Optimization
CAIO	Computer Aided Internal Optimization
CAO	Computer Aided Optimization
CFAO	Continuous Fiber Angle Optimization
CONLIN	Convex Linearization Problem
CPU	Central Processing Unit
CSD	Constrained Steepest Descent
DMO	Discrete Material Optimization
ESEDEN	Elastic Strain Energy Density (Abaqus)
ESO	Evolutionary Structural Optimization
FEM	Finite Element Method
FMO	Free Material Optimization
FRP	Fiber Reinforced Polymer
FSD	Fully Stressed Design
GA	Genetic Algorithms
GCMMA	Globally Convergent Method of Moving Asymptotes
GFRP	Glass Fiber Reinforced Polymer
LC1	Loadcase 1
LC2	Loadcase 2
MFD	Method of Feasible Directions
MLC	Multiple Loadcase
ML-CAIO	Multi-Layer Computer Aided Internal Optimization
MMA	Method of Moving Asymptotes
MMFD	Modified Method of Feasible Directions
OC	Optimality Criteria
PSO	Particle Swarm Optimization
Q-Iso	Quasi-Isotropic Standard Topology Optimization
RAMP	Rational Approximation of Material Properties
RVE	Representative Element Volume
SA	Simulated Annealing
SERA	Sequential Element Rejection and Admission
SI	Swarm Intelligence Algorithms
SIMP	Solid Isotropic Material with Penalization
SKO	Soft Kill Option
SLC	Single Loadcase
SLP	Sequential Linear Programming
SQP	Sequential Quadratic Programming

List of Figures

List of Tables

1. Introduction

In recent years one of the ultimate goals in engineering has been set on the pursuit of extremely light weight structures as well as the efficient use of raw material for reduction of energy in order to preserve the environment. Structural optimization has seen accelerated deployment throughout all industries in the past decade, mainly due to the fact that tremendous efficiency gain can be achieved at the concept design level. Therefore, structural optimization, in particular topology optimization, is a powerful and already widely used tool for designing weight optimized structural components. Topology optimization consists in determining the best size, shape and connectivity of a structure. Most approaches to topology optimization are based on a density formulation. In other words, the design variable is a factor to the material stiffness. Therefore, the objective is to determine a discrete "black-and-white" solution containing either full material or voids within a given design domain. Topology optimization has reached a certain maturity concerning the design of structures with isotropic material, essentially metals [1, 2, 3, 4].

In terms of extremely lightweight components, composite structures are a key-player due to their high stiffness-to-mass and strength-to-mass ratio. Furthermore, composites offer the possibility of tailoring a material to a specific application and therefore offer additional degrees of freedom in the optimization process. Indeed, it is possible to adapt a composite material according to the stress distribution within a structure, i.e., to adapt the orientation and the anisotropy of the local material tensor which is controlled by the composite microstructure. In practice, the local control over the microstructure is rather limited. The only eligible design factors are: the volume ratio of the matrix and the reinforcement, the orientation of a given microstructure and the topology of the microstructure, all within a fixed set of design variables.

Existing approaches for material optimization focus on directly finding a physically meaningful solution based on a limited number of predefined candidate materials (*Discrete Material Optimization*, DMO) [5]. In the context of orientation optimization, different "candidate materials" simply refers to the same material oriented at various angles in space (fiber angles). The principal material direction is assumed to coincide with the principal stress direction. However, for each additional "candidate material" an additional design variable must be added leading to an increased computational effort. It is obvious that *Discrete Material Optimization* implies the risk of local optimum solutions. The restriction to a prescribed set of orientations is resolved in the *Continuous Fiber Angle Optimization* (CFAO) where local design variables

are included to parameterize a continuous rotation of an anisotropic base material [6]. However, most CFAO approaches focus on two-dimensional problems (e.g., laminates for shells or plates), far less research is dedicated to three-dimensional problems. Other approaches for optimizing anisotropic materials work with a locally unconstrained configuration of material. For the so-called *Free Material Optimization* (FMO) the individual entries of the material stiffness tensor are defined as design variables [7]. FMO is the least restrictive approach but faces the problem that the optimization may yield a theoretically optimal structure but not always a physically feasible structure, especially for more complex structures or loading scenarios.

The introduction of composite materials as part of the design formulation of structural optimization require to determine the optimal spatial distribution as well as the optimal use of the material itself. However, the traditional approach to structural design is to select a material and then design the structure that best utilizes the given material, e.g., by using topology optimization. On the other hand, advanced composites (e.g., fiber-reinforced plastics, FRPs) are often used as "black metal" by simply keeping the geometry of a metal component and replacing it with composite structures that are lighter. In both cases the design of structure and material is inherently decoupled and yet the performance and quality of the designs are inextricably linked across the structural and material scales. Since a change in topology affects the local stress situation, it also affects the adjustment of material parameters (orientation, degree of anisotropy) and vice-versa. As a consequence, and to address untapped potentials in terms of lightweight design, there is an urgent need for a systematic approach to couple structural (topology) and material optimization. This coupling on design level is expected to enable products with better performance compared to designs that stem from approaches where structural topology and materials are not concurrently considered.

Further aspects that influence the optimal design, especially when dealing with advanced composite materials, are of course challenges to existing manufacturing techniques and the associated costs. Today, manufacturing methods are emerging for anisotropic materials, for instance *3D printing* for fiber-reinforced polymers and *Automated Fiber Placement*. Certainly, other manufacturing methods with the possibility of manufacturing new materials with complex composition will arise in the coming decades. However, including manufacturing constraints such that the practical feasibility of the optimized design can be taken into account in the optimization process is not the main focus of this thesis.

The objective of this thesis is to develop a method for simultaneous optimization of topology and material that shall start from a prescribed maximum design volume, prescribed boundary conditions, and loading, but without any initial "guess" on the shape of the structure. A computational scheme which concurrently updates the topology and the anisotropic material properties based on the local loading conditions is proposed. In the framework of this

thesis a continuous glass fiber reinforced polymer (GFRP) is used, i.e., infinitely long cylindrical inclusions (glass fiber) embedded in a matrix. Homogenized properties of the anisotropic material are used to characterize the elasticity tensor coefficients. The optimization of the anisotropy distribution consists of adjusting the local material orientation and adjusting the local material (stiffness) tensor, based on the local loading conditions in terms of resulting element stress tensors from a finite element analysis. The emerging principal stress trajectories are used for the material orientation in each element of the finite element model. The degree of anisotropy is based on the ratio of principal stresses for the respective element. Depending on the number of loadcases, several possible update schemes are proposed.

The new method, proposed in this thesis, opens up the design space as the material can be directly optimized for the functional needs at the structural scale. Compared to existing methods for material optimization, the concept yields physically feasible material configurations and is based on a reasonable amount of design variables but without adding unnecessary restrictions to the design space. The new approach to simultaneous topology and material optimization is illustrated for simple, 2-dimensional test cases. It is noted, however, that the concept can be generalized to 3-dimensional composite topologies in a straight forward way.

2. Theoretical Background

In the following sections, the basic terminologies of structural optimization as well as the general mathematical formulation of a structural optimization problem are introduced. Furthermore, the basic methods, namely size, shape and topology optimization, shall be briefly described followed by a presentation of the various optimization algorithms. As this thesis deals with the simultaneous optimization of topology and material, these topics will be dealt with in detail in Section 2.5, Section 2.6 and Section 2.7.

2.1. General Formulation of an Optimization Problem

The general mathematical formulation of a nonlinear optimization problem with n design variables, l inequality constraints, and m equality constraints is as follows [2, 8, 3] :

$$\begin{aligned}
&\text{minimize:} && f(\boldsymbol{x}) && \text{(2.1a)}\\
&\text{subject to:} && x_i^{\mathsf{L}} \leq x_i \leq x_i^{\mathsf{U}};\ i = 1, ..., n, && \text{(2.1b)}\\
& && g_j(\boldsymbol{x}) \leq 0;\ j = 1, ..., l, && \text{(2.1c)}\\
& && h_k(\boldsymbol{x}) = 0;\ k = 1, ..., m. && \text{(2.1d)}
\end{aligned}$$

Equation 2.1a defines the minimization of an objective function $f(\boldsymbol{x})$ depending on the vector of the design variable $\boldsymbol{x} \in \mathbb{R}^n$, $\boldsymbol{x} = [x_1, x_2, ..., x_n]^{\mathrm{T}}$. The design variables can be either discrete (binary) or continuous. Optimization problems that have their design variables restricted to discrete values are referred to as discrete optimization problems. The minimization problem in Equation 2.1a is subjected to inequality constraints $g_j(\boldsymbol{x})$ and equality constraints $h_k(\boldsymbol{x})$ (see Equation 2.1c and Equation 2.1d). For practical applications, equality constraints are of minor importance as in real world problems it is mostly important to keep upper or lower limits instead of keeping an exact target value [2]. Restrictions on the searchable design-space are the upper and lower bounds x_i^{L} and x_i^{U}, see Equation 2.1b. These are also referred to as explicit restrictions or side constraints on the design variables. An optimization problem is considered as constrained if it has one or more equality and/or inequality constraints. An unconstrained problem thus has no equality or inequality constraints, but may have side constraints on the design variables. The objective and constraint functions can either be linear or non-linear and explicit or implicit functions. Implicit functions usually appear, when, for example, a numerical simulation (e.g., finite element simulation) is used to evaluate a response function (e.g., displacement).

The fact that the optimization problem is formulated as a minimization rather than a maximization problem is not restrictive since instead of maximizing a function it is always possible to minimize the negative of it [2]:

$$\max\left(f(\boldsymbol{x})\right) = -\min f(\boldsymbol{x}). \tag{2.2}$$

In the same way, an inequality constraint

$$g_{\mathrm{j}}(\boldsymbol{x}) \leq 0, \tag{2.3}$$

can be reformulated to a greater-than-zero inequality constraint by simply multiplying Equation 2.3 with (-1).

2.2. Terminology

The following terms, variables, and functions are always present in the definition of a structural optimization problem and therefore are briefly introduced here:

Design Variable

For an optimization problem, the design variables are the set of parameters which are subject to variation during the optimization process. Design variables may represent the geometrical dimensions of individual members, e.g., "size variables" such as the width or depth of a member section or the cross-sectional area of a bar. Further examples of design variables include mechanical or physical properties of the structural materials, the configuration or geometrical layout of the structure as well as other relevant aspects of a design. Depending on the type of structural optimization being performed, design variables may be continuous or discrete. As shown in Section 2.1, mathematically, the full set of design variables for a given structure is represented as a vector $\boldsymbol{x} = [x_1, x_2, ..., x_n]^{\mathrm{T}}$ in an n-dimensional space which hereinafter will be referred to as design space. The design space is not to be confused with the design domain which is the region of a structure which is designable during optimization. The design domain can be either a subset of the model (containing only selected regions of the model) or the whole model itself. In contrast, non-designable regions are regions that may not be changed during optimization.

Design Objective

The objective function depends on the design variables and defines the goal of the optimization. Therefore, the objective which is a scalar value, represents the single most important property of a design. In engineering applications, typical objectives are minimizing weight, maximizing stiffness, or maximizing strength.

Sometimes it is necessary to deal with multiple objectives, e.g., minimizing the weight and at the same time maximizing strength. Similarly, it is possible to have multiple objective functions that arise from multiple different loadcases. In both cases, the optimization problem consists in finding a single optimal solution that optimizes simultaneously all the objective functions. One possibility to deal with multiple objectives is to use weighting factors that scale the influence of the respective objective function on the optimization. A famous example of combining several objective functions is the so-called *Weighted Sum* method where the objective functions are summed with a "weight factor of importance" (preference ratio). For instance, Sigmund [9] proposes to combine the objective functions from different loadcases, so that the problem is changed to a scalar optimization problem. This is exemplarily shown in Equation 2.4 for the objective of minimizing the compliance as

$$\min \sum_{i=1}^{m} w_i C_i, \tag{2.4}$$

where C_i denotes the compliance of the loadcase i, m is the total number of loadcases, and w_i is the weight factor of the respective loadcase. The above formulation with a linear combination of the individual cases is simple, but the design solution naturally depends on the chosen linear combination factors. The difficulty of this method lies in finding the correct value of the weight factors prior to the optimization because small perturbations of these values may lead to very different design proposals.

An alternative to the linear combination of several load cases is to optimize with focus on the "worst case" out of several loadcases as proposed by Bendsøe et al. [1]. For example one could decide to minimize the compliance of the loadcase which leads to the worst stress state. However, evaluating which load case is most relevant is not trivial since it depends on the geometry of the structure that changes at each optimization iteration step. Furthermore, this method does not consider the contribution of the other loadcases.

Constraints / Feasible Design / Infeasible Design

Constraints are restrictions placed on the design space of the optimization problem. Therefore, constraints limit the domain of options available to a designer for generating new design solutions. Constraints can be classified as constraints on the design responses (e.g., stiffness, displacement, mass, stress), so-called design constraints, or constraints on the design variables, which are referred to as side constraints. Design constraints restrict the value of a design response, for instance prevent the structure from violating stress limits, displacement values and so on. Like the objective functions, the design constraints are expressed as a function of the design variables. Design constraints on the design variables are upper and/or lower limits on the searchable design space. Figure 2.1 schematically shows the design space for a cantilever beam where the aim (objective) is to minimize its weight.

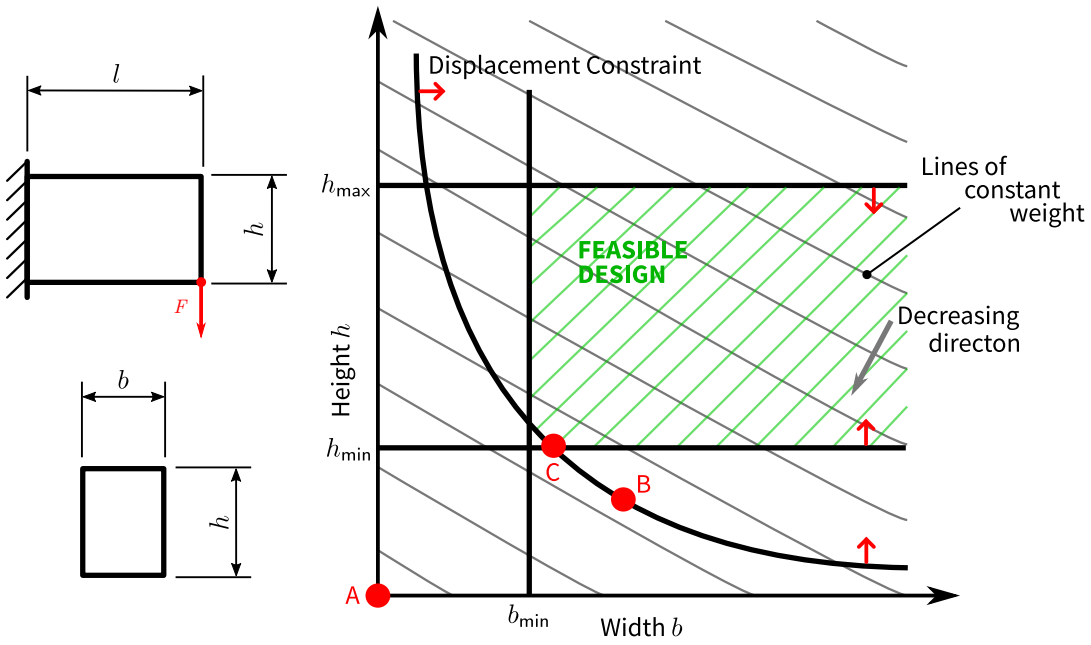

Figure 2.1.: Design Space showing feasible and infeasible design regions

The design variables are the height h and the width b of the beam. A design constraint is placed on the optimization, namely a displacement constraint. Furthermore, there are side constraints: a lower bound h_{min} and an upper bound h_{max} on the height and a lower bound b_{min} on the width of the beam. In this context a *Feasible Design* is a design that satisfies all constraints whereas an *Infeasible Design* is one that violates one or more constraints.

Optimum Design

The optimum design refers to the set of design variables which define the maximized or minimized objective without violating one of the constraints. Depending on the problem definition, sometimes constraints are necessary to achieve a meaningful result at all, as Figure 2.1 illustrates. Without any constraints the optimum solution would be at "point A", which is quite useless for practical applications. Adding a displacement constraint gives a practical design and the optimum is at "point B". Placing side constraints on the design variables h and b further restricts the design space (feasible design space) and the optimum is at "point C".

Stopping Conditions

If objective and/or constraints are nonlinear functions of the design variables, the design problem is called a nonlinear programming problem. Most engineering problems fall in this category. These problems are frequently solved using numerical, rather than analytical methods. As numerical optimization algorithms are iterative procedures, a termination criterion is needed to stop the iterative process.

An optimization algorithm has converged (can be stopped) if it cannot reach new solution candidates anymore or if it keeps on producing solution candidates from a "small" subset of the problem space. According to Harzheim [2], there are three termination criteria mostly used in structural optimization to determine the end of an optimization procedure.

The first termination criterion is based on defining a limit on the number of iterations. When the limit on the number of iterations exceeds a specified value, the optimization is terminated. However, this termination criterion is not very useful unless there are exact time constraints on the optimization. The final design represents an improvement but rarely an optimum because it is unrealistic to expect that a problem will converge at a certain iteration. A variation of this is to provide a quite large number as the maximum iteration. However, in such a case obviously the computing expense will be unnecessarily high.

Another possibility is the so-called "objective value convergence test": when all the objective values are close within a specified tolerance, the iteration is terminated. These convergence criteria are used to terminate an optimization at a point after which no further significant improvement in the objective function is expected. When the convergence criterion is satisfied, it can be assumed, that the optimum has been determined with sufficient accuracy. Therefore, the second termination criterion is a convergence method that evaluates the absolute change of the objective function. It requires that the actual change of the objective function of the last two iterations of the optimization is less than or equal to a certain value as follows:

$$\left| f\left(\boldsymbol{x}^{(k)}\right) - f\left(\boldsymbol{x}^{(k-1)}\right) \right| \leq \varepsilon_{\text{abs}}, \tag{2.5}$$

where $f\left(\boldsymbol{x}^{(k)}\right)$ is the value of the objective function of the current iteration k and $f\left(\boldsymbol{x}^{(k-1)}\right)$ is the value of the objective function of the previous iteration $(k-1)$. ε_{abs} is a user-selected convergence tolerance value, which determines the termination of the optimization procedure. However, the major disadvantage is that the limit ε_{abs} must always be adapted to the respective objective function.

According to Harzheim [2], the third type of termination criteria is also a convergence criterion and is the most universal stop criterion. It is based on the relative change of the objective function from one optimization iteration to the next optimization iteration. This termination condition requires that the relative change in the objective function is less than or equal to the user-selected convergence tolerance ε_{rel} as follows:

$$\frac{\left| f\left(\boldsymbol{x}^{(k)}\right) - f\left(\boldsymbol{x}^{(k-1)}\right) \right|}{\left| f\left(\boldsymbol{x}^{(k)}\right) \right|} \leq \varepsilon_{\text{rel}}, \tag{2.6}$$

The major advantage is that the user-selected convergence tolerance ε_{rel} must not be adapted to the respective objective function.

2.3. Structural Optimization Techniques

Optimization has earned a key place in the drive to improve products based on a wide range of performance criteria. Optimization technology has advanced rapidly over the past decade and the engineer faces a bewildering variety of tools and methods. Modern structural optimization has evolved since the 1940s, mainly driven by the aerospace industry but expanding to other industrial sectors as well. According to Harzheim [2], in the early years structural optimization mainly dealt with applications for civil engineering truss structures, with the design variables being the cross-sectional areas of the elements. The development moved from the original stage of considering only the geometrical dimensions (sizing or dimensioning) of a structure as illustrated in Figure 2.2, to a more general form of optimizing the outer boundaries (shape) of a structure as illustrated in Figure 2.3, and finally to determining the best topological layout while still considering the geometry and physical dimensions as well as connectivity of members and joints, as illustrated in Figure 2.4.

From an engineering point of view structural optimization techniques can be classified into the following three categories [2]: sizing optimization, shape optimization, and topology optimization. All these methods have in common that a physical quantity is optimized while equilibrium of forces and other constraints on the design are satisfied.

Size Optimization

In a typical size optimization, the basic layout (topology) of the structure is prescribed. The design variables are structural parameters like the length, width or depth of a member section, the cross-sectional area of a bar in a frame, the thickness of a plate or the moment of inertia of a flexural member. Figure 2.2 shows an example for size optimization of a truss structure with predefined structural connectivity and a predefined cross-section shape. In this case, the design variable for sizing optimization is the cross-section diameter D.

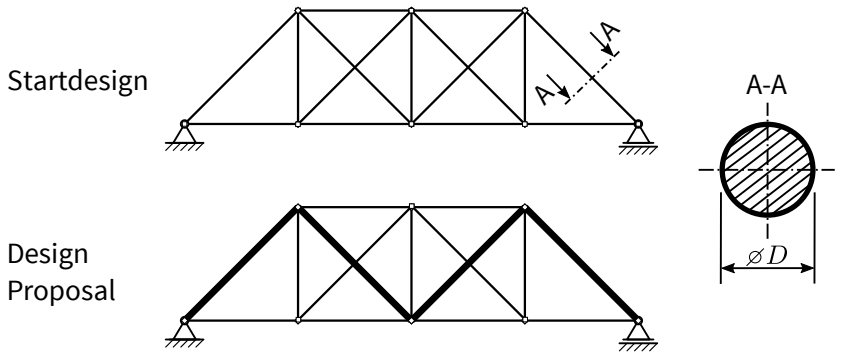

Figure 2.2.: Size optimization

Shape Optimization

Like with size optimization, in shape optimization, the basic layout (topology) of the structure is known and remains unchanged during the optimization process. The aim is to improve the performance of the structure by modifying its boundaries [3]. There are several approaches to represent the shape of a structure and to follow its evolution during shape optimization. For instance in the *Lagrangian Approach*, the shape boundary is sampled in a relatively dense and uniform manner to obtain a sufficiently accurate outline of the shape. The design variables are the coordinates of the boundary points. The optimal shape can be evolved by gradually moving those boundary points.

Figure 2.3 shows two examples of shape optimization. Figure 2.3(a) illustrates a shape optimization of a startdesign with known structural connectivity but unknown cross-section shape. The design proposals are the respective optimized cross-section shapes (e.g., circular or I-beam). Figure 2.3(b) shows a common engineering application of shape optimization. In this case, shape optimization is used for "fine tuning" the shape of cavities/holes from topology optimization in order to reduce stress concentrations which in turn influences fatigue life positively.

Topography optimization can be considered as a special case of shape optimization. It refers to pattern shaped reinforcements applied to shell and thin-walled structures.

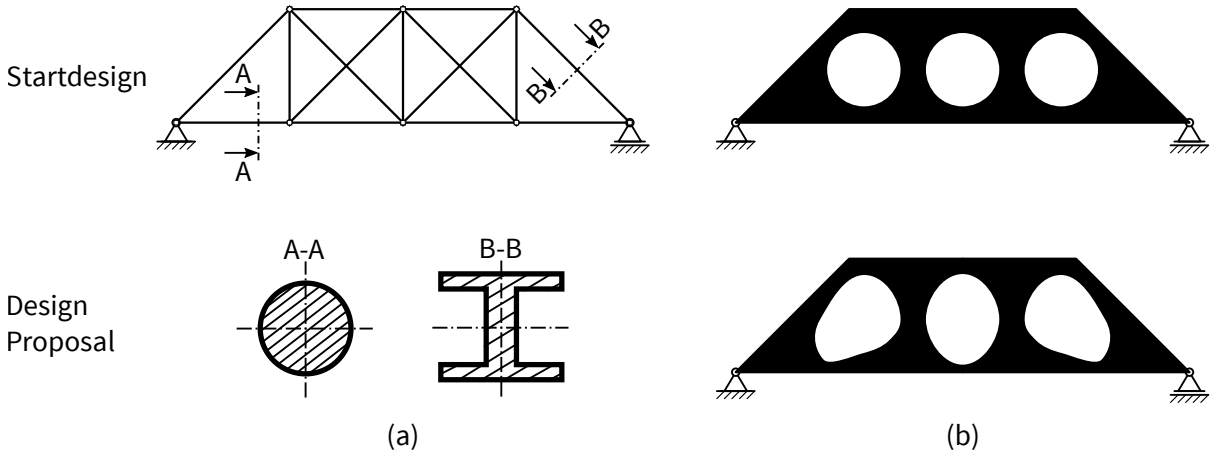

Figure 2.3.: Examples of shape optimization: (a) optimal cross-section shape, (b) shape optimization as applied to "fine tuning" after topology optimization

Topology Optimization

The topology of a structure, referring to the arrangement of material or the positioning of structural elements, is crucial for its optimality. Therefore, with topology optimization, the aim is not to look for the most suitable shape but rather for the optimal distribution of material ("optimal load path") inside a predefined design domain for a given set of loads and boundary conditions. Topology optimization is used when the actual fundamental layout of

a structure is unknown. It solves the most general structural optimization problem of distributing a given amount of material freely in the design domain such that the performance of the structure is optimized without violating predefined constraints. This means, unlike size and shape optimization, structures optimized through topology optimization can attain any shape within the design domain.

Topology optimization can be classified into methods for discrete structures and methods for continuum structures [3]. Figure 2.4 illustrates the two types of topology optimization with discrete topology optimization shown on the left-hand side (Figure 2.4(a)) while the continuum topology optimization is shown on the right-hand side (Figure 2.4(b)). Topology optimization for discrete structures is also referred to as *Ground Structure Approach* [10]. This approach considers a fixed grid of nodes, a so-called "basic structure", initially with a high degree of connectivity. This means that the nodes are connected by as many structural elements, e.g., trusses, in as many ways as possible. In extreme cases each node may be connected to each other node. These links between the nodes are potential structural members corresponding to the design variables. Topology optimization can be applied to remove "under-utilized" members. In contrary, topology optimization for determining the optimal material distribution for continuum structures, as illustrated in Figure 2.4(b), does not need any basic structure. The topology optimization problem of a continuum structure is how to distribute a certain amount of material within a design domain.

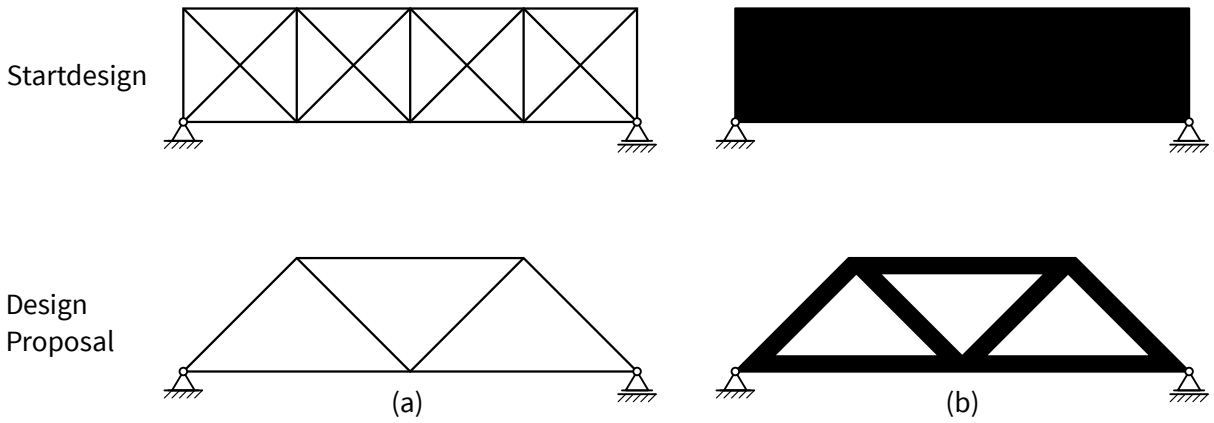

Figure 2.4.: Principles of topology optimization in the (a) discrete and (b) continuous case

Structural topology optimization is of great practical importance as it can result in great material savings. In this sense, according to Bendsøe et al. [1], topology optimization is the most straightforward approach to solve a typical problem in engineering, namely "construct a failsafe device with the least possible amount of material".

The aforementioned categorization of methods for structural optimization (size, shape, topology) is rather idealized. Often, structural optimization consists of a mixture of these techniques. For instance, one could use size optimization for the optimization of the cross-section of a truss structure while at the same time consider topology optimization to remove unnec-

essary trusses. From the point of view of product development, there are several levels with respect to structural optimization. *Concept Level Design* implies that the optimization is performed at a very early or even at the first stage of a design process in order to create the best design from which to progress. The second level, *Fine Tuning Design*, refers to optimization strategies that allow detailed changes to the structure in order to satisfy objective / constraint criteria but without making any changes to the overall topology. Among the aforementioned categories of structural optimization, topology design is used at a *Concept Design Level* to find the optimal layout of a structure. Size and shape optimization, belong to the level of the so-called *Fine Tuning Design*.

2.4. Algorithms for Optimization

Nowadays, it is common practice to use numerical optimization methods to deal with multidisciplinary industrial design problems [1]. The algorithms deal with the mathematical form of the optimization problem interfaced with computer models representing the physical structure. The physical properties of the structure to be optimized are represented by the design variables, objective function(s), and the design constraint(s). The model is used to perform structural analyses requested by the optimization algorithm.

Optimization algorithms are used to find the solution to the problem specified in Equation 2.1. The optimization procedure consists of finding a specific combination of design variable values that results in the best objective function value, while at the same time satisfying all equality, inequality and side constraints. Optimization is an iterative process that roughly consists of the following steps [1], where step 2.-4. constitute the iterative part of the procedure:

1. An initial design (startdesign) is suggested.
2. The design is evaluated, e.g., for mechanical structures by means of computer based methods like the Finite Element Method (FEM).
3. The design requirements are checked for fulfillment (stopping condition).
4. If the design requirements are fulfilled, the optimization process stops. Else, modifications to the design are made and a new, improved design is proposed. Subsequently step $2. - 4.$ are repeated.

In each iteration step, the algorithm decides by which value $\Delta \boldsymbol{x}^{(k)}$ the design, defined by the design variables $\boldsymbol{x}^{(k)}$, needs to be changed for the following iteration $(k+1)$:

$$\boldsymbol{x}^{(k+1)} = \boldsymbol{x}^{(k)} + \Delta \boldsymbol{x}^{(k)}. \tag{2.7}$$

Several approaches for solving the design update problem in Equation 2.7, i.e., how $\Delta \boldsymbol{x}^{(k)}$ can be determined, exist. These approaches can be roughly classified as search direction strategies, global optimization techniques and optimality criteria.

Depending on the chosen structural optimization technique (size, shape, topology) there are different requirements on the optimization algorithm. The following subsections provide a short overview of the most important attributes of a "good algorithm" as well as a discussion on local/global optimality of a solution. Furthermore, the most commonly used algorithms are discussed, including gradient-based algorithms, approximation methods, optimality criteria methods, and global optimization algorithms.

2.4.1. Local vs. Global Optimum

A globally optimal solution is a feasible solution with an objective value that is better than all other feasible solutions to the model. With a convex objective and a convex feasible region, there can be only one optimal solution, which is globally optimal. On the other hand, a non-convex optimization problem is any problem where the objective or any of the constraints are non-convex. Non-convexity implies that there are multiple optima, i.e., several local optima of which usually one is also the global or absolute minimum. A local optimum of an optimization problem is a solution that is optimal compared to all other feasible solutions in its immediate vicinity, whereas a global optimum is the best out of all such local optima. An example of such a non-convex function is illustrated in Figure 2.5.

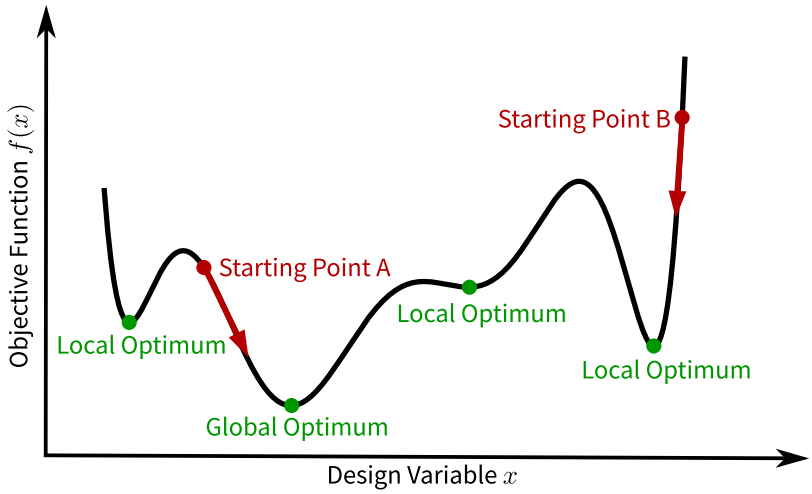

Figure 2.5.: Objective function with several local minima of which only one is the global optimum

It is important to consider that most problems of structural optimization are in fact non-convex. The probability that an optimization process gets caught in a local optimum depends on the characteristics of the optimization problem, the parameter settings and the features of the applied optimization algorithm. Local optimization algorithms are very efficient for finding local optima, namely determining an improving neighboring configuration starting from an initial configuration, see Figure 2.5 with starting point A and starting point B. These algorithms ensure only local optimality and they do not guarantee that the obtained design is the global optimum [11].

However, generally it is highly desirable for an algorithm to identify the global optimum. Global optimization algorithms employ measures that prevent convergence to local optima and increase the probability of finding a global optimum. The performance and efficiency of a global optimization algorithm is affected by the number of local optima as well as their location and surrounding gradients. The impact of distribution and number of local optima is discussed in detail by Törn et al. [12].

One of the problems regarding global optimization is that it is often not possible to determine whether the current best solution is situated on a local or a global optimum and thus, whether global convergence is achieved. In other words, it is usually not clear whether the optimization procedure can be terminated, whether the optimization procedure should concentrate on refining the current optimum or whether it should examine other regions of the design space instead. Furthermore, global optimization algorithms are not suitable for any kind of optimization problem as the computational burden increases with growing dimensionality of the optimization problem (i.e., the number of design variables) [13]. According to Sigmund [14], for instance, global algorithms for topology optimization require orders of magnitude more function evaluations compared to local algorithms which makes them computationally expensive. However, as global convergence is a major topic of research and is not the main focus of this thesis it will not be further discussed in detail.

Another problem is related to the non-uniqueness of solutions. Non-uniqueness of solutions refers to the problem that there exists more than one optimal designs with the same minimal objective function value (multiple global optima) [1]. An example of such a non-unique solution is the design of a structure in uni-axial tension, as shown in Figure 2.6 (a). The vertical black strip at the points of force application is assumed to be rigid. A structure consisting of one thick bar (Figure 2.6 (b)) will be just as good as a structure made up of several thin bars with the same overall area (Figure 2.6 (c)) [15]. However, this issue can be resolved by using regularization techniques.

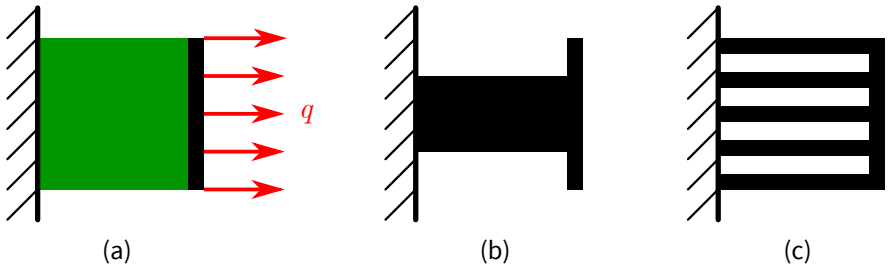

Figure 2.6.: Example of non-unique solutions for a structure in uni-axial tension (following [15])

2.4.2. Attributes of Algorithms

Algorithms for finding the optimum structural design have progressed rapidly within the past decades. In practice, one normally seeks algorithms that explore the feasible design space in a cost-effective manner, aiming for a better optimal solution within an acceptable level of accuracy depending on the nature and the size of the problem [2]. Most real-world structural optimization problems in engineering involve complexities like non-linearity, non-convexity, large dimensionality, design constraints, and mixed nature of variables. The latter refers to the fact that structural optimization problems may involve a mixture of continuous and discrete design variables. Therefore, from the optimization point of view, the choice of the right algorithm is crucially important. Several aspects must be considered when selecting an algorithm for practical applications. Considerations regarding the most important properties of a "good algorithm" can be summarized as follows:

Efficiency

The efficiency of an algorithm is defined as the computational effort that is required to solve an optimization problem. One possibility to judge the efficiency of an algorithm is the running time, measured either in terms of "wall clock time" or CPU time. "Wall clock time" refers to the amount of time the user has to wait to get an answer (e.g., the final design proposal) from the computer. The CPU time corresponds to the time the CPU spends on the algorithm, excluding tasks of the operating system and other processes. "Wall clock time" has been argued to be more useful in real-world settings by McGeoch [16]. In contrary Beiranvand et al. [17] states that the CPU time is considerably more stable as it is independent of background operations of the computer. However, according to Khompatraporn et al. [13] the execution times of algorithms are not directly comparable if the determined execution times are from machines with different specifications. Therefore, instead of relying on the execution time, Khompatraporn et al. [13] suggests to count the number of objective function evaluations, needed by the algorithm, to numerically converge to the optimum within some degree of predefined accuracy. This is similar to the measurement of algorithm efficiency by the number of so-called fundamental evaluations, proposed by Beiranvand et al. [17]. Fundamental evaluation refers to any subroutine that is called by the algorithm in order to gain fundamental information about the optimization problem, for instance objective function evaluation, constraint function evaluations or gradient evaluations. The algorithm should keep the amount of fundamental evaluations as small as possible so that the actual computation time is reasonable. In other words, an efficient algorithm should require relatively few iterations and thus converge quickly.

Accuracy

The accuracy of an algorithm refers to the quality of the algorithmic output which per se is a numerical issue according to Beiranvand et al. [17]. Algorithms should be able to identify a

solution with precision, without being overly sensitive to errors in the data or to arithmetic rounding errors that occur when the algorithm is implemented on a computer. Examples illustrating the effect of rounding errors can be found for instance in a publication by Brent [18].

Robustness/Reliability

For practical applications, it is of uttermost importance to use a method that is theoretically guaranteed to converge to the same solution starting from any initial design estimate. A method having such a guarantee is called robust [19]. In other words, robustness refers to the fact that the algorithm should be insensitive to choosing different "starting points", see Figure 2.5. Another way to define robustness is the following: according to Beiranvand et al. [17], the reliability and robustness of an optimization algorithm is defined as the ability of the algorithm to "perform well" over a wide range of optimization problems. In this context, the robustness of an algorithm can be verified if the algorithm is capable of treating different types of configurations of structural design problems with similar efficiency. Another way to define robustness is the following:

Ease of use

From the users point of view the ideal "user friendly" optimization algorithm is basically a *black box* that will output the final solution without too much preparation by the user. Algorithms that depend upon a large number of (externally set) parameters usually require pre-calibration or "tuning" for every new problem, indicating strong problem-dependency. An algorithm should need as little problem-specific parameter tuning as possible in order to enhance result reproducibility. However, this implies nontrivial compromises between user-friendliness for a non-expert or an average expert and sophisticated implementations [13].

It is noted, however, that there exists no algorithm for structural optimization that outperforms others in terms of being able to solve all types of optimization problems. The attributes of a "good algorithm" mentioned above may conflict and trade-offs between these attributes are usually inevitable. For instance, often an increase in computational cost (CPU time) has to be accepted in order to achieve a robust algorithm [17]. Therefore, the emphasis lies on finding the most appropriate algorithm for solving a particular structural optimization problem instead of finding the "best" optimization algorithm.

2.4.3. Gradient-Based Methods

Gradient-based methods are iterative optimization algorithms of mathematical programming (MP) for finding a (local) optimum for a differentiable function. Generally, mathematical programming refers to an iterative optimization procedure aiming at finding improved feasible designs with the knowledge of structural response and gradient (sensitivity) information [20].

According to Harzheim [2], gradient-based approaches fall into the category of so-called search-direction algorithms. The fundamental underlying structure of a search-direction algorithm is the following:

1. One starts with an initial point,
2. determines a direction of movement (according to a specified rule) in which to search for the next "design point",
3. and moves in that direction with a specified increment in order to improve the objective function.

At the new design point a new direction is determined and the process is repeated.

Gradient-based algorithms use local gradient information (function derivatives with respect to the design variables) to determine the most promising direction along which to search for the optimum. The gradient of a function $f\left(\boldsymbol{x}\right)$ is given by the vector of partial derivatives with respect to each of the n independent variables as

$$\boldsymbol{\nabla} f\left(\boldsymbol{x}^{(k)}\right) = \left[\frac{\partial f}{\partial x_1}, \frac{\partial f}{\partial x_2}, \ldots, \frac{\partial f}{\partial x_n}\right]^{\mathrm{T}}. \tag{2.8}$$

The gradient vector $\boldsymbol{\nabla} f\left(\boldsymbol{x}^{(k)}\right)$ is perpendicular to the hyperplane tangent to the contour surfaces of constant $f\left(\boldsymbol{x}\right)$. By determining the gradient, which is also referred to as the sensitivity of the design with respect to the design variables, it is possible to numerically (mathematically) determine how the design variables must be adapted to improve the objective while at the same time satisfying the constraints. A huge variety of such gradient-based methods is available today [4].

Using gradient-based algorithms, the design variables are updated at each major iteration k according to

$$\boldsymbol{x}^{(k+1)} = \boldsymbol{x}^{(k)} + \alpha^* \boldsymbol{p}^{(k+1)}, \tag{2.9}$$

where $\boldsymbol{p}^{(k+1)}$ is the so-called search direction for the major iteration k and α^* is the so-called step length. It is notable that the determination of the step length, which is performed with a so-called line search, usually involves multiple iterations that do not count towards the major iterations. This is an important distinction that needs to be considered when comparing computational cost of various approaches [1]. Equation 2.9 reveals that there are two subproblems for each major iteration, already indicated at the beginning of this subsection:

1) Originating from a starting point (the vector of design variables of the current design $\boldsymbol{x}^{(k)}$) a search direction $\boldsymbol{p}^{(k+1)}$ is determined.
2) The step length α^* is determined. The step length defines how the design variables must be adapted in order to improve the objective.

The procedure of determining a search direction $\boldsymbol{p}^{(k+1)}$ and finding the step length α^* is repeated until the stopping conditions (or conditions of convergence) are satisfied. The key point here is that all design variables are considered simultaneously according to their effect on the objective (and constraint) functions. The difference between the various types of gradient-based algorithms is the method that is used for computing the search direction (the first sub-problem).

The determination of the step length α^* is independent of the method that is used for determining the search direction. Therefore, the second sub-problem of determining the step length α^*, which is illustrated in Figure 2.7 (a), is explained first. To determine the step length along a given search direction $\boldsymbol{p}^{(1)}$ from a starting point ($\boldsymbol{x}^{(0)}$), a line search is performed. By using the line search strategy, the multi-dimensional optimization problem is reduced to a one-dimensional problem, i.e., the line search solves the one-dimensional optimization problem of finding the optimal step length along the search direction:

$$\alpha^* = \min\left(f\left(\alpha\right)\right). \tag{2.10}$$

The result of the above equation is used in Equation 2.9 to compute the next starting point $\boldsymbol{x}^{(k+1)}$.

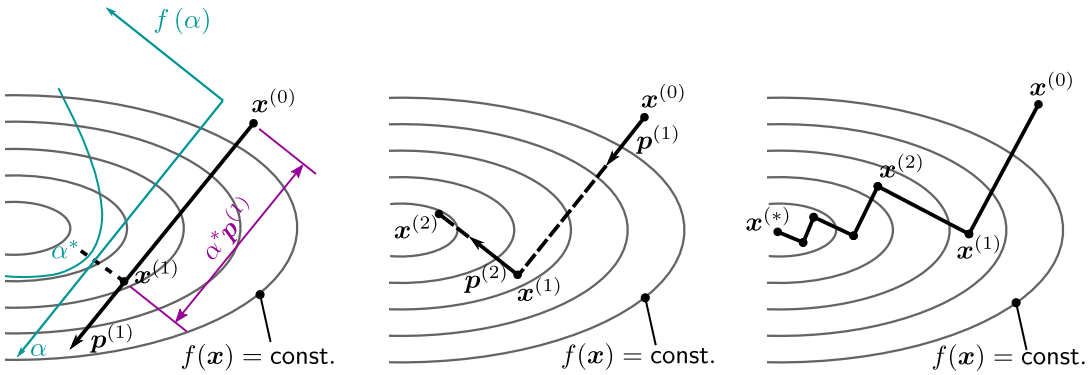

Figure 2.7.: General procedure of gradient-based search direction algorithms (following [2]). (a) Determination of the optimal step length α^* via line search, (b) Search direction procedure, (c) The convergence of the method of *Gradient Descent Method*

Getting back to the first sub-problem: the efficiency of gradient-based algorithms strongly depends on how the search directions are determined. *Gradient Descent Methods*, also referred to as *Steepest Descent Methods*, use the negative of the gradient of the function at the current point to determine the search direction. The gradient vector is orthogonal to the plane tangent to the isolines / isosurfaces ($f\left(\boldsymbol{x}\right) = \text{const.}$) of the function. The gradient vector at a design point, (e.g., at $\boldsymbol{x}^{(1)}$), is also the direction of maximum rate of change (maximum increase) of the function at that point. Therefore, in the case of a minimization problem, to improve the objective function and move further to a minimum, the search direction must be opposite to the gradient vector. Generally, for gradient based methods the determination of the function gradient signifies the main computational effort.

The procedure mentioned above can be visualized as a walk in high mountains with the design variables being the different paths to descend to the lowest point, the valley. The idea is that if the steps are not too large (causing the algorithm to jump over the target), following the most downward direction will result in finding the lowest point. Sometimes the terms gradient-based method and *Steepest Descent Method* are used interchangeably. However, in general, gradient-based methods refer to an optimization method in which the direction of descent is obtained by gradient information, that is, it is not limited to the negative gradient.

According to Harzheim [2], the *Steepest Descent Method* suffers from a slow convergence as two successive search-directions are always orthogonal such that a zigzagging pattern appears in the optimization process, as illustrated in Figure 2.7 (c). Although substantial improvement of the objective may be observed in the first few iterations, the method is usually very slow closing in on the optimum value. This is especially true for "long and narrow valleys". The step length gets smaller and smaller, crossing and recrossing the valley (shown as contour lines) as it approaches the minimum. The reason why the *Steepest Descent Method* converges slowly is that it has to take a right angle turn after each step and consequently search in the same direction as earlier steps.

To improve the convergence of the *Steepest Descent Method*, the method of *Conjugate Gradients*, developed by Fletcher et al. [21], can be used. This method is an attempt to mend the problem mentioned above by "learning" from experience. In the method of *Conjugate Gradients* the initial step in the first iteration is taken in the direction of the steepest descent. In all subsequent iterations, a contribution of the search direction from the previous iteration is added to the negative gradient of the current iteration

$$\boldsymbol{p}^{(k+1)} = -\boldsymbol{\nabla} f\left(\boldsymbol{x}^{(k)}\right) + \beta \boldsymbol{p}^{(k)}, \tag{2.11}$$

where the coefficient β is given, for example, by the so-called Fletcher-Reeves formula

$$\beta = \begin{cases} 0 & \text{when } k = 0 \\ \dfrac{\left|\boldsymbol{\nabla} f\left(\boldsymbol{x}^{(k)}\right)\right|^2}{\left|\boldsymbol{\nabla} f\left(\boldsymbol{x}^{(k-1)}\right)\right|^2} & \text{when } k > 0 \end{cases}, \tag{2.12}$$

With this small modification in the determination of the search direction, taking into account the history of the gradients, the algorithm moves more directly towards the optimum.

The methods described so far use first-order information (first-order derivatives) to obtain a local model of the objective function to find the optimum design. This is referred to as linear approximation.

In contrast, the *Newton Method* uses second-order information (second-order derivatives) to approximate the given function $f(\boldsymbol{x})$ in each iteration by a quadratic function, and then move to the minimum of this quadratic function. The geometric interpretation of this method is that in each iteration a paraboloid is fitted to the surface of the objective function $f(\boldsymbol{x})$ at the current design point $\boldsymbol{x}^{(k)}$, having the same slopes and curvature as the surface at that point. Subsequently, the minimum of that paraboloid is determined. If $f(\boldsymbol{x})$ happens to be a quadratic function, the exact optimum can be found in one step. According to Harzheim [2] the *Newton Method* results in faster convergence but not necessarily less computation time. While the gradient of a function of n variables is an n-vector, the "second derivative" of an n-variable function is defined by n^2 partial derivatives (the derivatives of the n first partial derivatives with respect to the n variables). The second-order partial derivatives can be represented by a square symmetric matrix called the Hessian matrix which contains $\frac{n(n+1)}{2}$ second-order derivatives:

$$\boldsymbol{\nabla}^2 f\left(\boldsymbol{x}^{(k)}\right) = \boldsymbol{H}(\boldsymbol{x}) = \begin{bmatrix} \frac{\partial^2 f}{\partial x_1 \partial x_1} & \cdots & \frac{\partial^2 f}{\partial x_1 \partial x_n} \\ \vdots & & \cdots \\ \frac{\partial^2 f}{\partial x_n \partial x_1} & \cdots & \frac{\partial^2 f}{\partial x_n \partial x_n} \end{bmatrix}, \tag{2.13}$$

where $\boldsymbol{H}(\boldsymbol{x})$ is the Hessian matrix of f at $\boldsymbol{x}^{(k)}$. The computation of the second-order derivatives and the handling of this matrix can be very time-consuming. *Quasi-Newton* methods approximate the Hessian matrix to speed up the algorithm by avoiding the computationally expensive step of determining the exact Hessian matrix. The various *Quasi-Newton* methods, like the *Davidon-Fletcher-Powell* (DFP) method and the *Broydon-Fletcher-Goldfarb-Shanno* (BFGS) method, differ in how they update the approximate Hessian matrix.

All the methods described so far are algorithms for solving an unconstrained optimization problem. However, most engineering problems have constraints that must be satisfied during the design process, see Equation 2.1c and Equation 2.1d. Therefore, it is also important to examine gradient-based algorithms that involve constraints. Associated with search direction algorithms one can say that a constraint is a boundary which prevents the optimizer from continuing in certain directions. Gradient-based algorithms for constrained optimization problems can be categorized into *indirect methods* and *direct methods*. With indirect methods, the constrained problem is converted into a sequence of unconstrained optimization problems. Penalty functions are used to take the constraints into account. Due to this, indirect methods are also referred to as penalty function methods. The *Exterior Penalty Method* appends a penalty for violating constraints while the *Interior Point Method* appends a penalty as one approaches infeasibility of the design. With direct methods the constraints are taken into account explicitly in the solution algorithm. These methods are also referred to as constrained methods.

Gradient-based methods for solving the constrained optimization problem include the *Constrained Steepest Descent Method* (CSD), *Constrained Quasi-Newton-Method* and *Method of Feasible Directions*(MFD) as well as it's modification the *Modified Method of Feasible Directions*(MMFD). According to Harzheim [2], direct methods are more efficient than indirect methods. The reason is that the optimal solution frequently lies on the boundary of the feasible region. Therefore, restricting the search to only feasible solutions (e.g., when using the *Interior Point Method*) or imposing very severe penalties makes it difficult to find the optimum. In practice it also might be better not to use the solution right on the boundary of the feasible region. On the other hand, if the penalty is not severe enough, then a too large region is searched and much of the search time will be used to explore regions far from the feasible region.

Like with the unconstrained methods, the design variables for constrained methods are modified successively during the design process by moving in the design space from one point to another. Constrained methods consist of the following computational steps:

1. Determine the set of active constraints at the current design point:
   For any point $\boldsymbol{x}^{(k)}$ in the feasible region, a constraint $g_j\left(\boldsymbol{x}^{(k)}\right) \leq 0$ is called active at $\boldsymbol{x}^{(k)}$ if $g_j\left(\boldsymbol{x}^{(k)}\right) = 0$, and inactive at $\boldsymbol{x}^{(k)}$ if $g_j\left(\boldsymbol{x}^{(k)}\right) < 0$. The active set of constraints at a design point $\boldsymbol{x}^{(k)}$ is made up of those constraints $g_j\left(\boldsymbol{x}^{(k)}\right)$ that are active at the current point [8].

2. Determine a search direction in the design space, based on the objective function and the set of active constraints.

3. Determine how far to go in the direction found in the previous step (step length).

4. Check convergence of objective.

Consequently, a search direction which leads to an improvement in the objective function without violating the constraints must be determined first. The basic concept is as follows: as long as there are no active constraints, the optimization is performed as an unconstrained gradient-based search. If a constraint becomes active, a different concept is needed for determining the search direction. A very illustrative description is to divide the design space into three domains [22]:

1. Usable Domain:
   A search direction within the usable domain (usable search direction) leads to an improvement of the objective function values. An improvement of the objective function (minimization) is achieved if the search direction $\boldsymbol{p}$ and the gradient of the objective function $\boldsymbol{\nabla} f\left(\boldsymbol{x}\right)$ are antiparallel:

$$\boldsymbol{p}^{\mathrm{T}} \boldsymbol{\nabla} f\left(\boldsymbol{x}\right) < 0. \tag{2.14}$$

2. Feasible Domain:
   A search direction within the feasible domain (feasible search direction) maintains that active constraints are not violated. This is the case if the search direction $\boldsymbol{p}$ and the gradient of the active constraint function $\boldsymbol{\nabla} g(\boldsymbol{x})$ are antiparallel:

$$\boldsymbol{p}^{\mathrm{T}} \boldsymbol{\nabla} g(\boldsymbol{x}) \leq 0. \tag{2.15}$$

3. Usable-Feasible Domain:
   The intersection between the usable and feasible domain is denoted as usable-feasible domain. For more than one constraint function the usable-feasible domain is the intersection of the usable domain with all feasible domains of the set of active constraints.

Figure 2.8(a) illustrated the three domains described above for one active constraint. If it is no longer possible to identify a usable and feasible search direction, that is, there is no usable-feasible domain anymore, the optimum is reached. For one active constraint $g(\boldsymbol{x})$ this is the case if the gradient of the objective function $\boldsymbol{\nabla} f(\boldsymbol{x})$ and the gradient of the active constraint $g(\boldsymbol{x})$ are antiparallel.

When a constraint becomes active, the aim is to move downwards as far as possible along the constraint limits as shown in Figure 2.8(b). For every k-th iteration, the search direction must have the following properties:

$$\boldsymbol{p}^{(k)^{\mathrm{T}}} \boldsymbol{\nabla} f\left(\boldsymbol{x}^{(k-1)}\right) < 0 \quad \text{and} \quad \boldsymbol{p}^{(k)^{\mathrm{T}}} \boldsymbol{\nabla} g\left(\boldsymbol{x}^{(k-1)}\right) \leq 0. \tag{2.16}$$

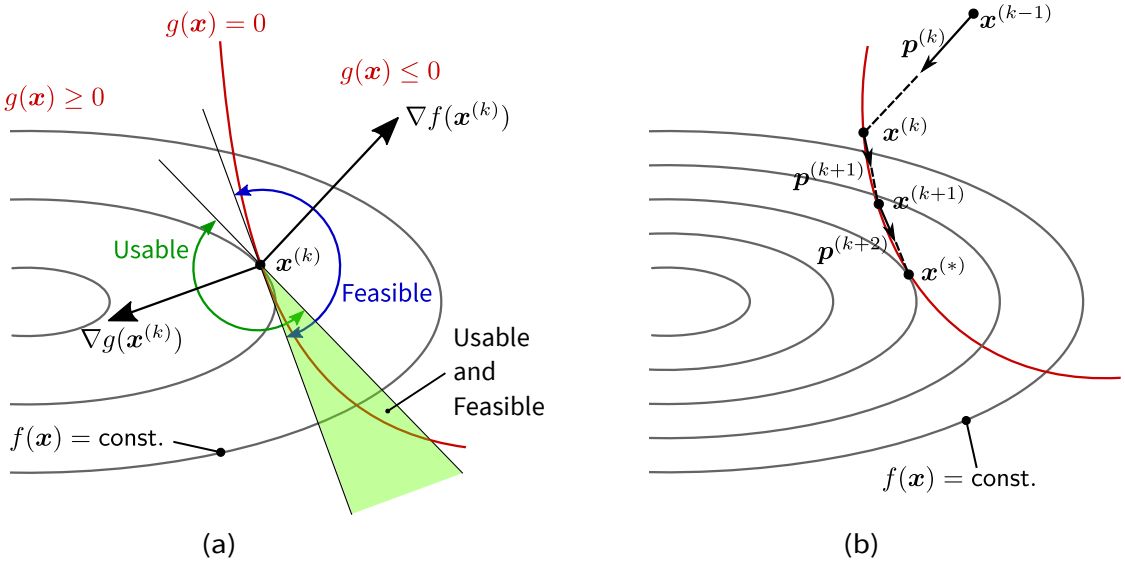

Figure 2.8.: Constrained optimization. (a) Usable and Feasible domain for the determination of the search direction, considering one active constraint. (b) Concept of the *Method of Feasible Directions* (following [2])

Using the *Method of Feasible Directions*, a certain tolerance range is defined for determining whether a constraint is active or not. The reason is that in terms of efficiency it is highly desirable to move as far as possible along a search direction. For instance, if one uses an unconstrained search when already close to the constraint limit, the step length may be very small and a new search direction must be determined, again requiring the time consuming computation of gradients. Figure 2.9 illustrates the idea of such a tolerance range, defined by the limits ε and δ. The tolerance range implies that a constraint is considered active before reaching the exact value $g(\boldsymbol{x}) = 0$. Furthermore, a slight violation of the constraint is tolerated. According to Harzheim [2], typical values for the tolerance limits are $\varepsilon = -0.03$ and $\delta = 0.003$. However, the *Method of Feasible Directions* shows a tendency to run along a "zigzag" course when moving along the constraint limit. With the *Modified Method of Feasible Directions*, which shall not be discussed in detail here, this tendency of "zigzagging" is suppressed [2].

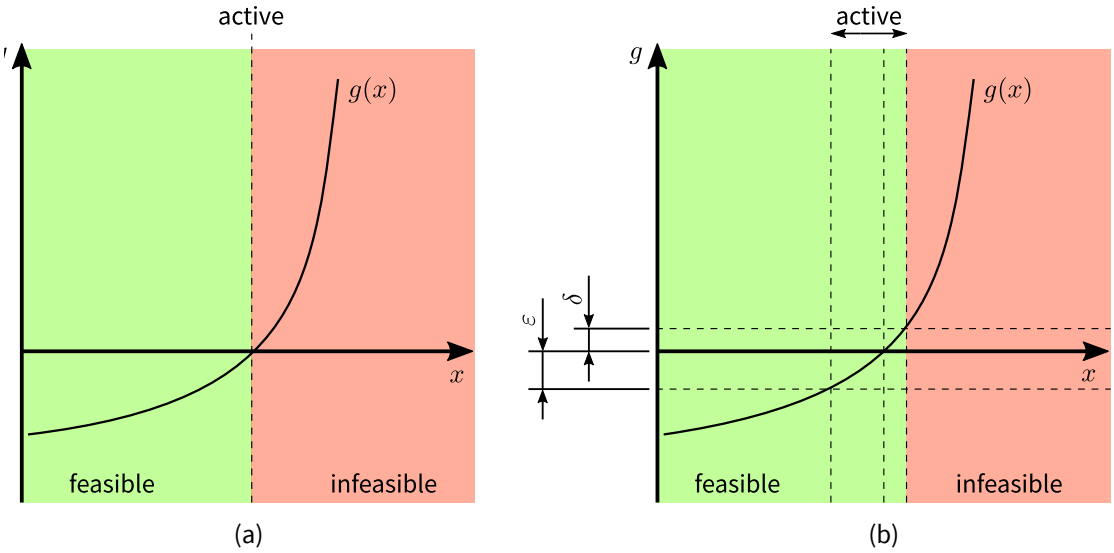

Figure 2.9.: Active constraint for the *Method of Feasible Directions*. (a) Exact constraint. (b) Introduction of tolerances ε and δ to form a tolerance band at both sides of a constraint (following [2])

Gradient-based methods are widely used for solving a variety of optimization problems in engineering, especially when dealing with topology optimization based on element-wise design variables. According to Bendsøe et al. [1] this is due to the fact that one of the key-advantages of these methods is that they are efficient for solving optimization problems where the number of design variables is high and considerably exceeds the number of constraints and objectives. Typically, a large number of design variables appears in topology optimization after discretization since for a good representation of the design one has to work with rather fine finite element meshes. However, most gradient-based algorithms have problems when dealing with discontinuous functions and they are not designed to handle multimodal problems (multiple local optima) or discrete and mixed discrete-continuous design variables. Figure 2.10 illustrates various types of functions that are problematic for gradient-based optimization algorithms.

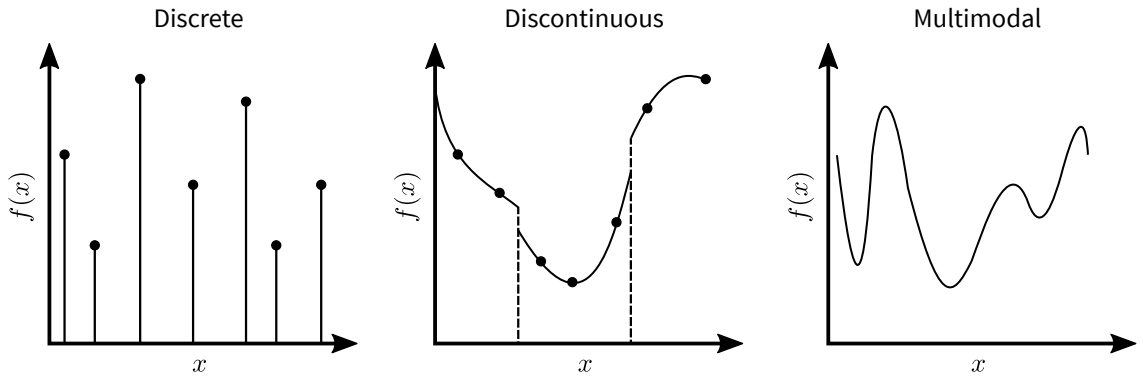

Figure 2.10.: Graphs of various types of functions that are problematic for gradient-based algorithms

Gradient-based methods in particular are known to be limited by a characteristic referred to as the 'local optima' problem (although they are very efficient in finding such a local optimum for high-dimensional, non-convex problems). Since these methods use only local information (functions and their gradients at a point) in their search process, they converge only to a local optimum. During the search for an optimum solution, e.g., global minima, these techniques can encounter local minima from which they cannot escape due to the 'descent' nature of the approach. Consequently, one can obtain different solutions to the same discretized problem, when using different starting points, and global optimality cannot be guaranteed [23]. Search methods based on local optimization, like the gradient-based algorithms, usually require some type of diversification to overcome local optimality. One way to achieve diversification is to start the optimization using different starting points. This is called *Multistart Strategy* [2]. The key-idea behind the *Multistart Strategy* is to select several starting points for a subsequent efficient local gradient-based optimization, as indicated in Figure 2.5 with starting point A, leading to the global optimum, and starting point B leading to a local optimum.

2.4.4. Approximation Methods

As already pointed out, the determination of the gradient (sensitivity) of objective functions and constraint functions signifies the main computational effort of gradient-based algorithms. Therefore, a multitude of methods have arisen with the aim of increasing the computational efficiency of gradient-based methods by replacing the original optimization problem by a sequence of sub-problems. These methods are referred to as *approximation methods*, where the actual objective function is replaced by a (simpler) approximation function. The number of structural analyses needed to determine the solution of an optimization problem can be reduced when appropriate approximations are used [2]. Their accuracy increases with the number of parameters they contain and/or the way they are computed [24]. Approximation methods can be categorized into methods of local approximation, where the approximation is only sufficiently accurate in the immediate vicinity of the actual design point $\boldsymbol{x}^{(k)}$, and methods of global approximation where the approximation is sufficiently accurate in

the entire design space. Therefore, local approximations are only used for one iteration step whereas global approximations can be used for the entire optimization. When using approximation methods, the quality of approximations determines the accuracy and the efficiency of the scheme. Consequently for structural optimization, expertise of the user is needed as these methods can be very complex to use [2].

The key idea of methods of local approximation is to use simple functions that are expected to provide a good approximation of the actual function in the immediate vicinity of the current design point. In consequence, a sequence of sub-problems is solved, each of which is an approximation of the real optimization problem. The idea of local approximation can be combined with any of the aforementioned gradient-based methods. Figure 2.11 illustrates the idea of local approximation for the *Method of Feasible Directions*. Starting with the design point $\boldsymbol{x}^{(k-1)}$, the objective function and constraint function(s) near that point are approximated. The approximated optimization problem is solved using the "line search" strategy leading to the optimal design point $\boldsymbol{x}^{(k)}$ for which the exact structural responses (objective/-constraints) are determined. This procedure is repeated until the optimum has been determined.

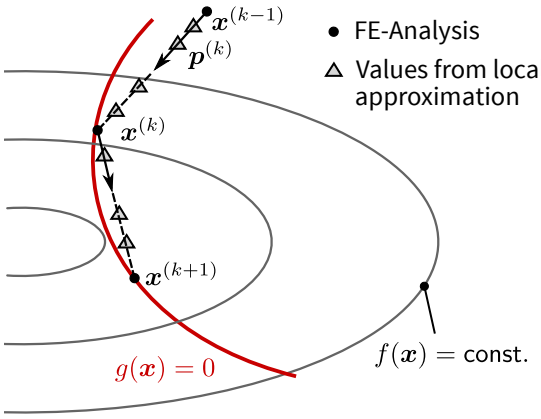

Figure 2.11.: *Method of Feasible Directions* using local approximation (following [2])

Methods of local approximation include *Sequential Linear Programming* (SLP), *Sequential Quadratic Programming* (SQP), *Convex Linearization Problem* (CONLIN), the *Method of Moving Asymptotes* (MMA) as well as the *Globally Convergent Method of Moving Asymptotes* (GCMMA). *Sequential Linear Programming* is a gradient-based optimization algorithm that relies solely on linear approximation. Gradient-based optimization algorithms that rely on nonlinear but convex separable approximation functions are: SQP, CONLIN, MMA and GCMMA. An example of global approximation is the so-called *Response Surface Method*.

The *Sequential Linear Programming* (SLP) method sequentially solves the non-linear optimization problem as a series of linear problems. A linear approximation of a function $y\,(x)$ is illustrated in Figure 2.12 (a). The linear approximation is obtained by using Taylor's expansion in the first order.

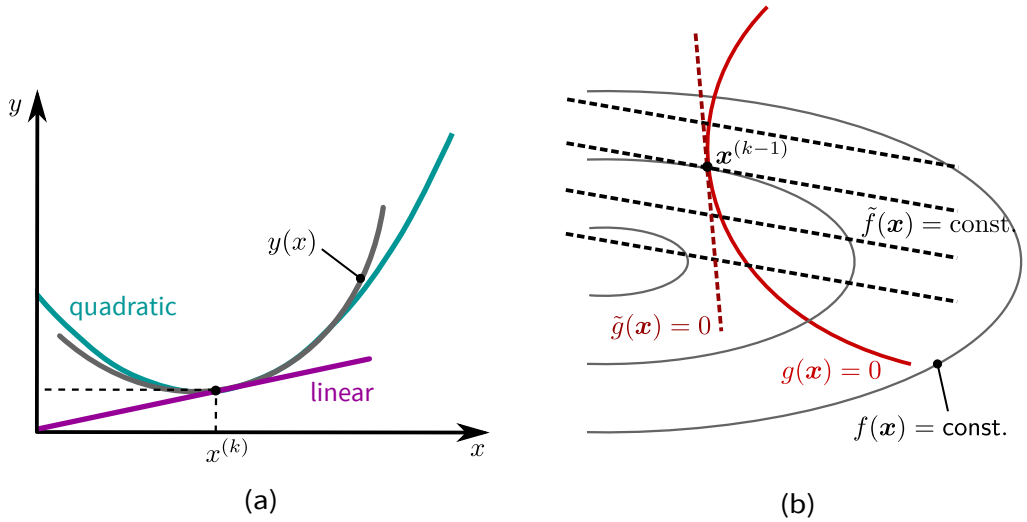

Figure 2.12.: (a) Linear and quadratic approximation of a function $y\,(x)$ in the one dimensional case, (b) *Sequential Linear Programming* Algorithm for objective function $f\,(\boldsymbol{x})$ and constraint $g\,(\boldsymbol{x})$ with approximated objective function $\tilde{f}\,(\boldsymbol{x})$ and the approximated constraint $\tilde{g}\,(\boldsymbol{x})$ (following [2])

Therefore, the approximated problem of minimizing the objective function can be written as:

$$\min(\tilde{f}\,(\boldsymbol{x})) = f\left(\boldsymbol{x}^{(k-1)}\right) + \boldsymbol{\nabla}^{\mathrm{T}} f\left(\boldsymbol{x}^{(k-1)}\right)\left(\boldsymbol{x} - \boldsymbol{x}^{(k-1)}\right), \tag{2.17}$$

The linear approximation only requires the determination of the function value and the gradient at the current design point, see Equation 2.17. If a gradient-based method is used to solve the optimization problem, the computation of the linear approximation does not require any additional effort since the gradients need to be determined anyway. The entire line search is carried out on the approximated function. A visualization of the SLP algorithm is shown in Figure 2.12 (b) where $\tilde{f}\,(\boldsymbol{x})$ denotes the iso-lines of the approximated objective function and $\tilde{g}\,(\boldsymbol{x})$ denotes the linear approximation of the constraint. The resulting subproblems of linear programming can be solved via linear programming (LP) methods like the *Simplex Method* [2]. Since a linearly approximated function has no extremum, SLP problems require additional constraints, termed as move limits. These move limits represent the maximum allowed change of the design variables in the current iteration. The reason for limiting the change of the design variables is the following: too large step lengths impose the risk of reaching regions where the approximation of the function is very poor, leading to the risk of violating constraints. According to Iqbal [8] the SLP algorithm is simple to apply, but should be used with caution in engineering design problems as it can easily run into convergence problems.

The *Sequential Quadratic Programming* (SQP) method solves a quadratic approximation of the non-linear optimization problem, as depicted in Figure 2.12 (a). SQP uses a quadratic approximation for the objective function, whereas a linear approximation is used for the constraint function(s). According to Iqbal [8], the big advantage of using SQP is that the subproblem represents a convex programming problem. Gradually changing the optimization from

an (artificial) convex problem to the original (non-convex) design problem, using gradient-based optimization algorithms in each step until convergence, helps to circumvent the problem of local optima. Therefore, compared to using solely a gradient-based algorithm without approximation, there is an increased chance of obtaining a global optimum [1].

Schumacher [3] states that the quality and range of validity of an approximation can be significantly improved if "information" of the parameter to be approximated is already considered when choosing the respective approximation. For instance, for the examples depicted in Figure 2.13, the volume and mass show a linear dependency on the design variable x. Therefore, these system responses can be linearly approximated. However, system responses like stresses and displacements, show a reciprocal dependency on the design variable, as exemplarily shown in Figure 2.13. Approaches of reciprocal approximation include the method of *Convex Linearization* and the *Method of Moving Asymptotes*.

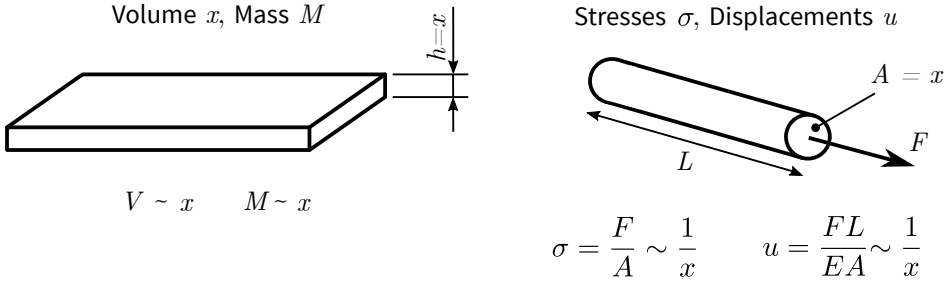

Figure 2.13.: Examples of simple system responses which can be determined analytically with linear and reciprocal dependency on the design variable

With reciprocal approximation Equation 2.17 can be written as

$$\min(\tilde{f}(\boldsymbol{x})) = f\left(\boldsymbol{x}^{(k-1)}\right) + \sum_{i=1}^{n} \frac{\partial f\left(\boldsymbol{x}^{(k-1)}\right)}{\partial z_i}(z - z_i), \tag{2.18}$$

where $z_i = x_i^{-1}$ is the reciprocal of the design variable x_i.

The *Convex Linearization* (CONLIN) method uses a so-called hybrid or mixed approximation where the selection of approximation depends on the algebraic sign of the first derivative. A linear approximation is selected if the first derivative with respect to the design variable is positive whereas a reciprocal approximation is selected if the first derivative with respect to the design variable is negative.

With the *Method of Moving Asymptotes* [25] the choice of the approximations is also based on the gradient information at the current iteration design point. An important role in the generation of these subproblems is played by a set of parameters which influence the "curvature" of the approximations, and also act as "asymptotes" for the subproblem. Bendsøe et al. [1] states that the MMA has proven itself to be very versatile and well suited for large scale topology optimization problems. However, it must be noted that the MMA, as well as all other approximation methods do not resolve the issue of local optima.

2.4.5. Optimality Criteria Methods

Gradient-based methods, approximation methods, and meta-heuristic methods (which will be dealt with in Subsection 2.4.6) are based on the philosophy of numerically searching the design space for optimum designs. In other words, starting with an estimate of the optimum design for the problem, the design is improved iteratively until the optimum is determined. *Optimality criteria* (OC) methods are based on a different philosophy. Using OC methods, a criterion/some criteria are defined such that when this criterion/these criteria are satisfied, the optimum is found. Therefore, optimality criteria are the conditions a function must satisfy at its minimum point. In order to generate an optimum design, a recursive algorithm is employed to update the design variables for satisfying the optimality criteria. Algorithms based on optimality criteria are indirect methods as the objective function is not directly optimized. The respective optimality criteria can be

- derived from physics, e.g., *Principle of the Fully Stressed Design* (FSD) or *Simultaneous Failure Mode Design*,
- based on observations from nature (Principle of Adaptive Growth), e.g., *Computer Aided Optimization* (CAO) or *Soft Kill Option* (SKO), or
- be derived mathematically, e.g., *Kuhn-Tucker-Conditions* [26]

The *Principle of the Fully Stressed Design* (FSD) is one of the earliest optimality criteria approaches used in structural design and is applicable to structures that are subject only to stress and "minimum cross-section" constraints (gage constraints) [2]. Therefore, it is widely practiced for member sizing of frame structures. The FSD optimality criterion states that for an optimum design, each member of a structure that is not at its minimum gage must be fully stressed under at least one of the design load conditions. [1]. This optimality criterion implies that in order to obtain a weight optimized structure, material should be removed from members that are not fully stressed unless prevented by a minimum gage constraint (e.g., minimum allowable cross-section). This requires the explicit assumption that the primary effect of adding or removing material from a structure is to change the stress in that member, with negligible or no effect on the rest of the structure. Since in statically determined structures internal forces are independent of member dimensions, the condition of the *Fully Stressed Design* leads to minimum weight. However, in statically indetermined structures, internal forces are influenced by member dimensions. Therefore, in these cases such a condition does not necessarily result in minimum weight. According to Harzheim [2], there might be members that are not fully stressed because they help to relieve stresses in other members.

According to Bendsøe et al. [1], optimality criteria have proven to be an attractive alternative to overcome the high numerical cost of mathematical programming methods when dealing with a high number of design variables. This is mainly due to the fact that these methods only need few numbers of mechanical analyses. However, the disadvantage is that the concept of optimality criteria can only be used for specific problems as it can only handle few

constraints and a restricted choice of objective functions. Applications of optimality criteria in structural optimization are discussed in detail in the publications of Chiandussi et al. [27], Yin et al. [28] as well as Kriechbaum [29].

2.4.6. Global Optimization Algorithms

One possibility to overcome some deficiencies of gradient-based methods is to use so-called gradient-free or non-gradient-based methods. The key strength of non-gradient-based methods is their ability to solve problems that are difficult to solve using gradient-based methods. The most commonly used gradient-free algorithms are: *Nelder-Mead Simplex* (Nonlinear Simplex), *Simulated Annealing* (SA), *Divided Rectangles Method*, *Genetic Algorithms* (GA) and *Particle Swarm Optimization* (PSO). Many gradient-free algorithms mimic mechanisms observed in nature or use heuristics. Furthermore, many of them are designed as global optimization algorithms. Therefore, these methods will be discussed in Section 2.4.6. Unlike gradient-based methods in a convex design space, gradient-free methods are not necessarily guaranteed to find the true global optimum. However, they are able to find many good solutions (mathematician's point of view vs. engineer's point of view).

Global optimization algorithms aim at finding the global optimum of an optimization problem. According to Weise [30], the most efficient way to solve global optimization problems currently is to use methods that contain stochastic features. Therefore, the found solution is dependent on the set of random variables generated. These algorithms are often referred to as heuristic, although recent literature tends to refer to them as meta-heuristic. Meta-heuristic methods are inspired by nature or physics combined with simple statistical and/or probabilistic methods [31]. These methods are iterative in nature and use stochastic operations in their search process to modify one or more initial candidate solutions. These candidate solutions are usually generated by random sampling of the design space. As global optima are at least highly desirable, extensive research has been undertaken in the field of meta-heuristic methods, leading to a huge variety of methods [2, 32, 33]. Among meta-heuristics the most prominent algorithms for structural optimization are *Genetic Algorithms* (GA), *Swarm Intelligence Algorithms* (SI), and *Physics Based Algorithms* [2]. According to Gandomi et al. [31], the two main characteristics of meta-heuristic methods are intensification and diversification. This implies focusing on a local region, knowing that a current good solution can be found in this region (intensification) while at the same time generating diversified solutions to explore the global design space (diversification). A balanced combination of those two aspects of meta-heuristic algorithms will generally ensure to determine the global or at least the "near global" optimum.

Genetic Algorithms (GA) are inspired by concepts of evolutionary biology. GAs simulate a natural process by generating an initial population of designs and subsequently applying evolutionary principles to improve the design. They are based on three essential components:

- Natural Selection (survival of the fittest)
- Crossover (reproduction processes where genetic traits are propagated)
- Mutation (variation)

Genetic Algorithms is the most general term used when expressing a large family of optimization algorithms that make use of the three components mentioned above. However, when reviewing literature one may also come across names like *Evolutionary Algorithms*, *Evolutionary Programming*, *Genetic Programming* and so forth. These similar techniques differ in genetic representation and other implementation details and the nature of the particular applied problem [2].

Another category of global optimization algorithms are *Swarm Intelligence* (SI) algorithms. The term swarm intelligence refers to collective intelligence. Swarm intelligence systems are typically made up of a population of simple and individually unsophisticated agents. The interaction with each other and the environment leads to the emergence of "intelligent" global behavior which is unknown to the individual agents. SI algorithms are inspired by the observation of the collective behavior in "societies" in nature. These "societies" efficiently solve complex problem such as finding the shortest path between their nest and food source or organizing their nest. Examples of SI algorithms include *Particle Swarm Optimization* (PSO), *Ant Colony Optimization* (ACO), and *Artificial Bee Colony Algorithm* (ABC). For instance the PSO algorithm is based on observations from nature that some animals, such as birds and fish, are able to share information among their group. E.g., identifying the best place to land is a complex problem (maximizing the availability of food, minimizing the risk of existence of predators) which depends on both memory of each individual as well as the knowledge gained by the swarm, known as social knowledge. The ACO algorithm is inspired by the way that ant colonies find the shortest route between the food source and their nest. Ants communicate with each other via pheromone trails. When an ant finds some amount of food it carries as much as it can carry. When returning to the colony it deposits pheromone on it's paths based on the quantity and quality of the food. When choosing their way, ants tend to choose, in probability, paths marked by strong pheromone concentrations. Consequently, the higher the pheromone level the higher the probability that more ants follow the path, implying that the pheromone will further increase on that path.

Physics Based Algorithms are inspired by physical phenomena. For instance the algorithm of *Simulated Annealing* (SA) is inspired by the physical process of crystallization rather than biological evolution. In metallurgy and material science annealing is the heat treatment of material with the aim of altering its properties such as hardness. This heat treatment involves controlled heating and cooling of a material to increase the size of its crystals and

reduce their defects. Metal crystals have small defects (dislocations of ions) which weaken the overall structure. When the metal is heated, the energy of the ions and consequently their diffusion rate is increased. By this, the dislocations can be destroyed and the structure of the crystal is reformed as the material is cooled down and approaches its equilibrium state. The initial temperature must not be too low and the cooling must be done sufficiently slow such that the system doesn't get stuck in a meta-stable, non-crystalline state, representing a local minimum of energy. The *Simulated Annealing* algorithm is a copy of this physical process. It is based on the analogy between the way in which the crystalline structure of a metal achieves near global minimum energy states during the process of annealing and the way in which a function may reach a global minimum during statistical search of the design space.

It is important to note, that no algorithm can guarantee convergence to a global optimum and it may be more accurate to refer to the algorithms above as having global properties. Global optimization algorithms that contain stochastic features typically involve the manipulation of a sample drawn from a uniform distribution over the design space. Obviously, these methods can never provide an absolute guarantee that the global optimum has been found. All that can be assured is that the probability of finding the global optimum approaches 1 as the sample size goes to infinity [30]. However, according to Bandaru et al. [11] most metaheuristics have the ability to recover from local optima due to inherent stochasticity or heuristics specifically meant for this purpose (e.g., simulated annealing).

One of the negative predicates attributable to global optimization strategies with respect to local optimizations (e.g., gradient-based algorithms) is the relatively large number of evaluations that are necessary to find an acceptable minimum. Schumacher [3] states, that generally, to identify a global optimum, an infinite number of analysis steps is necessary. Global optimization algorithms provide only an increased probability that a global optimum can be determined within a finite amount of analyses. Therefore, it is important to keep in mind that algorithms which improve the chances of finding a global optimum come at increased computational cost. This is also the reason why most applications, so far, have been on small scale problems [31].

Harzheim [2] states, that one of the major problems in global optimization is the choice of an adequate stop criterion. The respective criterion should be stringent enough so that the algorithm do not waste too many function evaluations after the global minimum has been found. On the other hand, the stop criterion should also be loose enough to ensure that the algorithm does not terminate before the global optimum has been found.

Another issue is that global optimization methods, e.g., simulated annealing, generally find the optimal solution of unconstrained optimization problems. They are not capable of directly considering constraints in the optimization algorithm. Therefore, the constraints must be taken into account using penalty functions [3]. To recall, penalty functions are used to convert the constrained global optimization problem to an unconstrained one by adding a

penalty term to the objective function. However, it is difficult to choose a static value of the penalty parameter such that the unconstrained (penalty) problem and the original problem have the same global optimum [30]. With evolutionary algorithms, another option is to impose that only individuals fulfilling the constraints are retained during the new generation and new individuals are generated until the desired number of feasible individuals are obtained. Another very 'rough' option is to generate a sufficiently large set of solutions, provided that they are equally well distributed (sub)optimal solutions, and sort out the feasible solutions after the optimization has stopped.

2.5. Topology Optimization

Compared to size and shape optimization, topology optimization is a relatively new topic. Nevertheless, numerical methods for topology optimization have been intensively investigated since the late 1980s [2]. This is mainly due to the fact that topology optimization is an extremely rapidly expanding research field having many interesting theoretical implications in mathematics, mechanics, multiphysics and computer science as well as important practical applications for manufacturing industries (i.e., automotive and aerospace) [34]. The importance of topology optimization lies in the fact that the choice of the appropriate topology in the conceptual design phase is generally the most decisive factor for the efficiency of a product.

A very straightforward way to categorize methods for topology optimization is to differentiate between methods for discrete structures and methods for continuum structures, see Figure 2.14. Methods for discrete structures use a so-called "basic structure". A "basic structure" is defined as a space of points which are connected by as many structural elements, e.g., bars, in as many ways as possible. In this case, the design problem consists in determining the optimal number, position, and mutual connectivity of the structural members. In contrast, methods for continuum structures do not need any basic structure but require the definition of the design domain for the optimization. Topology optimization for continuum structures means simultaneously optimizing the shape of external as well as internal boundaries and the number of inner holes. Within topology optimization for continuum structures one can further distinguish between two main types of solution techniques: the *Microstructure (Material)* approaches, which are also referred to as *Eulerian* approaches, and the *Macrostructure (Geometrical)* approaches, which are also referred to as *Lagrangian* approaches. In the *Microstructure* approach, which is more commonly used for structural problems, the entire admissible design domain is discretized, e.g., with finite elements, to describe the geometry and the mechanical response fields. In the *Macrostructure* approach, the topology optimization is performed in conjunction with a shape optimization. Therefore, in contrast to the *Microstructure* approach, which uses a fixed finite element mesh, the mesh must change with the changes of the boundaries of the design.

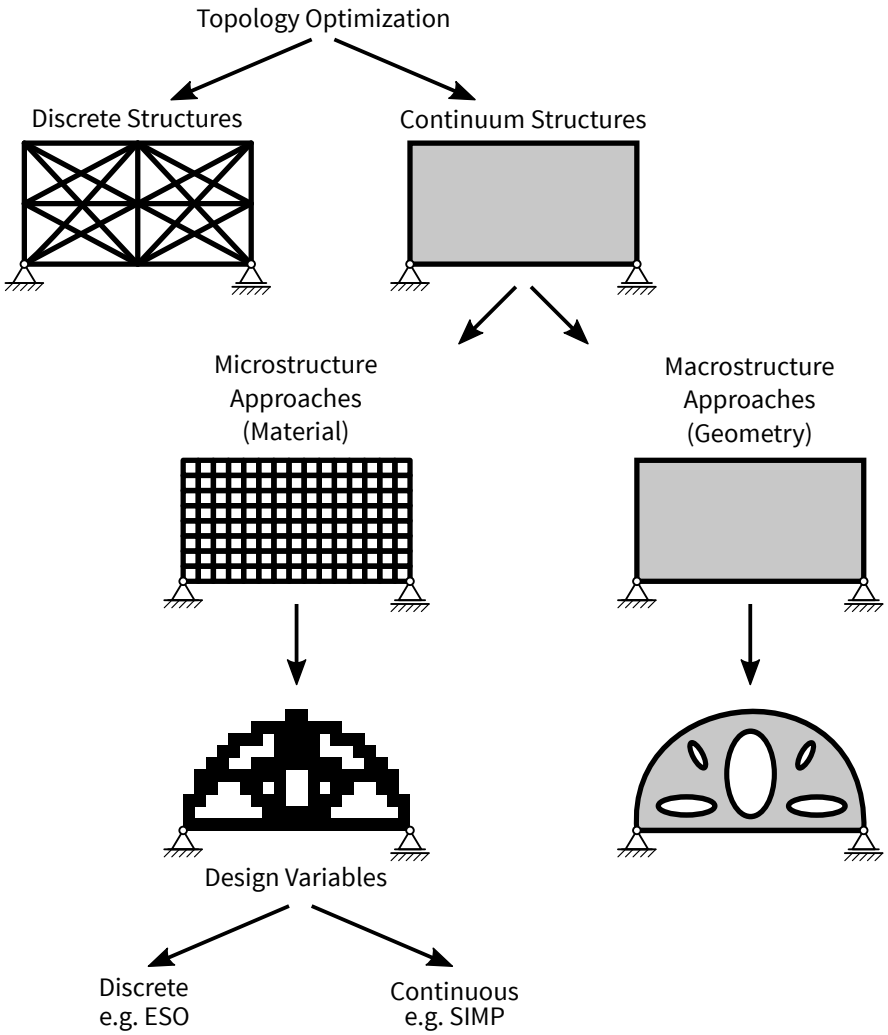

Figure 2.14.: Categorization of methods for topology optimization (following [3])

As the focus of this thesis is on the *Microstructure* approaches, *Macrostructure* approaches will not be discussed in more detail. The *Microstructure* approach for continuum structures introduces a set of design variables that describe the presence or absence of material within the design domain. These design variables are defined either within the element of the mesh or on every node point of the mesh [1]. Therefore, topology optimization using the *Microstructure* approach is synonymous with the presence of many design variables.

Generally, methods for the *Microstructure* approach are distinguished between those solving the discretized topology optimization with discrete variables and those using continuous design variables [35], see Figure 2.14. Using discrete design variables (e.g., methods of *Evolutionary Structural Optimization*), constitutes the basis for a great part of topology optimization approaches. However, according to Sigmund et al. [36], using design variables that can only take discrete values (0 or 1), imposes numerical difficulties when solving the topology optimization problem. These numerical issues are discussed in detail in Section 2.6.

The formulation of continuous (density) design variables constitutes the basis for the major part of recent research on topology optimization [36]. Methods which use continuous design variables are for instance the *Homogenization* approach and *Solid Isotropic Material with Penalization* (SIMP). A very illustrative example of the *Microstructure* approach for topology optimization for a continuum structure, published by Sigmund [37] is shown in Figure 2.15. This approach typically involves the following steps:

1) Definition of the design domain (colored green), see Figure 2.15 (a)
2) Definition of the load(s) and boundary condition(s), see Figure 2.15 (b)
3) Discretization of the design domain (e.g., finite elements) and iterative procedure to solve the optimization problem, see Figure 2.15 (c)
4) Post-processing and final design proposal, see Figure 2.15 (d)

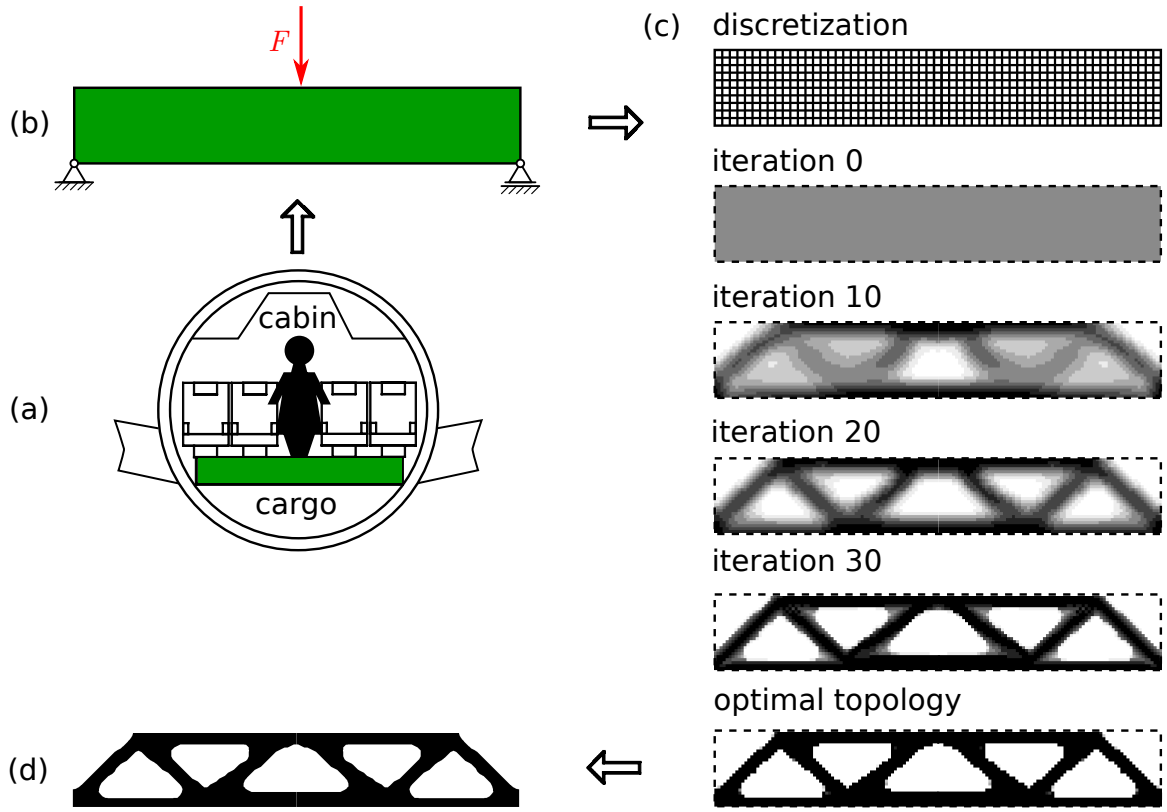

Figure 2.15.: Concept of Topology Optimization Procedure (following [37])

In the most simple form, where there is only one objective function, a topology optimization problem can be defined the following way [1]:

$$\text{minimize:} \qquad f(\boldsymbol{x}) \tag{2.19a}$$

$$\text{subject to:} \qquad V = \sum_{i=1}^{N} x_i V_i \leq V^*, \tag{2.19b}$$

$$\text{where:} \qquad 0 \leq x_i \leq 1. \tag{2.19c}$$

V^* is the prescribed target volume of the structure, V_i is the volume of the respective element and N is the total number of elements in the design domain. The material distribution is described by N elemental design variables x_i. The design variables are assumed to attain constant values within each finite element. The aim of the optimization is to determine whether each element in the continuum should contain material or not. The design variable x_i determines the presence ($x_i = 1$) or the absence ($x_i = 0$) of an element. In other words, the limit 1 denotes solid material (shown in black in Figure 2.15 (d)) and the limit 0 denotes void or very weak material (shown in white in Figure 2.15 (d)). The result is a rough description of the outer and inner boundaries of the structure that represents the optimal overall topological layout.

A large number of algorithms exist for solving the discretized topology optimization problem, ranging from mathematically well-founded methods that use the gradient of the objective/-constraint function to non-gradient meta-heuristic approaches (like genetic algorithms). As already pointed out in Section 2.4.3, gradient-based methods are very efficient when dealing with huge optimization problems with a high number of design variables. These approaches have the advantage of ensuring convergence within a reasonable number of iterations. In his publication "On the usefulness of non-gradient approaches in topology optimization" Sigmund [14] points out that non-gradient, nature inspired methods like genetic algorithms, swarms and most differential evolution techniques are not viable alternatives for the vast majority of topology optimization problems due to the high number of design variables. According to Bendsøe et al. [1], the most commonly used methods for solving topology optimization problems include *CONLIN*, *Method of Moving Asymptotes*, and *Optimality Criteria*.

2.5.1. Mathematical Formulation for Continuum Structures

To discuss the mathematical formulation for topology optimization of a continuum structure the simplest type of design problem formulation in terms of objective and constraint is used. According to Bendsøe et al. [1], the classical problem of topology optimization is to design for the maximum stiffness of a statically loaded, linearly elastic structure under a single load condition under simple source constraints, i.e., a limit on the amount of material at our disposal. The inverse of stiffness is flexibility or compliance. Therefore, designing for maximum stiffness is equivalent to designing for minimum compliance.

When solving this optimization problem by computational means a typical approach is to use finite elements. The optimization problem can thus be expressed as:

$$\begin{aligned} &\text{minimize:} && \boldsymbol{f}^{\mathrm{T}}\boldsymbol{u} \\ &\text{subject to:} && \boldsymbol{K}\left(E_e\right)\boldsymbol{u} = \boldsymbol{f}, \\ & && E_e \in E_{ad}, \end{aligned} \tag{2.20}$$

where $\boldsymbol{K}$ is the stiffness matrix, $\boldsymbol{u}$ is the global displacement vector and $\boldsymbol{f}$ is the load vector. The stiffness matrix $\boldsymbol{K}$ depends on the stiffness E_e in element e, numbered as $e = 1, ..., N$. Again, N is the total number of elements in the design domain. $\boldsymbol{K}$ can be written in the following form:

$$\boldsymbol{K} = \sum_{e=1}^{N} \boldsymbol{K}_e\left(E_e\right), \tag{2.21}$$

where $\boldsymbol{K}_e$ is the (global level) element stiffness matrix. In Equation 2.20 E_{ad} denotes the set of admissible stiffness tensors.

For topology optimization, the task is to determine which points of space should be material points and which points should remain void (no material). Therefore, the aim is to determine the optimal subset of active material points Ω^{mat} of the design domain Ω, where Ω denotes the entire design domain and Ω^{mat} denotes the domain occupied by isotropic material. Thus, for a discrete valued design problem (a so-called 0-1 problem) the set of admissible stiffness tensors consist of those tensors for which

$$E_{ijkl} = 1_{\Omega^{\mathsf{mat}}} E^0_{ijkl}\,,\; 1_{\Omega^{\mathsf{mat}}} = \begin{cases} 1 & \text{if } x \in \Omega^{\mathsf{mat}} \\ 0 & \text{if } x \in \Omega \setminus \Omega^{\mathsf{mat}} \end{cases}. \tag{2.22}$$

E^0_{ijkl} denotes the stiffness tensor for the given isotropic material. The design variable $1_{\Omega^{\mathsf{mat}}}$ is a binary indicator function with $1_{\Omega^{\mathsf{mat}}} = 1$ denoting solid and $1_{\Omega^{\mathsf{mat}}} = 0$ denoting void material. A simple source constraint defines a limit on the amount of material at our disposal. This is expressed by the following inequality:

$$\int_{\Omega} 1_{\Omega^{\mathsf{mat}}} d\Omega = \mathsf{Vol}\left(\Omega^{\mathsf{mat}}\right) \leq V. \tag{2.23}$$

Therefore, the minimum compliance design is for a limited (fixed) volume V.

It is well-known that this integer (0-1) parametrization of the optimization problem in its general continuum setting is ill-posed [1, 15, 38]. A physical explanation of this ill-posedness is, that for a given structure with a certain volume it is possible to improve the stiffness by introducing a lot of small holes without changing the actual volume. The solution tends towards a design with infinite perforation and finally microstructures that are typically not isotropic and cannot be represented within the original design description of only isotropic material and thus are not in the feasible (isotropic) design set anymore.

Typically, the topology optimization problem is treated by discretizing the design domain Ω. If the structure is discretized, e.g., using N finite elements, the size of the holes is limited by the discretization. However, in this case the ill-posedness of the optimization problem is indeed found in the numerical solution and is often termed mesh-dependency.

In order to obtain a well-posed problem, a regularization of the topology optimization problem formulation is required. According to [15], one option to achieve this is to relax the binary condition and include intermediate material densities in the problem formulation. This is referred to as *Relaxation*. For instance, the *Homogenization* approach assumes a periodically perforated microstructure. Different microstructures lead to different intermediate densities. The mechanical properties of the material are determined using the homogenization theory. An alternative to the homogenization theory is to relax the binary problem using a continuous density value with no microstructure. The mechanical properties are then determined using a power-law interpolation function between "solid" and "void". With this power law, intermediate densities are implicitly penalized, driving the structure towards the desired black-and-white configuration. This black-and-white solution is also often referred to as "$0-1$" design, where "0" stands for "void" and "1" stands for "solid" material configuration. This approach is usually referred to as the *Solid Isotropic Material with Penalization* (SIMP). The *Homogenization* approach as well as the *Solid Isotropic Material with Penalization* are discussed in more detail in Subsection 2.5.2. It is obvious that relaxation methods usually result in optimized design regions of intermediate density (gray regions) or perforated microstructures. The high complexity of these design proposals yields structures that cannot be easily interpreted for manufacturing purposes and therefore might be complicated and expensive to manufacture.

From a manufacturing point of view it is attractive to generate "$0-1$" solutions on a macroscopic level. Therefore, one can do quite the opposite of enlarging the design space to resolved the ill-posedness problem, namely restricting it. The aim of *Restriction* methods is to reduce the original feasible design set to a sufficiently compact subset which possesses sufficient closedness and therefore solutions to the optimization problem defined in Equation 2.22. Methods of restriction are for instance the *Perimeter Control*, *Gradient Control* or *Mesh-Independent Filtering*. These methods are discussed in more detail in Section 2.6.

However, there are methods that directly deal with the discrete (binary) formulation of the problem, without modifying the original problem by relaxation or restriction. These approaches use heuristic rules to avoid unwanted effects such as mesh-dependency or checkerboard patterns, caused by the ill-posedness of the topology optimization problem. These methods are discussed in more detail in Subsection 2.5.3.

2.5.2. Topology Optimization with Continuous Design Variables

As mentioned before, one possibility for solving the discretized topology optimization problem is to use continuous design variables. Approaches to continuous topology optimization use material models that allow the density of the material to cover the complete range from 0 (void) over intermediate values (composite) to 1 (solid). These methods have the advantage of providing regularization (well-posedness) of typical topology optimization problems when introduced in the mathematical formulation. The approaches differ in how the relation between density and material property is determined and how "intermediate" densities are handled. Using the *Homogenization* approach, the design domain is filled with a porous material whereas the *Solid Isotropic Material with Penalization* (SIMP) uses an isotropic material and an empirical approach.

Homogenization Approach

The homogenization method was the first practical methodology for topology optimization, published by Bendsoe et al. [39] in 1988. The key idea of this approach is to derive the relation between the density design variable and the material property based on the homogenization of a periodic microstructure (micromechanical model). In other words, the material density is introduced by representing the material as a microstructure. Common types of material models with periodic, perforated microstructure are the *hole-in-cell* microstructure, layered 2D-microstructures, and layered 3D-microstructures [1].

An example of a material model with periodic, perforated microstructure - namely the *hole-in-cell* microstructure - is illustrated in Figure 2.16.

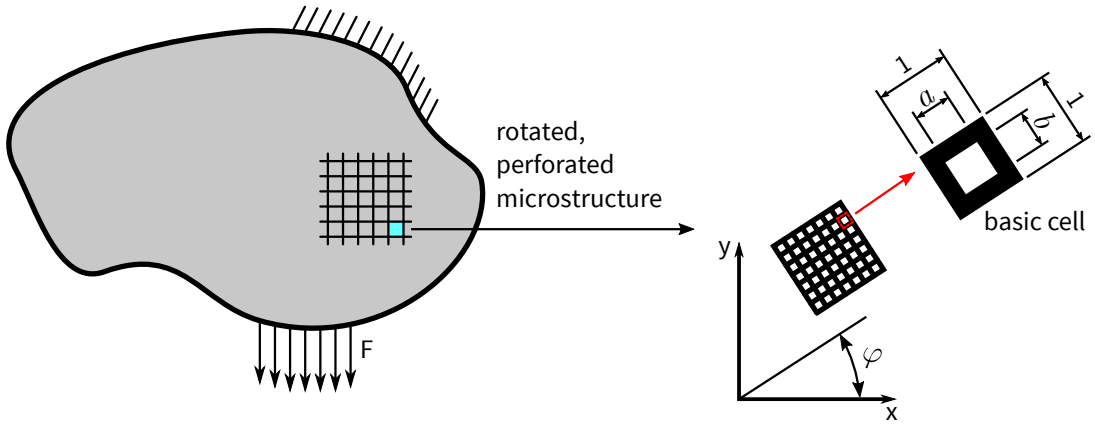

Figure 2.16.: Example of a *hole-in-cell* microstructure with rectangular holes for a two dimensional continuum topology optimization problem (following[1])

The microstructure consists of periodically arranged microcells (basic cells) and has an infinite number of infinitely small voids [1]. This leads to a porous "composite" that can have a density that varies between $0\,\%$ and $100\,\%$. The 2-dimensional square microcell consists of an isotropic material with rectangular holes.

The geometry of the holes is defined by the geometric parameters a and b. Since the macroscopic properties of the microstructure are not isotropic an orientation angle is also needed. The orientation of the microscopic cells is defined by the angle φ. The geometric parameters a, b as well as the orientation φ are the design variables. The same concept applies for the 3-dimensional case. However in this case, a total of 5 design variables per microcell are required: three variables for the edge length of the cavity in the unit cube as well as two angle variables for the alignment of the cavity.

As mentioned above, the aim is to derive a homogenized material property, based on the microcells, that only reflects the macroscopic behavior and depends on the geometric parameters of the microcell. In the finite element based homogenization method for topology optimization, those effective properties are assigned to the elements of the finite element model of the structure. This means, each element represents a material consisting of a large number of microcells. The parametrization of the cells is made in such a way that the density of the material covers the range of values from completely void ($\rho_i = 0$) to completely solid ($\rho_i = 1$) elements. This means, for instance, by changing the dimensions of the void (in this case the edge lengths of the void a and b), the void region can cover the whole area of the microcell. Therefore, the final topology may contain three types of regions: solid ($a = b = 0$), void ($a = b = 1$) and "porous" (with different cavity sizes). Figure 2.17 illustrates the basic concept of the homogenization method using a square microcell with a centrally placed square hole with the geometrical parameters $a = b$ and $\varphi = 0$. Figure 2.17 (a) shows the design domain before optimization, Figure 2.17 (b) shows the design proposal after optimization. Prior to the optimization, all elements of the discretized structure have a uniform homogenized material. After optimization, the elements have different material densities depending on the choice of the design variables $a = b$.

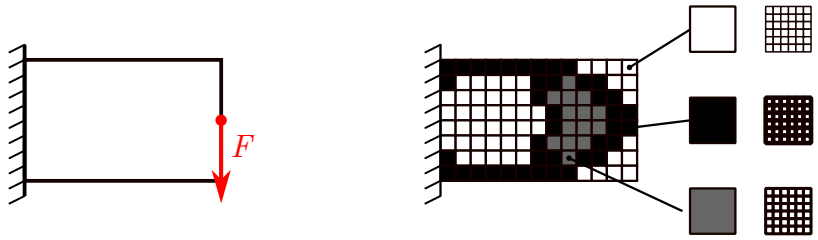

Figure 2.17.: Basic concept of homogenization method using a square microcell with a centrally placed square hole

Using the homogenization method, the optimization does not only yield an optimal material distribution but also the optimized orthotropic material properties for each element. However those orthotropic material properties cannot be easily transferred to a real structure. Furthermore, the "grey" areas found in the final design proposal contain microscopic length-scale holes that are difficult or even impossible to manufacture.

In fact, for the material distribution of a real manufacturable structure with isotropic material only the two extreme values of the density $\rho_i = 0$ and $\rho_i = 1$ are of interest, leading to an isotropic material, where only 1 design variable is needed instead of 3 (in the 2-dimensional case) or 5 (in the 3-dimensional case) [2]. The homogenization method was the inspiration for the development of another important structural optimization approach, namely the *Solid Isotropic Material with Penalization* method which is described in more detail in the next passage.

Density-Based approach

An alternative, that avoids the application of the homogenization, is the so-called *Density-Based* approach. The aim of this approach is to reduce the complexity of the homogenization approach and to improve its convergence to 0-1 solutions. The key idea is to relax the binary topology optimization problem using a continuous density value with no microstructure.

In the *density-based* approach, the material distribution is parametrized by the material density distribution. The design variables x_i are represented by the "artificial density" for the i-th element, defined as the normalized density:

$$x_i = \frac{\rho_i}{\rho_i^0}, \tag{2.24}$$

where ρ_i^0 is the element's initial density and ρ_i is the element's density after the optimization. In practical terms, this solution approach is similar to a sizing optimization where the sizing variables are the densities of the elements. The key issue when using the *density-based* approach is to define a relationship between material properties of the element, i.e., the stiffness tensor, and the continuous design variable x_i. In his original study, Bendsøe [35] used a so-called power-law approach as material interpolation scheme. In Bendsøe's approach, the material stiffness is expressed as a power function of the design variable:

$$E_i = (x_i)^p \, E_i^0, \quad p > 1. \tag{2.25}$$

E_i is the elastic modulus after optimization and E_i^0 is the elastic modulus of a given solid isotropic reference material. As the design variable is free to move between 0 and 1 ,it can also take on some intermediate values also referred to as "intermediate densities". From a practical viewpoint, this is an undesirable feature as the primary goal of isotropic topology optimization is to find a real and manufacturable shape, namely a density taking only the values 0 and 1. Therefore, this power-law implicitly penalizes intermediate densities to drive the structure towards a so-called "black-white" ("$0-1$") configuration. This penalization procedure is usually referred to as *Solid Isotropic Material with Penalization* (SIMP). It is the most common technique to solve material distribution optimization problems. The penalization factor p, also referred to as penalty factor, is used to steer the solution to discrete $0/1$ values: with increasing values of the exponent $p > 1$, the optimized design moves more and more to a design without intermediate density values ("gray" zones), as indicated in Figure 2.18.

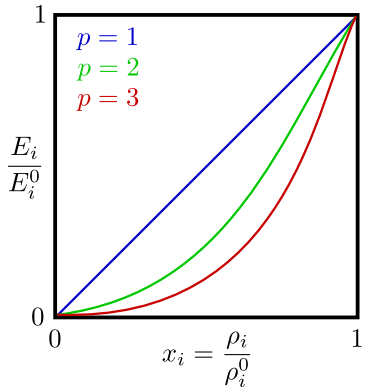

Figure 2.18.: Relative stiffness as a function of normalized density with different values of penalization factor p

However, Sigmund et al. [36] states that the proper choice of the penalization factor is not trivial. Choosing p too low might cause too much grey scale elements. Choosing p too large, there is the risk to attain a feasible region too fast that is not the one giving the global optimum [1]. In his publication *"Material interpolation schemes in topology optimization"* Bendsøe et al. [40] suggest to use a continuation method which, for instance, for the SIMP method means that the penalty exponent is gradually increased during the optimization process. According to Sigmund et al. [36] this will often result in convergence to better design.

Further approaches to interpolation schemes with isotropic materials exist that all serve the same purpose, namely to provide a continuous interpolation between "solid" and "void" material with a penalization of intermediate densities. These are for instance the *Rational Approximation of Material Properties* (RAMP) approach published by Stolpe et al. [41] or schemes that use explicit penalization [42]. According to [1], these alternative interpolation schemes have certain theoretical or computational advantageous features for specific problems but shall not be explained in more detail here.

All density-based optimization approaches mentioned above represent smooth-differentiable problems that can be solved by gradient-based methods (e.g., *Method of Feasible Directions* [43]), sequential convex programming methods (e.g., *Method of Moving Asymptotes* [44]), optimality criteria methods (e.g., public codes [9], [45]) or by other mathematical programming based optimization algorithms.

2.5.3. Topology Optimization with Discrete Design Variables

An important branch of approaches that directly deal with the discrete valued (continuum) optimization problem are the *Evolutionary Structural Optimization* (ESO) approaches. Further approaches include the *Discrete Level Set* approach [46] as well as *Discrete Density* approaches that use convex approximation and mathematical programming approaches [47, 48].

The approaches of *Evolutionary Structural Optimization* are subject of this subsection, as this method is used for optimizing the topology in the framework of this thesis. ESO, and its variations, are numerical methods combined with FEM. The original *Evolutionary Structural Optimization* (ESO) method, developed by Xie et al. [49], has undergone tremendous development over the past decades. Its variants include the *Additive Evolutionary Structural Optimization* (AESO) and *Bi-Evolutionary Structural Optimization* (BESO). It has to be mentioned that the term "evolutionary" is somewhat misleading because it usually refers to Darwinian processes (as in genetic algorithms). For ESO and its representatives the term "evolutionary" rather indicates the underlying concept of sequential element rejection and admission such that a structure can evolve towards an optimum.

All ESO approaches have in common that the initial finite element mesh is used throughout the whole optimization process. This means that the position of nodes and elements are fixed and only the number of "active" elements changes during the optimization. The elements themselves are considered as design variables. Thus, the elemental design variable x_i, which is also referred to as "element property number", is used to declare the existence ($x_i = 1$) or absence of an element ($x_i = 0$). In the isotropic case, each element within the design domain is assigned a design variable $x_i = 1$ in the beginning which equals a solid isotropic material (with the respective material properties such as Young's modulus and Poisson's ratio). When an element is eliminated during the process, its design variable is switched to $x_i = 0$. Therefore, this element physically does not exist in the current structure and thus is ignored in assembling the global stiffness and/or mass matrices. Approaches to evolutionary structural optimization differ in two aspects: how the criterion for the element rejection (and addition) is defined and how the elements to be removed are handled, i.e., whether they are completely deleted from the structure (hard-kill) or merely removed by setting the element stiffness to a low value (soft-kill).

The concept of the original *Evolutionary Structural Optimization* approach, first published by Xie et al. [49] in 1993, is based on the assumption, that the optimal use of material goes along with an evenly distributed stress field within the structural domain. This concept is clearly reflected in the fully stressed design (FSD). The original ESO concludes that lowly stressed material is inefficiently used and therefore can be gradually removed according to a predefined rejection criterion based on the local stress level. By gradually removing inefficient material, it is expected that the resulting structure evolves towards an optimal shape and topology. This approach is the so-called *stress approach* since it uses the element stress, e.g. von Mises stress, as the driving criterion in the evolution process. The gradual removal works as follows: the stress field of a loaded structure easily can be determined by means of a numerical simulation method, e.g. finite element method. As the design is over-sized and far from being optimal, the element stress level σ_e^{vM} may vary significantly throughout the design domain. Lightly stressed elements are "inefficient" and can be removed from the structure.

An inequality, which compares the element von Mises stress σ_e^{vM} with a critical (maximum) von Mises stress $\sigma_{\mathsf{critical}}^{\mathsf{vM}}$, is defined to identify those inefficient elements as follows:

$$\sigma_e^{\mathsf{vM}} < c_{\mathsf{rr}} \sigma_{\mathsf{critical}}^{\mathsf{vM}}, \tag{2.26}$$

where c_{rr} is a so-called rejection ratio (rejection rate). Those elements that satisfy the inequality, defined by Equation 2.26, are removed from the structure. The removal of material happens by simply deleting elements from the finite element model, for which the original ESO method is also referred to as "hard-kill" method. The rejection ratio can also be increased, for each iteration, according to a defined evolutionary ratio c_{ER}:

$$c_{\mathsf{rr}}^{\mathsf{new}} = c_{\mathsf{rr}}^{\mathsf{old}} + c_{\mathsf{ER}}. \tag{2.27}$$

As the rejection ratio increases, more and more relatively inefficient material is removed from the structure. The cycle of finite element analysis and element removal is repeated until a desired optimum is reached (i.e., until the tolerance is fulfilled).

Apart from the strength requirement, a structure may also need to comply with requirements on stiffness/displacement, frequency or buckling load. For these problems the so-called *sensitivity approach* is used. The *sensitivity approach*, which is also referred to as sensitivity analysis, is to study the effect of material removal on the above mentioned structural behavior. For instance, to maximize the stiffness of a structure, the stress criterion for element addition and removal is replaced by an elemental strain energy criterion as published by Chu et al. [50] for ESO and later by Yang et al. [51] for BESO. In literature this is also referred to as *stiffness criterion*.

Generally, the goal of the optimization is to maximize the stiffness of a structure which is equivalent to minimizing the compliance since compliance is defined as the inverse of stiffness. When loads are applied in terms of nodal forces only (i.e., no displacement load) the global mean compliance C^{global} of a structure is proportional to its internal energy:

$$C^{global} \propto \frac{1}{2} \sum_i \boldsymbol{f}_i{}^{\mathrm{T}} \boldsymbol{u}_i, \tag{2.28}$$

where $\boldsymbol{f}_i$ is the nodal load vector and $\boldsymbol{u}_i$ is the corresponding displacement vector. Therefore, to minimize the compliance, the expression in Equation 2.28 needs to be minimized.

In the finite element method, the static behavior of a structure is represented by

$$\boldsymbol{K}\boldsymbol{u} = \boldsymbol{f}, \tag{2.29}$$

where $\boldsymbol{K}$ is the global stiffness matrix, $\boldsymbol{u}$ is the global nodal displacement vector and $\boldsymbol{f}$ is the nodal load vector.

As the propotionality, shown in Equation 2.28, plays no role for the minimization problem and in order to be consistent with literature, the following formulation is used:

$$C = \frac{1}{2}\boldsymbol{u}^{\mathrm{T}}\boldsymbol{K}\boldsymbol{u}. \tag{2.30}$$

If an element i is removed from a structure with N finite elements, the mean compliance will have a change which is defined as the element stiffness sensitivity number α_i:

$$\alpha_i = \Delta C \tag{2.31}$$

Similarly, for dynamic problems and the buckling behavior of a structure, sensitivity numbers can be defined [52]. The sensitivity number represents the contribution of element modification to the concerned structural behavior. For stiffness optimization, the mean compliance is reduced. Therefore, eliminating elements with the smallest absolute value of sensitivity will be the most effective. Similarly, in frequency or buckling optimization (if the goal is to frequency or buckling load), elements with the largest sensitivity number can be removed.

As mentioned above, in the original ESO approach "inefficient" elements are completely removed from the structure (hard-kill). As deleted elements physically do not exist in the updated structure, there is no information about the effects of these elements on the objective function in later stages of optimization. Furthermore, the main criticism concerning original ESO approaches is that the approach is limited to removing elements from the structure as an element cannot be readmitted once it has been prematurely or "wrongly" removed from the structure. According to Xia et al. [53], as a consequence, the original ESO approach requires an over-sized initial design domain to ensure that the final design is represented by adequate elements as in certain cases the optimization can be misled due to an inappropriately defined initial setting.

The *Additive Evolutionary Structural Optimization* (AESO) approach, proposed by Querin et al. [54], is a reverse method to the original ESO algorithm. With AESO the structure evolves from a base structure (design domain) with little material, gradually adding material to highly stressed regions. However, like ESO, AESO also only allows for one directional variation of the structural material layout.

The key idea of the *Bi-Evolutionary Structural Optimization* (BESO) approach is to devise a scheme to restore deleted elements in later stages of optimization if necessary. In other words, in comparison to ESO and AESO, BESO is capable of turning elements "on" (addition) and "off" (removal) during the optimization process. Again, one has to distinguish between the *stress based* approach and the so-called *sensitivity based* approach. Furthermore, depending on how the elements to be removed are handled, BESO is referred to as "hard-kill" BESO or "soft-kill" BESO.

The original stress-based BESO approach, published by Querin et al. [55], is a combination of ESO and AESO. In this improved version of the ESO method, elements can be removed from the "least efficient" regions but also added to the "most efficient" regions of the finite element model of the structure.

In this original *stress based* BESO approach, elements to be removed or added are treated separately with a rejection ratio c_{rr} and inclusion ratio c_{ir}:

$$\sigma_e^{\text{vM}} < c_{\text{rr}}\sigma_{\text{critical}}^{\text{vM}}, \tag{2.32a}$$

$$\tilde{\sigma}_e^{\text{vM}} \geq c_{\text{ir}}\sigma_{\text{critical}}^{\text{vM}}, \tag{2.32b}$$

where $\tilde{\sigma}_e^{\text{vM}}$ is an approximation of the von Mises stress for void elements. Elements with the lowest von Mises stress are removed, satisfying the criterion in Equation 2.32a. Void elements near the highest von Mises stress regions are switched to solid when satisfying the criterion defined in Equation 2.32b. In contrast, when using the *sensitivity based* approach for stiffness maximization the sensitivities of the objective function with respect to a local variation of the material are calculated for each element of the FEM mesh inside the design area. Subsequently, the elements are ranked using the corresponding sensitivity numbers. The solid elements with the lowest sensitivity numbers are removed from the structure and the void elements with the highest sensitivity numbers are changed to solid elements. As this approach is used in the framework of this thesis, it is discussed in detail in Chapter 3.

The difference between "hard-kill" and "soft-kill" BESO is as follows: in the hard-kill BESO an element which is regarded as being "inefficient" is completely deleted from the structure, similarly to ESO. Hard-kill BESO shows a very high computational efficiency due to the fact that eliminated elements are not involved in the finite element analysis. However, this approach sometimes fails in rectifying incorrect elemental rejection. This is shown by Zhou et al. [56] for a simple example which shows the complete breakdown of ESO and "hard-kill" BESO. The example of Zhou et al. is illustrated in Figure 2.19.

It shows a simple topology optimization problem of a beam in which the total compliance is minimized. The beam has a fixed support at the left and a roller support at the top. The load condition consists of a horizontal load and a vertical load. The design domain is discretized by 100 elements. In the original structure, see Figure 2.19 (a), the lowest strain energy density is in the element colored blue. Therefore, the rejection criterion for minimum compliance will take out this element first. After removing the blue element in the vertical tie, the resulting structure becomes a cantilever where the vertical load is transmitted by flexural action, see Figure 2.19 (b). This structure has a much higher compliance than that of any intuitive design obtained by removing one element from the horizontal beam. The region with the highest strain energy density is at the left bottom of the cantilever. According to the BESO algorithm, an element may be added in that region rather than recovering the deleted element in the vertical tie.

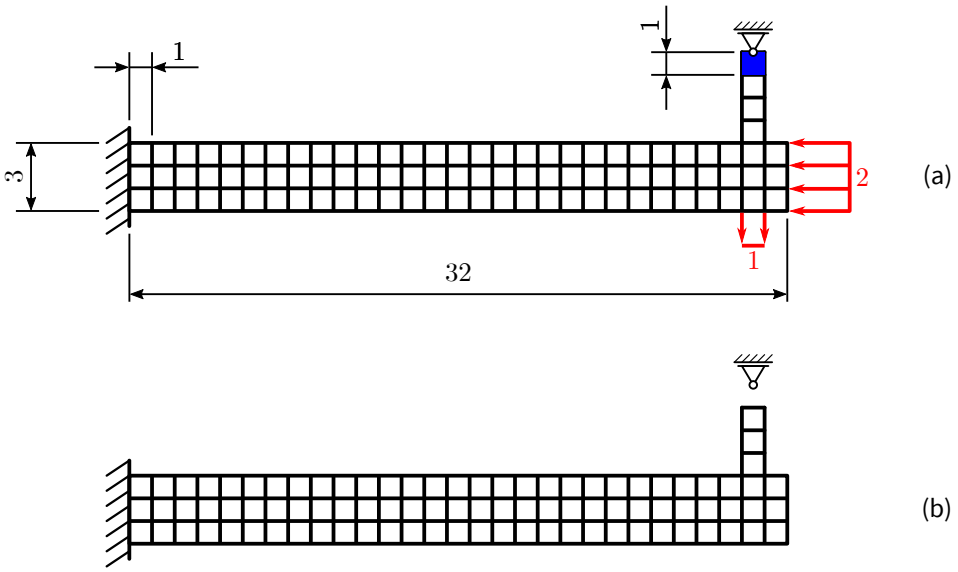

Figure 2.19.: Illustration of the breakdown of hard-kill BESO: (a) boundary and loading conditions defined by Zhou et al. [56], (b) BESO design for a volume fraction $VF = 99\,\%$

Therefore, Zhou et al. [56] conclude, that hard-kill optimization methods such as ESO/BESO may produce highly non-optimal solutions. However, it may be more appropriate to call such a solution a highly inefficient local optimum than a non-optimum [52].

A very effective alternative way to "remove" elements from the design domain is to set the element stiffness to a very low value (e.g., adjusting elastic modulus, density, thickness, ...). For instance, Hinton et al. [57] reduced the elastic modulus of elements to be "removed" by dividing it by a predefined large factor. Rozvany et al. [58] suggest a *Sequential Element Rejection and Admission* (SERA) method which considers two separate material models: a real material and a virtual material with negligible stiffness. Huang et al. [59], in 2009, proposed a sensitivity based "soft-kill" BESO method, using an artificial material interpolation scheme with penalization similar to the treatment in the SIMP approach. In this method, the element's effective properties are determined according to the power-law material scheme

$$E\left(x_i\right) = x_i^p E_1, \tag{2.33}$$

where E_1 denotes the elastic modulus for solid material and p is the penalty exponent. The design variable x_i is limited to a minimum value x_{min}, e.g., $x_{\text{min}} = 0.001$. Therefore, the void elements are not completely removed from the structure but replaced by a very soft material. The soft-kill BESO approach, by Huang et al., uses the sensitivity approach for element addition and rejection. Although this soft-kill BESO approach has been introduced quite recently it has shown its capability for solving a wide range of shape and topology optimization problems with high computational efficiency [60], [61], [52], [62].

Considering practical engineering aspects, ESO/BESO approaches to structural optimization have some attractive features: they can be easily implemented as a post-processing algorithm to most FEM analysis packages and require a relatively small amount of computational time. In addition, as the optimization is performed with discrete design variables, the resulting topology consists of a clear distinctive region without gray regions of "intermediate material", which eases the interpretation of the results.

According to Sigmund [14], the "soft-kill" BESO approach, by Huang et al. is capable of efficiently solving topology optimization problems with discrete design variables as this approach is inspired by continuous methods and makes use of gradient information (sensitivity approach). Therefore, Sigmund et al. [36] claim that this approach should not be categorized as a separate approach but rather as a discrete update version of the standard SIMP scheme. Due to their simplicity, both in theory and application, ESO and its further developments have gained great popularity since their primary introduction and have been the subject of further extensive studies [53].

Most of the early work on ESO/BESO neglected important numerical problems in topology optimization such as dependency on the discretization of the structure (checker-board and mesh-dependency), computational efficiency (convergence), and so on [34]. Mesh-dependency is in fact a common issue for almost all topology optimization methods, not only to BESO [15]. Therefore, this will be discussed further in the next section.

2.6. Mathematical and Numerical Problems of Topology Optimization

As mentioned before, discrete valued topology optimization problem is ill-posed. Numerically, this deficiency manifests itself as dependency of the resulting optimized topology on the discretization, i.e., mesh-dependency. In order to obtain a well-posed problem, a regularization of the problem formulation is required. This can be achieved, for instance, with *relaxation* (e.g., *Homogenization Approach*, *Density Approaches*), already discussed in Section 2.5.2. Although density-based topology optimization is a relatively mature algorithm, several inherent numerical instabilities still exist. In this section, approaches for making the discrete-valued design problem well-posed by including restrictions against formation of microstructures, are explained. These restrictions are considered directly in the problem formulation. Furthermore, methods to prevent the formation of checkerboard like patterns are discussed.

2.6.1. Mesh-Dependency

Mesh dependency refers to the phenomenon that performing the same optimization on a finer mesh yields a qualitatively different solution. So, while refining the mesh-size, optimal topology results can change correspondingly. If the mesh is fine enough such that a global optimum can be attained, further refining the mesh should lead to a better finite element modeling of the same optimal structure as well as a better and smoother description of the boundaries. Mesh-refinement should not lead to a qualitatively different structure. An illustration of the mesh-dependency effect can be seen in Figure 2.20.

Comparing the design proposal for a discretization by 800 elements (Figure 2.20(a)) with a discretization of 1600 elements (Figure 2.20(b)) reveals that the finer mesh results in a qualitatively different structure as more holes appear in the "optimal solution".

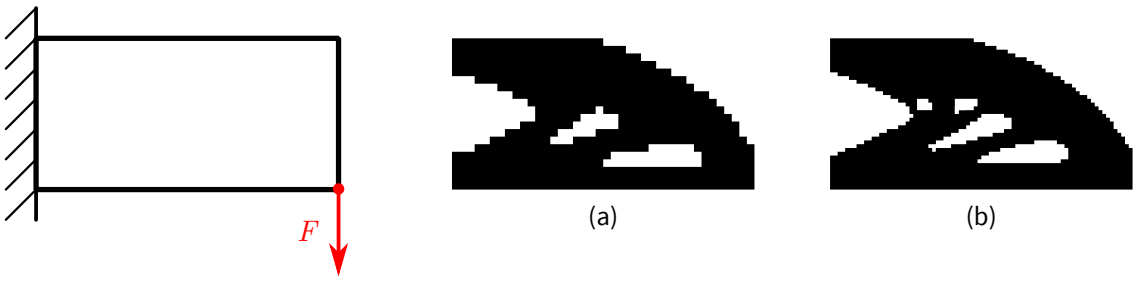

Figure 2.20.: Example of mesh-dependency

According to Bendsøe et al. [1], one way to efficiently achieve mesh independent designs is to reduce the original feasible design set to a sufficiently compact subset by adding some local or global restrictions on the variation of density to the design problem. Therefore, for density based approaches like the SIMP method, the design space is restricted such as to remove the possibility of rapid oscillations in the density of material in the structure. The aim of all these methods is that finer meshes shall offer improved solutions without altering the design, which is regarded as convergent solutions with respect to mesh refinement [1].

According to Sigmund et al. [15] *restriction methods*, to prevent mesh-dependency, can be roughly divided into the following categories:

- *Constraint Methods* such as, *Perimeter Control* [63], *Global Gradient Control* [64] and *Local Gradient Control* [65].
- *Mesh-independent filtering methods* such as, *Density Filters* [66] and *Sensitivity Filters* [67, 15]
- *Alternative methods* like, for instance, *wavelet parametrizations* [68], *phase-field* approaches [69] and *level-set* approaches [70].

In general, constraint methods may be difficult to use because they require a problem and geometry dependent choice and tuning of the respective constraint value. Mesh-independent filtering methods are probably the most popular ones due to their ease of implementation and their efficiency both for preventing mesh-dependency (density filtering and sensitivity filtering) and formation of checkerboards (sensitivity filtering). Alternative methods, according to Sigmund [71], are mostly still in their infancy and have yet to be applied to advanced problems with many constraints.

Perimeter Control

The method of *Perimeter Control* is also referred to as a global control method. The perimeter is the sum of the lengths (2-dimensional structures) or areas (3-dimensional structures) of all inner and outer boundaries of the structure. Designs with fewer, larger holes have lower perimeter measures than designs of equal volume with more numerous smaller holes, see Figure 2.21.

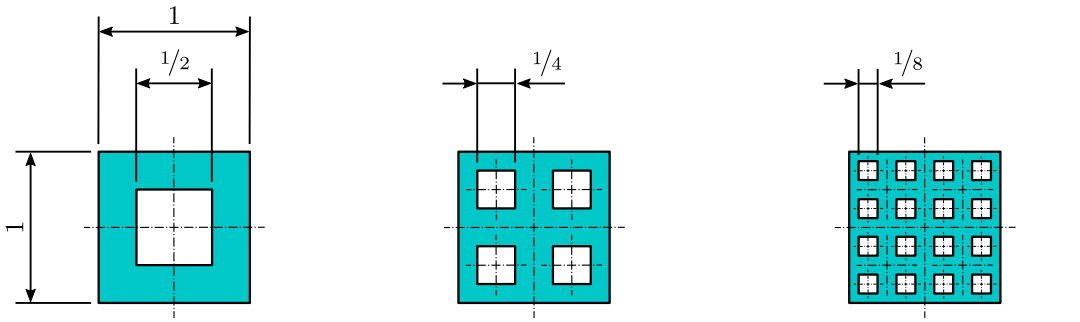

Figure 2.21.: 2-dimensional example of how smaller holes increase the perimeter P for a fixed volume V

Such designs, which are also referred to as chattering designs in literature, are characterized by unbounded perimeter measures [38]. Therefore, by defining an upper bound constraint on the perimeter, such chattering designs can be avoided. Furthermore, according to Sigmund et al. [15], a bound on the perimeter controls the number and sizes of holes in the macroscopic design without otherwise restricting the shape or layout of the holes. By incorporating perimeter control, one additional constraint, namely on the perimeter, has to be considered. However, the method is not capable of controlling the minimum member size of the emerging features in the design domain. Therefore, perimeter control allows the formation of locally very thin bars (even if in limited numbers).

According to Sigmund et al. [15], to determine the bound of the perimeter constraint for new design problems is a serious problem. The value of the perimeter constraint must be determined by experiments since there is no direct relation between local scale in the structure and the perimeter bound. If the bound is too large, the constraint remains inactive, i.e., it

has no regularizing effect. Choosing the "correct" perimeter constraint is particularly tricky for three-dimensional topology optimization problems as reported by Fernandes et al. [72]. However, Ambrosio et al. [63] proved that the existence of solutions to the perimeter controlled topology optimization is assured for both the discrete 0-1 setting and the interpolated version using SIMP.

Gradient Control

Instead of restricting the perimeter, one can also define a bound on the gradient of the density function ρ. Gradient control schemes can be categorized as global or local. With local gradient control, also referred to as strict gradient control, the key idea is to constrain the local gradient of element densities by imposing pointwise bounds on the derivatives of the function ρ with respect to the design variables:

$$\left| \frac{\partial \rho}{\partial x_i} \right| \leq G \tag{2.34}$$

Therefore, the local gradient scheme defines a local length scale under which structural variation is filtered out. At the same time, this local length scale corresponds to a lower limit on the width of the thinnest features of a feasible design. This is, of course, of great importance for manufacturing considerations.

However, the local gradient constraint adds a high number of extra constraints (in order of the number of finite elements after discretization) to the design problem, since it needs to be derived for each element. Therefore, this method is considered as being computationally expensive and too slow for practical design [1]. Although advanced large scale mathematical programming algorithms can handle a large number of constraints, practice has shown that the implementation of the constraints can lead to convergence problems [73].

Gradient constraints presuppose that the density function ρ is sufficiently smooth and defined for intermediate values. This is the case, for instance, when the SIMP approach is applied to the ill-posed topology optimization problem. Unlike the perimeter control, this method makes no sense for the discrete-valued 0-1 setting of topology optimization with discrete variables, i.e., ESO methods.

Filtering Techniques

Methods of perimeter control and gradient control impose explicit limitations on the design variables and therefore have to be considered as constraints in the optimization formulation. A possibility to circumvent additional constraints to the optimization problem are so-called filtering techniques which can be categorized as *Filtering of Densities* and *Filtering of Sensitivities*.

In the *Filtering of Densities* approach, each element density is redefined as a weighted average of the densities in a mesh-independent neighborhood of the element. The neighborhood of an element e, here referred to as Ω_e, is generally specified by elements that have centers within a given filter radius r_{min} of the center of element e:

$$\Omega_e = \{f \,|\, ||x_f - x_e|| \leq r_{\text{min}}\}, \tag{2.35}$$

where x_f is the spatial center location of element f.
Therefore, the modified element density $\tilde{\rho}_e$ is a function of the neighboring element densities (design variables) $\rho_{f \in \Omega_e}$:

$$\tilde{\rho}_e = \tilde{\rho}_e \left(\rho_{f \in \Omega_e}\right). \tag{2.36}$$

According to Bendsøe et al. [1], typical weighting functions for density filtering are linearly decaying functions or the Gaussian distribution function. The modified (filtered) densities are then used to determine the stiffness matrix, e.g., for the SIMP model:

$$E_{ijkl}\left(x\right) = \tilde{\rho}_e\left(x\right)^p E^0_{ijkl}. \tag{2.37}$$

In the *Filtering of Sensitivities* approach, the main idea is to base the design updates on filtered sensitivities instead of the sensitivities according to Equation 2.31 . Thus, after the finite element problem is solved, the sensitivities are calculated and subsequently modified. The modified (filtered) design sensitivity of each element is then determined as a linear weighted average of the sensitivities of elements within a predefined distance r_{min} of the corresponding element. As the weighting function is defined as a linearly decaying function, the closer the elements, the larger the weight factor. The successful deployment of this approach for evolutionary ESO/BESO methods has been proven for instance by Li et al. [74] and Huang et al. [75]. As the method of sensitivity filtering is used in the framework of this thesis, this approach is discussed in detail in Section 3.1.2.

The big advantage of using filtering schemes is that they do not require extra constraints added to the optimization problem and that they are easy to implement. According to Sigmund et al. [15], the likely reason for the filtering of sensitivities to be so effective and favorable, is that it enhances the convergence to global optima, especially for minimum compliance problems. However, it has to be mentioned that the filter scheme is purely heuristic.

2.6.2. Checkerboard Patterns

Checkerboards refer to the problem of obtaining regions of alternating solid and void elements ordered in a checkerboard like fashion. The checkerboard problem is illustrated in Figure 2.22. Diaz et al. [76] shows, that the checkerboard configuration has artificially high stiffness compared to the stiffness of uniformly distributed material. The authors conclude,

that the main cause for the formation of checkerboard patterns lies in poor numerical modeling of the structure, especially when low-order finite elements are used. Sigmund et al. [15] confirms that the use of linear shape function finite elements gives rise to the formation of checkerboard patterns. Checkerboards are numerical "artifacts" that lead to difficulties in interpreting and manufacturing the optimized design proposals. Therefore, it is highly desirable to suppress the formation of checkerboard patterns in topology optimization of continuum structures.

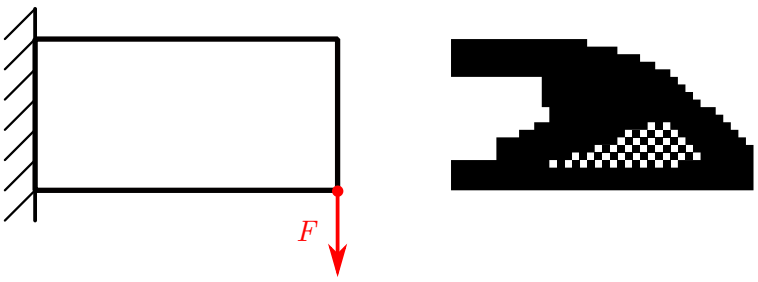

Figure 2.22.: Example of checkerboards

The restriction methods, mentioned in Section 2.6.1, also have the effect of reducing or removing checkerboards. By enforcing a constraint (directly or indirectly) on the variation of density, checkerboard patterns with a strong oscillating density from element to element are suppressed. Further approaches to circumvent the formation of checkerboards are for instance the usage of higher-order finite elements, smoothing, patch design, and the *NoHinge* constraint.

For instance, Sigmund et al. [15] suggest to use higher order elements for the modeling of the structure so that the stiffness properties of checkerboard patterns can be accurately calculated and checkerboards are avoided. The author states that checkerboards can be prevented when using 8 or 9-node quadrilaterals for the displacement in combination with an element wise constant discretization of density. However, as these elements have more degrees of freedom per material design variable (compared to four-node element meshes), they are seldom used in topology optimization [76]. Increasing the degrees of freedom enhances the accuracy of the numerical analyses but at the same time increases computational cost. Furthermore, Diaz et al. [76] proved that the application of elements of higher order often does not necessarily yield a checkerboard-free result when using a high value of penalization factor p with the SIMP approach.

Many commercial post-processing codes use smoothing by image processing of the output images of the "optimal solution" [15]. However, this method ignores the underlying problem and therefore should be avoided.

2.7. Material Optimization

Over the past two decades, the demand for lighter and stronger structures, supported by remarkable advancements in manufacturing techniques, has resulted in an increasing use of advanced materials, such as composite materials. The development and application of composites is mainly driven by the aerospace industry but at the same time is expanding to other industrial sectors as well. This includes structural applications for cars, trains and ships as well as wind turbine blades and civil engineering applications like bridge structures.

As the response of structures depends on the materials they are built of, a central aspect is the optimal use of material. Therefore, it has been natural to extend the optimization of structures to the material choice and the consideration of designing the material properties [1]. However, the corresponding design problem, the so-called material optimization (i.e., with composite materials), is quite complex and an important area in its own right.

In terms of weight reduction, the trend nowadays is to replace highly loaded and massive structures with composite structures. The concept and application of composite materials can be traced back to ancient history [1]. The purpose of combining two or more constituents to form a composite is to gain a new material that has better overall properties compared to the properties of its constituents. The overall properties are influenced by the constituent materials themselves, their distribution, but also the interaction between them. In fact, composite structures can be tailored by choosing, among other relevant factors, the individual constituent materials, their volume fractions, and their orientations.

Fiber-reinforced composite materials, also referred to as fiber-reinforced polymers (FRPs), are particularly competitive for light-weight design due to their high stiffness-to-mass and stiffness-to-strength ratio, compared for example to metallic materials. FRPs are composed of fibers of various forms, with superior properties in fiber direction, embedded in a matrix. The fibers constitute the most important component as they provide the superior properties of a composite. The matrix groups the fibers together, puts them in fixed positions and protects them from environmental effects such as oxidation, corrosion, and so on. From a mechanical point of view the matrix provides a load transferring mechanism for the fibers.

The directional nature of fiber-reinforced composites provides the ability to construct a material which can meet specific loads and/or stiffness requirements without wasting material by providing stiffness and strength where they are not needed. This anisotropic behavior of composites, while allowing the engineer to tailor the material more closely to the design requirements, is a big challenge in product development because the lightweight potential can only be fully exploited if the fibers are arranged properly. Even small deviations from the ideal fiber orientation can result in dramatically lowered strength and stiffness characteristics of the composite part because the matrix (with significantly lower stiffness and strength values) is increasingly loaded. Therefore, selecting proper material orientations for the application is of utmost importance.

A polar plot is a useful tool to visualize and quantify the orientation dependent characteristics of composites – namely showing the variation of a specific material characteristic (e.g., Young's Modulus, Shear Modulus, ...) with the loading direction. Figure 2.23 shows a polar plot for the elastic modulus E_1 of a carbon fiber reinforced polymer (AS4/3501-6 epoxy) with a fiber volume content of $\varphi_f = 60\%$ for quasi-isotropic, unidirectional, and cross-ply material behavior under various loading directions.

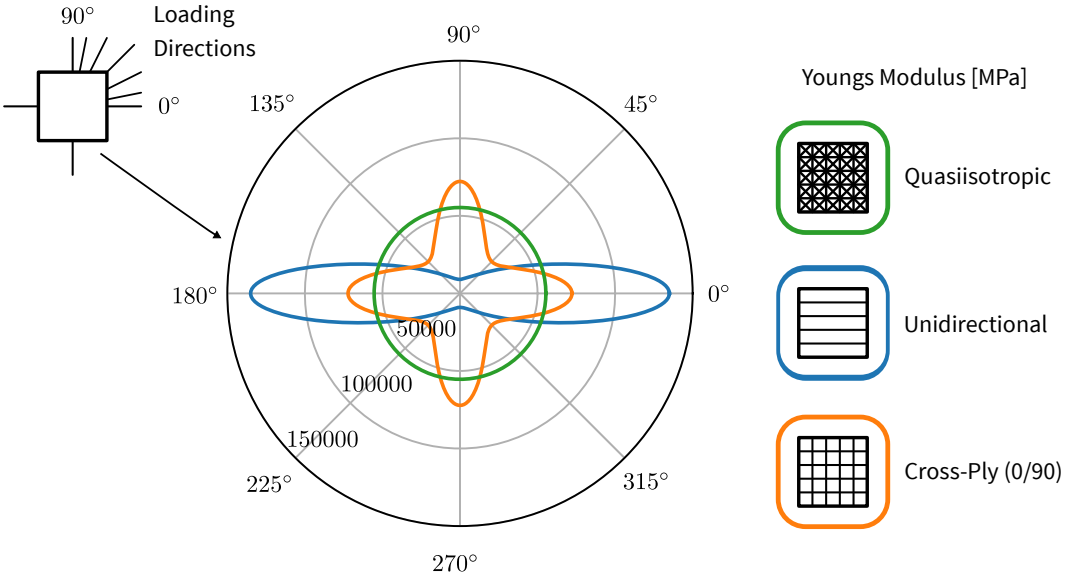

Figure 2.23.: Polar diagram for the variation of the elastic modulus E_1 with respect to the loading direction

To attain the best results when designing materials with improved properties, adequate optimization methods have to be implemented to find practical optimal solutions that satisfy a given set of design constraints. For instance, significant mass savings can be achieved by so-called "black-metal" solutions. A black metal solution is a composite structure whose shape is derived from the former metallic structure (e.g., determined by topology optimization). However, the black metal solution is not optimal because it is not fully harnessing the benefits of composite materials, i.e., that they are strong along the fiber direction. In order to obtain an optimal solution, structure and material must be designed simultaneously to gain load-tailored composite parts. This implies, that there is no a priori on the initial topology and unlike e.g., the black metal design, there are no simplifying assumptions on the material behavior. In present design practice, the optimization of structure and material are inherently decoupled and yet the performance and quality of the designs are inevitably linked across the structure and material scales. Hence, a lot of effort has been put on developing a general continuum based structural optimization method, especially for simultaneous structural (topology) and material optimization [1].

Early topology optimizations based on the homogenization method [39] already consider composite structures with continuously varying material orientation and material distribution. As mentioned above, a decisive factor for effective lightweight design is the fiber ori-

entation according to load path trajectories [77]. Various methods exist to optimize the orientation of orthotropic materials ranging from heuristic-based methods like the *Computer Aided Internal Optimization* [78] to methods of *Continuous Fiber Angle Optimization* [6] and *Load Path Computation* [79]. Existing discrete approaches for simultaneous topology and material optimization, e.g., *Discrete Material Optimization* focus on directly finding a physically meaningful solution based on a limited number of predefined candidate angles and/or candidate materials, with the risk of local optimum solutions.

However, other approaches which avoid the local optimum problem by relaxation of the design space (*Free Material Optimization*) face the problem that the optimization may yield a theoretically optimal structure but not always a physically feasible structure, especially for more complex structures or loading scenarios
The approaches of *Computer Aided Internal Optimization* (CAIO), *Discrete Material Optimization* (DMO), *Continuous Fiber Angle Optimization* (CFAO) as well as *Free Material Optimization* (FMO) are described in more detail in the following sub-sections.

2.7.1. Computer Aided Internal Optimization (CAIO)

An example of a stress-based method for orientation optimization of orthotropic materials is the *Computer Aided Internal Optimization* (CAIO) by Mattheck [78, 80, 81]. This method determines an optimized fiber layout for parts made of FRPs, starting from an initial shell geometry and a given load case. CAIO copies the principle of internal optimization of trees, i.e., the biological fiber orientation, in order to minimize shear stresses within orthotropic or multilayer composite material structures. The aim of this heuristic-based algorithm is to obtain lightweight structures with high stiffness and high strength. The reduction of failure-critical shear stresses is achieved by aligning fiber orientations with principal normal stress trajectories. For this purpose, the principal normal stress eigenvector with the largest eigenvalue is used. From this new state of fiber orientation, a new stress state emerges, determined by a finite element analysis. This new stress state is then used as input for the next CAIO iteration until, for instance, the shear stresses are "sufficiently" reduced [78]. An overview of the CAIO method is illustrated in Figure 2.24. According to Reuschel et al. [81], this method of fiber orientation optimization naturally depends on a sufficiently fine mesh to allow proper local adaption of orientation.

Several mathematical studies, for instance by Gea et al. [82], prove the efficiency of the method described above to obtain stiff structures. However, most real-world problems exhibit complicated geometries and loadcases, leading to multiaxial stress states. As mentioned above, the orientation of the largest absolute eigenvalue, i.e., the corresponding eigenvector, is chosen for orienting the fibers. This is referred to as the ’maximum absolute’ method.

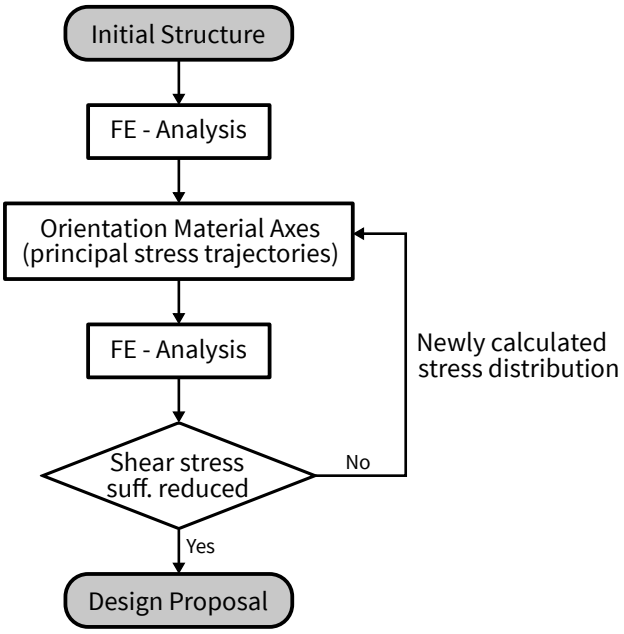

Figure 2.24.: Flowchart of the CAIO method adapted from Mattheck et al. [78]

For stress states that do not provide a single largest principal normal stress but, for instance, two (nearly) equal principal normal stresses, aligning fiber orientations with principal normal stress trajectories is not always unambiguous, as illustrated in Figure 2.25. This can lead to chaotic designs with alternating fiber directions [83].

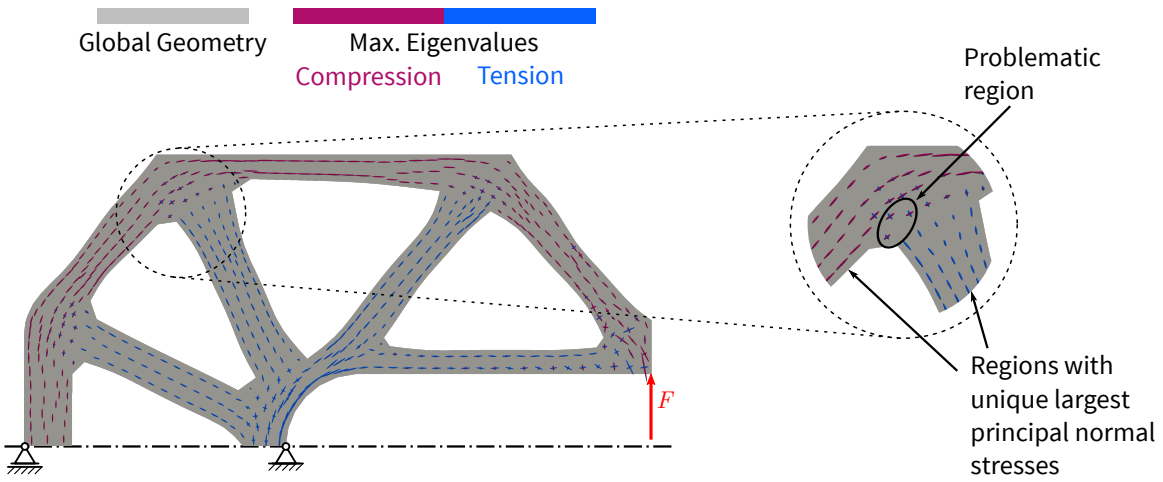

Figure 2.25.: Multiaxial stress states leading to ambiguous fiber trajectories

In 2014 Klein et al. [84] proposed a method for computing the resulting fiber orientation for multiple loadcases, referred to as 'proximity search' method. The aim of this method is to avoid chaotic, alternating fiber directions in regions with ambiguous (isotropic) stress states. Whereas the 'maximum absolute' method represents the mathematically optimal solution, the 'proximity search' method intentionally deviates from the optimal solution with the focus on improving the design in terms of manufacturability. First, every element is checked for an ambiguous (isotropic) stress state, i.e., if the principal normal stresses are (nearly) equal.

Voelkl et al. [83] introduce an equation, a so-called isotropy criterion, to detect this state as

$$I_{iso-crit} = \frac{|\sigma_I|}{|\sigma_{II}|} \in]1 - r_{iso}, 1 + r_{iso}[\tag{2.38}$$

where r_{iso} defines the range of the quotient of two principal normal stresses in which an element's stress state is considered ambiguous. If the criterion, defined in Equation 2.38, is true for an element's stress state, the neighboring elements are checked for their stress states as well. If there is an element, in the direct neighborhood, with an unambiguous (non-isotropic) stress state, the fiber orientation of the current element is set to the neighbor elements fiber orientation, see Figure 2.26. If all neighbor elements exhibit an ambiguous (isotropic) stress state as well, the neighborhood of the neighboring elements are checked as well until an element with unambiguous stress state is found. Again, the fiber orientation of the current element is adapted accordingly.

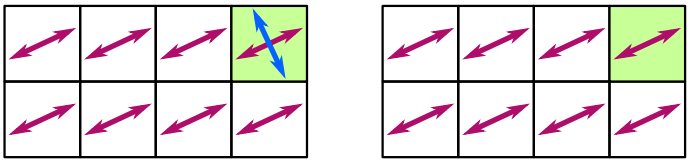

Figure 2.26.: Adaption of orientation for elements with ambiguous stress state using the 'proximity search' method. (a) Element with ambiguous stress state, (b) Adaption of the fiber orientation of the current element according to the neighbor elements fiber orientation

The original CAIO introduced above is useful in giving an idea of force flow within a given geometry and thus providing trajectories along which fibers should be placed. However, it is only capable of handling one single layer, not taking the advantage of great lightweight capabilities when using laminates with several different layers. Therefore, Klein et al. [85] propose a modification of the original CAIO for multi-layer capabilities, the so-called *Multi-Layer Computer Aided Internal Optimization* (ML-CAIO). The ML-CAIO is used to compute the fiber orientations and number of layers which are needed to transfer the loads within the structure. The results of the ML-CAIO are then used to determine areas of comparable fiber orientations (defining a so-called "patch structure"), to define the optimal stacking sequence and compute the layer thicknesses. An overview over the design approach using ML-CAIO is illustrated in Figure 2.27. According to Klein et al. [85], it is very important to point out that in general the results of the proposed approach is not a laminate structure that is completely ready to manufacture.

In the ML-CAIO approach at first a FEM model with shell elements (and all necessary boundary conditions) is created. Each shell element in the FEM model is a so-called layered shell element. This means that each shell element consists of several layers which are modeled

with the help of through thickness integration points. The initial number of layers is arbitrary but constant for all shell elements.

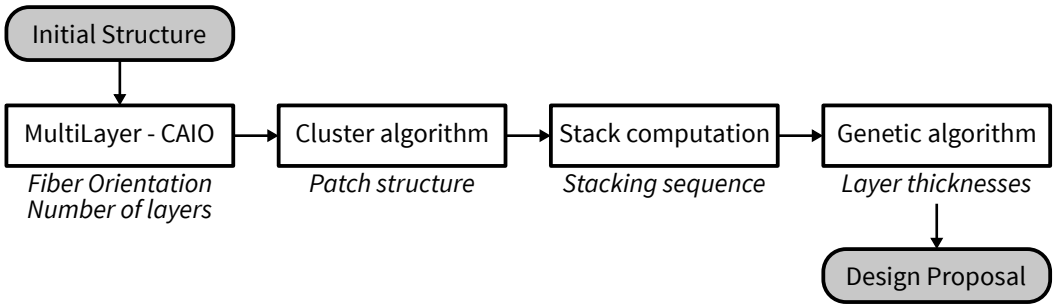

Figure 2.27.: Overview of the computational approach on the optimal design of composite parts using ML-CAIO [85]

Isotropic material behavior is assumed for the first FEM analysis. The procedure of ML-CAIO is illustrated in Figure 2.28. To optimize the fiber angles in each layer of every element, the stress tensor is computed for every element layer via FEM analysis. If there is more than one single loadcase, all the stress states which occur for the part have to be determined (see Figure 2.28 (a)). The stress states, resulting from each loadcase, are collected, as illustrated in Figure 2.28 (b). The collected stress states are the basis for determining the layer number and the fiber orientations. Whenever there is a significant principal stress, a layer with a corresponding fiber orientation is needed to bear the load. Figure 2.28 (b) illustrates the computation procedure for layer 1 and two different loadcases (*Loadcase 1*, *Loadcase 2*). The result of the FEM analysis for layer 1 are the principal stresses $\sigma_{11}^{\mathrm{LC}\,1}$ and $\sigma_{22}^{\mathrm{LC}\,1}$ (for *Loadcase 1*) as well as $\sigma_{11}^{\mathrm{LC}\,2}$ and $\sigma_{22}^{\mathrm{LC}\,2}$ (for *Loadcase 2*). At first, principal stresses with a small absolute value (in this case $\sigma_{22}^{\mathrm{LC}\,1}$ and $\sigma_{22}^{\mathrm{LC}\,2}$) are deleted because it is assumed that these stresses do not need an "own" layer. Next, the directions of the remaining principal stresses ($\sigma_{11}^{\mathrm{LC}\,1}$ and $\sigma_{11}^{\mathrm{LC}\,2}$) are compared. If there is no significant difference between the orientations, the principal directions (eigenvectors) are summed up. In the example depicted in Figure 2.28 (b), the difference between the principal directions of *Loadcase 1* and *Loadcase 2* is significant, so both loadcases need an own layer. Subsequently, layer 1 is extended to two different layers with the respective angles $\alpha = 45^{\mathrm{o}}$ (for $\sigma_{11}^{\mathrm{LC}\,1}$) and $\beta = 15^{\mathrm{o}}$ (for $\sigma_{11}^{\mathrm{LC}\,2}$). This extension of the initial layers to multiple layers may lead to multiple layers with equal fiber orientation for instance for layer 1 and layer 5 in Figure 2.28 (b). Therefore, all "double" layers are deleted such that for each fiber orientation only one layer is remaining, see Figure 2.28 (c). The modified FEM model is solved again and the fiber orientations of the new model are compared to the preceding ones. If the difference is significant, a new iteration starts, otherwise the algorithm stops. By iterating like in the original CAIO method for single-layer optimization (first iteration isotropic material, then anisotropic material), the optimized solution is found.

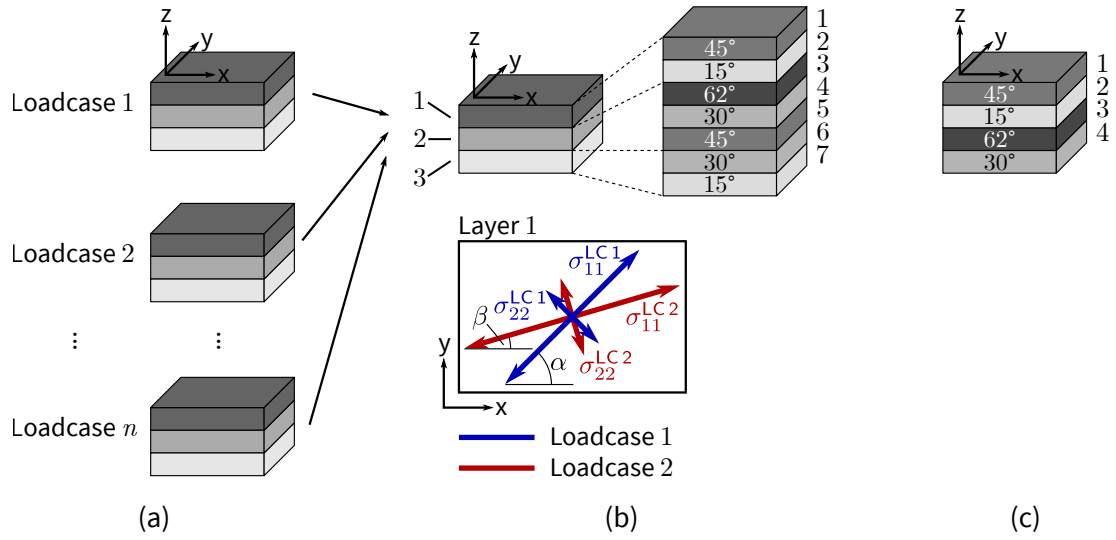

Figure 2.28.: Computation of fiber orientations and layer number according to ML-CAIO [85]

2.7.2. Discrete Material Optimization (DMO)

According to Lund [5], the *Discrete Material Optimization* (DMO) can be used to solve the orientation problem of orthotropic materials and the material selection problem as well as problems involving both. The key-idea of DMO is adopted from topology optimization. However, instead of selecting "solid" or "void" properties for each element of the finite element model (0-1 design), a fixed number of "candidate materials" is available for each element. The scope of DMO is to choose the best combination out of these predefined "candidate materials". In the context of orientation optimization, "candidate materials" simply refers to the same material oriented at various angles in space (fiber orientations), for instance FRP materials oriented at predefined angles (e.g., $0\,^{\circ}$, $+45\,^{\circ}$, $-45\,^{\circ}$, $90\,^{\circ}$). However, "candidate materials" might as well be polymer foams, steel, aluminum, or any other material at any orientation.

The method of discrete material optimization relies on ideas from multi-phase topology optimization where the total material stiffness is computed as a weighted sum of the "candidate materials" [86]. Similar to topology optimization, the parametrization of the DMO is invoked at the finite element level. The general methodology is as follows: the element constitutive matrix $\boldsymbol{E}^e$ is expressed as a weighted sum of the predefined "candidate materials".

$$\boldsymbol{E}^e = \sum_{i=1}^{n} w_i \boldsymbol{E}_i = w_1 \boldsymbol{E}_1 + w_2 \boldsymbol{E}_2 + ... + w_n \boldsymbol{E}_n, \quad 0 \leq w_i \leq 1. \tag{2.39}$$

Each "candidate material" is characterized by a constitutive matrix $\boldsymbol{E}_i$. n denotes the total number of predefined plausible material configurations, i.e., "candidate materials", per element. The number of "candidate materials" per element, n, is also the number of elemental design variables. Therefore, if N is the number of elements, the total number of design variables for a single layered structure is $N \cdot n$. Note, that the "classical topology optimization" formulation uses one design variable per element and therefore can be obtained by setting

$n = 1$ in Equation 2.39. As the constitutive matrices $\boldsymbol{E}_i$ may represent any type of "candidate material", this paramterization also allows for simultaneous optimization of fiber orientation and material choice. When working with anisotropic materials, the orientation can be implicitly included in the problem, i.e., the constitutive matrix is a function of the spatial orientation θ_i of the fibers (fiber angle). Therefore, in this case, the constitutive tensor of each individual "candidate material" is defined by an anisotropic base material rotated by a set of fixed angles as $\boldsymbol{E}_i = \boldsymbol{E}(\theta_i)$. In Equation 2.39, w_i are the so-called weight factors of the "candidate materials". The weight factors w_i are limited to values between 0 and 1 as a negative contribution $(w_i < 1)$ is physically meaningless and no matrix can contribute more than the physical material properties $(w_i > 1)$. In general it is important to define a "fair" starting guess so no materials are favored a priori. Therefore, the initial values of the weight factor (which may in principle be any set of numbers between 0 and 1) should be chosen such that the weighting is uniform.

The single most important requirement for the DMO method is that every element must have one single weight factor of $w_i = 1$ whereas all other weight factors have a value of $w_i = 0$, i.e., $\sum_i w_i = 1,\ i = 1, ..., n$ [86]. In other words, the design problem is to choose the best of the "candidate materials" by choosing the best of the constitutive matrices $\boldsymbol{E}_i$. Therefore, the performance of DMO relies heavily on the ability of the optimizer to push the weight factors to the limit values $w_i = 0$ and $w_i = 1$. Several formulations have been proposed for the formulation of the weight factor. For instance, for a single layered structure, the simplest choice of weight function would be to use the SIMP method with $w_i = x_i^p$ where x_i denotes the design variable. Therefore, Equation 2.39 can be written as:

$$\boldsymbol{E}^e = \sum_{i=1}^{n} (x_i)^p \boldsymbol{E}_i = (x_1)^p \boldsymbol{E}_1 + (x_2)^p \boldsymbol{E}_2 + ... + (x_n)^p \boldsymbol{E}_n, \quad 0 \leq x_i \leq 1. \tag{2.40}$$

The penalization factor p penalizes intermediate values of x_i, to push the design variables towards 0 and 1. However, in this formulation, each design variable scales only one constitutive matrix and has no influence on any of the other constitutive matrices and therefore is considered as inefficient [87]. Therefore, Sigmund [87] proposes the following formulation for two distinct materials $(\boldsymbol{E}_1, \boldsymbol{E}_2)$:

$$\boldsymbol{E}^e = (x_0)^p \left[(1 - (x_1)^p) \boldsymbol{E}_1 + (x_1)^p \boldsymbol{E}_2 \right], \quad 0 \leq x_i \leq 1. \tag{2.41}$$

The difference between Equation 2.41 and Equation 2.40 is the term $(1 - (x_1)^p)$ which links a single design variable to more than one constitutive matrix. Therefore, adding weight for one "candidate material" automatically reduces the weight for another "candidate material", thus helping to push the weights towards 0 or 1. In the formulation in Equation 2.41 the design variable x_0 scales the entire contribution to $\boldsymbol{E}^e$. Therefore, this formulation encompasses simultaneous topology optimization (through x_0) and multiple material optimization (through x_1).

The formulation can also be extended to include any number of "candidate materials" as shown by Stegmann et al. [86]:

$$\boldsymbol{E}^e = \sum_{i=1}^{n} w_i \boldsymbol{E}_i = \sum_{i=1}^{n} \left[(x_i)^p \prod_{j=1}^{n} \left[1 - (x_{j \neq i})^p \right] \right] \boldsymbol{E}_i. \tag{2.42}$$

Again, the term $(1 - (x_{j \neq i})^p)$ is included to drive the design towards a 0/1 design as an increase in x_i automatically involves a decrease in all other weights.

For multi-layered structures Equation 2.42 can be used directly [86]. The constitutive matrix $\boldsymbol{E}^l$ for a given layer l in a given element can thus be determined by

$$\boldsymbol{E}^l = \sum_{i=1}^{n^l} w_i \boldsymbol{E}_i = \sum_{i=1}^{n^l} \left[(x_i)^p \prod_{j=1}^{n^l} \left[1 - (x_{j \neq i})^p \right] \right] \boldsymbol{E}_i, \tag{2.43}$$

where n^l is the number of "candidate materials" for the layer. Consequently, for multi-layered elements, the number of element design variables (n) is the sum of the number of design variables per layer n_k^l over all layers N^l of an element

$$n = \sum_{k=1}^{N^l} n_k^l. \tag{2.44}$$

Again, the total number of design variables for the whole structure is $N \cdot n$ where N is the total number of elements. For multi-layered structures, this implies a significant increase in the total number of design variables.

The problem of the high number of design variables associated with DMO can be circumvented by using so-called patch design variables [86]. Patch design variables denotes merging several design variables from different elements and/or layers into a single variable. Patch design variables are inspired by the manufacturing process of composite laminates where fiber mats covering larger areas are often used. For instance, a single patch design variable can govern the fiber orientation of a layer (fiber mat), even though it covers several elements. Such patches can also be used to enforce laminate symmetry (to avoid unwanted coupling effects) by assigning the same design variable to the opposite layer. However, one major drawback is that the layout of these patches is left up to the engineer a priori. Consequently, the final result will be dependent on the engineers insight and the initial patch layout.

2.7.3. Continuous Fiber Angle Optimization (CFAO)

The restriction to a prescribed set of "candidate orientations" of *Discrete Material Optimization* is resolved in the *Continuous Fiber Angle Optimization* (CFAO). In CFAO additional (local) design variables are included for a continuous rotation of an anisotropic base material.

Therefore, the design variables are the local orientations (rotation angle of the material), namely the continuous parameters θ_i, relative to the reference coordinate system. The fiber angle θ_i can be oriented at any angle in the interval $-90\,^{\circ} \leq \theta_i \leq +90\,^{\circ}$. Figure 2.29 illustrates the classical concept of this local orientation optimization in a finite element framework where θ_i is the fiber angle which can be adapted element wise.

The continuous parametrization of the fiber angle provides flexibility in the solution. However, the major difficulty of this continuous parametrization is that the global design space becomes highly non-convex [1]. Figure 2.30 shows an example of such a non-convex design space where the objective is to minimize the compliance based on the two design variables (local orientations) θ_1 and θ_2. The problem of finding a global optimum becomes even more complex as the scale of the problem grows. Therefore, design proposals obtained with CFAO will often be sub-optimal (local optimum) results. Nevertheless, it is still a valuable design tool as it can provide engineers with a significant performance increase [1].

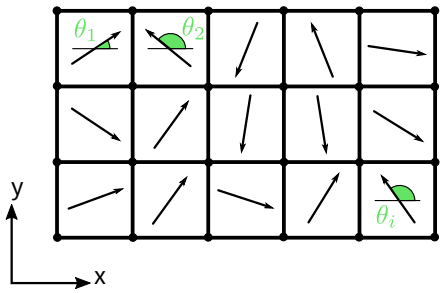

Figure 2.29.: Concept of continuous fiber angle optimization in a finite element framework

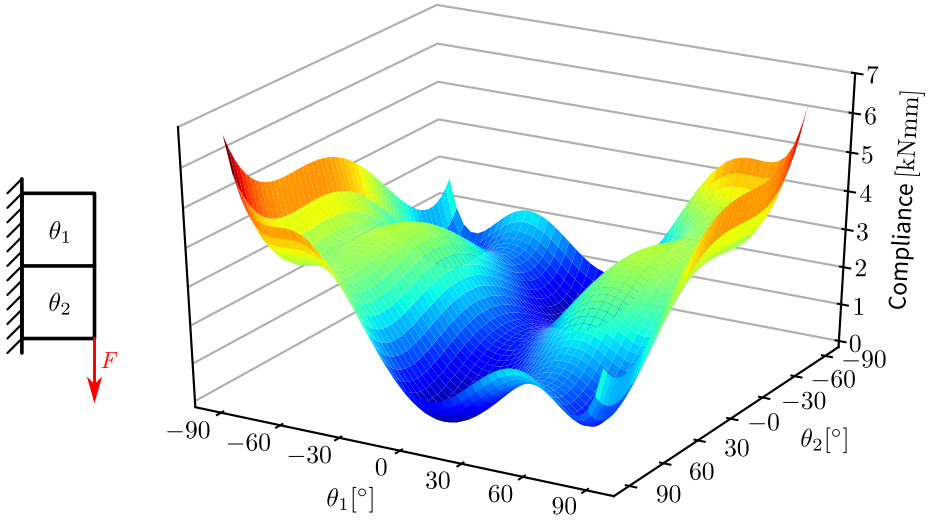

Figure 2.30.: Variation of the compliance of a cantilever beam discretized with two elements with respect to the local orientation variables θ_1 and θ_2

Like for the standard topology optimization, several methods have already been proposed to circumvent the problem of local solutions with CFAO. For instance, Pedersen [88] proposed an optimality criteria method to optimize 2D continua, beams, and plates. Parametrization methods where the aim is to change the parametrization to obtain a convex design space have been successfully applied for the orientation optimization of plates and shells by Foldager et al. [89] and for plates by Miki et al. [90]. Additionally, regarding manufacturability it is desirable to control the smoothness of material orientation pathways within CFAO approaches. For instance, Nomura et al. [91] proposes a specialized parametrization and projection scheme so that the designer can control the complexity of the orientation angles.

2.7.4. Free Material Optimization (FMO)

The least restrictive approach to material optimization is the so-called *Free Material Optimization* (FMO). *Free Material Optimization* is a branch of structural optimization that gains more and more attention in recent years leading to a wide range of models, methods and theories [1]. Whereas DMO is based on determining the best discrete material selection, for instance for laminated composite structures, FMO extends this discrete set of admissible materials, avoiding any restriction to pre-existing materials and searching for more general material properties.

The main difference to other methods of material optimization is that the design parametrization of *Free Material Optimization* allows the entire elastic stiffness tensor to vary freely at each point of the design domain. The only requirements imposed on the stiffness tensor are necessary conditions that the stiffness tensor has to be symmetric and positive semidefinite. However, this does not imply that the material is thermodynamically consistent of physically reasonable. FMO thus can be used to obtain conceptual optimal structures characterized by optimal material distribution and optimal material properties. This is also the reason why FMO is considered as the "ultimate" generalization of the structural optimization problem.

FMO uses certain invariants of the stiffness tensor as objective. According to Stingl et al. [92] a frequently used measure of the stiffness of the material tensor is its trace. Pointwise stiffness restrictions are used to define the set of admissible materials. This is done in order to avoid overly stiff materials $(\mathrm{Tr}\,(E) \leq \bar{\rho})$ and to define a lower limit on the stiffness $\left(\mathrm{Tr}\,(E) \geq \underline{\rho} \geq 0\right)$ where $\overline{\rho}$ and $\underline{\rho}$ are finite real numbers [92]. These constraints on the local stiffnesses do not depend on coordinate systems due to the invariance property of the trace under orthogonal transformations.

One of the main difficulties concerns the nature and size of FMO problems. As the design variables are the entries of the symmetric stiffness tensor which are allowed to vary pointwise throughout the structure, the number of independent variables in each stiffness tensor is 6 for two-dimensional and 21 for three-dimensional problems. Additionally, according to

Kočvara et al. [7], it is important to work with relatively fine finite element discretizations to obtain essentially predictive solutions which, in turn, leads to large-scale problems.

According to [7] the results of FMO, within the assumption of a locally unconstrained configuration of material, can be regarded as ultimately best structure among other possible elastic continua in terms of optimal material distribution and optimal local material properties. The fact that the optimal material, as proposed by FMO, does not already exist in nature is seen as one of the major drawbacks of this optimization method. However, it is a fundamental idea of FMO to overcome the boundaries of traditional materials as well as laminate manufacturing standards and to motivate the construction of entirely new materials by pointing out the high potential provided by advanced materials. Free material optimization can thus be used to generate benchmark solutions for other models and besides to propose novel ideas for new design situations.

3. A Method for Simultaneous Topology and Material Optimization

Structural optimization, in particular topology optimization, is a powerful and already widely used tool for the design of weight optimized structural components. Topology optimization has reached a high level of maturity for isotropic materials [1]. In terms of extremely lightweight components, composite structures are a key player, offering the possibility of tailoring the material to a specific application. However, few publications exist on concurrently optimizing the layout of the structure and the mechanical constitutive behavior of the structure. Indeed, considering the material properties (i.e., orientation and anisotropy of the local material tensor, which is controlled by the composite micro-structure) in the optimization process is considered complex. The aim of this chapter is to propose an optimization methodology for the simultaneous structural (topology) and material optimization.

As outlined in the previous chapter, structural optimization deals with the improvement of the mechanical performance of load carrying structures. The most common measures of structural performance are weight, stiffness, stresses, strains, critical loads, displacements, and geometry. The optimization problems can thus be formulated by taking one or more of these measures as an objective and some of the other measures as constraints. Engineers usually prefer to minimize the mass of a structure while at the same time imposing constraints on the global structural stiffness (i.e., displacement constraints). Nonetheless, a similar problem can be solved by maximizing the global structural stiffness and imposing constraints on the mass. The problem of maximizing the global stiffness of an elastic structure can be formulated as the minimization of the compliance. The compliance of a body, in elasticity, corresponds to the global work done by the external forces for the field of the displacements that are solution of the elastic problem. Therefore, the problem of maximizing the stiffness, which is subject to a mass constraint, is synonymous to minimizing the compliance of a structure, which in turn is subject to a constraint on the volume fraction. The optimization problem of minimizing the compliance is mostly discussed in literature and therefore is taken up in the framework of this thesis. Therefore, the global design objective for the simultaneous structural and material optimization is to minimize the compliance of a structure, subject to a constraint on the amount of material that is at our disposal, i.e., a constraint on the volume fraction.

The following sections describe how the "State of the Art" (isotropic) topology optimization procedure is extended to anisotropic material behavior. Subsequently, a computational scheme which updates the anisotropic material properties (local material orientation as well as the local material tensor) based on the local loading conditions (i.e. principal stresses and principal stress directions) is proposed. The general concept of the optimization procedure for the simultaneous optimization of topology and material is shown in Figure 3.1. For both, the isotropic as well as the anisotropic case, a convergence criterion is checked in each iteration prior to the update of topology and material. As real structures are subjected not only to one loadcase but multiple loadcases, the method is extended to multiple loadcases as well.

The next sections explain in detail how the topology update is determined (Section 3.1), how the optimized material properties are determined (Section 3.2), and how the simultaneous optimization of topology and material is implemented (Section 3.3).

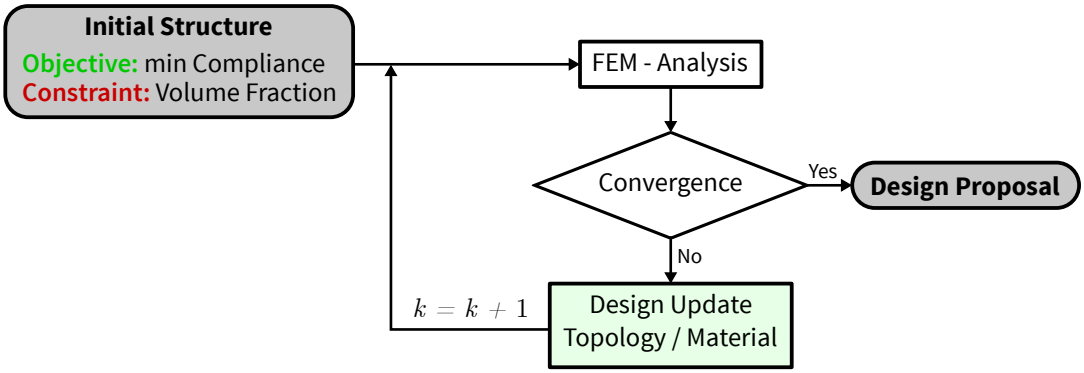

Figure 3.1.: General concept for the simultaneous structural and material optimization for minimizing the compliance subject to a volume constraint

3.1. Topology update scheme

In the framework of this thesis, the soft-kill *Bi-Evolutionary Structural Optimization* (BESO) algorithm, proposed by Huang et al. [59], is used to determine the best topological layout that yields the stiffest structure with a predefined volume of material. Furthermore, a filter scheme to overcome numerical issues like mesh-dependency and checkerboard patterns, as proposed by Huang et al. [75], is used. According to Huang et al. [52], this BESO method for stiffness optimization offers many advantages as opposed to other methods like for instance SIMP. These include high quality topology solutions which can be easily interpreted in terms of manufacturability as the final topology does not contain regions of intermediate densities. Furthermore, the BESO algorithm provides excellent computational efficiency and is easy to implement as a post-processing algorithm to most FEM packages. The BESO algorithm as well as the filter scheme are implemented in Python based on the publication by Zuo et al. [93]. The Python code takes advantage of the advanced FEM analysis capacities of the Abaqus software and employs the Abaqus Scripting Interface (ASI) to communicate with Abaqus.

3.1.1. Soft-kill BESO

In 2009 Huang et al. [59] proposed a soft-kill BESO algorithm to solve the topology optimization problem that yields the stiffest structure with a prescribed amount of material. To maximize the stiffness of a structure, the total strain energy of the structure or mean compliance C is minimized for a predefined volume of the material:

$$\text{minimize:} \qquad C = \frac{1}{2}\boldsymbol{u}^{\mathrm{T}}\boldsymbol{K}\boldsymbol{u}, \tag{3.1a}$$

$$\text{subject to:} \qquad V^* - \sum_{i=1}^{N} x_i V_i = 0, \tag{3.1b}$$

$$\text{where:} \qquad x_i = x_{\text{min}} \text{ or } 1. \tag{3.1c}$$

$\boldsymbol{K}$ is the global stiffness matrix of the structure and $\boldsymbol{u}$ is the displacement vector. The volume constraint, see (Equation 3.1b), limits the amount of material that is at disposal for the optimization. V_i is the volume of an individual element, V^* is the prescribed structural volume, N is the total number of finite elements in the structural model, and x_i denotes the design variable of the ith element. As outlined in Section 2.5.3, in evolutionary algorithms the element itself is considered as the design variable. A small value x_{min} is introduced as lower bound for the design variable to avoid singularity of the stiffness matrix. This lower bound denotes the soft (void) elements and is set to $x_{\text{min}} = 0.001$.

The formulation of the material interpolation scheme of the BESO algorithm, published by Huang et al. [59], makes use of the SIMP material interpolation model. Therefore, the Young's modulus is interpolated as a function of the element design variable as

$$E_i = E\left(x_i\right) = \left(x_i\right)^{\mathrm{p}} E_i^0, \tag{3.2}$$

similar to Equation 2.25. E_i^0 denotes the Young's modulus of the solid isotropic material and p is the penalty factor. It is assumed that the Poisson's ratio is independent of the design variables x_i. Thus, the global stiffness matrix $\boldsymbol{K}$ is expressed by the element stiffness matrix $\boldsymbol{K}_i$ and the design variables as follows:

$$\boldsymbol{K}\left(\boldsymbol{x}\right) = \sum_{i=1}^{N} \boldsymbol{K}_i\left(E_i\right) = \sum_{i=1}^{N} \left(x_i\right)^{\mathrm{p}} \boldsymbol{K}_i^0. \tag{3.3}$$

$\boldsymbol{K}_i^0$ denotes the element stiffness matrix of solid elements, N is the total number of elements in the structure, and $\boldsymbol{x}$ denotes the vector of the design variables.

The design variable update is based on the elemental sensitivity. In other words, a sensitivity analysis is performed to study the effect of material elimination on the structural behavior. Consequently, the sensitivity number represents the contribution of element modification to the concerned structural behavior.

For deriving the sensitivity of the objective with respect to the removal or addition of an element, the adjoint method is used. The adjoint method is a numerical method for efficiently computing the gradient of a function in a numerical optimization method. The sensitivity of the structural compliance with regard to the change in the i-th element can be easily derived by differentiating the objective function C as

$$\alpha_i = \frac{\partial C}{\partial x_i}. \tag{3.4}$$

By using Equation 3.1a, Equation 3.1c and Equation 3.3 the equation above evolves to

$$\frac{\partial C}{\partial x_i} = -\frac{1}{2} \mathrm{p} x_i^{\mathrm{p}-1} \boldsymbol{u}_i{}^{\mathrm{T}} \boldsymbol{K}_0^{\mathrm{e}} \boldsymbol{u}_i, \tag{3.5}$$

where $\boldsymbol{u}_i$ is the element displacement vector. The sensitivity is negative for all elements, so physical intuition is confirmed as additional material in any element decreases compliance, and therefore, makes the structure stiffer. Since BESO uses discrete design variables, only two bound materials ($x_i = 1$ and $x_i = x_{\mathsf{min}} = 0.001$) are allowed in the design. TThe sensitivity of an individual element, for both solid and soft elements, thus can be expressed by

$$\alpha_i = -\frac{1}{p}\frac{\partial C}{\partial x_i} = \begin{cases} \dfrac{1}{2} \boldsymbol{u}_i{}^{\mathrm{T}} \boldsymbol{K}_0^{\mathrm{e}} \boldsymbol{u}_i & \text{when } x_i = 1 \\ \dfrac{1}{2} x_{\mathsf{min}}^{\mathrm{p}-1} \boldsymbol{u}_i{}^{\mathrm{T}} \boldsymbol{K}_0^{\mathrm{e}} \boldsymbol{u}_i \approx 0 & \text{when } x_i = x_{\mathsf{min}} = 0.001. \end{cases} \tag{3.6}$$

This equation indicates that the sensitivity numbers of solid elements (x_i) are equal to the elemental strain energy and the sensitivity numbers of soft elements are approximately zero. The element strain energy, which is the amount of elastic energy stored in a finite element, can be directly obtained from FEM analysis. Elements with large values of strain energy indicate the location of large elastic deformation (energy). Therefore, by knowing the amount of the element strain energy one can immediately determine the areas of the structural model where modifications (changes of the design variable) will have the most impact. It is common to normalize the strain energy by unit volume, which is referred to as strain energy density. The element elastic strain energy densities are retrieved from the Abaqus Field Output (using the keyword "ESEDEN").

3.1.2. Filter Scheme

As already mentioned in Section 2.6, topology optimization is prone to numerical instabilities like mesh-dependency and checkerboard patterns. To recall, mesh-dependency refers to the problem of obtaining qualitatively different optimized structures when using different mesh sizes for the modeling of the structure. Checkerboards are referred to as patterns of alternating solid and void elements ordered in a checkerboard like fashion. According to Sigmund et al. [15], these numerical issues can be circumvented, to a large extent, by imposing restrictions on the variation of the design variables by including for instance a filter scheme for densities or sensitivities.

To simultaneously address numerical instabilities like mesh-dependency and checkerboard patterns, a sensitivity filter scheme for soft-kill BESO, as suggested by Huang et al. [75], is implemented. The filtering of the elemental sensitivities is performed prior to the update of the design variables. The key idea of the filter scheme is to replace the raw sensitivity number α_i^{e} of each element (retrieved from the FEM analysis) with a filtered elemental sensitivity α_i. The filtered elemental sensitivity α_i for the i-th element depends on the sensitivities of the element itself and its neighboring elements within a certain circular "domain of influence" Ω_i defined by a scale parameter denoted as filter radius r_{min}. The principle of the filter scheme is illustrated in Figure 3.2.

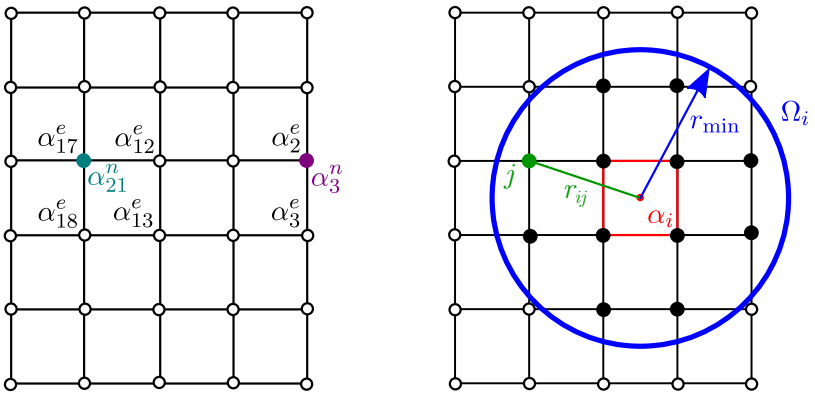

Figure 3.2.: Filter scheme used for filtering the elemental sensitivities

As a first step, the nodal sensitivity numbers α_j^{n}, are determined. Nodal sensitivity numbers do not carry any physical meaning on their own but rather are needed for the recalculation of the element sensitivities. They are determined by averaging the raw elemental sensitivities α_i^{e} of the elements connected to the respective node. Therefore, nodal sensitivity numbers are calculated as

$$\alpha_j^{\mathrm{n}} = \frac{\sum_{i=1}^{M^{\mathrm{e}}} V_i \alpha_i^{\mathrm{e}}}{\sum_{i=1}^{M^{\mathrm{e}}} V_i}, \tag{3.7}$$

where M^{e} denotes the total number of elements connected to the j-th node and V_i is the volume of an individual element. For instance, for determining the nodal sensitivity α_3^{n} for node 3 in Figure 3.2 (a), the raw elemental sensitivities of the connected elements α_2^{e} and α_3^{e} are averaged. Similarly, the nodal sensitivity α_{21}^{n} for node 21 is calculated by averaging the raw elemental sensitivities α_{12}^{e}, α_{13}^{e}, α_{17}^{e}, and α_{18}^{e}. The nodal sensitivity numbers α_j^{n} are used to calculate the improved, filtered elemental sensitivity numbers α_i as:

$$\alpha_i = \frac{\sum_{j=1}^{M^{\mathrm{n}}} w\left(r_{ij}\right) \alpha_j^{\mathrm{n}}}{\sum_{j=1}^{M^{\mathrm{n}}} w\left(r_{ij}\right)}, \tag{3.8}$$

where M^{n} is the total number of nodes within a sub-domain Ω_i.

The sub-domain Ω_i, centred at the centroid of the i-th element with the scale parameter r_{min}, is illustrated in Figure 3.2 (b). Nodes located inside Ω_i contribute to the computation of the filtered sensitivity number α_i and $w(r_{ij})$ is a linear weight function for averaging the raw sensitivities and is defined as:

$$w(r_{ij}) = \begin{cases} r_{\text{min}} - r_{ij} & \text{for } r_{ij} < r_{\text{min}} \\ 0 & \text{for } r_{ij} \geq r_{\text{min}} \end{cases}, \tag{3.9}$$

where r_{ij} is the distance between the center of the i-th element and the j-th node. As mentioned before, the primary role of the scale parameter r_{min} is to identify the nodes that influence the filtered sensitivity of the i-th element. The scale parameter r_{min} is specified by the user and can be used to control the minimum member size of the emerging features in the design domain. Huang et al. [75] note that r_{min} needs to be at least larger than the size of the smallest finite element in use, in order to have an effect. Furthermore, Huang and his co-workers suggest that r_{min} is selected to be about 1-3 times of the size of one element to successfully avoid checkerboard patterns and mesh-dependency.

To improve the accuracy of the sensitivities the sensitivity history of each element is considered, as suggested by Huang et al. [75]. The current filtered sensitivity α_i is averaged with the sensitivity of the previous iteration as

$$\alpha_i = \frac{\alpha_i^k + \alpha_i^{k-1}}{2}, \tag{3.10}$$

where k denotes the current iteration and $k-1$ denotes the previous iteration. Based on the filtered and history averaged α_i the design variables are updated as described in the next section.

3.1.3. Update of Design Variables

The presence ("solid material") or absence ("soft material") of each element of the discretized structure defines the material spatial distribution, i.e., the topology of the structure. Soft-kill BESO starts from a full design, iteratively evolving to an optimal structural layout by switching element status from "solid" ($x_i = 1$) to "soft" ($x_i = x_{\text{min}} = 0.001$) or vice versa. Before elements are added to or removed from the design by switching the element status, the target volume for the current design iteration V^k needs to be determined. The target volume decreases step by step until the predefined, constrained volume V^* is reached. Thus, the structural volume is gradually reduced by a so-called Evolution Rate ($ER > 0$) which determines the percentage of material to be removed from the design in each iteration step, as shown in Figure 3.3. The target volume of the current iteration V^k is determined based on the volume of the previous iteration V^{k-1} and the Evolution Rate ER as follows

$$V^k = V^{k-1}(1 - ER). \tag{3.11}$$

Selecting a high value of ER reduces the computational time, i.e., it reduces the number of iterations. However, according to Huang et al. [52], very high values of ER may result in local optima. Once the constrained volume is reached, the optimization runs with a constant redistribution factor (Evolution Rate $ER = 0$). Therefore, once the target required material volume usage is attained, the optimization algorithm alters the topology but keeps the volume constant ($V = \text{const.}$). From this point on, the cycle of finite element analysis, element removal and addition (and material adaption in the case of anisotropic material) continues until the convergence criterion, defined for instance in the variation of the objective functions, is satisfied. The convergence criterion is described in detail in Section 3.3. The procedure described above is different from other methods, e.g., SIMP, where the target volume is kept constant from the very beginning and the compliance decreases gradually until a convergence criterion is satisfied.

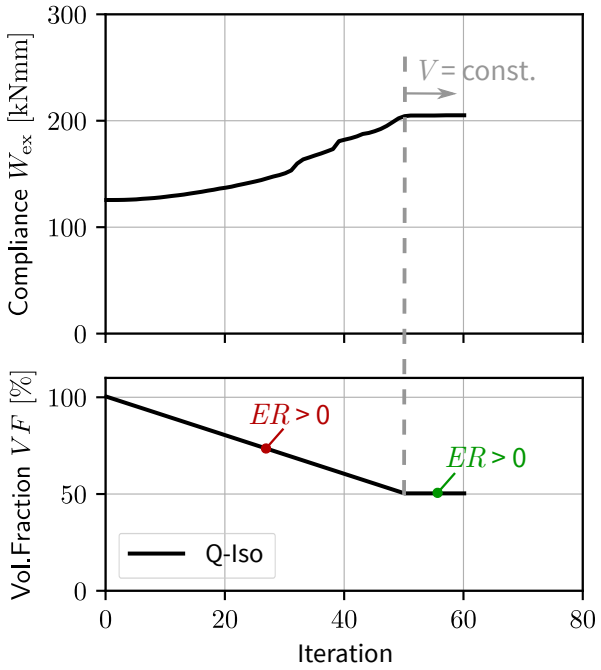

Figure 3.3.: Illustration how the compliance (objective) and volume fraction (constraint) evolves with the number of iterations for the BESO algorithm

The update of the design variables x_i, implemented in the numerical simulations of this thesis, is based on the update scheme proposed by Huang et al. [59]. Listing A.1 in Appendix A shows the Python code of a simple bisection method that is used in the framework of this thesis to determine a threshold parameter for the elemental sensitivities in order to decide which elements are "efficient" and therefore shall be included in the design, and which are not. Solid elements with a sensitivity number below the threshold are removed from the structure whereas solid elements with a sensitivity number above the threshold are kept as solid. Likewise, void elements are recovered when their sensitivity number is greater than the threshold. Void elements are kept as void when their sensitivity number is lower than the threshold.

The target volume tv gives volume, i.e., the number of elements, that shall be reached in the current design iteration. The threshold is changed progressively until the target volume of the current iteration is reached. The bisection algorithm returns the updated design variables $x_{i,\text{new}}$ as input for the next optimization iteration.

3.1.4. Implementation of the Topology Update Scheme

The implementation of the topology update scheme, described in the previous sections, is illustrated in Figure 3.4 (a) for the single loadcase (SLC) and Figure 3.4 (b) for multiple loadcases (MLC).

The initial structure is discretized with finite elements. Control parameters like the Evolution Rate ER, volume fraction constraint V^*, and the scale parameter r_{min} (filter radius) are defined. A linear static FE-Analysis is carried out to determine the system responses which are required for the determination of the updated topology, i.e., element elastic strain energy density. In the next step, the actual volume fraction of the design domain is checked against the target volume fraction V^*. If the target volume fraction has not been reached, a new target volume for the current iteration is determined by decreasing the actual volume by the evolution rate ER. Otherwise the volume stays constant. The filter scheme, described before, is used to filter the raw sensitivities determined from the element elastic strain energy density to prevent numerical instabilities. Subsequently, the filtered elemental sensitivities are checked against a threshold value: elements with a sensitivity value below the threshold are "removed" from the structure ($x_i = x_{\text{min}} = 0.001$) which implies that they are set to a very soft material. Elements with a sensitivity value higher than the threshold are set to "solid" ($x_i = 1$). The new material distribution is determined based on the current elemental design variables (x_i) and the material properties for "solid elements" and "soft elements". If the design variable of an element has a value of $x_i = 1$, the material properties of this element for the next iteration equal the material properties of a solid element (e.g., isotropic material). Otherwise, if the design variable of an element has a value of $x_i = 0.001$ the elements material properties are set to a very soft, isotropic, material with the material parameters $E = 0.001^3,\ \nu = 0.3$ where the penalization factor is set to $\mathrm{p} = 3$.

When designing structures for complex systems, the handling of Multiple Load Cases (MLC) is an essential part of the design process, as complex systems may be subject to a large number of different loading conditions. Therefore, an efficient strategy for multiple loadcase problems is crucial in engineering activities. Topology optimization for multiple loadcases involves the balance among multiple optimal load transferring paths. Generally, each loadcase is considered as an objective function to be optimized. In order to extend the BESO algorithm to multiple loadcases, the criterion for the addition and removal of the elements is adapted, as proposed by Zuo et al. [93]. For multiple loadcases the linear static FE-Analysis of the structure is carried out for each of the loadcases separately.

Likewise, filtering of the elemental sensitivities is performed for each of the loadcases separately. The filtered sensitivities are summed up for all loadcases as

$$\alpha_i = \sum_{j=1}^{n} \alpha_i^{\mathrm{LC}\,j}, \tag{3.12}$$

where n is the total number of loadcases and $\alpha_i^{\mathrm{LC}\,j}$ denotes the elemental sensitivity of the respective loadcase j. The value of α_i is then checked against the threshold, similarly to the single loadcase procedure. According to Young et al. [62], this is equivalent to a logical "AND" condition for the element removal process and a logical "OR" condition for the element addition process. This means that the designs obtained for each individual load case are superimposed to produce the new design, whilst satisfying the target volume constraint. Therefore, if an element is needed for any of the loadcases it must be set to $x_i = 1$. Only if an element is considered "inefficient" for both loadcases it can be removed from the structure.

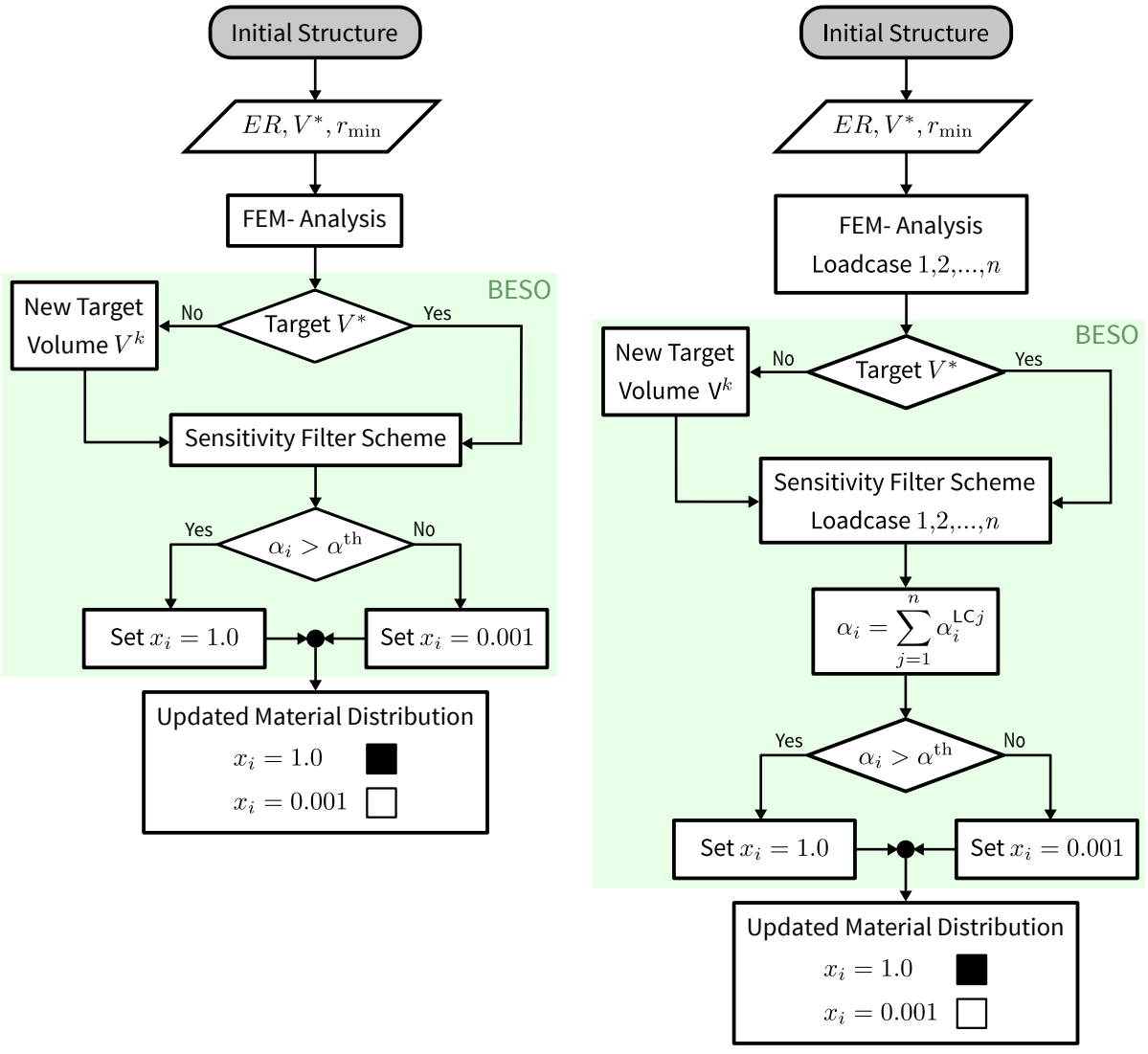

(a) (b)

Figure 3.4.: BESO algorithm. (a) Single Loadcase, (b) Multiple Loadcases

3.2. Material Update Scheme

For a given load and boundary conditions, the stress usually varies in each point of the structure. Some areas are mainly stressed in tension or compression, whereas others are stressed in shearing. Consequently, the material should be adapted to the local stresses which are applied on it. The second aspect of simultaneous optimization developed in the framework of this thesis, namely the material optimization, tackles this problem by determining the optimal material orientation as well as the optimal material anisotropy which vary throughout the structure. Thus, the update of the material within each iteration step of the optimization consists of two aspects: (1) adjusting the local material orientation and (2) adjusting the local material (stiffness) tensor, based on the local loading conditions.

The following subsections explain in detail how the material is modeled (see Subsection 3.2.1), how the update of the local material orientation is determined (see Subsection 3.2.2), and how the update of the local material anisotropy is performed (see Subsection 3.2.3).

3.2.1. Material Modeling

In mechanics of materials, the length-scale at which a problem is considered is of great importance. Typically, a material is an inhomogeneous agglomeration of constituents. For instance composites consist of dissimilar constituents ("phases") that are distinguishable at some (small) length scale(s). Each constituent shows different material properties and/or material orientations and may itself be inhomogeneous at some smaller length scale. The behavior of inhomogeneous materials is determined, on the one hand, by the relevant material properties of the constituents. On the other hand, the behavior of inhomogeneous materials is determined by the geometry and topology of the constituents (the so-called "phase arrangement"). The process for "bridging length scales" for determining a unique constitutive behavior for inhomogeneous materials is called *Homogenization* [94]. The aim is to determine the overall "effective material properties" (e.g. stiffness, thermal expansion, strength properties) from the corresponding material behavior and from the geometrical arrangement of the phases. The principle of homogenization is illustrated in Figure 3.5. The left picture shows the inhomogeneous composite with it's constituents, i.e., different phases p (different materials or pores) with the respective material properties $E_i^{(p)}, G_{ij}^{(p)}, \nu_{ij}^{(p)}, ...$ The picture on the right shows the "homogeneous equivalent medium" after homogenization with the "effective material properties" $E_i^*, G_{ij}^*, \nu_{ij}^*, ...$

Approaches for modeling inhomogeneous materials are for instance simple analytical methods, like the *Rule of Mixture*, which lack thermodynamical consistency and are limited to simple topologies (e.g., unidirectionally aligned long-fibers). Other methods, like for instance *Mean Field Homogenization* methods, allow for different inclusion shapes (e.g., spherical inclusions, continuous cylindrical inclusions, penny-shaped inclusions, ...) and two or more phases.

The key idea of *Mean Field Homogenization* methods is to give a macroscopic response as well as basic information on the state of deformation within the phases based on assumptions of the interaction laws between the different phases (which define the homogenization scheme). A good summary of micromechanics and approaches for modeling inhomogeneous materials can be found in "A Short Introduction to Basic Aspects of Continuum Micromechanics" by Böhm [95]. Böhm [95] also states that, the effective field method of *Mori-Tanaka* [96] is the simplest mean field approach to model inhomogeneous materials and it is specifically suited for matrix-inclusion-type microtopologies (composites).

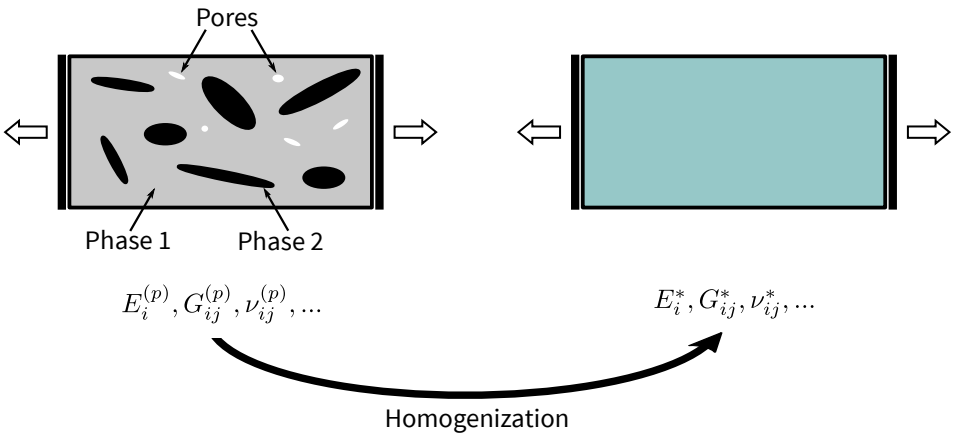

Figure 3.5.: Principle of homogenization for bridging length scales for inhomogeneous materials by determining the overall "effective material properties" (e.g., stiffness, thermal expansion, strength properties) from the corresponding material behavior and from the geometrical arrangement of the phases

According to Pierard et al. [97], direct homogenization schemes might lead to physically unacceptable macro predictions, i.e., a non-symmetric overall stiffness tensor. Pierard et al. [97] propose a two-step homogenization procedure which gives physically acceptable results. The composite is decomposed into "grains" where each grain contains only one inclusion family (i.e., inclusions which have the same material properties, aspect ratio, shape, and orientation). In a first step, each grain is homogenized individually, e.g., by using the method of *Mori-Tanaka*. In the second step the representative volume element (RVE) is considered as a set of different grains where each grain is characterized by its stiffness and orientation (determined in the first step). This "aggregate" denotes a multi-phase composite and therefore can be homogenized by one of several homogenization schemes. However, Pierard et al. [97] suggests to use models which are suitable for aggregates or polycrystals (e.g. Voigt, Reuss). Using Mori-Tanaka also for the second step is not a viable option as this is equivalent to a direct Mori-Tanaka homogenization on a multiphase composite and therefore leads to the problems mentioned above.

In the framework of this thesis a continuous glass fiber reinforced polymer (GFRP) is used, i.e., infinitely long cylindrical inclusions (glass fiber) embedded in a matrix. The orientation and volume fraction of the inclusions are determined for each optimization iteration via update

schemes for the material orientation and the degree of anisotropy (see Subsection 3.2.2 and Subsection 3.2.3). The predefined input data for the *Mori Tanaka* calculations, i.e., mechanical and thermal properties of the continuous cylindrical inclusions (fibers) and the matrix, are listed in Table 3.1 and Table 3.2.

Table 3.1.: Mechanical and thermal properties of Silenka E- Glass fiber [98]

Fibre type	Symbol	Unit	Silenka E- Glass 1200tex
Longitudinal Young's modulus	E_{f1}	GPa	74
Transverse Young's modulus	E_{f2}	GPa	74
In-plane shear modulus	G_{f12}	GPa	30.8
Major Poisson's ratio	ν_{f12}	$-$	0.2
Transverse shear modulus	G_{f23}	GPa	30.8

Table 3.2.: Mechanical and thermal properties of matrix [98]

Matrix type	Symbol	Unit	MY750
Young's Modulus	E_{m}	GPa	3.35
Shear modulus	G_{m}	GPa	1.24
Poisson's ratio	ν_{m}	$-$	0.35

3.2.2. Material's 1-Direction

The determination of the ideal orientation of the given material is of fundamental importance as even small deviations from the ideal fiber alignment result in significantly lowered strength and stiffness characteristics of the structure because the matrix (with significantly lower strength and stiffness values, see Table 3.1 and Table 3.2) is increasingly loaded.

Single Loadcase

The optimal local fiber orientation for each element is determined based on the resulting element stress tensors from the finite element analysis. The emerging principal stress trajectories are used for the material orientation in each element of the finite element model. For this purpose, the principal normal stress eigenvector (principal direction) with the largest absolute eigenvalue (maximum absolute principal normal stress eigenvalues) is used. This principal direction defines the material's 1-direction. The update of the local material axes for a single loadcase is illustrated in Figure 3.6, where the principal direction with the largest absolute principal normal stress (indicated with the blue arrows) determines the material's 1-direction (fiber orientation) for the respective element.

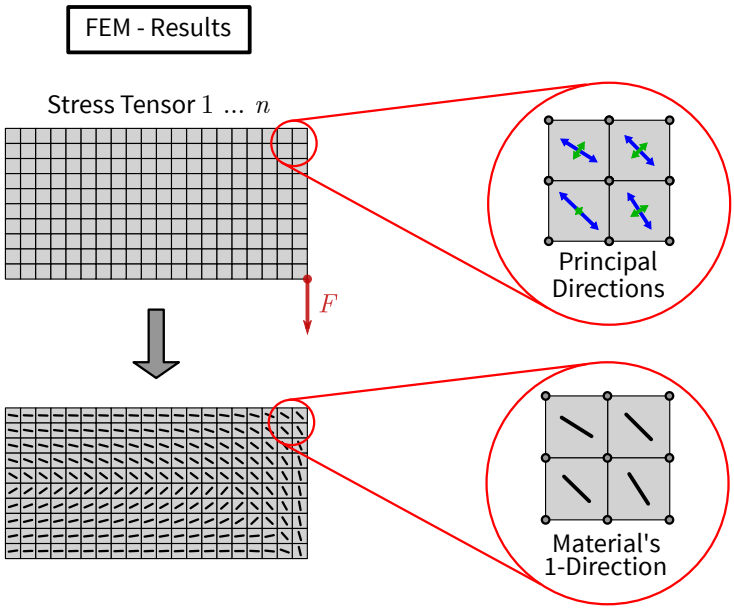

Figure 3.6.: Principle of material orientation update for a single loadcase

Multiple Loadcases

Similar to the update procedure described above, for multiple loadcases the basic idea is to align the fibers along the principal stress trajectories with the biggest absolute value. However, compared to the single loadcase, the orientation is updated according to the principal directions of the design loadcase, see Figure 3.7. In the framework of this thesis, *Loadcase 1* is denoted as "Design Loadcase", therefore, the material orientation is updated according to this loadcase. The principal directions of all further loadcases do not contribute to the determination of the local material orientation. However, these loadcases do contribute to the determination of the local material tensor, as described in the next section.

3.2.3. Local Stiffness Tensor

In addition to the update of the local material orientation, the local stiffness tensor is updated. The overall volume content of the continuous cylindrical inclusions is set to $\xi_f = 60\,\%$ for all simulations. The optimal degree of anisotropy depends on the nature of the stress field. Several procedures for updating the local stiffness tensor for single loadcase and multiple loadcases are described in detail below. All the procedures designations contain the prefix *Anisotropic-Orient-Material* (*AOM*) as the basis for all of these procedures is the update of the material orientation described in the previous section and all of these procedures update the local stiffness tensor with every iteration step of the optimization. The several methods of *AOM* described in this subsection differ in how the degree of anisotropy is determined.

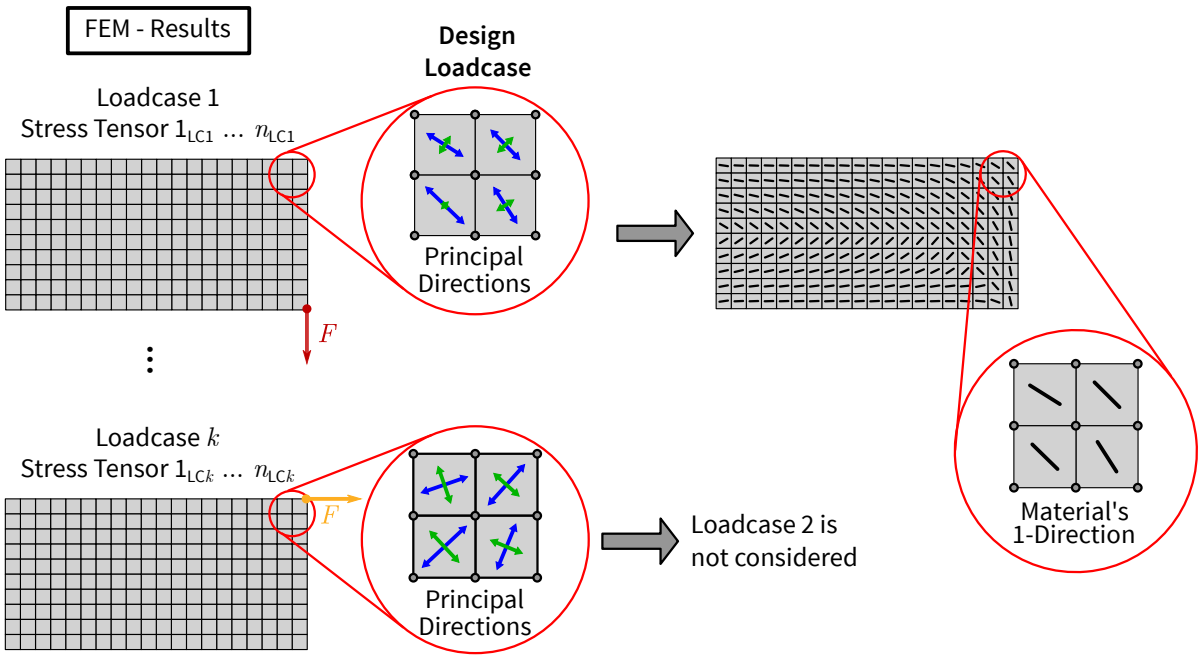

Figure 3.7.: Principle of material orientation update for multiple loadcases where *Loadcase 1* is the design loadcase

AOM-I Single

For the update of the local stiffness tensor for a single loadcase (*AOM-I Single*) only inclusions oriented at $0\,^{\circ}$ and $90\,^{\circ}$ are allowed, leading to an orthotropic material. The respective volume fractions, ξ_{0° and ξ_{90°, are based on the ratio of the principal stresses σ_{11} and σ_{22} (absolute values) and on the requirement that the sum of those volume fractions must amount to ξ_f:

$$\frac{\xi_{90^\circ}}{\xi_{0^\circ}} = \frac{\sigma_{22}}{\sigma_{11}}, \tag{3.13a}$$

$$\xi_{0^\circ} + \xi_{90^\circ} = \xi_\mathrm{f}. \tag{3.13b}$$

The principle of the material update for a single loadcase is illustrated in Figure 3.8. Different stress states lead to different volume fractions, ξ_{0° and ξ_{90°, for the inclusions. For instance, *element 200* shows a predominantly uni-axial stress. Therefore, an almost transversely isotropic material is used. In other words, the volume fraction of the $90\,^{\circ}$ inclusions is approximately 0. However, a transversely isotropic material that exhibits a privileged direction is not sufficient for covering the multi-axial stress state in *element 1*. In this case inclusions of $0\,^{\circ}$ and $90\,^{\circ}$ ($\xi_{0^\circ} > 0$ and $\xi_{90^\circ} > 0$) are required. The material's 1-direction ($0\,^{\circ}$ inclusion) coincides with the local material orientation determined in the course of the orientation update.

For updating the local material tensor for multiple loadcases three different material update schemes are proposed. These material update schemes are denoted as *AOM-I Multiple*, *AOM-II* and *AOM-III*.

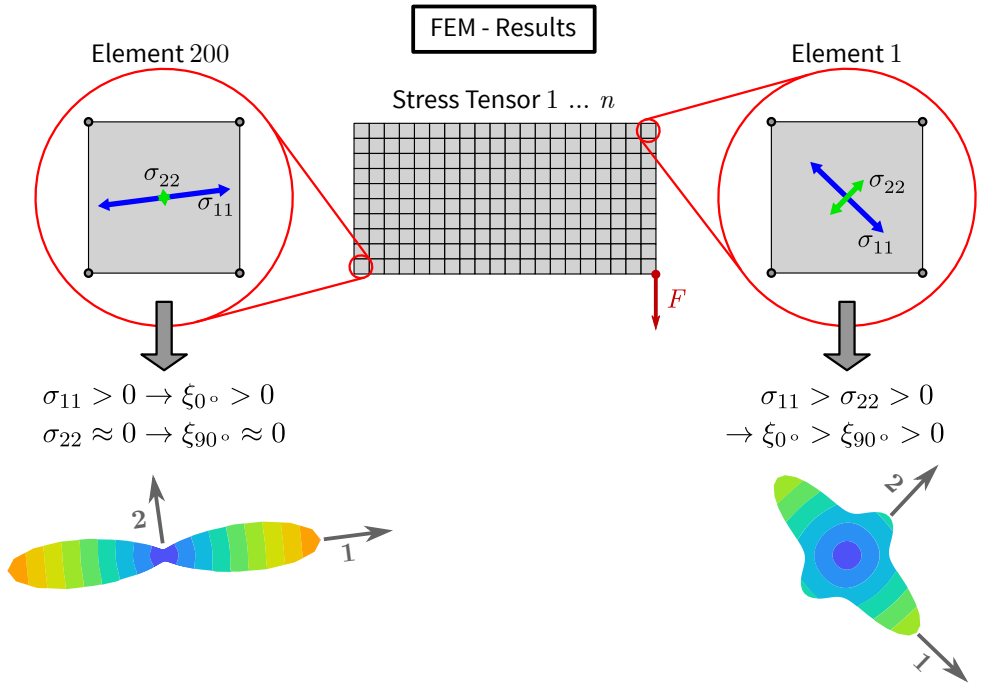

Figure 3.8.: *AOM-I Single*: Update of the local material tensor for a single loadcase based on the ratio of the principal stresses σ_{11} and σ_{22}

AOM-I Multiple

The update procedure *AOM-I Multiple* for multiple loadcases is equal to the procedure used with a single loadcase, as described in the previous subsection. In this case, only the design loadcase is used to determine the respective volume fractions of the 0° and 90° inclusions. The *AOM-I Multiple* procedure is illustrated in Figure 3.9 for two loadcases. The volume fractions of the inclusions for the material update (ξ_{0° and ξ_{90°) are determined based on the ratio of the principal stresses $\sigma_{11}^{\mathrm{LC}\,1}$ and $\sigma_{22}^{\mathrm{LC}\,1}$ emerging from the design loadcase (in this case *Loadcase 1*), disregarding stress states resulting from *Loadcase 2*. Furthermore, again there is the requirement that the sum of the volume fractions must amount to ξ_{f}. The stiffness tensor glyph, exemplarily shown for *element 5* , clearly shows that the material is only optimized for *Loadcase 1*. However, the material is not optimized for *Loadcase 2*.

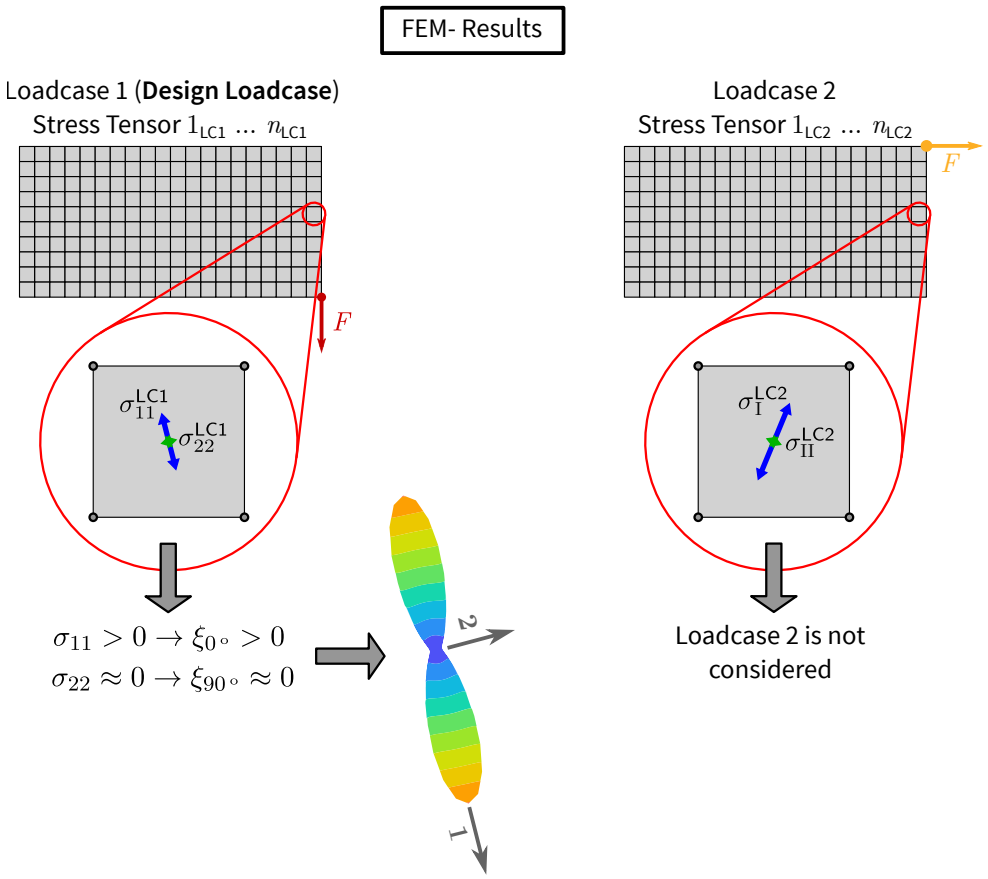

Figure 3.9.: *AOM-I Multiple*: Update of the local material tensor for multiple loadcases assuming that only the design loadcase is the deciding loadcase for the degree of anisotropy

AOM-II

The key idea of the procedure *AOM-II* for dealing with multiple loadcases is to consider the design loadcase with inclusions of 0° and 90° and all further loadcases with additional inclusions (e.g., θ_3, θ_4 for a second loadcase). The orientations of these additional inclusions depend on the principal directions of the respective loadcase with in relation to the principal directions of the design loadcase. Therefore, the additional inclusions, pertaining to one specific loadcase, are also orthogonal. It is assumed, that this procedure gives the most design freedom since the inclusions can be directly adapted to the needs of the further loadcases, but may lead to non-orthotropic material tensors. Figure 3.10 exemplarily shows the update procedure *AOM-II* for two loadcases. First, the principal stresses and principal directions of the element under consideration are determined for both loadcases. Generally, *Loadcase 1* (design loadcase) adds inclusions of 0° and 90° whereas *Loadcase 2* adds inclusions of θ_3 and θ_4. However, for the element exemplarily shown in Figure 3.10 ξ_{90° and ξ_{θ_4} are approximately 0 as the respective principal stresses, σ_{II} are approximately 0. The orientation of inclusion θ_3 is determined as the angle between the maximum (absolute) stress principal direction of the design loadcase (*Loadcase 1*) and the maximum (absolute) stress principal direction of *Loadcase 2*.

As the inclusions of *Loadcase 2* must be orthogonal, θ_4 is calculated as $\theta_4 = \theta_3 + 90°$. The respective volume fractions depend on the ratios of the principal stresses of the two loadcases (superposition of loadcases) and on the requirement that the sum of those volume fractions ($\xi_{0°}, \xi_{90°}, \xi_{\theta_3}, \xi_{\theta_4}$) must amount to ξ_f.

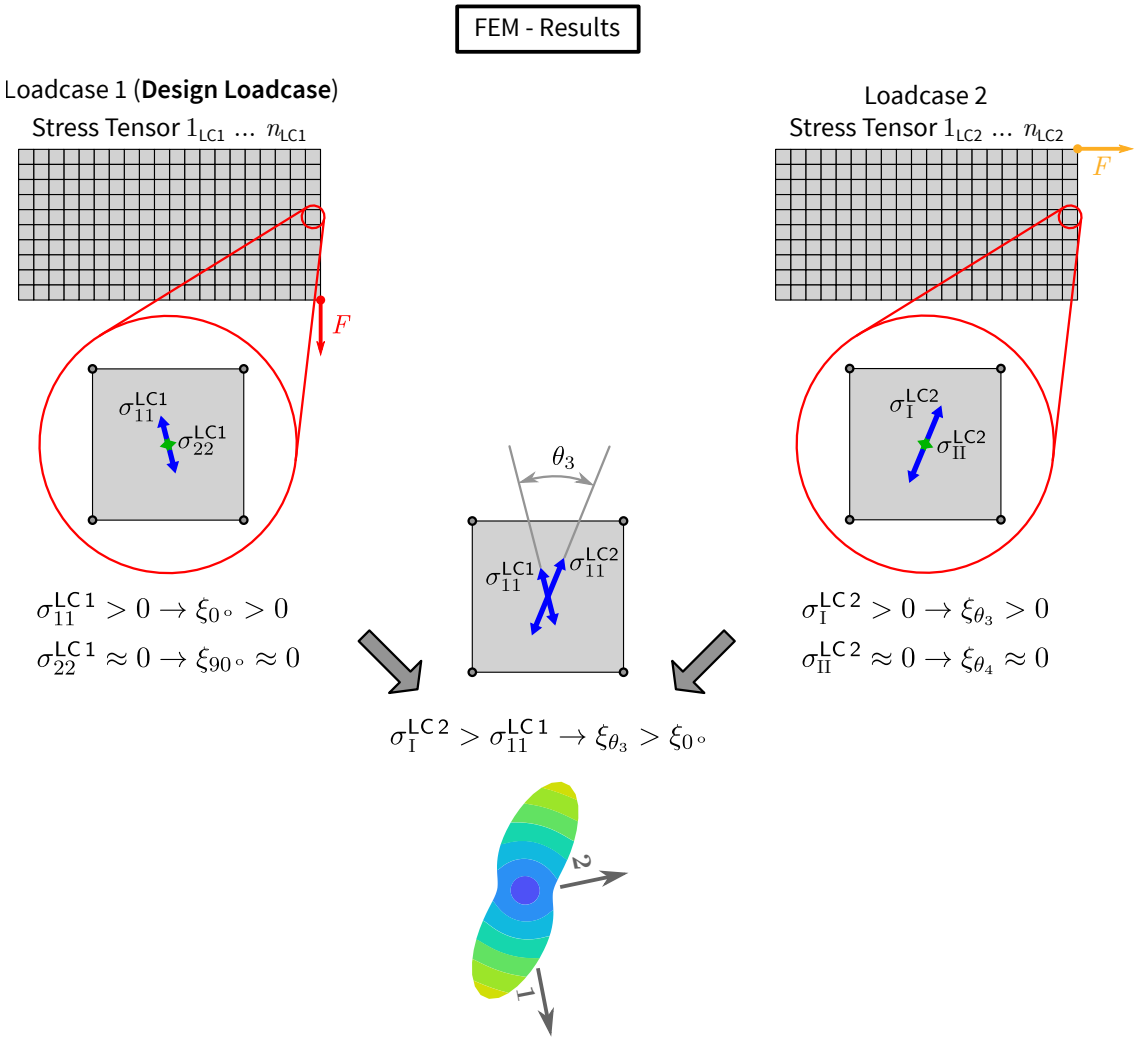

Figure 3.10.: *AOM-II*: Update of the local material tensor for multiple loadcases assuming that the design loadcase contributes with cylindrical inclusions of $0°$ and $90°$ whereas the second loadcase contributes with inclusions (θ_3, θ_4) where the orientation is based on the principal directions of *Loadcase 2* with respect to the principal directions of the design loadcase

AOM-III

In the third approach for updating the local material tensor, *AOM-III*, inclusions of $0°$, $\pm 45°$ and $90°$ are used. These inclusion orientations correspond to the standard composite ply-orientations employed in traditional material lay-ups. The *AOM-III* approach is exemplarily illustrated for *element 12* in Figure 3.11 for two loadcases. Again, there is a design loadcase (*Loadcase 1*) which determines the orientation, i.e., material's 1-direction and therefore local orientation of the $0°$ inclusion. The principal stresses σ_{11}^{LC1}, σ_{22}^{LC1} as well as the corresponding principal directions of the design loadcase are determined.

The stress tensor resulting from *Loadcase 2* is rotated to the major principal axis of the design loadcase. This results in normal stresses, denoted as $\sigma^{\mathrm{LC}\,2}_{11,\mathrm{rotated}}$, $\sigma^{\mathrm{LC}\,2}_{22,\mathrm{rotated}}$, and shear stresses $\tau^{\mathrm{LC}\,2}_{12}$ (indicated by pink arrows in Figure 3.11). These shear stresses are the basis for adding $\pm 45^\circ$ inclusions to the material formulation. For determining the volume fractions ξ_{0°, ξ_{90° and $\xi_{\pm 45^\circ}$, first the stresses contributing to the volume fractions of $0\,^\circ$ and $90\,^\circ$ inclusions are compared, i.e., $\sigma^{\mathrm{LC}\,1}_{11}$ and $\sigma^{\mathrm{LC}\,2}_{11,\mathrm{rotated}}$ for the $0\,^\circ$ inclusions and $\sigma^{\mathrm{LC}\,1}_{22}$ and $\sigma^{\mathrm{LC}\,2}_{22,\mathrm{rotated}}$ for the $90\,^\circ$ inclusions. In each case the greater value is used for determining the volume fractions. For the element exemplarily shown in Figure 3.11, this implies that $\sigma^{\mathrm{LC}\,2}_{11,\mathrm{rotated}}$ and $\sigma^{\mathrm{LC}\,2}_{22,\mathrm{rotated}}$ along with $\tau^{\mathrm{LC}\,2}_{12}$ are used for determining the volume fractions. Again, the respective volume fractions are determined based on the ratio of the stresses (σ_{11}, σ_{22} and τ_{12}) and on the requirement that the sum of the volume fractions ξ_{0°, ξ_{90° and $\xi_{\pm 45^\circ}$ must amount to ξ_f. It has to be noted, that the volume fraction of $+45^\circ$ and -45° inclusions are assumed to be equal (balanced). Therefore, $\xi_{+45^\circ} = \xi_{-45^\circ} = \dfrac{\xi_{\pm 45^\circ}}{2}$.

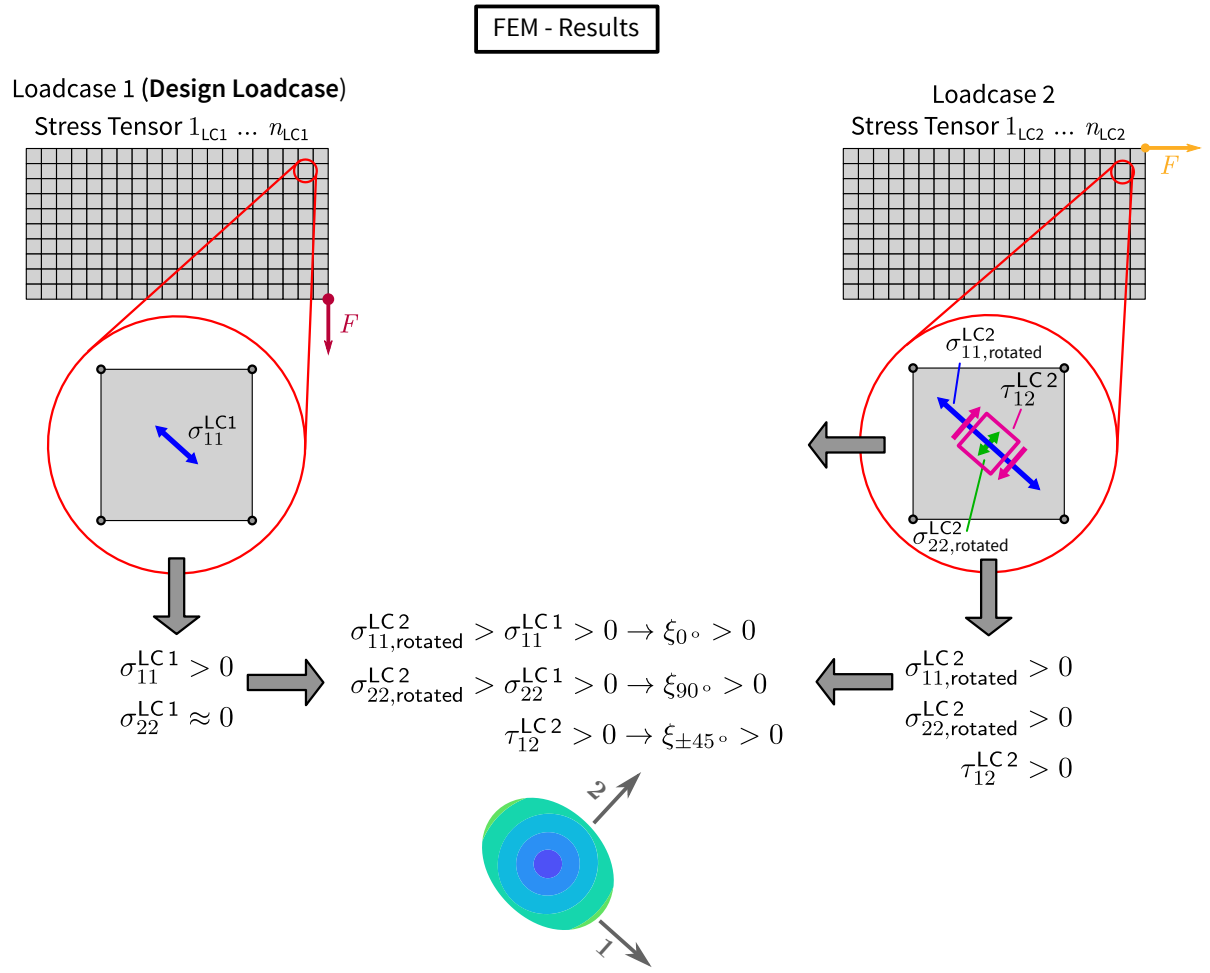

Figure 3.11.: *AOM-III*: Update of the local material tensor for multiple loadcases assuming standard composite ply orientations of $0\,^\circ$, $\pm 45\,^\circ$ and $90\,^\circ$ as inclusion orientations

Methods for Reference

To evaluate the potential of simultaneously optimizing topology and material (*AOM*), two further schemes are defined to be compared to the standard "State of the Art" topology optimization with quasi-isotropic material.

The *Anisotropic* (*A*) scheme denotes the topology optimization with an anisotropic (unidirectional) material but without altering the material properties in every iteration step. In other words, after determining the startdesign (see Section 3.3.1) the local material orientation and degree of anisotropy remain unchanged throughout the optimization. Only the topology is altered based on the *BESO* algorithm.

The second update scheme *Anisotropic Orient* (*AO*) is an extension to the *Anisotropic* update scheme and corresponds to the idea of *Continuous Fiber Angle Optimization* (CFAO) presented in Section 2.7.3. Similar to the *Anisotropic* update scheme, at first the startdesign for the optimization is determined. However, in this case, in addition to the topology update the orientation of the material is updated with every optimization iteration step. The degree of anisotropy remains unchanged, i.e., the optimization is performed with the unidirectional material defined for the startdesign.

3.3. Computational Scheme

This section introduces the strategy for the proposed optimization method. Figure 3.12 shows the computational scheme when topology update and material update (i.e., update of the local orientation and degree of anisotropy) are combined.

The optimization problem is non-convex and therefore admits several local minima. The initial structure to be optimized is modeled with a quasi-isotropic material. Quasi-isotropic denotes a material having isotropic properties, but only in-plane. In other words, the stiffness of the material within the plane of the part is independent of the direction in which the material is loaded. To obtain the quasi-isotropic material inclusions of equal content are specified in $0\,^{\circ}$, $+45\,^{\circ}$, $-45\,^{\circ}$, and $90\,^{\circ}$, i.e. since $\xi_{\mathrm{f}} = 60\%$, $\xi_{0^{\circ}} = \xi_{90^{\circ}} = \xi_{+45^{\circ}} = \xi_{-45^{\circ}} = 15\%$. The quasi-isotropic material is also used for the "State of the Art" standard topology optimization (*Q-Iso*).

The iterative part of the optimization procedure, which builds on the startdesign, is the following: in every iteration step a FEM-Analysis is performed. As long as the constraint on the volume fraction is not fulfilled the topology as well as the material properties are updated as described in the previous sections. Figure 3.12 shows the update of the topology and the material update in terms of local material orientation and local degree of anisotropy (visualized with stiffness tensor glyphs).

When the constraint on the volume fraction is fulfilled, after 10 further iterations at constant volume fraction, a convergence criterion is checked to determine whether the optimization can be stopped or another design update is necessary. The convergence criterion is described in detail in Subsection 3.3.2.

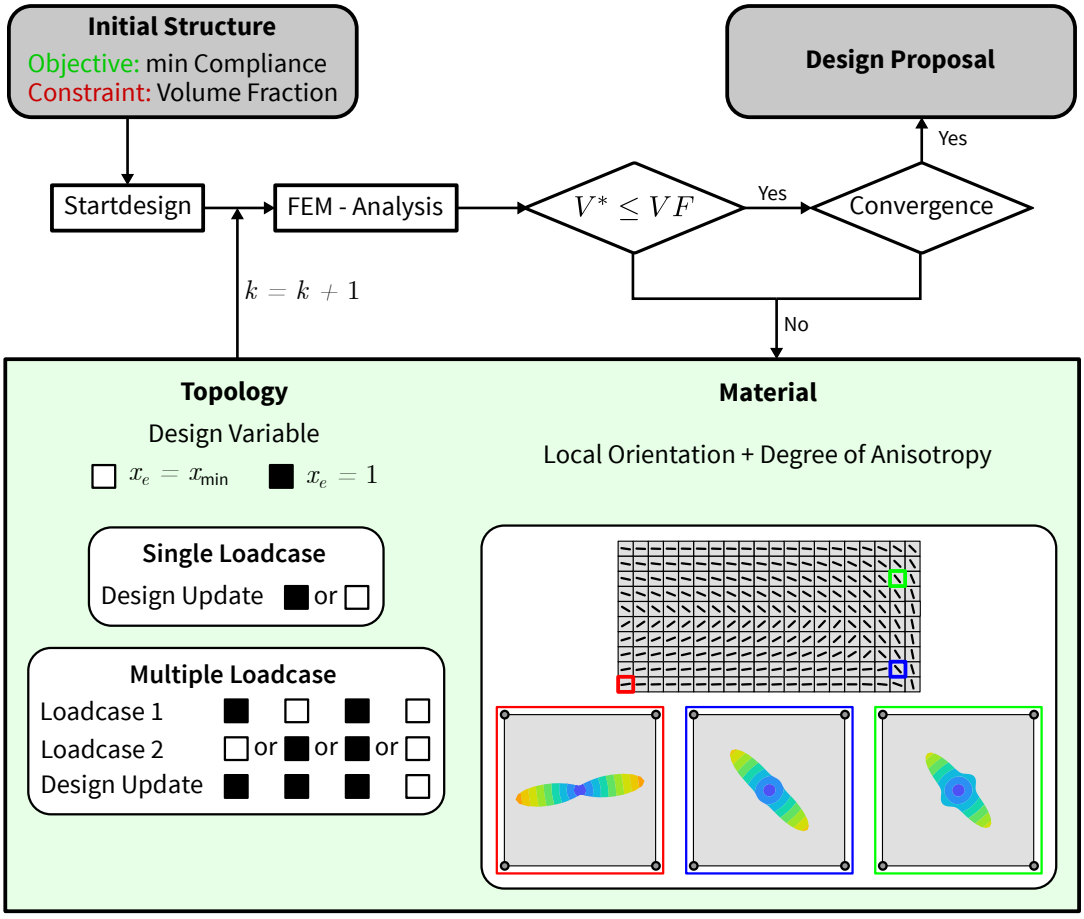

Figure 3.12.: Computational scheme developed for the simultaneous optimization of topology and anisotropic material properties *(AOM)*

3.3.1. Startdesign

Several suggestions for the startdesign for the optimization can be found in literature. For instance Mattheck et al. [99] suggest to use a unidirectional orientation of the orthotropic axes for the initial material orientation. Reuschel et al. [81] propose to use an orthotropic material with arbitrary orientation assigned to the FEM model to be optimized. Völkl et al. [100] propose to use an isotropic material for the startdesign of the optimization.

In the framework of this thesis, several startdesigns are investigated in order to determine if the startdesign has an influence on the optimization result, see Section 4.1. The investigations show, that aligning the fibers along principal stress axes for the startdesign gives the best result compared to other startdesigns. The initial design exhibits quasi-isotropic material properties, indicated by the respective stiffness tensor glyphs.

The fiber orientation for the startdesign is determined by performing a finite element analysis with the quasi-isotropic material setup and subsequently aligning the material's 1-direction according to the principal stress directions as described in Section 3.2.2. The material used for the startdesign for the optimization is a unidirectional material (i.e., fiber inclusions of 0° with $\xi_{0^{\circ}} = 60\%$). The procedure of determining the startdesign is illustrated in Figure 3.13.

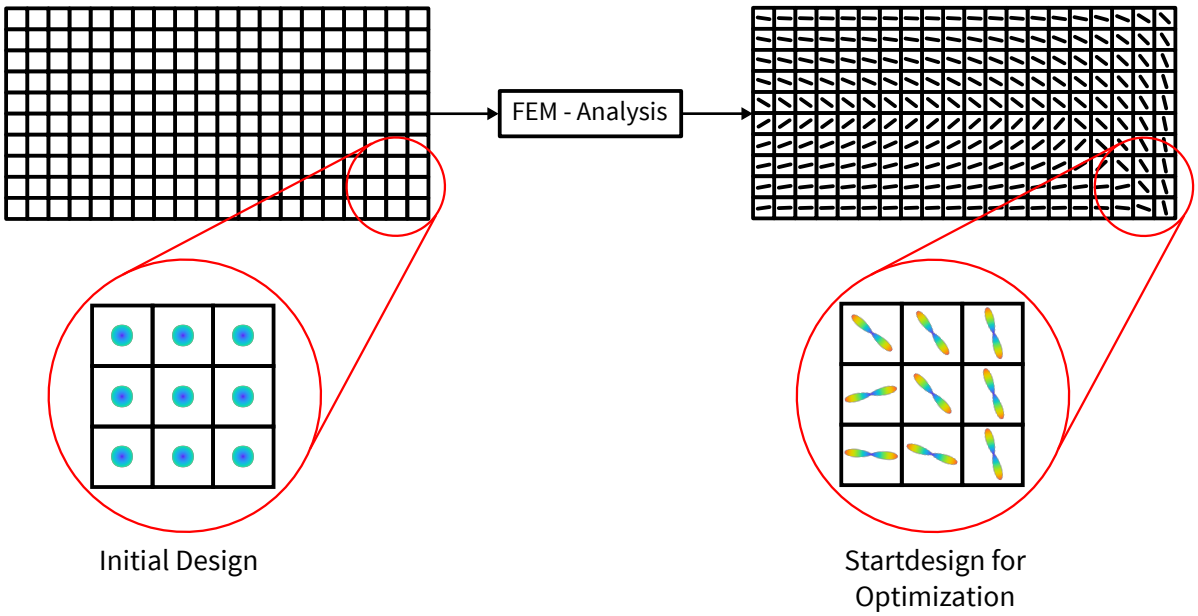

Figure 3.13.: Determination of a startdesign for the optimization by performing a FEM analysis for the initial, quasi-isotropic structure

3.3.2. Convergence Criterion

For checking if the sensitivity-based optimization has converged a convergence criterion, as proposed by Xia et al. [53], is implemented. The convergence criterion is expressed as the change in the objective function in the previous iterations and is given by

$$\left| \frac{\sum_{j=1}^{n} (C_{k-j+1} - C_{k-n-j+1})}{\sum_{j=1}^{n} (C_{k-j+1})} \right| \leq \varepsilon_{\text{tol}}, \tag{3.14}$$

where k is the current iteration number, n is an integer number and ε_{tol} is the allowable convergence error. The integer number n is chosen as $n = 5$, as proposed by Xia et al. [53], which means that the changes in the objective function in the last 10 iterations are within the specified allowable convergence error.

Most studies that deal with minimum compliance problems in topology optimization use $\tau_{\text{tol}} = 0.001$ as the convergence tolerance value [53]. Therefore, when dealing with a single loadcase, the allowable convergence error is set to $\varepsilon_{\text{tol}} = 0.001$. Therefore, the changes in the objective function in the last 10 iterations are within $0.1\,\%$ tolerance.

When dealing with multiple loadcases, the convergence of the design loadcase (*Loadcase 1*) is determined as above. When the convergence criterion is fulfilled for the design loadcase, all other loadcases are checked for convergence, but with a slightly higher tolerance of $\varepsilon_{\text{tol}} = 0.005$.

4. Application of the Method to a Single Loadcase

In this chapter the method of simultaneous structural and material optimization, described in the previous chapter, is validated for a single loadcase for simple test cases. The aim is to verify if the method is capable of efficiently determining concurrently the material distribution (topology) and anisotropy distribution.

As compliance is one of the most popular measures regarding the efficiency of a structure in topology optimization, the objective of the optimization is to minimize the compliance of a cantilever beam with a constraint on the volume fraction, $VF = 50\,\%$. The simulations are conducted using a continuous glass fiber reinforced polymer (GFRP), i.e., infinitely long cylindrical inclusions (glass fiber) embedded in a matrix. The mechanical and thermal properties of the continuous cylindrical inclusions (fibers) and matrix are listed in Table 3.1 and Table 3.2.

The design domain and boundary conditions are shown in Figure 4.1 (a) (in the x-y plane). The size of the design domain is 40 mm x 20 mm x 1 mm and it is discretized with $80 \times 40 \times 1$ linear brick elements with reduced integration, unless otherwise stated. Therefore, the mesh size in the x-y plane is denoted as m_{size} and amounts to $0.5\,\mathrm{mm}$. The design domain is modeled in 3D. However, as plane stress is assumed, stresses exist in the xy-plane as σ_x and σ_y (normal stresses) and σ_{xy} (in-plane shear stress). Each of these stresses is constant along the element thickness. In addition there is no stress in the z-direction as well as no through-thickness shear stresses. Therefore, the determination of the material orientation and material degree of anisotropy is reduced to a 2D problem.

The left side of the design domain is fixed ($u_{\mathrm{x}}, u_{\mathrm{y}} = 0$). A single load is applied to the lower right edge of the design domain, indicated with a red dot in Figure 4.1. The translational degrees of freedom (x- and y-direction) of the nodes of this edge are coupled to a reference point. The concentrated force is applied to this reference point. Figure 4.1 (b) shows the various loading scenarios which were investigated, namely *Loadcase A* (vertical load), *Loadcase B* (load at $-45\,^{\circ}$), and *Loadcase C* (horizontal load). The loads are applied to the lower right edge of the design domain. For all loading scenarios the load is set to $|F| = 10\mathrm{N}$.

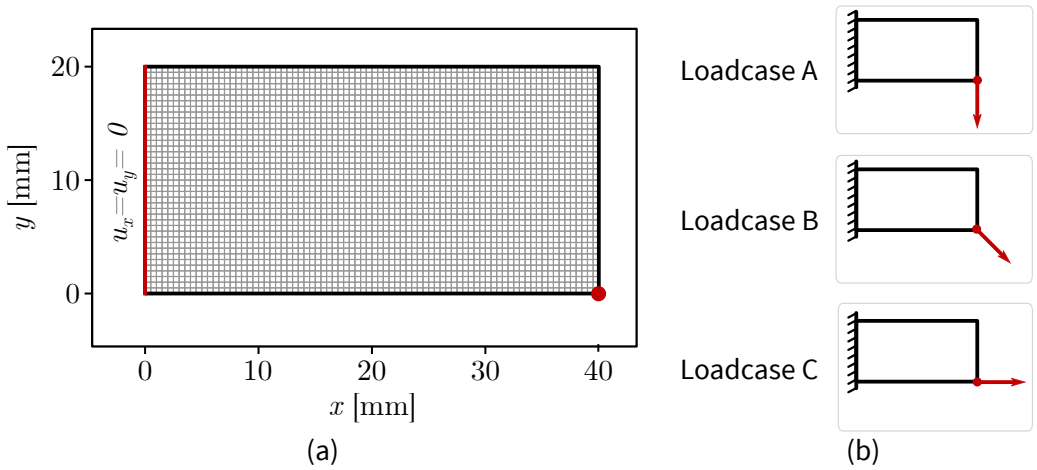

Figure 4.1.: Loading scenarios for comparing the optimization methods for a single loadcase

As the problem of optimizing the topology and material is non-convex, the optimal solution is very sensitive to the initialization. This initialization encompasses the initial material setup (startdesign) as well as control parameters like the scale parameter r_{min} (filter radius) and Evolution Rate ER. Therefore, the influence of the initialization of the model on the optimization results is presented. Furthermore, the influence of the scale parameter r_{min} and its use for mesh-dependency are studied. The algorithms *A*, *AO*, and *AOM-I Single* are compared to the standard topology optimization with quasi-isotropic material *Q-Iso*.

4.1. Comparison of Startdesigns

In Subsection 3.3.1 a strategy for initializing the model, in terms of the initial material setup (startdesign), is proposed. In the framework of this thesis the following startdesigns are investigated:

- Initialization with a quasi-isotropic material (no startdesign)
- Initialization with a unidirectional material oriented at $0\,^{\circ}$
- Initialization with a unidirectional material oriented at $45\,^{\circ}$
- Initialization with a unidirectional material oriented at $-45\,^{\circ}$
- Initialization with a unidirectional material oriented at $90\,^{\circ}$
- Initialization with the procedure proposed in Subsection 3.3.1, i.e., determining a startdesign based on the principal directions of a preliminary FEM analysis. From here on this startdesign is referred to as "PD-startdesign".

The results for the various startdesigns are illustrated in Figure 4.2. As the results show the same tendency for all loading scenarios (A, B, C) , only *Loadcase A* is shown here. The results for *Loadcase B* and *Loadcase C* can be reviewed in Appendix B.1.

The startdesigns (see Figure 4.2), from left to right, are the following: no startdesign, startdesign $0\,^{\circ}$, startdesign $45\,^{\circ}$, startdesign $-45\,^{\circ}$, startdesign $90\,^{\circ}$, and "PD-startdesign". The plot shows the comparison of the compliance for the optimization methods *AO* and *AOM-I Single* relative to the standard topology optimization *Q-Iso*. Furthermore, the optimal topologies resulting from various startdesigns are shown.

The plot reveals, that the *AO*-method is very sensitive to the initialization with regard to the orientation of the material's 1-direction. Especially those startdesigns oriented at $45\,^{\circ}$ and $90\,^{\circ}$ show a significantly higher compliance compared to all other startdesigns. This is also reflected in the optimal topologies which clearly differ from the optimal topologies determined with no startdesign, "PD-startdesign", and startdesigns with an initial orientation of $0\,^{\circ}$ and $-45\,^{\circ}$.

Furthermore, it has been observed that the optimization with the startdesign oriented at $45\,^{\circ}$ and $90\,^{\circ}$ need many more iterations for the objective function to converge (e.g., 79 iterations for the startdesign oriented at $45\,^{\circ}$ as compared to 60 iterations for the PD-startdesign).

In contrast, the method of simultaneously optimizing the topology and material (*AOM-I Single*) does not show a significant dependency of the optimal result on the startdesign. For instance, for the startdesign with $45\,^{\circ}$ the compliance of the final design amounts to the highest compliance value out of all startdesigns ($W_{\text{ex}} = 85.575\,\text{Nmm}$). For the PD-startdesign the compliance of the final design amounts to the lowest compliance value out of all startdesigns ($W_{\text{ex}} = 85.231\,\text{Nmm}$). This corresponds to a difference of $0.4\,\%$.

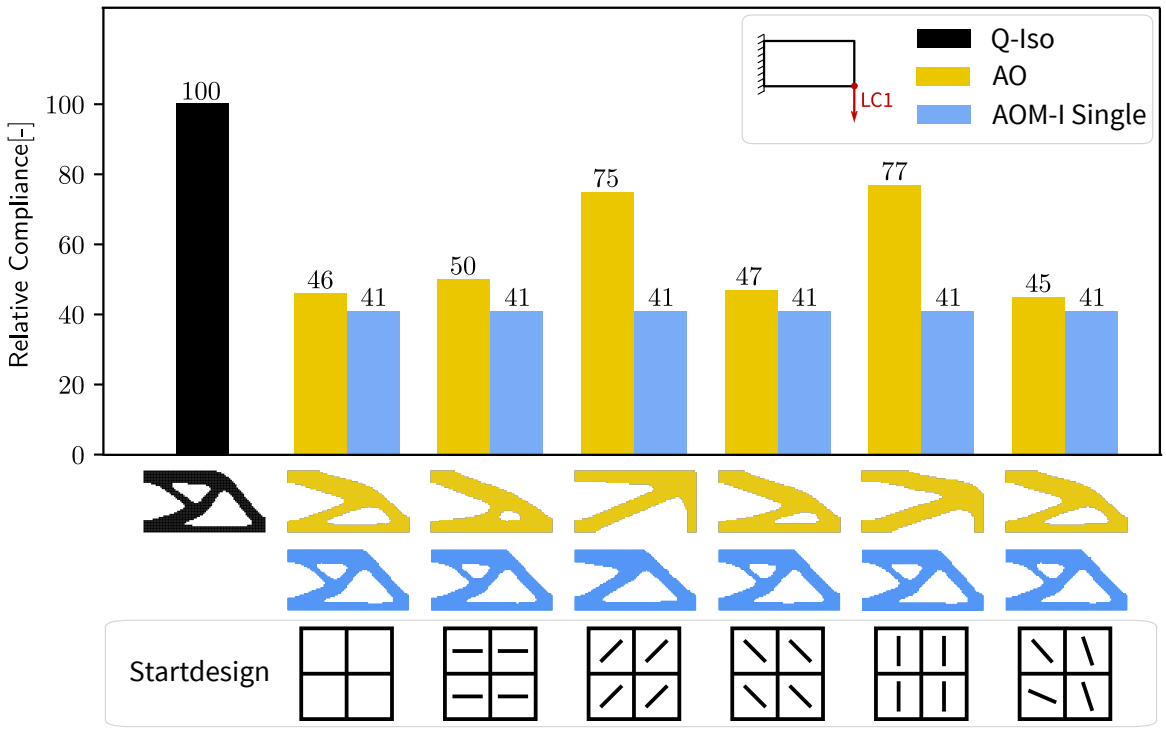

Figure 4.2.: Influence of startdesign on the compliance and final topologies for the optimization methods *AO* and *AOM-I Single* ($m_{\text{size}} = 0.5\,\text{mm}$, $r_{\text{min}} = 3\,\text{mm}$, $ER = 0.01$)

Furthermore, the number of iterations that are needed are more or less the same (e.g., 65 iterations for the startdesign with $45\,^{\circ}$ and 62 iterations for the PD-startdesign). Concerning the optimal topologies, the design proposal determined with a startdesign oriented at $45\,^{\circ}$ shows a slightly different topology. In this case the small shearing triangle (which can be observed with the final topologies of all other startdesigns) is replaced by two thicker bars.

Based on the results shown above it is concluded that the initialization with a startdesign with an orientation based on the principal directions determined with a preliminary finite element analysis (PD-startdesign) is the most suitable as this startdesign also leads to the best performance in terms of compliance for the *AO* method. Therefore, this startdesign is used for all further simulations.

4.2. Influence of Control Parameters

4.2.1. Influence of Filter Radius

As mentioned in Chapter 3, a sensitivity filter scheme is used to avoid the problem of mesh-dependency of the solutions and to eliminate checkerboard patterns. When applying the filter scheme, the sensitivities are heuristically modified as weighted averages of the sensitivities in the mesh-independent neighborhoods. The concept is to take into account the influence of neighbor elements inside a certain "domain of influence" defined by the scale parameter $r_{\min}$ (filter radius). By doing so, the evolution of the sensitivities is expected to become smoother without abrupt discontinuity in the sensitivity distribution. As the filter scheme prevents sharp changes of material sensitivities it is expected that the optimization leads to designs with smoothly varying geometries. However, using sensitivity filtering makes the optimization sensitive to the scale parameter r_{min} as input for the optimization [71]. Therefore, several values for the scale parameter r_{min} are investigated, to show its influence on the complexity of the topology and to draw a conclusion which scale parameter $r_{\min}$ shall be used for the simulations.

Figure 4.3 illustrates the influence of the filter scheme on the sensitivities distribution. The figure exemplarily shows the sensitivities distribution as well as the corresponding final topologies without filter scheme and with filter scheme. The sensitivities are obtained from a simulation using the *AOM-I Single* method for *Loadcase A* with a discretization of $80\,\text{x}\,40$ elements (mesh size $m_{\text{size}} = 0.5\,\text{mm}$) and a scale parameter of $r_{\text{min}} = 1.5\,\text{mm}$. The original sensitivities distribution, without filter scheme, is shown in Figure 4.3 (a1). Figure 4.3 (b1) shows the sensitivities distribution with filtered sensitivities. The corresponding final topologies are shown in Figure 4.3 (a2) and Figure 4.3 (b2). The original sensitivities show a very strong gradient, i.e., they change abruptly from one element to another. Note, an element which is colored in dark gray has a higher sensitivity compared to elements which are colored in light gray. This abrupt change in sensitivities is also reflected in the final design topology,

as elements with a high sensitivity are set to "solid" whereas elements with a low sensitivity are set to "soft" ("void"). The topology in Figure 4.3 (b2) reveals that, besides avoiding mesh-dependency and checkerboard patterns, the filter scheme can be used to control the minimum size of the emerging features in the design domain, i.e., to avoid too detailed structures.

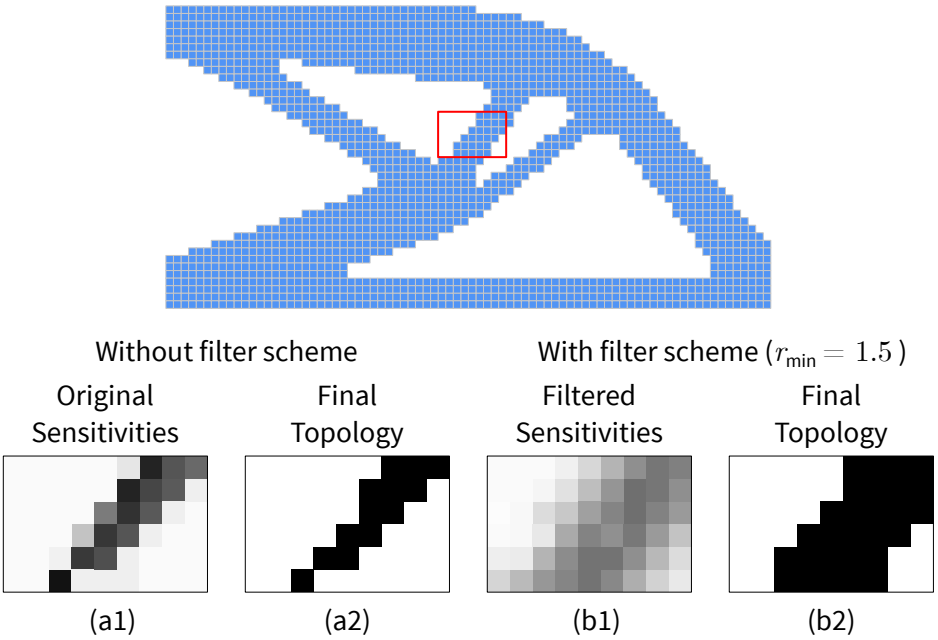

Figure 4.3.: Effect of the filter scheme ($m_{\text{size}} = 0.5\,\text{mm}$, $r_{\text{min}} = 1.5\,\text{mm}$, $ER = 0.01$)

Following the recommendation of Huang et al. [75], that r_{min} should be at least about 1-3 times the size of one element, several values of r_{min} were investigated. A mesh size of $m_{\text{size}} = 0.5\,\text{mm}$ is used for the simulations. For the simulations the scale parameter r_{min} is set to the following values:

n	1	3	6	9
$r_{\text{min}} = n \cdot m_{\text{size}}\,[\text{mm}]$	0.5	1.5	3.0	4.5

Figure 4.4 and Figure 4.5 show the influence of the scale parameter on the compliance W_{ex} for *Loadcase A* and *Loadcase B*. As *Loadcase C* shows the same tendency, the results are shown in Appendix B.2. For the standard topology optimization *Q-Iso*, there is an overall tendency for the compliance to increase with the scale parameter r_{min}. This means, the smaller r_{min}, the better the objective function value. For the *AOM-I Single* method, the compliance determined with different values of r_{min} is within a narrow range (e.g., $25.36\,\text{Nmm}$ for $r_{\text{min}} = 0.5\,\text{mm}$ to $25.61\,\text{Nmm}$ for $r_{\text{min}} = 4.5\,\text{mm}$ for *Loadcase B* which means a difference of $0.9\,\%$).

The topological results for *Loadcase A* (Figure 4.4) and *Loadcase B* (Figure 4.5) show that the use of large filter radii restricts the design field from expressing fine structural features. The largest scale parameter r_{min} used in these simulations ($r_{\text{min}} = 4.5\,\text{mm}$) gives a topology with thicker bars. For a small r_{min} the material distribution is less constrained as there are less elements that influence the behavior of the considered element.

The topological results for $r_{\text{min}} = 0.5\,\text{mm}$ and $r_{\text{min}} = 1.5\,\text{mm}$ show very thin features, especially for the *Q-Iso* method. Generally, such fine features are unwanted, especially with regards to aspects of finite element stress analysis. A minimum value for the scale parameter r_{min} of three times the element size is necessary to maintain that stresses, which represent the basis for the material optimization, are determined accurately. Therefore, for the conducted simulations, it is concluded that a scale parameter $r_{\text{min}} = 3\,\text{mm}$ is sufficient to prevent the formation of too thin features but at the same time offers enough design freedom as compared to larger values of r_{min}. Consequently, this value is used for all further simulations.

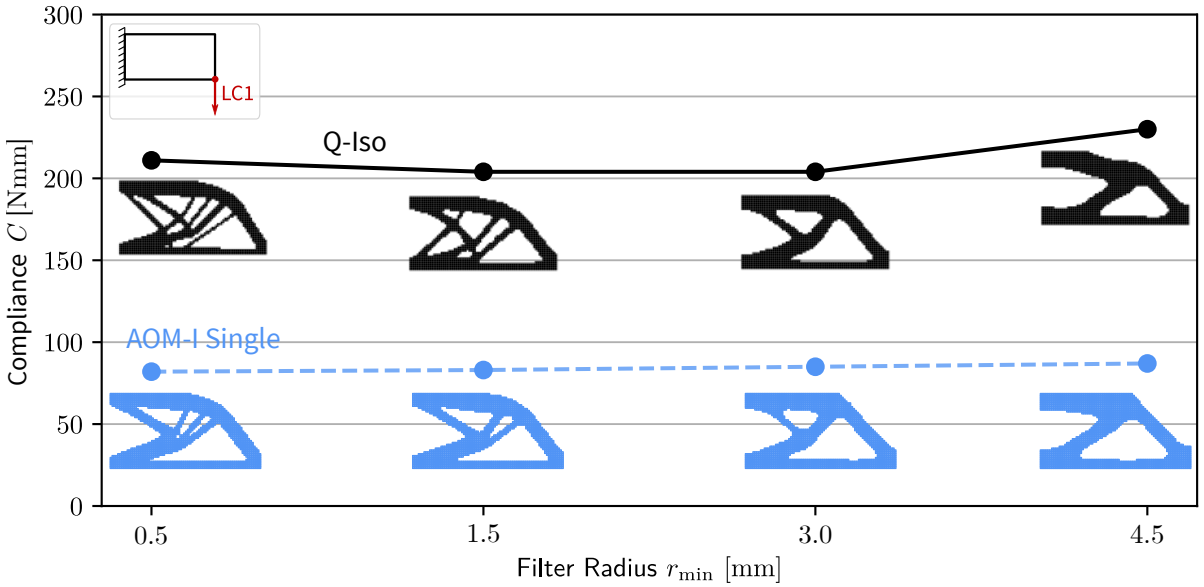

Figure 4.4.: Influence of scale parameter r_{min} on the compliance and final topologies of *Q-Iso* and *AOM-I Single* for *Loadcase A* ($m_{\text{size}} = 0.5\,\text{mm}$, $ER = 0.01$)

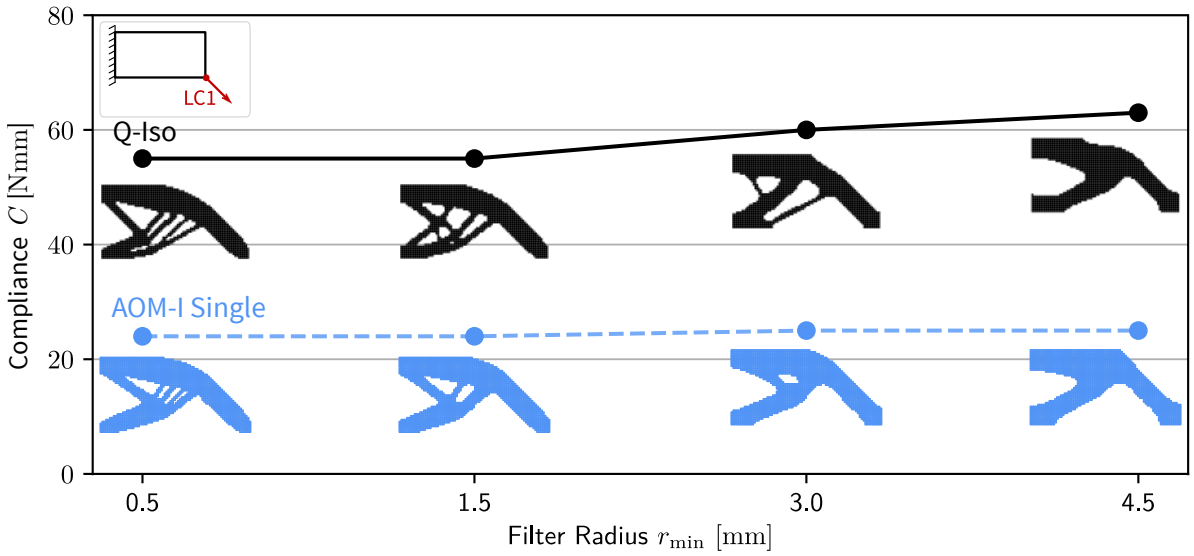

Figure 4.5.: Influence of scale parameter r_{min} on the compliance and final topologies of *Q-Iso* and *AOM-I Single* for *Loadcase B* ($m_{\text{size}} = 0.5\,\text{mm}$, $ER = 0.01$)

4.2.2. Influence of Evolution Rate

Using the BESO algorithm the structural volume is gradually reduced by the so-called Evolution Rate ER until the constrained target volume is reached. Therefore, ER determines the percentage of material to be removed from the design of the previous iteration. In order to evaluate the sensitivity of the optimization regarding the evolution rate ER several simulations are conducted using the following values of $ER = 0.01$, 0.025, and, 0.05. By performing the material removal with a lower evolution rate, less change is applied to the topology at each iteration, i.e., less elements are removed within every iteration. As a logical consequence, a lower evolution rate generally corresponds to a higher number of evolutionary iterations (i.e., number of iterations until the constrained volume fraction is attained). However, the simulations revealed that the number of iterations to convergence (after the attaining the constrained volume fraction of $50\,\%$) does not depend on the evolution rate.

The results in terms of final topology and compliance of the final design for using the aforementioned values of ER are shown for *Loadcase A* in Figure 4.6. The results for *Loadcase B* and *Loadcase C* can be reviewed in Appendix B.2. Figure 4.6 reveals, that for the standard topology optimization *Q-Iso* the topology changes as the evolution rate increases. Furthermore, the compliance significantly increases with higher evolution rates. The compliance of the final designs determined with evolution rates $ER0.01$ and $ER = 0.05$ differs by $28\,\%$. For *AOM-I Single*, the topology for $ER = 0.05$ is different from the topologies determined for $ER = 0.025$ and $ER = 0.01$. However, for $ER = 0.025$ and $ER = 0.01$ the final topologies are almost the same. However, the compliance doesn't significantly change. In this case the compliance of the final designs determined with evolution rates $ER = 0.01$ and $ER = 0.05$ differs by $0.2\,\%$.

As *Loadcase B* and *Loadcase C*, shown in Appendix B.2, show the same tendency as described above it is concluded that the evolution rate of $ER = 0.01$ is a good option for the proposed optimization method and problem. Therefore, this evolution rate is used for all further simulations.

4.3. Mesh-Dependency

To prove the functional capabilities of the implemented filter scheme proposed in Subsection 3.1.2, a study on the mesh-dependency of the optimal design is conducted. The results are presented for *Loadcase A* in Figure 4.7. The optimal topologies as well as the compliance are shown for $r_{\text{min}} = 3\,\text{mm}$ for several mesh sizes. The simulations were conducted with discretization with $20\,\text{x}\,10$ ($m_{\text{size}} = 2.0\,\text{mm}$), $40\,\text{x}\,20$ ($m_{\text{size}} = 1.0\,\text{mm}$), $80\,\text{x}\,40$ ($m_{\text{size}} = 0.5\,\text{mm}$), $160\,\text{x}\,80$ ($m_{\text{size}} = 0.25\,\text{mm}$), and $400\,\text{x}\,200$ ($m_{\text{size}} = 0.1\,\text{mm}$) elements. Again, the results are only displayed for the loading scenario *Loadcase A* as all other loading scenarios show the same tendency.

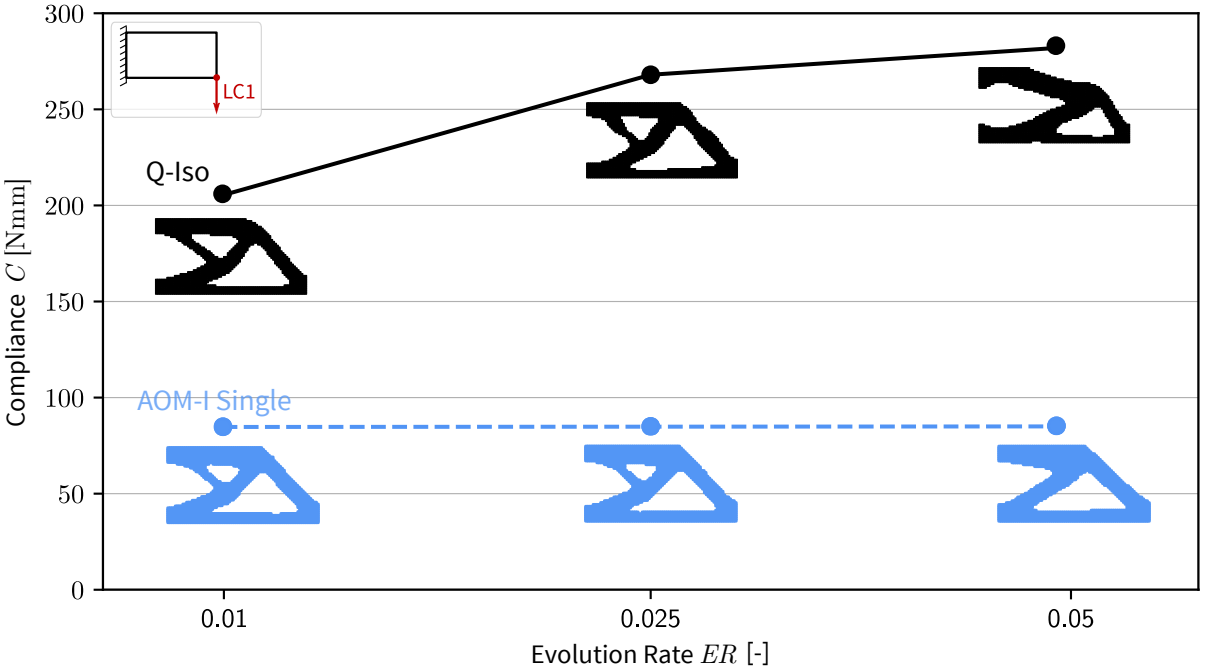

Figure 4.6.: Influence of volume evolution rate ER on the compliance and final topologies of *Q-Iso* and *AOM-I Single* for *Loadcase A* ($m_{\text{size}} = 0.5\,\text{mm}$, $r_{\text{min}} = 3\,\text{mm}$)

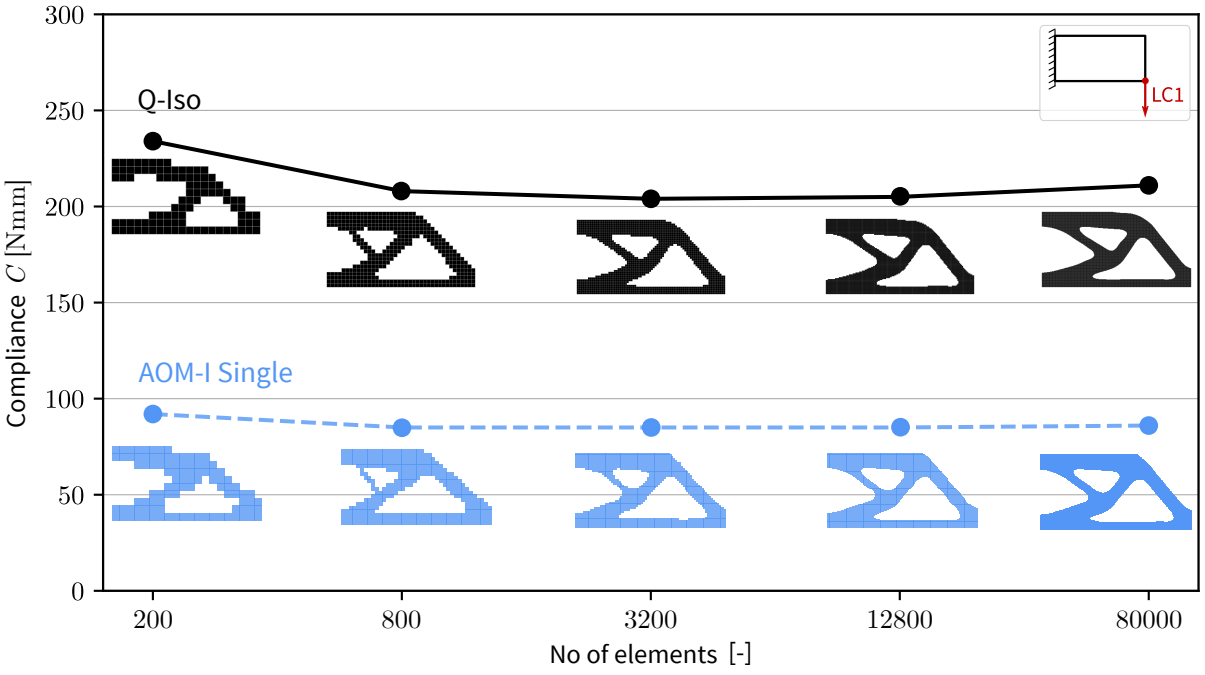

Figure 4.7.: Mesh-independent results for the standard *Q-Iso* topology optimization and the simultaneous optimization method *AOM-I* for *Loadcase A* ($r_{\text{min}} = 3\,\text{mm}$, $ER = 0.01$)

The lowest discretization with 200 elements ($m_{\text{size}} = 2.0\,\text{mm}$) shows a different topology and a slightly higher compliance compared to the discretization with 800 elements ($m_{\text{size}} = 1.0\,\text{mm}$) or higher. For a discretization with 800 elements or higher, the optimal topology does not depend on the discretization in terms of layout and number of bars, for both the *Q-Iso* and *AOM-I* method.

The only difference between the topologies for different discretization is that the boundaries of the structure become smoother when refining the mesh.

Regarding the compliance, Figure 4.7 demonstrates that the *Q-Iso* shows a certain (even if not significant) mesh-dependency in terms of compliance results. For the simultaneous topology and material optimization (*AOM-I*), the solutions are very stable in terms of compliance when using a discretization equal or higher than 800 elements.

4.4. Comparison of Methods Q-Iso, A, AO, and AOM-I Single

4.4.1. Loadcase A

The results of the various optimization methods, namely *Q-Iso*, *A*, *AO*, and *AOM-I Single*, are summarized in Figure 4.8 and Figure 4.9. Figure 4.8 shows the comparison of the relative compliance for all optimization methods. The standard topology optimization *Q-Iso* serves as a reference. A decrease in compliance can be observed for the optimization methods *A*, *AO*, and *AOM-I Single*, compared to *Q-Iso*.

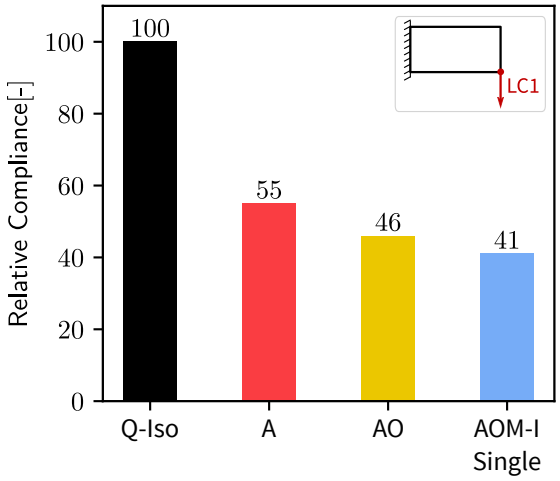

Figure 4.8.: Comparison of the relative compliance of the proposed optimization methods with regard to the compliance of the *Q-Iso* standard topology optimization for *Loadcase A*

Figure 4.9 (a) shows the evolution of the compliance and the volume fraction as a function of the iteration number. The compliance initially increases as the material is gradually removed from the design domain. After 50 iterations the volume fraction reaches its target value of $50\,\%$. In the subsequent iterations, while the volume remains unchanged, the compliance gradually converges to a constant value.

Figure 4.9 (b) shows a detailed illustration of the evolution of the compliance at the very beginning of the optimization procedure. For the standard topology optimization, *Q-Iso*, the sequential removal of elements starts at Iteration 1. Therefore, from this point on the compliance increases.

For all other methods, the sequential removal of elements starts at Iteration 2 after the determination of the startdesign . At Iteration 2 *A*, *AO*, and *AOM-I Single* show a significantly lower compliance compared to *Q-Iso*. The reason is that the startdesign consists of a unidirectional material oriented along the principal directions determined with a the preliminary finite element analysis of the initial structure with quasi-isotropic material. Therefore, the startdesign for *A*, *AO*, and *AOM-I Single* is stiffer compared to the *Q-Iso* design at Iteration 2. The compliance of *AOM-I Single* further decreases towards Iteration 3 as the orientation and the degree of anisotropy are optimized. Apparent bumps in the compliance, e.g., for *AOM-I Single* for iterations 40 to 42, are attributed to a significant change in topology, namely the breaking up of connecting bars. Thereafter, the compliance is quickly recovered.

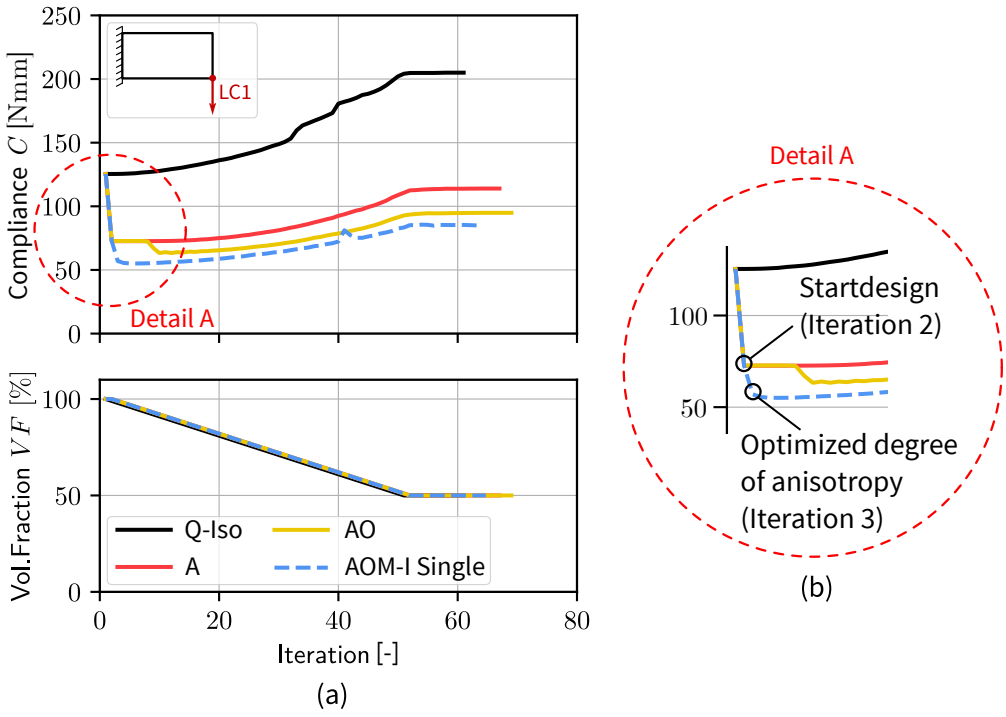

Figure 4.9.: Comparison of compliance for optimization methods for *Loadcase A* ($m_{\text{size}} = 0.5\,\text{mm}$, $r_{\text{min}} = 3\,\text{mm}$, $ER = 0.01$). (a) Evolution histories of compliance and volume fraction, (b) Detailed illustration of the compliance at the very beginning of the optimization procedure

The evolution of topology for *AOM-I Single* is illustrated in Figure 4.10, also showing the elimination of a bar from iteration 40 to iteration 42. This effect of "bar elimination" is even more evident when using a coarser mesh, see Figure 4.11.

The final design topologies for all optimization methods as well as the corresponding material's 1-directions (for *A*, *AO*, and *AOM-I Single*) are shown in Figure 4.12. The final topologies of *Q-Iso* and *AOM-I Single* show similarities, as well as the final topologies of *A* and *AO*. For the orientation optimized unidirectional material (*AO*) and the algorithm *AOM-I Single* the material's 1-direction is aligned with the direction of the principal stress with the highest absolute value within every iteration step.

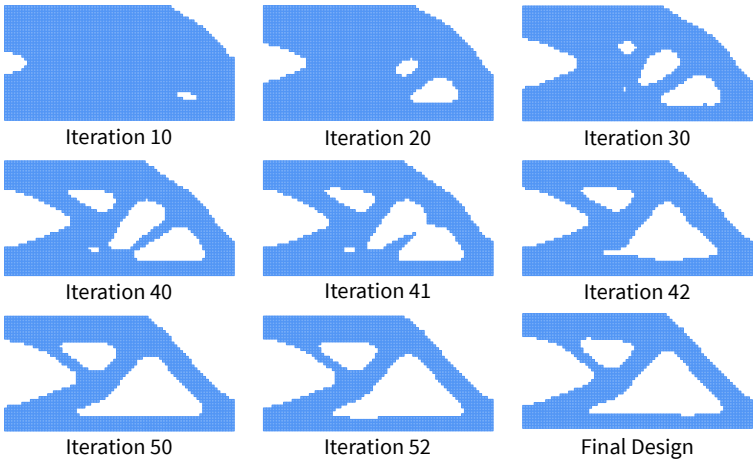

Figure 4.10.: Evolution of topology for optimization method *AOM-I Single*, *Loadcase A*

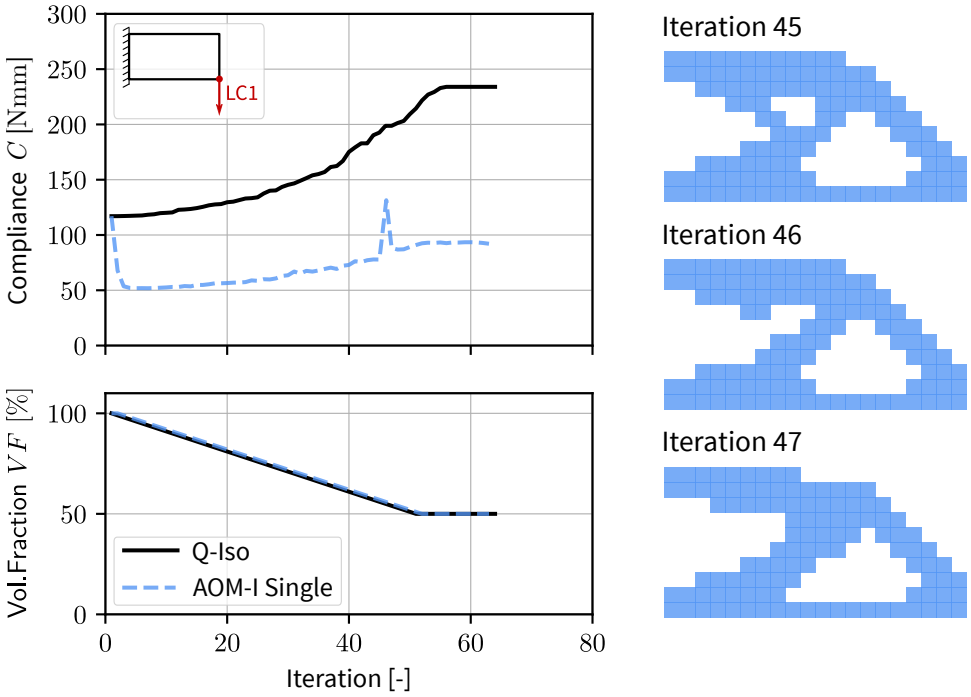

Figure 4.11.: Significant bump in compliance between iteration 45 and iteration 47 for *Loadcase A* using a discretization of 20×10 elements ($m_{\text{size}} = 2\,\text{mm}$, $r_{\text{min}} = 3\,\text{mm}$, $ER = 0.01$)

Since the stress field is continuous throughout the structure, the material orientation is continuous as well, except in areas that are loaded in shear. The optimal material orientation follows the shape of the structure. However, for the structure determined with method *A*, there are regions where the material's 1-direction does not follow the shape of the structure, e.g., in the region highlighted with a black frame in Figure 4.12 (b). The "disorientation" of the material's 1-direction in this region for method *A* is attributed to the fact that the material's 1-direction is still the same as determined for the startdesign. For *AO* the material orientation can be adapted to the "needs" of the structure within every iteration. Therefore, this "disorientation" doesn't occur in the final design for the structure optimized with *AO* as highlighted with a black frame in Figure 4.12 (c).

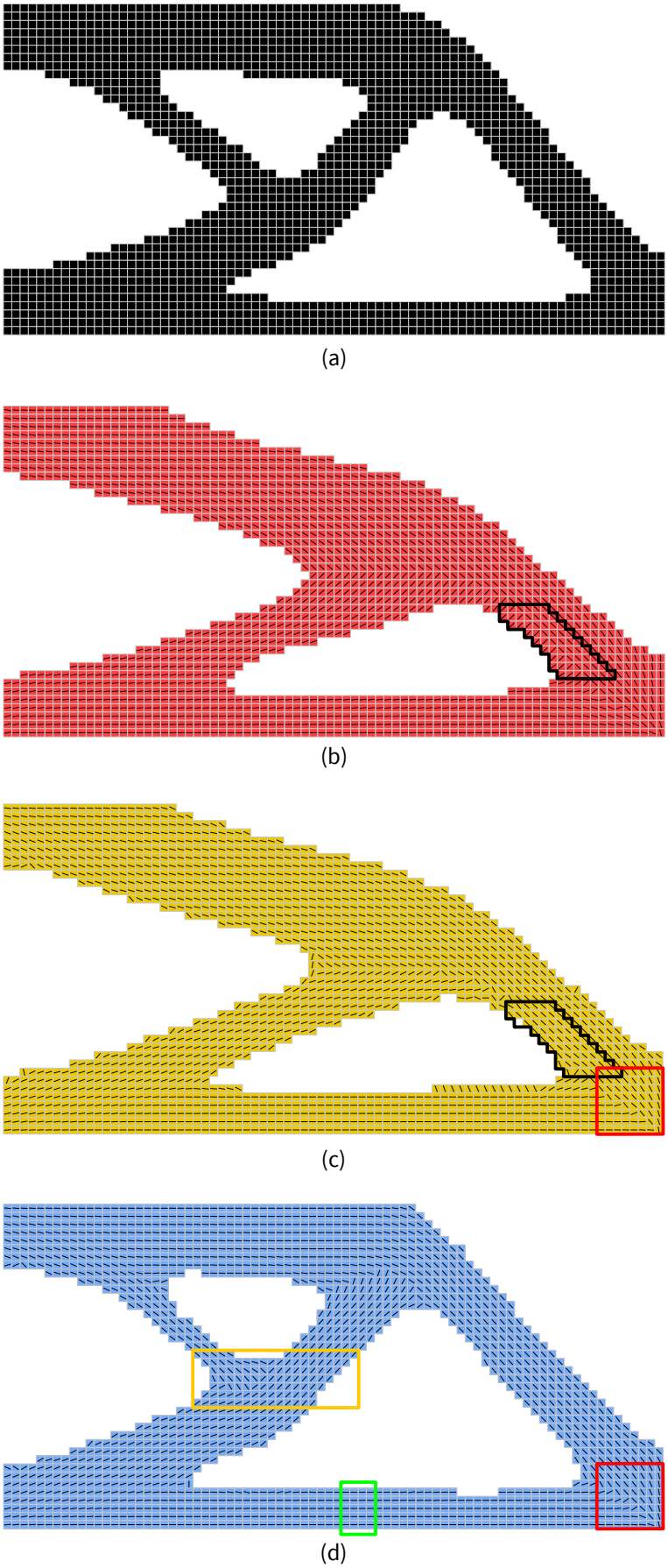

Figure 4.12.: Comparison of the proposed final design topologies and material's 1-directions for *Loadcase A*

The differences between the optimization methods in terms of the materials degree of anisotropy are visualized by stiffness tensor glyphs in Figure 4.13, Figure 4.14, and Figure 4.15. Figure 4.13 shows a comparison of the optimization methods *A* and *AO* for the regions highlighted with a black frame in Figure 4.12 (b) and (c). The visualization of the stiffness tensor glyphs once more points out that for the structure determined with algorithm *A*, for some elements, the material's 1-direction is not aligned correctly with the force flow, i.e., the unidirectional material is not loaded along it's fiber direction and therefore is not optimally used.

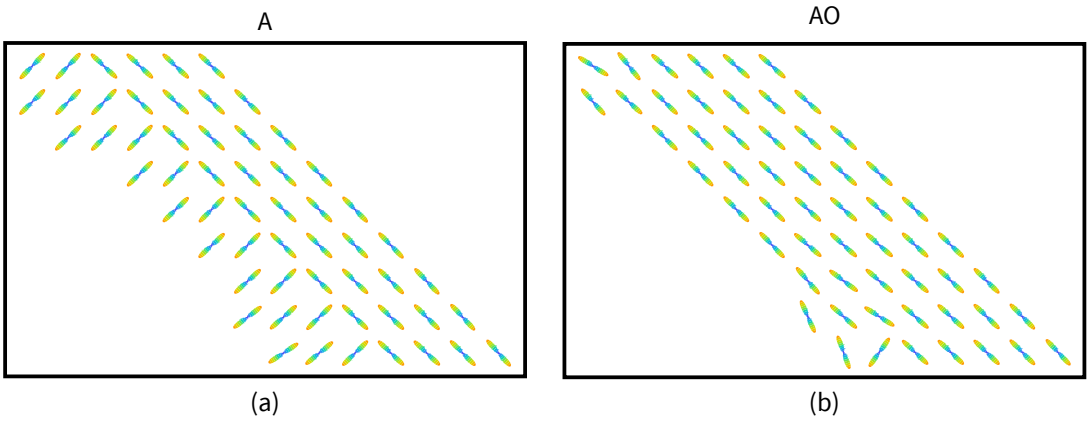

Figure 4.13.: Detailed illustration of the material tensor of the highlighted regions in black in Figure 4.12 (b) and (c) for optimization methods (a) A and (b) AO.

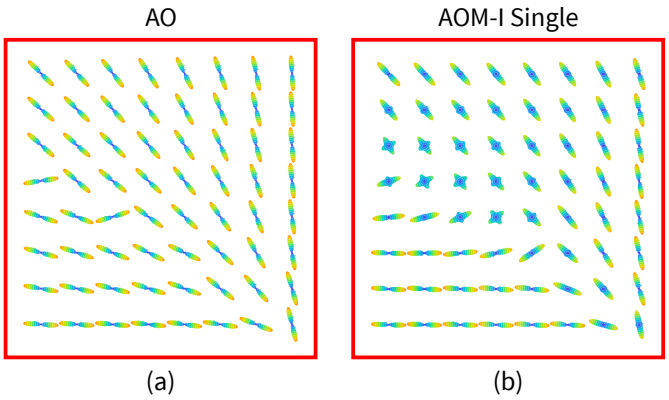

Figure 4.14.: Detailed illustration of the material tensor of the highlighted regions in red in Figure 4.12 (c) and (d) for optimization methods (a) AO and (b) AOM-I.

Figure 4.14 shows a comparison of the optimization methods *AO* and *AOM-I Single* for the regions highlighted with the red frame in Figure 4.12 (c) and (d). In this region, the material's 1-direction shows no significant difference. However, there is a clear difference in degree of anisotropy in the region where the lower bar in compression and the slanted bar in tension intersect. In this region, the material is loaded in shear. Therefore, the optimal material determined with *AOM-I Single* is stiffened in two orthogonal directions, i.e., by adding inclusions of $90\,^{\circ}$. The ability of the material optimized with *AOM-I Single* to bear shear stresses is also the reason why the overall topology of *AO* and *AOM-I Single* clearly differ.

For *AO*, the topology must be adapted in such a way that shear stresses are avoided as much as possible, i.e., avoiding intersections of bars, for instance, like the region highlighted by the yellow frame in Figure 4.12 (d) for *AOM-I Single*. The respective stiffness tensor glyphs are illustrated in Figure 4.15 (a). When shear occurs, the material is stiffened with 0° and 90° inclusions. However, when stress is predominant in one direction, the material is stiffened mainly in one direction. This can be seen in Figure 4.15 for the region highlighted in green in Figure 4.12 (d). The lower bar is loaded in uni-axial compression which is counteracted by using a unidirectional material (i.e., only 0° inclusions).

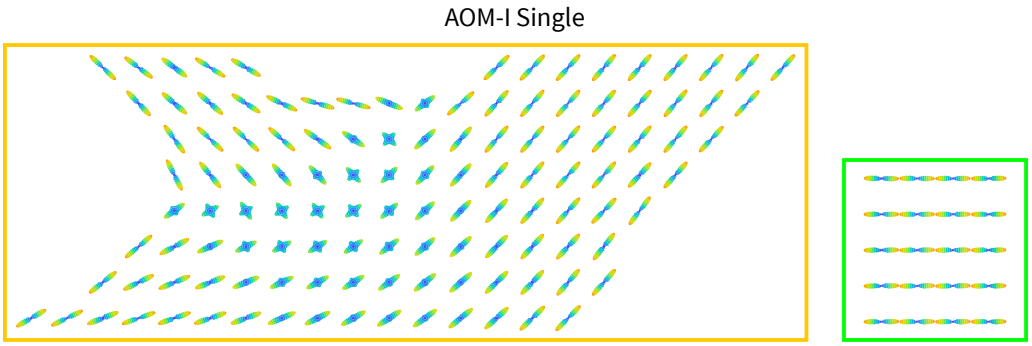

Figure 4.15.: Detailed illustration of the material tensor of the highlighted regions in yellow and green in Figure 4.12 (d) for optimization method AOM-I.

4.4.2. Loadcase C

To confirm the tendency of the results observed for *Loadcase A*, the results of *Loadcase C* are shown here. In this case the cantilever beam is loaded with a horizontal single load at the lower right edge. The results are illustrated in Figure 4.16. Figure 4.16 (a) shows the evolution of the compliance and volume fraction with the optimization iterations. Figure 4.16 (b) shows the comparison of the relative compliance for all optimization methods. As with *Loadcase A*, the standard topology optimization *Q-Iso* serves as a reference. Similar to *Loadcase A*, a decrease in compliance can be observed for the optimization methods *A*, *AO*, and *AOM-I Single*, compared to *Q-Iso*. However, as Figure 4.16 (b) reveals, the difference in performance in terms of compliance between *AO* and *AOM-I Single* for *Loadcase C* is smaller compared to *Loadcase A*.

Figure 4.17 illustrates the final topologies for *Loadcase C* as well as the material's 1-direction of the final design for the optimization methods *A*, *AO*, and *AOM-I Single*. Like for *Loadcase A*, the final topologies determined with *Q-Iso* and *AOM-I Single* show similarities as well as the final topologies determined with *A* and *AO* show similarities. Again, the final design determined with the optimization method *A* shows regions where the material's 1-direction is misaligned leading to a poorer performance in terms of compliance compared to *AO*.

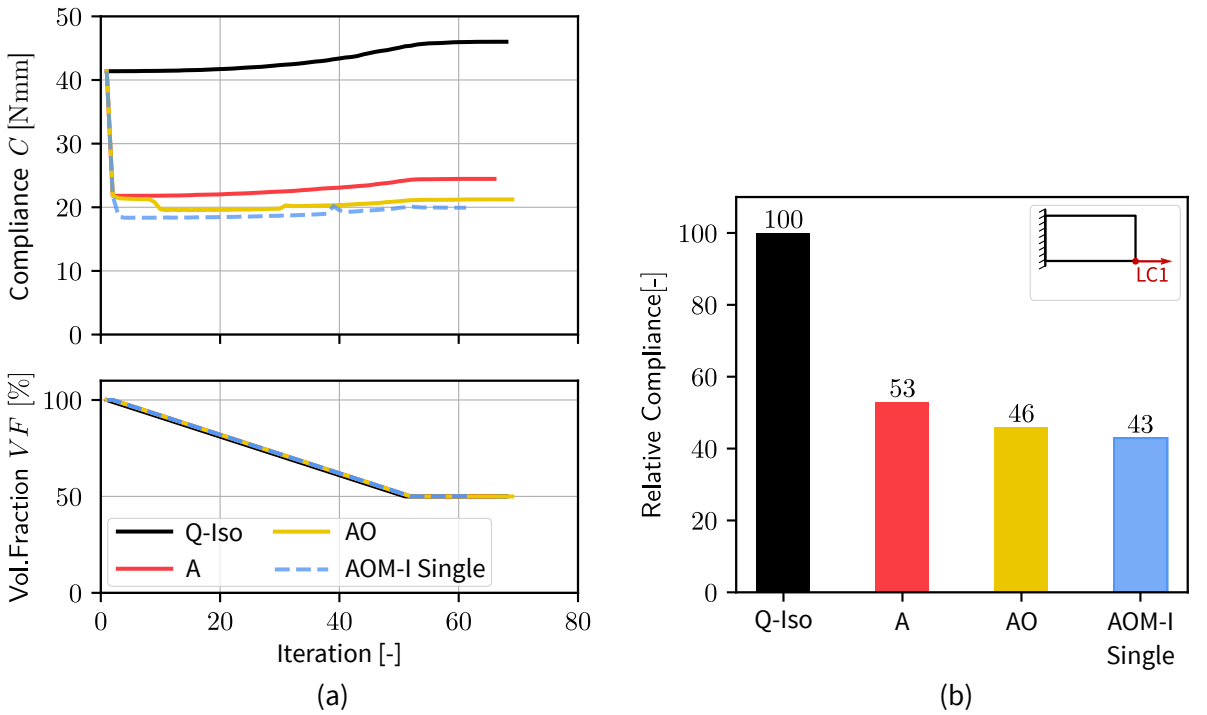

Figure 4.16.: Comparison of compliance for optimization methods for *Loadcase C* ($m_{\text{size}} = 0.5\,\text{mm}$, $r_{\text{min}} = 3\,\text{mm}$, $ER = 0.01$). (a) Evolution histories of compliance and volume fraction, (b) Comparison of the relative compliance of the proposed optimization methods with regard to the compliance of the *Q-Iso* standard topology optimization

The regions highlighted by a red frame in Figure 4.17 (c) for the optimization method *AO* and in Figure 4.17 (d) for the optimization method *AOM-I Single* are compared in detail in Figure 4.18. Figure 4.18 (a) shows the stiffness tensor glyphs for the orientation optimized unidirectional material determined with *AO*. Figure 4.18 (b) shows the stiffness tensor glyphs for the material determined with *AOM-I Single*. The plots reveal that for this region where the load is applied there is almost no difference in material's 1-direction and degree of anisotropy between *AO* and *AOM-I Single* except for some elements. The areas highlighted in blue for *AO* (see Figure 4.17 (c)) and green for *AOM-I Single* (see Figure 4.17 (d)) again reveal that the material of *AO* is not capable of effectively bearing shear stresses whereas *AOM-I Single* is capable of adapting the material in terms of adding inclusions of $90\,^{\circ}$ to stiffen the material loaded in shear, see Figure 4.19. This is also the reason why the structure determined with *AOM-I Single* still performs better than the structure determined with *AO*. However, for *Loadcase C* the regions where unidirectional material is sufficient are predominate. Therefore, the difference in compliance between *AO* and *AOM-I Single* is not as big as for *Loadcase A*.

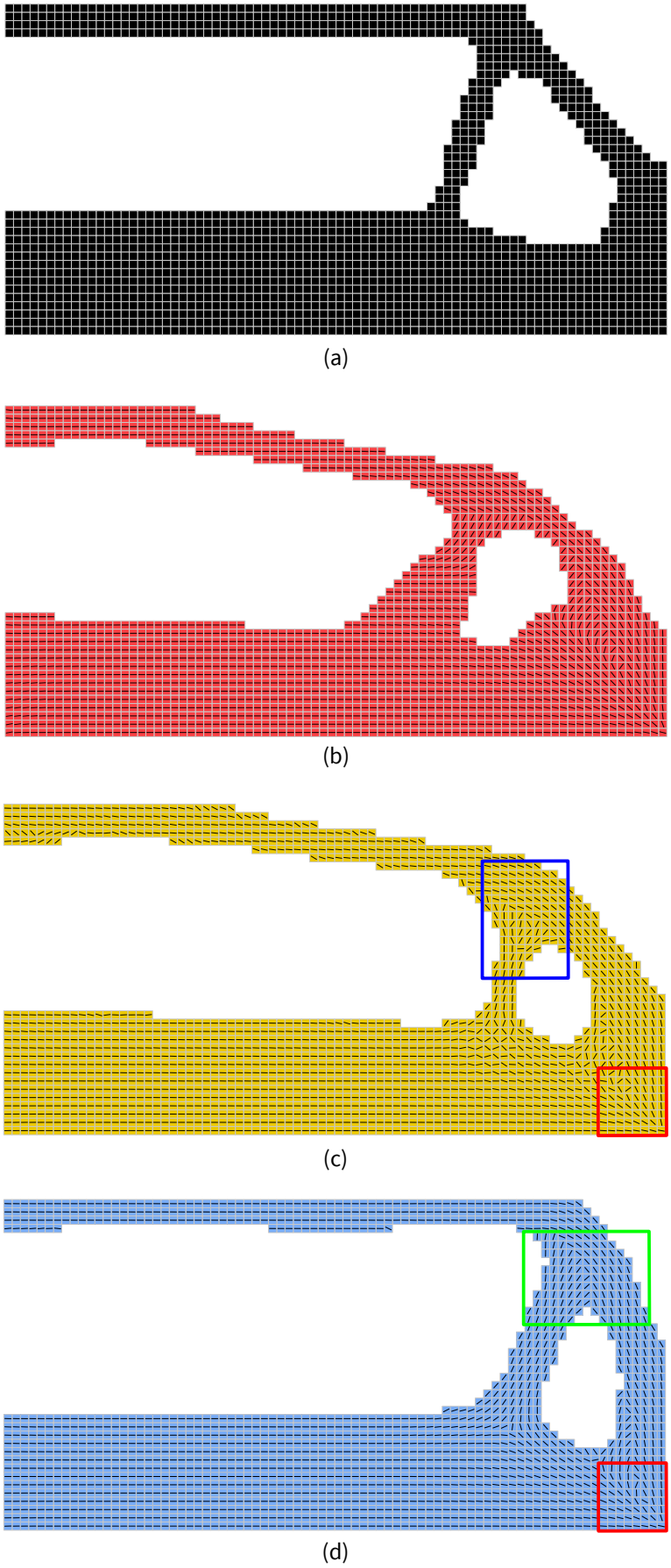

Figure 4.17.: Comparison of the proposed final design topologies and material's 1-directions for *Loadcase C*

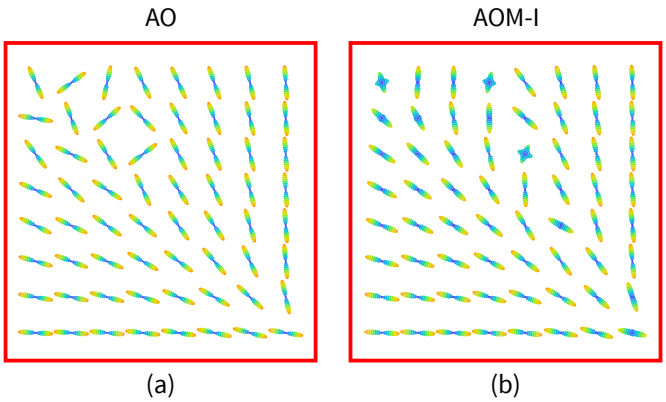

Figure 4.18.: Detailed illustration of the material tensor of the regions highlighted in red for (a) *AO* optimization method and (b) *AOM-I* optimization method.

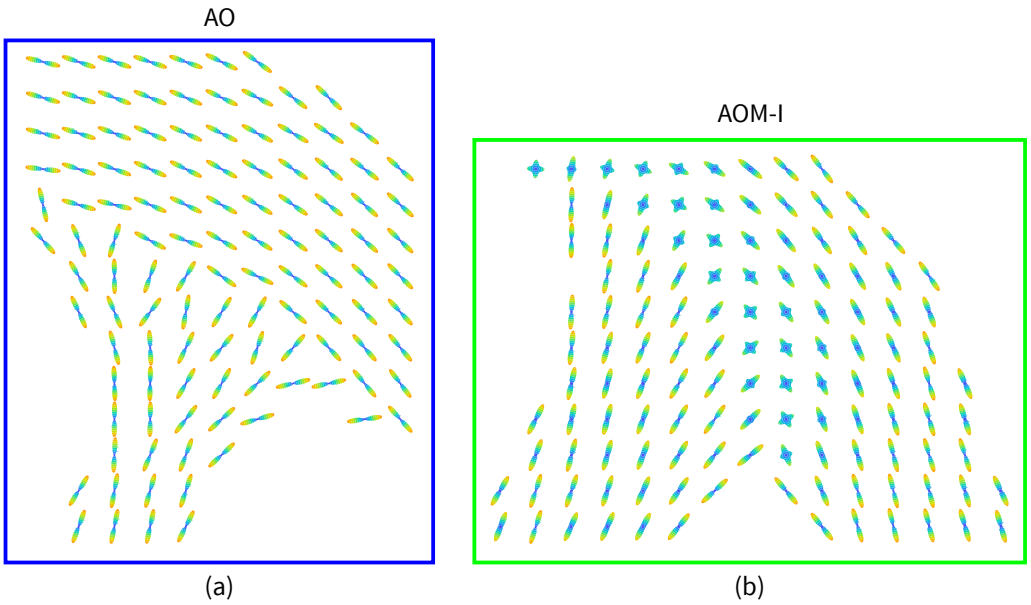

Figure 4.19.: Detailed illustration of the material tensor of the highlighted regions for (a) *AO* optimization method and (b) *AOM-I* optimization method.

4.5. Sequential versus Simultaneous Optimization

So far the results reveal that the full advantage of anisotropy is exploited when optimizing the material orientation and the degree of anisotropy. This can be performed either simultaneously with the optimization of the material distribution (topology) or sequentially. Sequential optimization consists in optimizing first the topology of a structure with a fixed isotropic (or quasi-isotropic) material, and the material anisotropy is optimized for the obtained topology. In contrast, simultaneous optimization consists in finding the optimal topology and the optimal material anisotropy in one step. In this section, the sequential optimization of topology and material and the simultaneous optimization method *AOM-I Single*, as proposed in this thesis, are compared.

As indicated above, sequential optimization requires two steps of optimization. Two sequential optimization methods are proposed for comparison to the simultaneous optimization method:

- *Sequential-I*: For this optimization method the first step is a standard topology optimization with quasi-isotropic material, *Q-Iso*, leading to an optimal topology. This topology stays fixed for the second optimization step. In the second step the optimal material anisotropy, in terms of material orientation and degree of anisotropy, is determined. A modified version of *AOM-I Single* is used for the second step: the material properties are adapted but the topology stays fixed. The second optimization step of *Sequential-I* requires only 1 iteration.

- *Sequential-II*: Again, the first step is a standard topology optimization using the quasi-isotropic material *Q-Iso*. However, in this case the second step of optimization comprises a "full" *AOM-I Single* optimization. In other words, the second optimization step is performed with respect to the material anisotropy but also with respect to the topology.

Figure 4.20 (a) shows the evolution of compliance and volume fraction for *Q-Iso*, *Sequential-I*, *Sequential-II*, and *AOM-I Single* for *Loadcase A*. The detailed results in terms of compliance of the final design as well as total number of iterations are listed in Table 4.1.

Table 4.1.: Compliance and iterations resulting from sequential (two steps) and simultaneous (1 step) optimization

Optimization	Steps	Compliance $[\mathrm{Nmm}]$	Iterations $[-]$
Sequential-I	1: *Q-Iso*	204.996	61
	2: Material anisotropy with fixed topology	87.986	1
Sequential-II	1: *Q-Iso*	204.996	61
	2: *AOM-I Single*	85.231	17
Simultaneous	1: *AOM-I Single*	84.922	62

Regarding the number of iterations, the results show that *Sequential-II* needs more iterations compared to the simultaneous optimization, owing to the fact that the optimization takes place in two steps. After 61 iterations the final design using the *Q-Iso* algorithm is determined. The sequential algorithms, *Sequential-I* and *Sequential-II*, use the material distribution (topology) from *Q-Iso* as basis for further optimization of the structure. Between the first and the second step in the sequential optimization, the compliance significantly drops. The reason is that the material anisotropy is optimized in the second step. Hence, compared to the initial quasi-isotropic structure, the anisotropic one is stiffer. For *Sequential-I*, only one iteration is performed for the second step of optimization as the material properties are only adapted once. The optimization performed in the second optimization step of *Sequential-II* requires 17 iterations. Regarding the performance in terms of minimizing the compliance, *Sequential-II* performs better than *Sequential-I*.

The final compliance obtained by these two optimization methods differs by $3\,\%$. However, the difference in compliance between *Sequential-II* and the simultaneous optimization *AOM-I Single* only amounts to $0.4\,\%$.

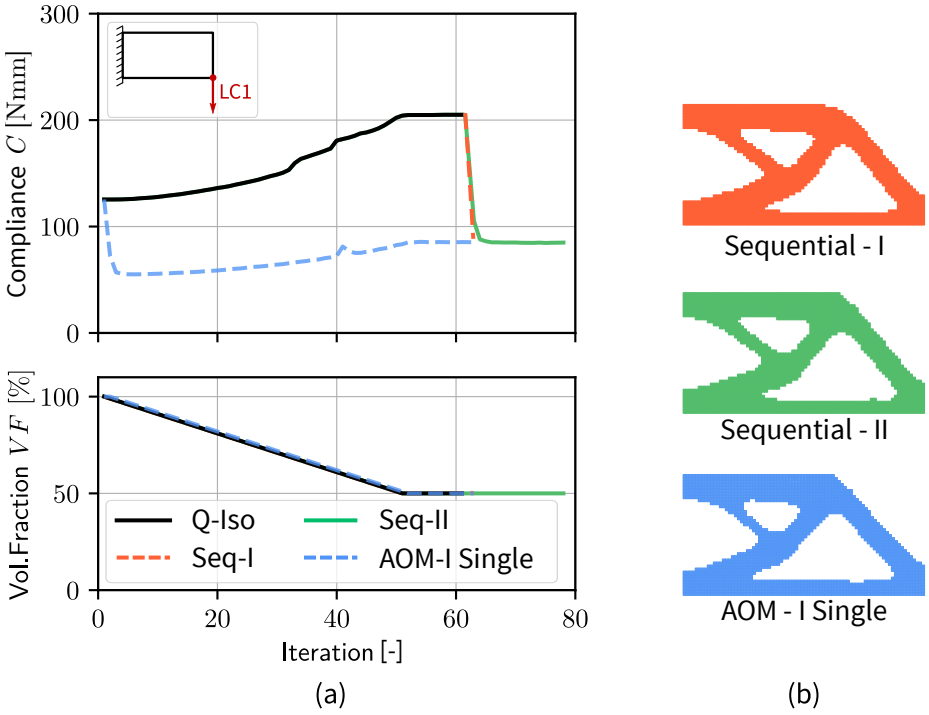

Figure 4.20.: Comparison of sequential and simultaneous optimization for a cantilever beam with dimensions $40\,\mathrm{mm} \times 20\,\mathrm{mm}$ for *Loadcase A* ($m_{\mathrm{size}} = 0.5\,\mathrm{mm}$, $r_{\mathrm{min}} = 3\,\mathrm{mm}$, $ER = 0.01$)

The final topologies for the sequential and the simultaneous algorithm, shown in Figure 4.20 (b), show only minor differences. However, applying the same algorithms to a cantilever beam with dimensions $60\,\mathrm{mm} \times 20\,\mathrm{mm}$ results in final topologies that clearly differ. Furthermore, the difference between *Sequential-I* and *AOM-I Single* increases to $12\,\%$. However, the difference between *Sequential-II* and *AOM-I* still is very low and amounts to $0.17\,\%$.

Figure 4.21.: Comparison of sequential and simultaneous optimization for a cantilever beam with dimensions $60\,\mathrm{mm} \times 20\,\mathrm{mm}$ for *Loadcase A* ($m_{\mathrm{size}} = 0.5\,\mathrm{mm}$, $r_{\mathrm{min}} = 3\,\mathrm{mm}$, $ER = 0.01$)

4.6. Discussion Single Loadcase

The results of the numerical test cases presented in this chapter demonstrate the efficiency of the proposed method of simultaneously optimizing the topology and the material in terms of material orientation and degree of anisotropy (*AOM-I Single*) for a single loadcase.

The influence of the startdesign in terms of the material's 1-direction and material definition (quasi-isotropic / unidirectional) was investigated. The results show that the method of *AOM-I Single* is not overly sensitive to the initialization as opposed to the optimization method *AO*. However, there are minor differences in the compliance of the final design, owing to the fact that the design space is highly non-convex. Consequently, unless a global optimization algorithm is used, different startdesigns lead to different optimal (local) solutions as outlined in Chapter 2. However, the differences between the compliance for the final designs are within a narrow range. The biggest difference for the considered startdesigns amounts to $0.4\,\%$.

The influence of the control parameters for the BESO optimization algorithm, namely the scale parameter r_{min} (filter radius) and Evolution Rate ER, were investigated. The scale parameter r_{min} is needed as input for the filter scheme. The filter scheme, which is a regularization technique, is required to control abrupt discontinuity in the sensitivity distribution in order to prevent numerical problems (checkerboard instabilities or mesh-dependency) and to smooth the final topology. It has to be noted that even if there might be some discontinuity in the anisotropy distribution as well, the anisotropy is not averaged in the framework of this thesis. However, the strategy of averaging the anisotropy could be similar to the strategy of filtering the sensitivities.

The influence of various values for the scale parameter r_{min} on the final topology and the compliance is shown in Section 4.2.1. A larger r_{min} will constrain the optimization to a chunkier type of material distribution, see Figure 4.4 and Figure 4.5. Generally, with increasing r_{min}, fewer void areas are formed inside the topological structure so that a simpler topology is obtained. In turn, if r_{min} is too low the final design shows many very thin strands of material which are unwanted, especially with regard to aspects of finite element simulation. Too thin features are unwanted especially when using lower order elements which use shape function which are unable to exhibit kinematics to represent the correct solution. Furthermore, such fine structures are also unwanted in terms of manufacturability. This further emphasizes a proper choice of the scale parameter r_{min} relative to the element size. The compliance of the final design of the method of *AOM-I Single* shows marginal dependency on the choice of r_{min}. Since the optimal topologies are different, the distribution of anisotropy differs as well. However, obviously the material can be adjusted equally well for different topologies.

The author is not aware of any detailed studies regarding the influence of the evolution rate ER on the results of optimization in terms of final topology and compliance of the final design. Therefore, various values of ER ($ER = 0.01$, $ER = 0.025$, and $ER = 0.05$) were investigated. $ER = 0.01$ corresponds to the lowest value and $ER = 0.05$ corresponds to the highest value reported in literature. The following observation was made: increasing the evolution rate leads to an increase in compliance for the standard topology optimization method *Q-Iso* but shows negligible effect on the compliance for *AOM-I Single*, see Figure 4.6. However, for both optimization methods, the topology for $ER = 0.05$ clearly differs. Recall, using a lower evolution rate implies that less material is removed within every iteration step. Therefore, big changes in topology within one iteration step are avoided. It is concluded that using a lower ER gives the optimization algorithm more time to evolve in the "right direction". Smaller changes in topology lead to smaller changes in material's 1-direction. The degree of anisotropy can be adapted optimally. This is supported by the observations of Huang et al. [52] that very high values of ER may result in local optima. Therefore, a constant value of $ER = 0.01$ is used for all simulations.

Regarding the issue of checkerboards, all simulations show checkerboard-free results. Mesh-dependency refers to the issue that for a specific optimization problem, given a target reduction in volume, the solution depends on the element size within the mesh. It is clearly unreasonable to allow the density of the mesh to control the topological configuration an optimization algorithm will deliver. The results shown in Figure 4.7 reveal, that mesh-dependency with a tendency towards a high level of porosity (i.e., foam-like "filigree" or "fibrous" configuration) doesn't occur. However, it has to be noted that there is always a certain mesh-dependency as certain structures can only evolve with a certain degree of discretization. This effect can be seen in Figure 4.7 for the standard topology optimization *Q-Iso* as well as for the simultaneous method *AOM-I Single* when comparing the final topologies of the discretization with 200 elements ($m_{\text{size}} = 2.0\,\text{mm}$) with all other discretizations. The optimal topologies for a discretization with 800 or more elements show a thin bar oriented at $-45\,^{\circ}$. This bar does not occur in the final topology when using a discretization with 200 elements since the mesh is too coarse. A thin bar oriented at $-45\,^{\circ}$ in the simulation with 200 elements would lead to "1-node hinges". The reason why such a bar does not occur in the design is that the filter scheme suppresses such "1-node hinges" as long as the scale parameter r_{min} is larger than the element size. The results furthermore show that a discretization using 3200 elements ($m_{\text{size}} = 0.5\,\text{mm}$) is sufficient for the simulations as all finer meshes lead to smoother boundaries but do not influence the results in terms of topology and compliance. Furthermore, finer meshes would imply a significantly higher computational effort which in this case does not represent any added value for the results of the simulations.

With the optimization methods presented in this thesis (*Q-Iso*, *A*, *AO*, and *AOM-I* Single) additional degrees of freedom (in terms of anisotropy distribution) are gradually added to the optimization procedure. By performing a topology optimization using a quasi-isotropic material (*Q-Iso*), the advantage of directionality of material properties is not exploited. Optimizing the material orientation in addition to the topology (*AO*) permits to take advantage of the

directionality of properties. Using the same constraint on the volume fraction the cantilever beam with optimized topology and material orientation (*AO*), is stiffer than a topology optimized structure made of quasi-isotropic material. As the stress field is continuous, the material's 1-direction (aligned with the direction of the principal stress with the highest absolute value) is continuous. The direction changes continuously throughout the structure, except on areas where bars intersect. In these areas, the material is loaded in shear. One step further, to take full advantage of material anisotropy, is to consider the degree of anisotropy in addition to the material distribution and the material orientation, in the design process (*AOM-I Single*). The proposed algorithm *AOM-I Single* is the least restrictive algorithm, leading to a general orthotropic material by adding inclusions of 0° and 90° with respect to the optimized material's 1-direction. It gives the most optimal material that can be reached inside the design space of a general orthotropic material. This ideal material goes beyond quasi-isotropic and orientation optimized unidirectional material (*AO*) as it can be fully adapted to the local loading conditions and is directly optimized for the functional needs at the structural scale. In other words, the material is used to its full potential. The ability of the material for *AOM-I Single* to adapt to the local loading conditions (i.e., shear stresses) is also the reason why the final topology shows similarities with the final topology determine with *Q-Iso* but clearly differs from the topologies determined with *A* and *AO*.

To verify the numerical effectiveness of the simultaneous method to allocate the optimal material distribution (topology) and anisotropy, the *AOM-I Single* method was compared to a sequential optimization of topology and material. The method of sequential optimization is based on the idea of the so-called "black metal" design. A "black metal" solution is a composite structure whose shape is derived from the former metallic structure. This process is mimicked in the optimization method *Sequential-I* where the optimization is divided into two steps: first, the optimal topology is determined using the standard topology optimization method *Q-Iso* for a quasi-isotropic material. Second, for the fixed topology, the optimal material in terms of material orientation and degree of anisotropy is determined. In contrast, for the simultaneous optimization *AOM-I Single*, there is no need to "guess" the initial shape (i.e., topology) of the structure that shall be used for the optimization of the anisotropic material. Throughout the optimization the anisotropy distribution depends on the stress field that in turn depends on the topology. This emphasizes the influence of the material anisotropy on the optimal topology and vice versa. The numerical results prove the relevance of the simultaneous optimization, since its resulting solution is stiffer than the solution for the sequential optimization *Sequential-I*. The simultaneous optimization *AOM-I Single* is also compared to an alternative formulation of sequential optimization, namely *Sequential-II*. *Sequential-II* first performs a standard topology optimization with quasi-isotropic material. This design serves as startdesign for a subsequent simultaneous optimization of topology and material *AOM-I Single*. The small difference in performance, in terms of compliance, between *Sequential-II* and *AOM-I Single* supports the observation that the *AOM-I Single* method is not overly sensitive to the startdesign. However, the final topologies of *Sequential-II* and *AOM-I Single* clearly differ supporting the fact that the design space is highly non-convex with several (even if almost equally good) local minima.

5. Application of the Method to Multiple Loadcases

The aim of this chapter is to present the results and the performance of the update schemes proposed in Subsection 3.2.3 when the method of simultaneously optimizing topology and material (orientation and degree of anisotropy) is extended to multiple loadcases. Therefore, the optimization algorithms proposed in Chapter 3, *Q-Iso*, *AOM-I Multiple*, *AOM-II*, and *AOM-III*, are compared. The main differences between those methods lies in how the material orientation and degree of anisotropy is updated. Therefore, the proposed methods are briefly summarized again in Table 5.1. For the simulations two loadcases are considered: a design loadcase (denoted as LC1) and a second loadcase (denoted as LC2).

Table 5.1.: Optimization methods for multiple loadcases

	Topology		Material 1-Direction		Degree of Anisotropy	
	LC1	LC2	LC1	LC2	LC1	LC2
Q-Iso	✓	✓	✗	✗	✗	✗
AOM-I	✓	✓	✓	✗	$0\,^{\circ}/90\,^{\circ}$	✗
AOM-II	✓	✓	✓	✗	$0\,^{\circ}/90\,^{\circ}$	θ_3/θ_4
AOM-III	✓	✓	✓	✗	$0\,^{\circ}/90\,^{\circ}$	$\pm 45\,^{\circ}$

The setup of the numerical test cases, introduced in Chapter 4 for the single loadcase, is used with respect to optimization objective and constraint, size of the design domain, discretization ($m_{\text{size}} = 0.5\,\text{mm}$), and boundary conditions. Furthermore, the control parameters for the filter scheme and the BESO algorithm remain unchanged: $r_{\text{min}} = 3\,\text{mm}$ and $ER = 0.01$. In Figure 5.1 (b) the loading scenarios which are used for the simulations are shown. Each of these loading scenarios represent a combination of two loadcases, already presented in the previous chapter. *Loadcase AC* is a combination of a vertical load applied to the lower right edge of the structure (same as *Loadcase A* in Chapter 4) and a horizontal load applied to the upper right edge of the structure (symmetric to *Loadcase C* in Chapter 4). *Loadcase BB* represents a symmetric loading of the cantilever beam. In this case, *Loadcase B*, which is applied to the lower right edge of the structure, is mirrored around the middle plane. For *Loadcase AC* the vertical load at the lower right edge is defined as the design loadcase (LC1). The horizontal load at the upper right hand is chosen as *Loadcase 2* (LC2). For *Loadcase BB* the load at the lower right edge is used as the design loadcase. Therefore, this load is chosen as *Loadcase 1* (LC1). The load at the upper right hand is chosen as *Loadcase 2* (LC2).

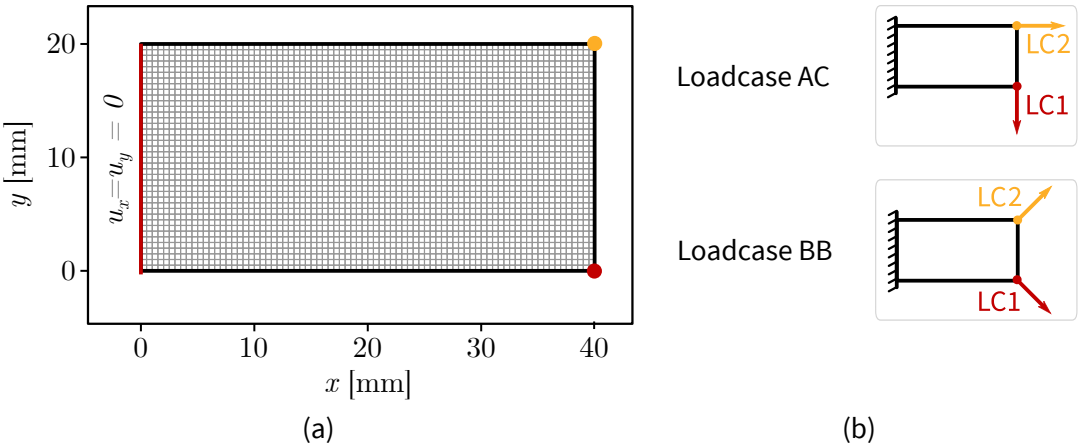

Figure 5.1.: Loading scenarios for comparing the optimization methods for multiple loadcases

For *Loadcase 1*, acting on the lower right edge of the design domain, the translational degrees of freedom (x- and y-direction) of the nodes of this edge are coupled to a reference point. The concentrated force is applied to this reference point. Similarly, for *Loadcase 2*, the translational degrees of freedom (x- and y-direction) of the nodes of the upper right edge are coupled to a reference point. The concentrated force is applied to this reference point. The loads are set to $|F| = 10\mathrm{N}$ for all loading scenarios.

5.1. Comparison of Startdesigns

Similar to the single loadcase several startdesigns are compared. The results for *Loadcase AC* are shown in Figure 5.2 for the optimization method *AOM-II* and in Figure 5.3 for the optimization method *AOM-III*. Each figure shows the compliance of the design loadcase (*Loadcase 1*) and *Loadcase 2* relative to the compliance determined with the standard topology optimization *Q-Iso*. Regarding *Loadcase 1*, for both optimization methods, *AOM-II* and *AOM-III*, there is no significant difference between the compliance of the final design for the investigated startdesigns. For instance for *AOM-II*, the difference between the compliance for the optimization with "no startdesign" and the optimization with "PD-startdesign" amounts to $0.02\,\%$. For *AOM-III*, the difference between "no startdesign" and "PD-startdesign" amounts to $0.13\,\%$. The compliance results for *Loadcase 2* clearly show differences, depending on the startdesign. For both loadcases, the best result in terms of minimum compliance is gained when the "PD-startdesign" is used.

Figure 5.2 and Figure 5.3 also show the optimal topologies determined with different startdesigns for the optimization. The final topologies for no startdesign and a startdesign with $90\,^{\circ}$ clearly differ from the topologies gained with the other startdesigns.

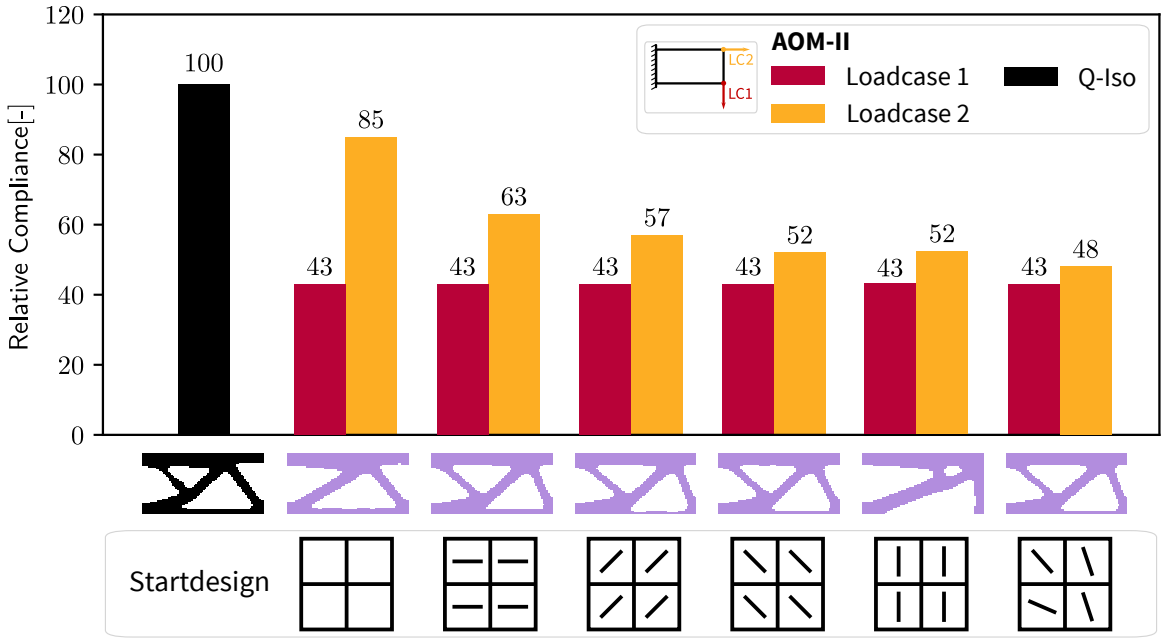

Figure 5.2.: Influence of startdesign on compliance and final topologies for the optimization method *AOM-II* for *Loadcase AC* ($m_{\text{size}} = 0.5\,\text{mm}$, $r_{\text{min}} = 3\,\text{mm}$, $ER = 0.01$)

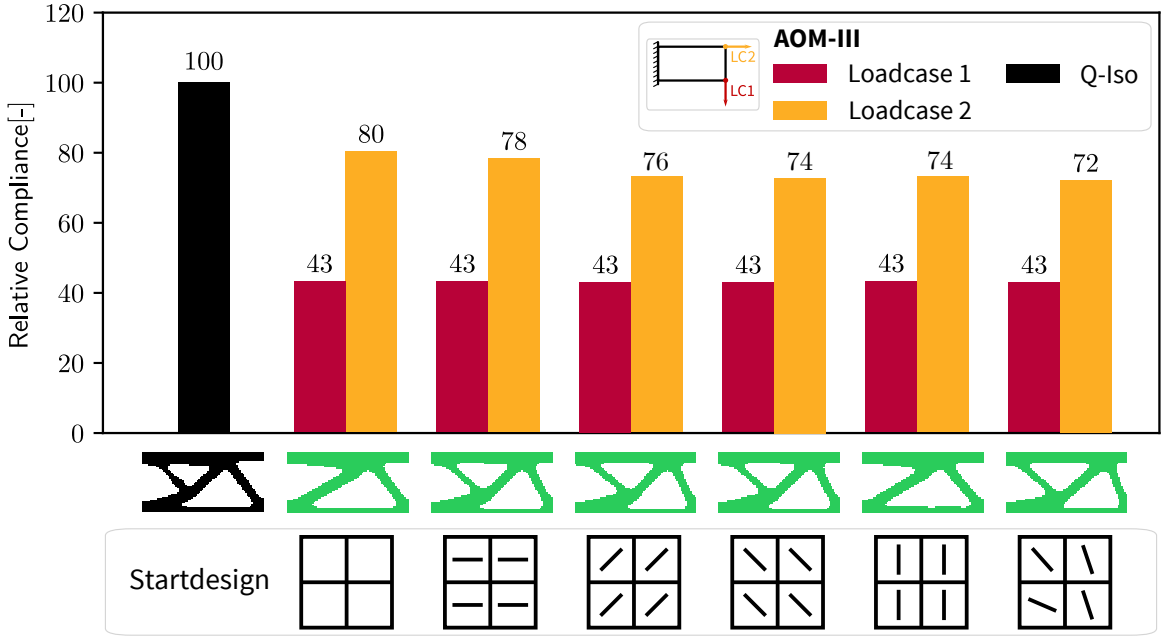

Figure 5.3.: Influence of startdesign on compliance and final topologies for the optimization method *AOM-III* for *Loadcase AC* ($m_{\text{size}} = 0.5\,\text{mm}$, $r_{\text{min}} = 3\,\text{mm}$, $ER = 0.01$)

5.2. Influence of Control Parameters

Similar to the results for the single loadcase, the results for multiple loadcases show no mesh-dependency and checkerboard patterns.

5.2.1. Influence of Filter Radius

As for the single loadcase, the choice of the scale parameter r_{min} and its influence on the final topology as well as the compliance of the optimized design is investigated. Figure 5.4 shows the compliance of the final design determined with various r_{min} and different optimization methods (*AOM-I Multiple*, *AOM-II*, and *AOM-III*). Figure 5.5 shows the respective final topologies.

Like for the single loadcase, a lager scale parameter r_{min} restricts the design field from expressing fine structural features. In turn, a small scale parameter r_{min} ($r_{\text{min}} = 0.5\,\text{mm}$) leads to very thin structures. Regarding the compliance of the final design, *Loadcase 1* shows a slight increase in compliance with increasing r_{min}. The design determined with $r_{\text{min}} = 4.5\,\text{mm}$ shows a significantly higher compliance compared to lower values of r_{min}. For *Loadcase 2* the compliance of the design determined with $r_{\text{min}} = 4.5\,\text{mm}$ is clearly lower compared to the design with $r_{\text{min}} = 3.0\,\text{mm}$ and $r_{\text{min}} = 1.5\,\text{mm}$ and slightly lower than the compliance for the design determined with $r_{\text{min}} = 0.5\,\text{mm}$.

The results for *Loadcase BB* can be reviewed in Appendix C.1.

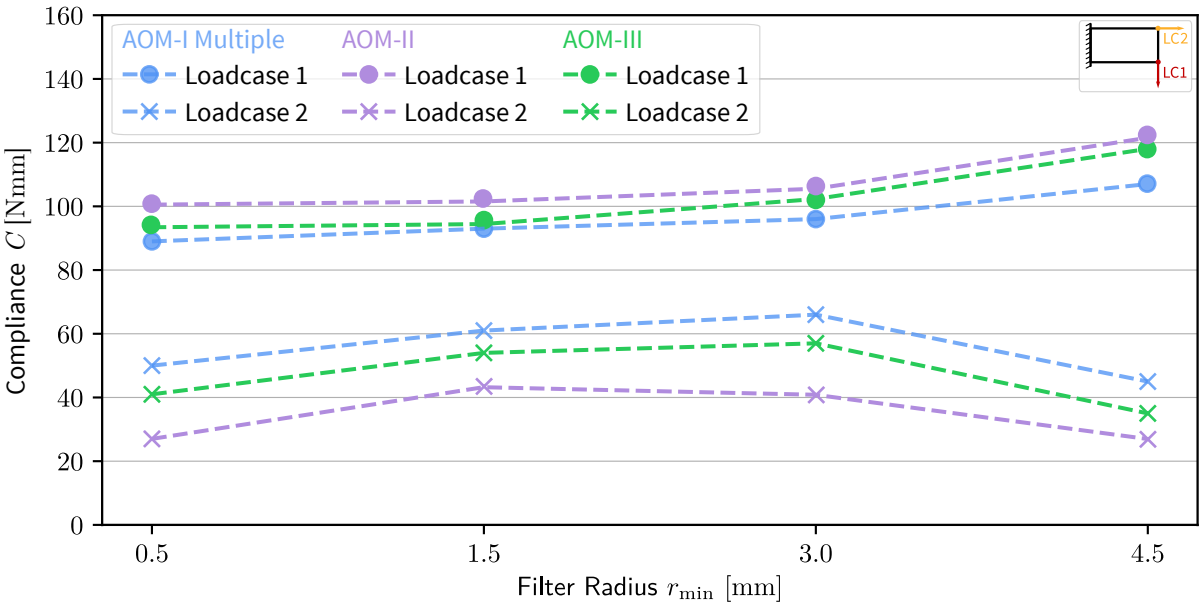

Figure 5.4.: Influence scale parameter r_{min} on the compliance of *AOM-I Multiple*, *AOM-II*, and *AOM-III* for *Loadcase AC* ($m_{\text{size}} = 0.5\,\text{mm}$, $ER = 0.01$)

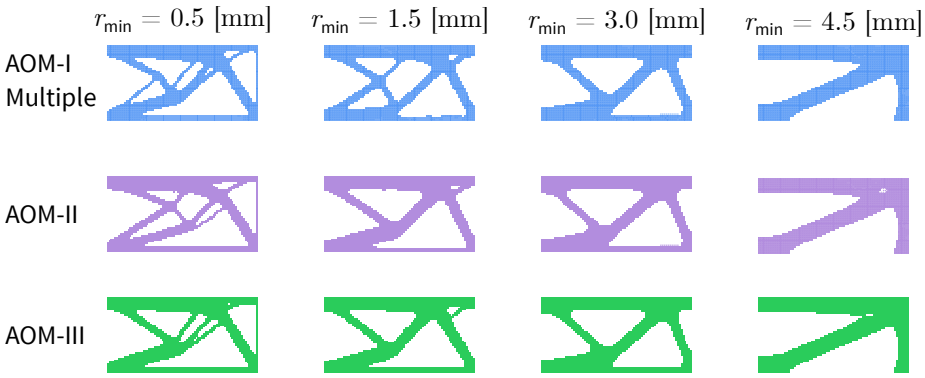

Figure 5.5.: Influence scale parameter r_{min} on the final topologies of *AOM-I Multiple*, *AOM-II*, and *AOM-III* for *Loadcase AC* ($m_{\text{size}} = 0.5\,\text{mm}$, $ER = 0.01$)

5.2.2. Influence of Evolution Rate

Similar to the single loadcase, the sensitivity of the optimization regarding the volume evolution rate ER is investigated. Therefore, simulations were conducted using several different values of $ER = 0.01, 0.025$, and, 0.05. The results, shown in Figure 5.6, reveal that the evolution rate has minor influence on the compliance of *Loadcase 1*. For instance, for *AOM-I Multiple*, the difference in compliance between $ER = 0.01$ and $ER = 0.05$ amounts to $0.5\,\%$ which is in the same range as observed for *AOM-I Single*, see Section 4.2.2.

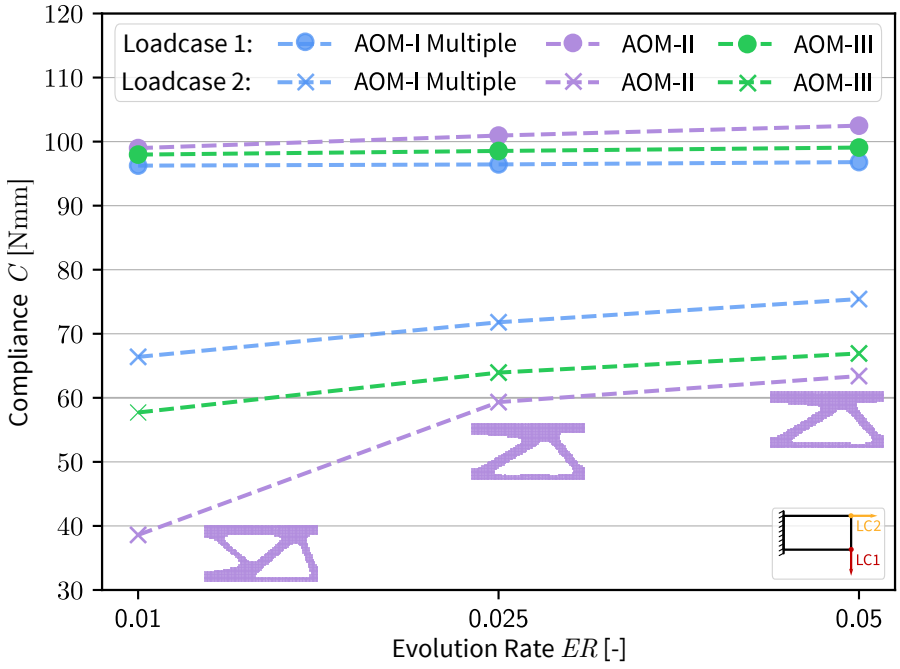

Figure 5.6.: Influence of volume evolution rate ER on the compliance of the final designs for *AOM-I Multiple*, *AOM-II*, and *AOM-III* for *Loadcase AC* ($m_{\text{size}} = 0.5\,\text{mm}$, $r_{min} = 3\,\text{mm}$).

For *AOM-II* and *AOM-III* the difference in compliance between $ER = 0.01$ and $ER = 0.05$ amounts to $3.4\,\%$ and $1.1\,\%$. However, the differences between the compliance determined with $ER = 0.01$ and $ER = 0.05$ are more significant for the second loadcase: $11.9\,\%$ for *AOM-I Multiple*, $40\,\%$ for *AOM-II*, and $13\,\%$ for *AOM-III*.

AOM-II shows the highest difference in compliance between the designs gained with different evolution rates. This is also reflected in the final topologies that clearly differ, see Figure 5.6. The results for further loading scenarios (*Loadcase BB* and *Loadcase BC*) can be reviewed in Appendix C.1.

5.3. Comparison of Methods Q-Iso, AOM-I Multiple, AOM-II, and AOM-III

5.3.1. Loadcase AC

When dealing with multiple loadcases, compromises are made at each iteration of the evolutionary process among these loadcases. The final structure is the optimal design in the sense that every part of the remaining material has its own role to play for at least one loadcase and possibly for all loadcases. Regarding the update of the topology, multiple loadcases mean that if an element is needed for any of the loadcases it is set to "solid". Only when an element is considered as being "inefficient" for both loadcases it is set to a very soft material and is removed from the design. As a logical consequence, the final topology for multiple loadcases clearly differs from the topologies that are gained when optimizing for single loadcases. This is exemplarily illustrated for the standard topology optimization of a quasi-isotropic material *Q-Iso* in Figure 5.7. However, of course, for the quasi-isotropic case it makes no difference which of the loadcases is seen as the design loadcase.

Figure 5.7.: Optimal design of the cantilever beam determined with the standard topology optimization method *Q-Iso*. (a) Optimized for *Loadcase A* (LC1), (b) Optimized for *Loadcase C* (LC2), (c) Optimized for both loadcases (*Loadcase AC*).

The evolution of compliance and volume fraction for both loadcases are shown in Figure 5.8. The compliance curve for *Loadcase 2* shows a significant bump at the very beginning of the optimization. This bump occurs as the second loadcase is ignored for the definition of the startdesign for the optimization. The startdesign is determined solely based on the design loadcase (*Loadcase 1*). Therefore, for the first iteration of *Loadcase 1*, the structure is stiffer than the quasi-isotropic design whereas for *Loadcase 2* it is less stiff than the quasi-isotropic design.

Figure 5.8 reveals that the anisotropic optimization algorithms (*AOM-I Multiple*, *AOM-II*, and *AOM-III*) require more iterations to converge than the standard quasi-isotropic topology optimization. Note, the convergence error defined in Section 3.3.2 ($\varepsilon_{\text{tol}}^{\text{LC1}} = 0.001$, $\varepsilon_{\text{tol}}^{\text{LC2}} = 0.005$) is checked for both loadcases irrespective of the optimization method that is used. The convergence error for *Loadcase 2* is not as stringent as for *Loadcase 1* since the focus of the optimization is on *Loadcase 1* which is considered as design loadcase.

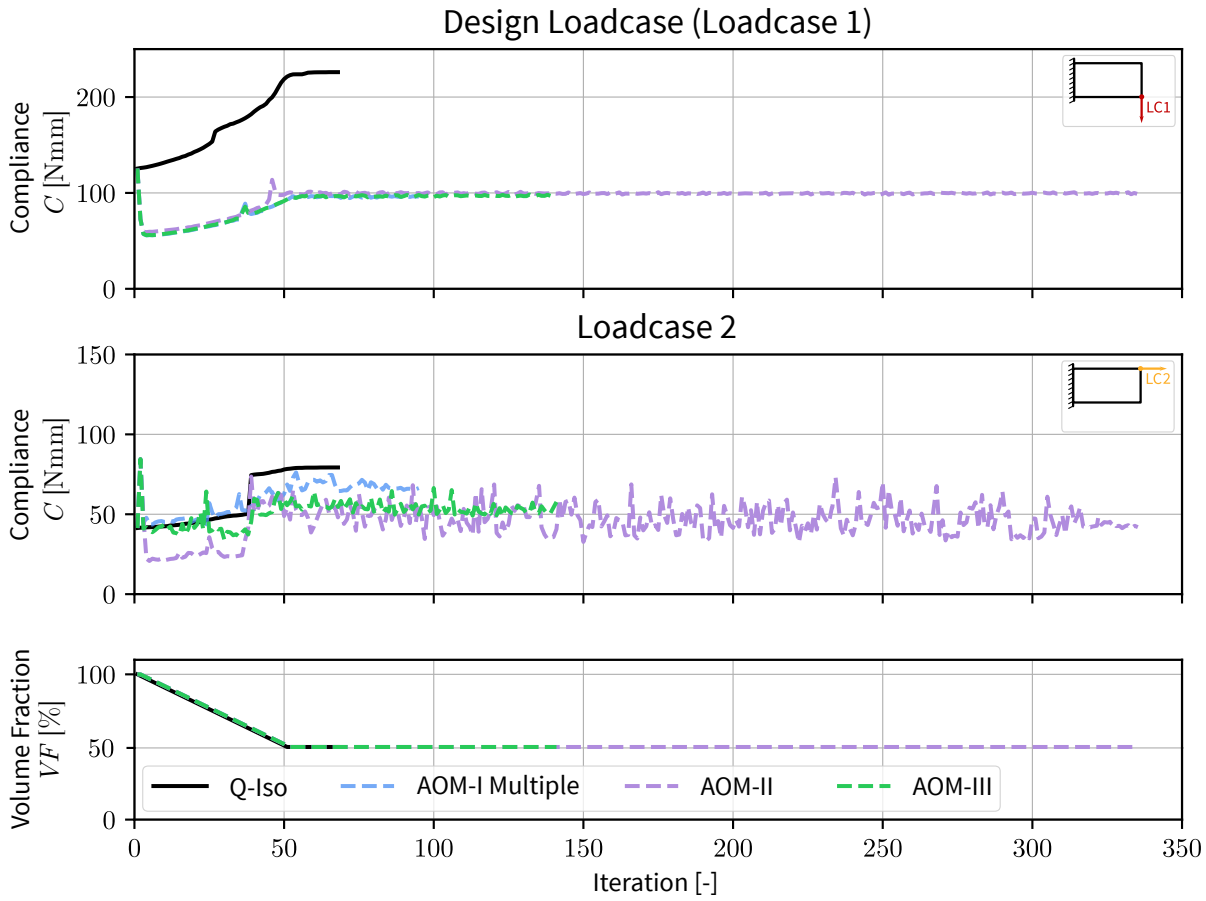

Figure 5.8.: Evolution histories of compliance and volume fraction for *Loadcase AC* ($m_{\text{size}} = 0.5\,\text{mm}$, $r_{\text{min}} = 3\,\text{mm}$, $ER = 0.01$)

The compliance curves show that *Loadcase 1* converges quite fast after the structure reaches the constrained volume of $50\,\%$. However, the optimization is not terminated until the results for *Loadcase 2* are within an acceptable tolerance range to avoid that the optimization procedure stops within a "bump". As the compliance curve for *Loadcase 2* reveals this is especially important for the optimization method *AOM-II* which leads to a compliance curve with significant fluctuations even for a high number of iterations.

All methods show a significant improvement of compliance compared to the standard topology optimization *Q-Iso*. The numerical results are summarized in Table 5.2. The improvement in compliance of the optimized structure for *Loadcase 1* in comparison to the standard topology optimization is quite similar for all anisotropic optimization algorithms. The results for *Loadcase 2* show significant differences. With regard to *Loadcase 2 AOM-II* performs best.

Table 5.2.: Comparison of compliance of the final design determined with optimization methods *Q-Iso*, *AOM-I Multiple*, *AOM-II*, and *AOM-III* (*Loadcase AC*)

	Compliance W_{ex} [Nmm]	
	Loadcase A (LC1)	Loadcase C (LC2)
Q-Iso	225.97	79.28
AOM-I Multiple	96.25	66.39
AOM-II	98.99	38.60
AOM-III	97.97	57.71

Figure 5.9 shows a detailed comparison of the relative compliance gained by the proposed anisotropic optimization methods (*AOM-I Multiple*, *AOM-II*, and *AOM-III*) for multiple loadcases. The compliance results of *AOM-I Multiple* serve as a reference. As already pointed out in Table 5.2, the compliance of *Loadcase 2* clearly drops when the structure is optimized using the algorithms *AOM-II* and *AOM-III*. This is plausible because when optimizing with *AOM-I Multiple*, *Loadcase 2* is not considered for the material update. In this case, *Loadcase 2* is only considered for the topology update, the material is solely optimized for *Loadcase 1*. This drop in compliance is especially evident for *AOM-II* in comparison to *AOM-I Multiple*.

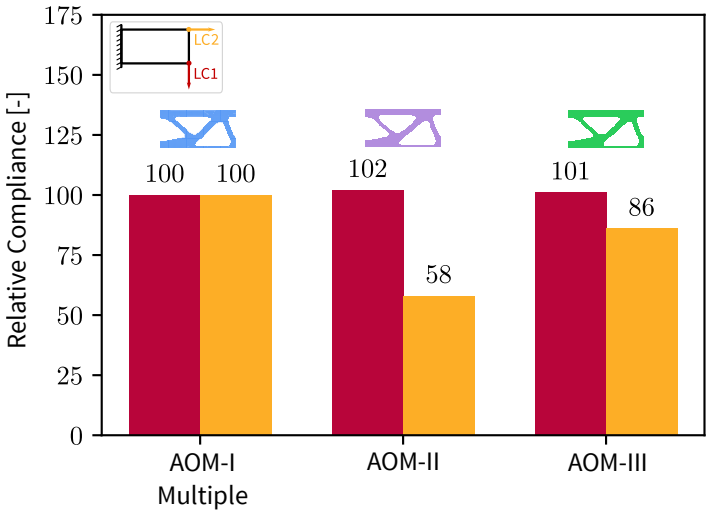

Figure 5.9.: Illustration of the performance of *Loadcase 1* (Design Loadcase) and *Loadcase 2* optimized with *AOM-I Multiple*, *AOM-II*, and *AOM-III* for loading scenario AC where the single loadcase optimization *AOM-I Single* serves as a reference. ($m_{\text{size}} = 0.5\,\text{mm}$, $r_{\text{min}} = 3\,\text{mm}$, $ER = 0.01$)

The final topologies as well as the material's 1-direction and stiffness tensor glyphs, for selected regions of the final design, are shown in Figure 5.10. The final topology determined with the standard topology optimization *Q-Iso* differs slightly. Compared to the anisotropic final designs, the quasi-isotropic final design shows a bigger and a smaller shearing triangle whereas for the other anisotropic optimization algorithms the shearing triangles are of almost equal size.

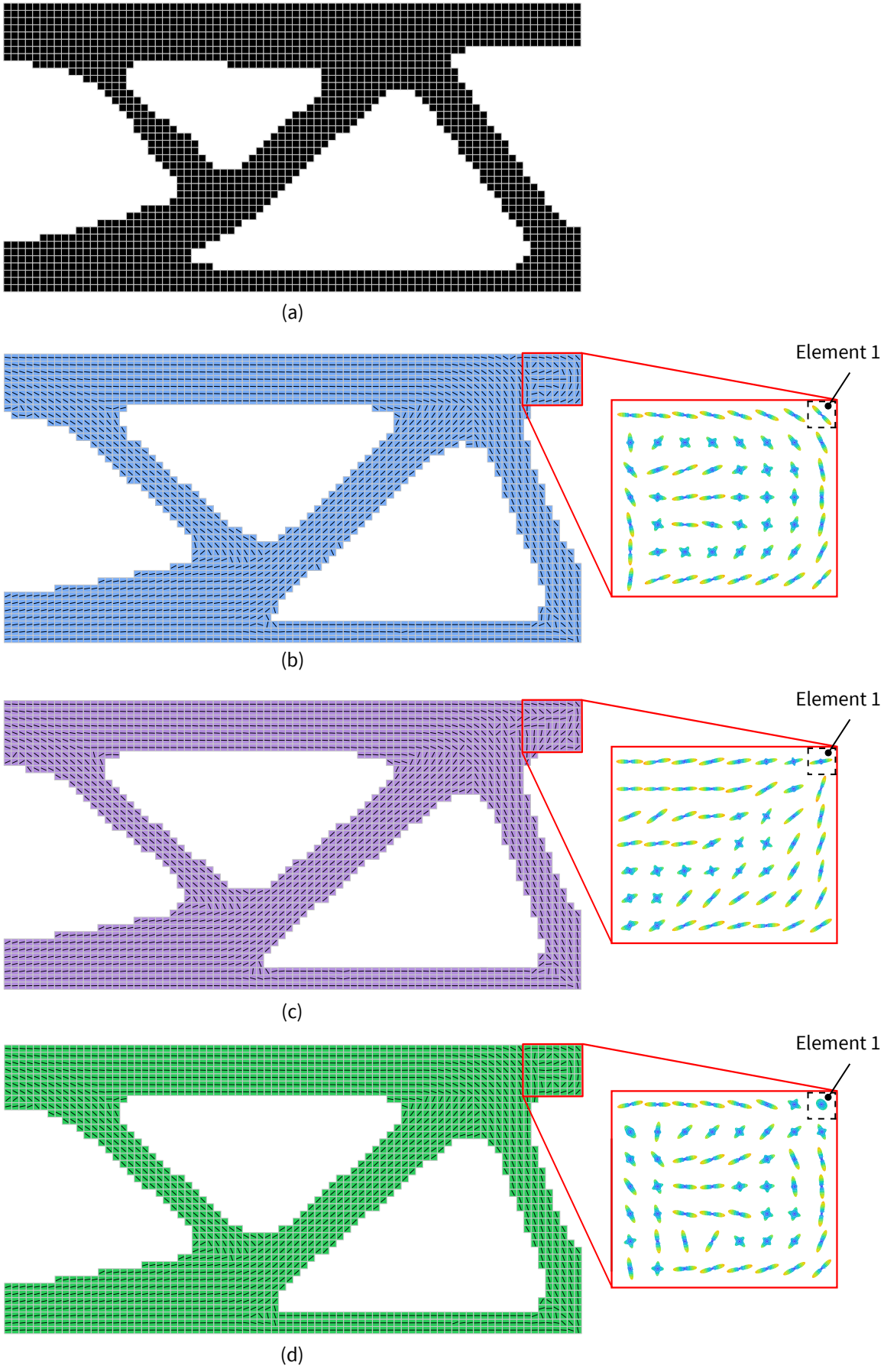

Figure 5.10.: Illustration of final topologies, material's 1-direction and stiffness tensor glyphs for selected regions of interest for the optimization methods (a) Q-Iso, (b) AOM-I Multiple, (c) AOM-II, (d) AOM-III for *Loadcase AC* ($m_{\text{size}} = 0.5\,\text{mm}$, $r_{\text{min}} = 3\,\text{mm}$, $ER = 0.01$).

There is almost no difference in terms of the final topology for the anisotropic optimization strategies *AOM-I Multiple*, *AOM-II*, and *AOM-III*. Consequently, the material's 1-direction (which is determined based on *Loadcase 1* for all anisotropic optimization strategies) is identical for the major part of the structure. An exception to this is the region where the second loadcase is applied, highlighted with a red frame in Figure 5.10. The stiffness tensor glyphs in these regions point out the differences between the optimization algorithms *AOM-I Multiple*, *AOM-II*, and *AOM-III*. A magnified view of the stiffness tensor glyph for *element 1* is shown in Figure 5.11. The respective volume fractions of the inclusions for this element are summarized in Table 5.3.

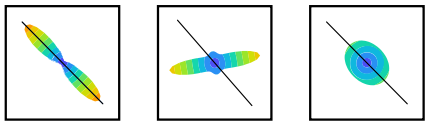

Figure 5.11.: Magnified view of stiffness tensor glyphs and material's 1-direction of element 1 highlighted in Figure 5.10

AOM-I Multiple (see Figure 5.10 (b)) adapts the degree of anisotropy according to the local loading conditions by adding inclusions of 0° and 90° based on the principal stresses resulting from *Loadcase 1*. For instance, for *element 1*, this results in a unidirectional material aligned with the optimal material's 1-direction determined by the orientation update for *Loadcase 1*, see Figure 5.11 (a). The respective volume fractions of the inclusions for this element are listed in Table 5.3.

Table 5.3.: Volume fractions for inclusions for optimization methods *AOM-I Multiple*, *AOM-II*, and *AOM-III* for an overall fiber volume content of $\xi_\mathrm{f} = 60\,\%$ (*Loadcase AC*)

	Volume Fractions of Inclusions				
	ξ_{0°	ξ_{90°	ξ_{θ_3}	ξ_{θ_4}	$\xi_{\pm 45^\circ}$
AOM-I Multiple	0.59	0.01	✗	✗	✗
AOM-II	≈ 0	≈ 0	0.48	0.12	✗
AOM-III	0.20	0.12	✗	✗	0.28

For *AOM-II*, (see Figure 5.10 (c)), the stiffness tensor glyphs in the region highlighted in red differ from those determined with *AOM-I Multiple*. The method of *AOM-II* is capable of considering the second loadcase for determining the optimal degree of anisotropy. In this case, further inclusions can be added to the material formulation depending on the principal stresses of the second loadcase. Therefore, the material can be optimized for the second loadcase as well. This is especially evident for those regions where the stresses due to *Loadcase 2* are significantly higher than the stresses due to *Loadcase 1*. For instance, for *element 1*, this means that the volume fractions ξ_{0° and ξ_{90° are close to zero whereas the volume fractions of the inclusions for the second loadcase ξ_{θ_3} and ξ_{θ_4} determine the degree of anisotropy, see Table 5.3. The orientations of these inclusions (θ_3 and θ_4) depend on the principal directions of the considered loadcase with respect to the principal directions of the design loadcase.

For instance, for *element 1* , the angle between the principal directions of *Loadcase 1* and *Loadcase 2* amounts to approximately $62\,^{\circ}$. This can be clearly seen in the magnified illustration of the stiffness tensor glyph for *element 1* , see Figure 5.11 (b).

The optimization algorithm *AOM-III* also considers the second loadcase for the material update. In this case, the second loadcase is capable of adding inclusions of $0\,^{\circ}$, $90\,^{\circ}$ if the second loadcase signifies higher stresses in these directions compared to *Loadcase 1*. Furthermore, inclusions of $\pm 45^{\circ}$ are added if shear stresses are introduced by the second loadcase. Therefore, the stiffness tensor glyph of *element 1* clearly differs from the stiffness tensor glyphs of *AOM-I Multiple* and *AOM-II*, see Figure 5.11 (c). In this case, the inclusions of $\pm 45^{\circ}$ play an important role for the degree of anisotropy, leading to an almost quasi-isotropic material, see Table 5.3.

5.3.2. Loadcase BB

Figure 5.12 illustrates the evolution histories of compliance and volume fraction for *Loadcase BB*. Again, the compliance curve for *Loadcase 2* shows a significant bump (for all optimization algorithms except *Q-Iso*) at the very beginning of the optimization. Like with *Loadcase AC* this is due to the fact that the startdesign for the optimization is determined based on the design loadcase (*Loadcase 1*).

For *Loadcase BB*, the *AOM-III* algorithm converges more quickly than the *AOM-I Multiple* and *AOM-II* algorithms. Furthermore, it is clearly visible that the evolution history of compliance for the second loadcase (determined with *AOM-II*) shows almost no bumps compared to *Loadcase AC*. As the loads are symmetric, the compliance curves for the *Q-Iso* optimization are identical.

All methods show a significant improvement of compliance compared to the standard topology optimization *Q-Iso*. The numerical results, summarized in Table 5.4, confirm the observations already made for *Loadcase AC*: for *Loadcase 1*, the compliance is significantly reduced for all optimization methods. Compared to *AOM-I Multiple*, the compliance of the structure with regard to *Loadcase 2* is significantly enhanced when the optimization algorithms *AOM-II* and *AOM-III* are used.

Table 5.4.: Comparison of compliance of the final design determined with optimization methods *Q-Iso*, *AOM-I Multiple*, *AOM-II*, and *AOM-III* (*Loadcase BB*)

	Compliance $W_{\text{ex}}\,[\text{Nmm}]$	
	Loadcase B (LC1)	Loadcase B (LC2)
Q-Iso	74.31	74.31
AOM-I Multiple	31.69	66.50
AOM-II	32.36	37.43
AOM-III	32.85	50.80

Like for *Loadcase AC* a detailed comparison of the compliance gained with the proposed anisotropic optimization methods for multiple loadcases *AOM-I Multiple*, *AOM-II*, and *AOM-III* is shown, see Figure 5.13. The compliance determined with *AOM-I Multiple* serves as a reference.

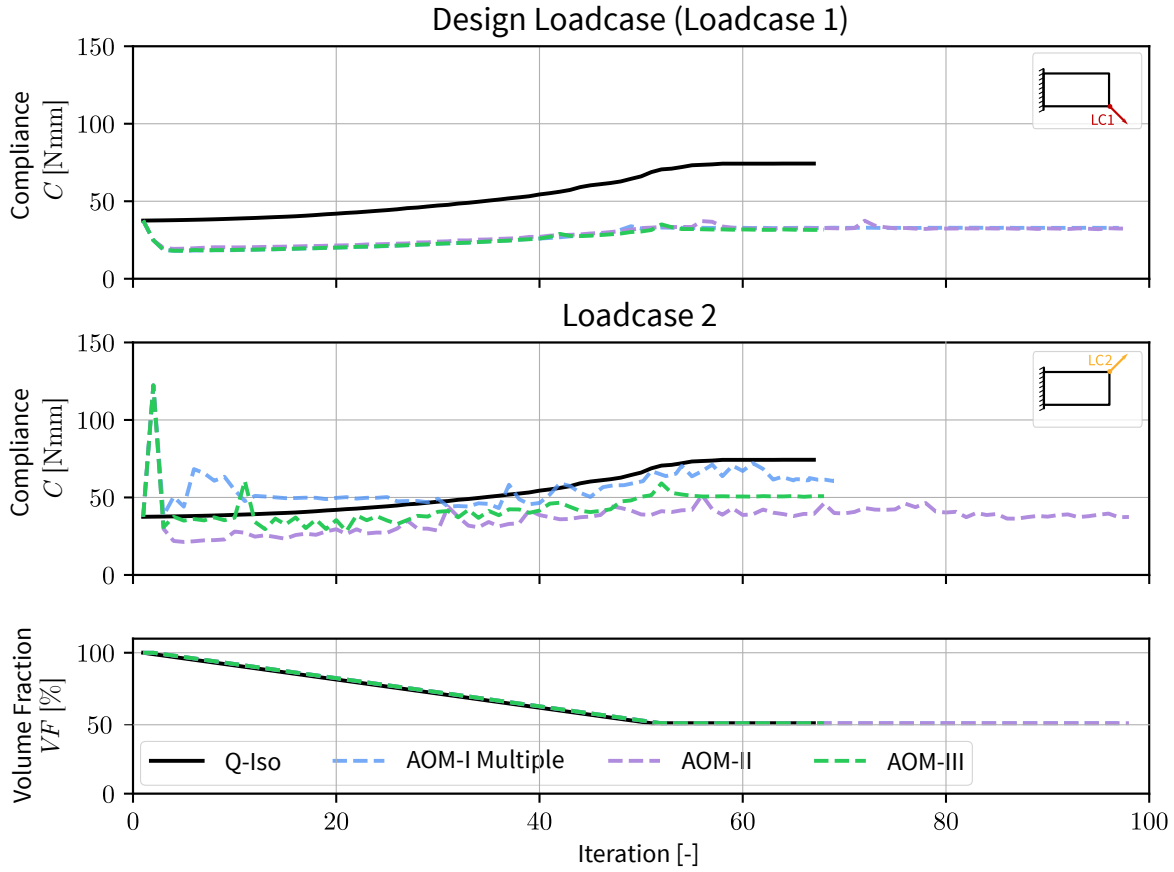

Figure 5.12.: Evolution histories of compliance and volume fraction for *Loadcase BB* ($m_{\text{size}} = 0.5\,\text{mm}$, $r_{\text{min}} = 3\,\text{mm}$, $ER = 0.01$)

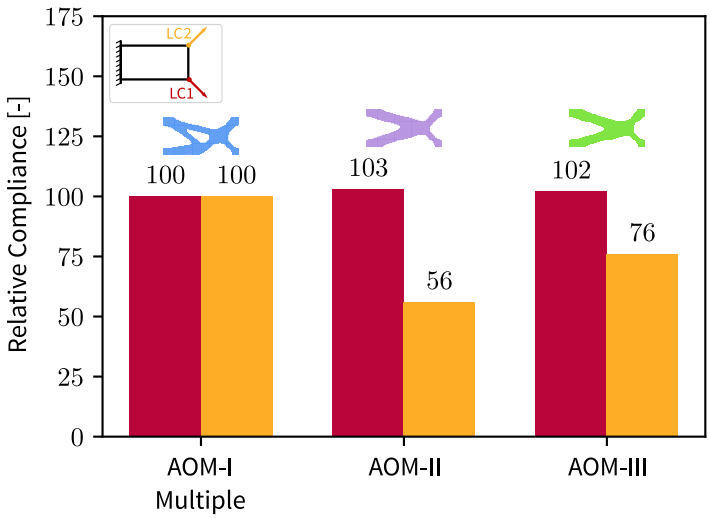

Figure 5.13.: Illustration of relative compliance and final topologies of *Loadcase 1* (Design Loadcase) and *Loadcase 2* optimized with *AOM-I Multiple*, *AOM-II*, and *AOM-III* for loading scenario BB. ($m_{\text{size}} = 0.5\,\text{mm}$, $r_{\text{min}} = 3\,\text{mm}$, $ER = 0.01$)

Figure 5.13 shows that, as opposed to *Loadcase AC*, the final topology gained with *AOM-I Multiple* clearly differs from the topologies gained with *AOM-II* and *AOM-III*.

To further compare the optimized designs resulting from the proposed optimization algorithms, the final topologies as well as the material's 1-direction and stiffness tensor glyphs, for selected regions of the final design, are shown in Figure 5.14. Due to the symmetric loading conditions, the topology of the standard topology optimization *Q-Iso* is symmetric, see Figure 5.14 (a). The structure optimized with *AOM-I Multiple* shows a non-symmetric design since the material is optimized for *Loadcase 1*, see Figure 5.14 (b). In comparison to *AOM-II* and *AOM-III* the topology of *AOM-I Multiple* shows an additional bar. The topologies of *AOM-II* and *AOM-III*, shown in Figure 5.14 (c) and (d), also show a non-symmetric final design but show a tendency towards a symmetric design due to the symmetric loading and the fact that the second loadcase is considered for the material update.

Regarding the degree of anisotropy, all three designs show large areas where the material is optimized as a unidirectional material aligned with the material's 1-direction based on the first principal direction of *Loadcase 1*. Exceptions are of course regions where bars intersect and especially the region where the structure is connected to the region where *Loadcase 2* is applied. With increasing proximity to the sphere of influence of *Loadcase 2*, the stresses for *Loadcase 1* decrease whereas the stresses resulting from *Loadcase 2* increase. For *AOM-II* and *AOM-III*, the material is capable of adapting to this circumstance by adding inclusions based on the local stress situation due to *Loadcase 2*.

Similarly to *Loadcase AC*, an element is picked out to show the differences in local material orientation and local material's degree of anisotropy between *AOM-I Multiple*, *AOM-II*, and *AOM-III*. Therefore, an enlarged view of *element 538* highlighted in Figure 5.14, which is subject to tensile loading due to *Loadcase 1* and *Loadcase 2*, is shown in Figure 5.15. The resulting volume fractions of the inclusions for the proposed optimization algorithms are summarized in Table 5.5.

Table 5.5.: Volume fractions for inclusions for optimization methods *AOM-I Multiple*, *AOM-II*, and *AOM-III* for an overall fiber volume content of $\xi_\mathrm{f} = 60\,\%$ (*Loadcase BB*)

	Volume Fractions of Inclusions				
	ξ_{0°	ξ_{90°	ξ_{θ_3}	ξ_{θ_4}	$\xi_{\pm 45^\circ}$
AOM-I Multiple	0.42	0.18	✗	✗	✗
AOM-II	0.17	0.05	0.31	0.07	✗
AOM-III	0.44	0.06	✗	✗	0.10

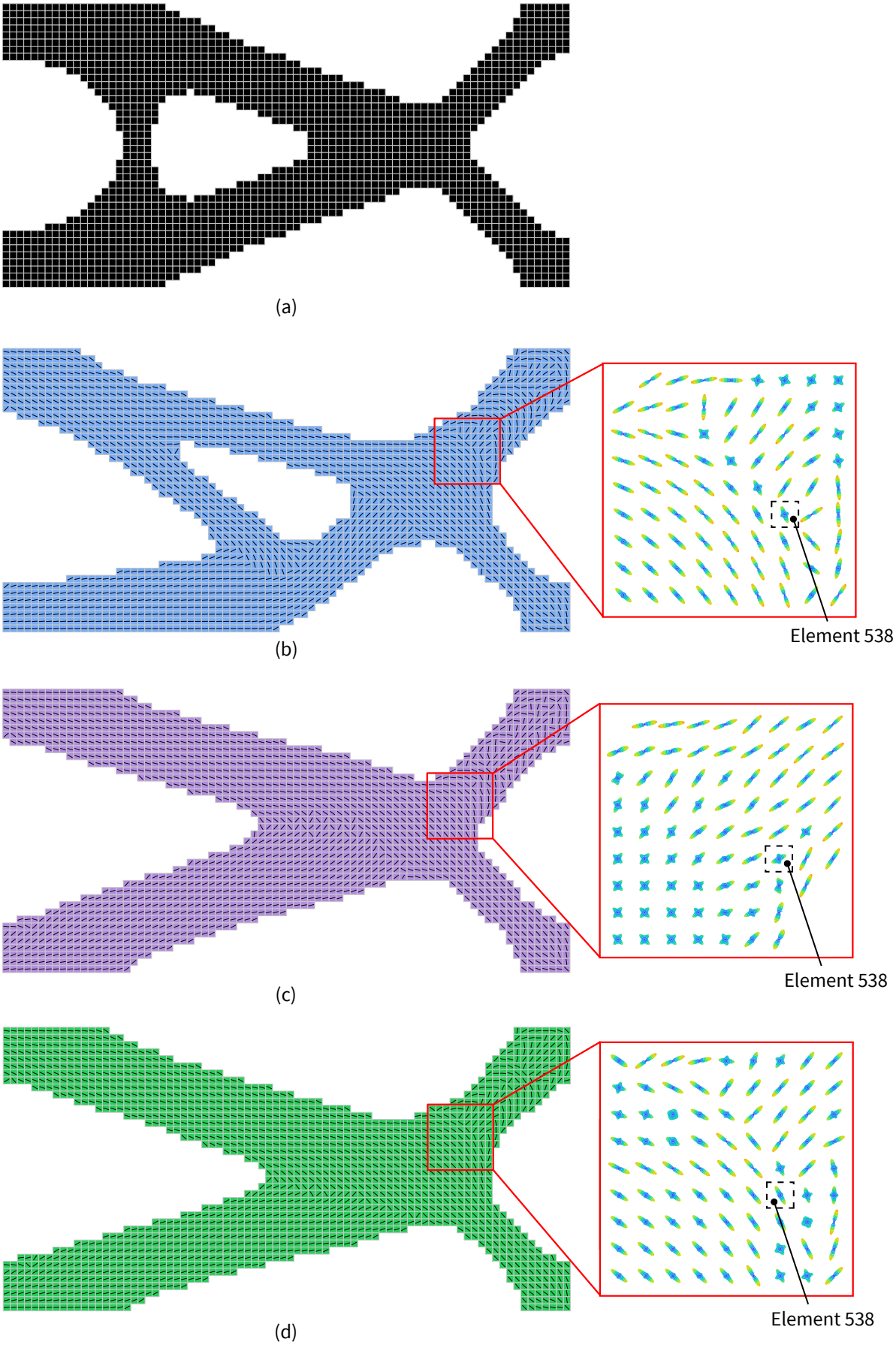

Figure 5.14.: Illustration of final topologies, material's 1-direction and stiffness tensor glyphs for selected regions of interest for the optimization methods for *Loadcase BB* (a) Q-Iso, (b) AOM-I Multiple, (c) AOM-II, (d) AOM-III.

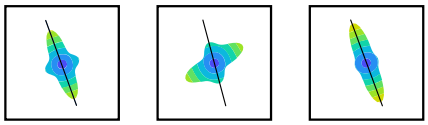

(a) (b) (c)

Figure 5.15.: Magnified view of stiffness tensor glyphs and material's 1-direction of *element 538* highlighted in Figure 5.14 for (a) *AOM-I Multiple*, (b) *AOM-II*, and (c) *AOM-III* ($m_{\text{size}} = 0.5\,\text{mm}$, $r_{\text{min}} = 3\,\text{mm}$, $ER = 0.01$).

In this case, for *AOM-I Multiple* the material properties are only optimized for *Loadcase 1*. However, *element 538* , is stiffened in $0\,^{\circ}$ and $90\,^{\circ}$ direction to bridge the transition between elements with unidirectional material definition, see Figure 5.15 (a).

For *AOM-II*, the resulting principal directions from *Loadcase 1* and *Loadcase 2* are at an angle of $69\,^{\circ}$. Therefore, the inclusions for *Loadcase 2* (θ_3 and θ_4) are at an angle of $69\,^{\circ}$ and $159\,^{\circ}$ with respect to the material's 1-direction determined for *Loadcase 1*. For *element 538* the stresses introduced by *Loadcase 2* are higher than the stresses introduced by *Loadcase 1*. Consequently, the volume fraction of the inclusion ξ_{θ_3} is larger than the volume fraction of the $0\,^{\circ}$ inclusion (see Table 5.5) which is also reflected in the stiffness tensor glyph in Figure 5.15 (b).

For *AOM-III*, the local stress situation leads to a material that is predominately stiffened with inclusions of $0\,^{\circ}$ but also shows a certain amount of inclusions of $\pm 45^{\circ}$ due to the stresses induced by *Loadcase 2*, see Figure 5.15 (b).

5.4. Discussion Multiple Loadcase

The numerical test cases presented in this chapter show the extension of the simultaneous optimization of topology and material *AOM-I Single*, proposed for a single loadcase, to multiple loadcases. Thus, the cantilever beam already used for the simulations with a single loadcase is subjected to two loads, where the design loadcase is denoted as *Loadcase 1*. For the *AOM-I Multiple* optimization method *Loadcase 2* is only considered for the update of the topology whereas for *AOM-II* and *AOM-III* the second loadcase contributes to the degree of anisotropy of the material by adding further inclusions.

For the optimization algorithms proposed for multiple loadcases, the influence of the startdesign in terms of the material's 1-direction and material definition (quasi-isotropic / unidirectional) was investigated. The results reveal that for the optimization methods *AOM-II* and *AOM-III* the compliance of *Loadcase 1* is not overly sensitive to the startdesign. However, similar to the observations made with a single loadcase, there are minor differences owing to the fact that the design space is highly non-convex. The results furthermore show that *Loadcase 2* performs different, in terms of compliance, for different startdesigns.

Both loadcases perform best with the startdesign based on a unidirectional material aligned with the main principal direction from a preliminary finite element analysis ("PD-startdesign"). A plausible explanation is that a quick stabilization of the design for the design loadcase (*Loadcase 1*) also implies that the material can be adapted more effectively for the second loadcase. If major changes, e.g., in terms of material orientation, are necessary for the design loadcase, the material obviously can not be optimally adapted for the second loadcase. As the algorithm *AOM-II* has more freedom concerning the inclusions that can be considered for the second loadcase this method is more sensitive to changes induced by the design loadcase. This is supported by the fact that the differences in compliance for different startdesigns for *Loadcase 2* are greater for *AOM-II* compared to *AOM-III*.

The influence of the control parameters for filter scheme and the BESO algorithm, namely scale parameter r_{min} and evolution rate ER were investigated. For *Loadcase AC* the restriction to a bulkier design, using a higher r_{min}, leads to a final design that performs worse for the design loadcase (*Loadcase 1*) compared to lower r_{min}. The final design performs better for *Loadcase 2* when defining a larger r_{min}. This observation is supported by the fact that the final topology for $r_{\text{min}} = 4.5\,\text{mm}$ clearly differs. The reason is obvious: the final topology that evolves for $r_{\text{min}} = 4.5\,\text{mm}$ is superior for *Loadcase 2* compared to all other topologies that evolve for lower r_{min}.

The investigation concerning the influence of evolution rate ER shows that a proper choice of ER is necessary with regard to the performance of the second loadcase. A lower ER leads to a better performance, in terms of compliance, compared to a higher ER. That seems logical as a higher ER means that more material is removed within every iteration step until the constrained volume of $50\,\%$ is reached. Obviously this prevents an optimal adaption of the degree of anisotropy for the second loadcase. Therefore, with a lower ER the design has more time to evolve in the "right" direction. This effect is even more evident for *AOM-II* as opposed to *AOM-III* confirming the observations made with the startdesign. The reason why the difference is most significant for *AOM-II* is that this optimization method offers the most design freedom concerning the adaption of the material to the second loadcase. Obviously, *AOM-II* reacts more sensitive to bigger changes in topology as well.

As expected, the results reveal that all anisotropic optimization algorithms (*AOM-I Multiple*, *AOM-II*, and *AOM-III*) show a significant over the standard topology optimization with quasi-isotropic material (*Q-Iso*).

As mentioned in Section 3.3.2, the allowable convergence error is set to 0.001 for the design loadcase (*Loadcase 1*) and to 0.005 for all other loadcases, in this case *Loadcase 2*. Therefore, the convergence error for *Loadcase 1* is more stringent. The reason is that the focus of the optimization is on the design loadcase. However, the optimization does not terminate before the result is within an acceptable convergence error range for *Loadcase 2* as well.

The compliance curves, presented in Figure 5.8 and Figure 5.12 underpin the necessity of a convergence criterion for the second loadcase. Especially the evolution of the compliance for the second loadcase of *Loadcase AC* shows many "bumps". It is undesirable that the algorithm terminates at a peak of such a "bump", therefore *AOM-II* needs significantly more iterations than the other algorithms. The reason for these "bumps" again lies in the fact that, concerning the material update, the algorithm *AOM-II* has more degrees of freedom compared to *AOM-III*. Therefore, this algorithm reacts more sensitive to changes, be it minor changes in topology or the associated minor change in material's 1-direction. This in turn makes it again seem logical why this algorithm reacts more sensitively to changes in the evolution rate. This effect is more obvious for *Loadcase AC* compared to *Loadcase BB*. A possible explanation is that for *Loadcase BB* the individual loads do not exclude each other to such an extent as it is the case for *Loadcase AC*.

The proposed algorithms for simultaneously optimizing topology and material were compared considering the following aspects: First, how is the performance of the final design in terms of compliance of the design loadcase affected when the second loadcase is considered for the material update. Second, how does the gain in performance of the second loadcase differ between the methods *AOM-II* and *AOM-III*. Concerning the compliance for the design loadcase, all algorithms perform almost equally well. For the design loadcase the differences between the algorithms are in the low single-digit percentage range. For the second loadcase the algorithm *AOM-II* shows the best performance. As the stiffness tensor glyphs of selected regions of the final design illustrate *AOM-I Multiple* adapts the degree of anisotropy according to the local loading conditions of *Loadcase 1* by adding inclusions of $0\,^{\circ}$ and $90\,^{\circ}$. Therefore, in this case, the second loadcase remains totally unconsidered with regard to the material properties. *AOM-II* is capable of considering the second loadcase in the material update by adding inclusions depending on the principal stresses and principal directions of the second loadcase with respect to the design loadcase. Therefore, in regions where the stresses resulting from the second loadcase are predominant, the material can be fully optimized for the local loading conditions. Even though the material's 1-direction is aligned with the main principal direction of the design loadcase (and therefore in the extreme case absolutely misaligned with regard to the second loadcase) this is compensated by the inclusions added for the second loadcase. The inclusions for the design loadcase can be reduced correspondingly if necessary. In the extreme case this means that the respective inclusions for the design loadcase are set to zero if the stresses resulting from the second loadcase are predominant. For the algorithm *AOM-III*, the local stress tensor for the second loadcase is rotated to the principal directions of the design loadcase. Therefore, the second loadcase contributes with inclusions of $0\,^{\circ}$ and $90\,^{\circ}$ but also with inclusions of $\pm 45^{\circ}$ depending on the induced shear stresses. In this case, too, the inclusions can be adapted to the local loading conditions, i.e., in regions where the stresses resulting from the second loadcase are predominant. However, as opposed to *AOM-II*, the inclusions are limited to certain directions. Therefore, *AOM-III*

signifies an improvement compared to *AOM-I Multiple*, although the improvement is not as significant as with *AOM-II*.

As it was expected, symmetric loading conditions (*Loadcase BB*) lead to a symmetric topology for the standard topology optimization *Q-Iso*. Both algorithms, where the second loadcase is considered for the degree of anisotropy of the local material tensor, show a tendency towards a symmetric design when subjected to symmetric loading conditions. However, the part of the structure which establishes the connection to the second loadcase is a bit thicker than the lower bar that establishes the connection of the structure to the design loadcase. As mentioned before, in those regions where the second loadcase predominates, the material can be fully adapted to the second loadcase as the volume fractions of the inclusions for the design loadcase can be reduced correspondingly. However, in regions where both loadcases play a role, compromises have to be made regarding the volume fractions of the inclusions for the design loadcase and the second loadcase. Consequently, if the material can not be used to its full potential for the second loadcase, this must be counteracted by making the structure "thicker". This observation is confirmed by the topology gained with *AOM-I Multiple*.

6. Summary & Conclusion

The motivation to study material design in a structural optimization framework comes both from the increased industrial use of advanced materials as well as from developments within the structural optimization field itself. Therefore, in the framework of this thesis, a tool was developed to provide an even better support for the design and engineering of competitive structures within a lightweight and material-oriented development process. The novelty of this work is the development of a new concept of structural optimization where the topology of the structure and the material, in terms of material orientation and degree of anisotropy, are designed simultaneously (*AOM* - Anisotropic Orient Material). The material properties of a continuous fiber reinforced polymer (FRP) with infinitely long cylindrical inclusions embedded in a matrix are tailored to the structural design and vice-versa. Thus, the material is directly optimized for the functional needs at the structural scale in order to gain lighter and more efficient structures applicable to many engineering sectors. This is contrary to the present design practice where the design of structure and material are inherently decoupled. Existing approaches to structural design either select a material and then design the structure that best utilizes the given material, thereby reducing the design space, or optimize the anisotropy distribution for a fixed structural shape.

In the framework of this thesis the aim was to develop a method for simultaneous topology and material optimization that minimizes the compliance of a structure subject to a volume constraint. The optimal design, in terms of topology and material properties, is a structure with high stiffness.

The developed algorithm is capable of handling a standard topology optimization with quasi-isotropic material (*Q-Iso*), a standard topology optimization for a predefined unidirectional material (*A*), a simultaneous optimization of topology and material orientation (*AO*), and a simultaneous optimization of topology, material orientation, and material anisotropy (*AOM*). To point out the potential of the simultaneous approaches, the respective material update schemes were compared to the standard topology optimization for a quasi-isotropic material. The anisotropic material is modeled by specifying the material's 1-direction as well as the orientations and volume fractions of the continuous fiber inclusions within each element in the fixed FEM mesh.

The numerical application of the method on simple (academic) test cases shows its effectiveness. For the single loadcase it is shown that the *AOM-I Single* approach makes use of the largest design space as opposed to *A* and *AO*. The orthotropic material determined with this method goes beyond topology optimized quasi-isotropic (*Q-Iso*) and orientation optimized unidirectional material (*AO*) as it can be fully adapted to the local loading conditions. In other words, the material is used to its full potential. However, for real structures, taking into account only one loadcase is not sufficient. Therefore, the *AOM* method was extended to multiple loadcases.

Regarding multiple loadcases, *AOM-I Multiple* defines a design loadcase. The design loadcase determines the material's 1-direction and the material's degree of anisotropy, i.e., adjustment of the local stiffness tensor, based on the local loading conditions in terms of resulting element stress tensors. In this case, further loadcases are only considered for the update of the topology. For the approaches *AOM-II* and *AOM-III* any additional loadcase contributes to the optimized topology but also to the degree of anisotropy of the material by adding further inclusions. Therefore, in comparison to the structure determined by *AOM-I Multiple*, the material of the resulting structure is also optimized with regard to these additional loadcases, see Section 5.3. It has been shown that the *AOM-II* approach makes use of the largest design space as this approach gives the most design freedom. The inclusions can be directly adapted to the needs of the further loadcases. It has to be noted that the present algorithm is not limited to two loadcases, as presented in Chapter 5, but can be applied to an arbitrary number of loadcases.

As outlined in Section 4.5, the sequential approach, where the topology is optimized first for a fixed (e.g., quasi-isotropic) material followed by an optimization of the material itself, limits the design space. It is found, that indeed, the material anisotropy influences the optimal shape of the structure as different topologies are obtained in the case of a sequential and a simultaneous approach to topology and material optimization. These observations verify that it is necessary to optimize the topology and the anisotropy distribution of the considered structure all at once, as opposed to the present design practice where the design of structure and material are inherently decoupled. The concurrent optimization of topology and the optimized use of fiber reinforced materials show the potential of significant improvement compared to traditional construction methods.

In the framework of this thesis, the influence of the control parameters which are needed for the filter scheme and the BESO algorithm (evolution rate ER and scale parameter $r_{\min}$) as well as the influence of the initial material setup (startdesign) were investigated. The results reveal, that the method of simultaneously optimizing the topology and the material for a single loadcase *AOM-I Single* is insensitive to the choice of evolution rate ER compared to the standard topology optimization with quasi-isotropic material *Q-Iso*.

The compliance shows negligible differences even if the final topologies differ. The material's local orientation and degree of anisotropy is adapted equally well for different values of ER. The same observations were made for multiple loadcases. The topologies for different values of ER differ, however, the compliance of the design loadcase is insensitive to the choice of ER. Regarding *Loadcase 2*, the resulting compliance depends on the choice of evolution rate ER. The compliance for *Loadcase 2* increases with increasing ER.

Regarding the scale parameter for the filter scheme, $r_{\min}$, it was concluded that a minimum value of three times the element size is necessary with regard to aspects of finite element analysis, i.e., that stresses are captured accurately. Furthermore, avoiding the formation of too thin features makes sense with regard to aspects of manufacturability. The compliance of the structure determined with *AOM-I Single* is insensitive to changes of $r_{\min}$. When dealing with multiple loadcases, the compliance of the design loadcase is very stable, showing a slight tendency towards increasing compliance with increasing values of $r_{\min}$. For *Loadcase 2* this is not generally the case: the compliance of the optimized structure with respect to *Loadcase 2* depends on the choice of $r_{\min}$. However, no overall tendency for the compliance of *Loadcase 2* was observed: for instance for *Loadcase AC* the compliance decreases for higher values of $r_{\min}$, for symmetric loading with *Loadcase BB* the compliance increases for higher values of $r_{\min}$.

With regard to the startdesign, similar observations were made: the compliance as well as the final topologies of the structure determined with *AOM-I Single* as well as *AOM-I Multiple*, *AOM-II*, and *AOM-III* for the design loadcase, show only minor differences. The results suggest, that due to the expanded design space and the non-convexity of the optimization problem multiple, almost equally optimal solutions can be determined with different startdesigns. Especially for the results observed with *AOM-I Single* this observation allows the presumption that this algorithm is capable of escaping local minima. The best results, particularly with regard to multiple loadcases, are achieved when choosing a startdesign where the orientation of a unidirectional material is based on the principal directions of a preliminary finite element analysis of a quasi-isotropic structure ("PD-startdesign").

In summary, it was observed, that *AOM-I Single* is a very robust algorithm for the single loadcase optimization problem. The method shows good convergence and little sensitivity to the startdesign and control parameters ER and r_{min}. With respect to the design loadcase, all methods proposed for multiple loadcases are very robust whereas the compliance of the second loadcase shows certain dependencies on the choice of the evolution rate ER, scale parameter $r_{\min}$, and startdesign. The reason is that *Loadcase 2*, which is only considered for the update of the topology and the material's degree of anisotropy, is very sensitive to changes in topology and the corresponding changes in material orientation induced by the design loadcase.

The concept of simultaneous topology and material optimization was illustrated on simple two dimensional (academic) test cases. It is noted, however, that the concept can be generalized to three dimensional composite topologies. The extension to three dimensional problems is necessary in order to use the proposed method in an industrial context. By doing so, the method is capable of covering a very general, even completely anisotropic, material.

The method was developed on a conceptual level. Including manufacturing constraints such that the practical feasibility of the optimized design can be taken into account in the optimization process, was not the main focus of this thesis. However, with the potential of additive manufacturing (i.e., 3D printing) perhaps it would be possible to determine a manufacturable material that is close to the optimal solution given by the present algorithm. Since the material optimization is based on a micromechanics approach with specific fiber orientations, the resulting material can be directly translated to actual fiber arrangements (in contrast to FMO). This feature can potentially also be used to implement manufacturing constraints. For this purpose it would be interesting to include a post processing step that determines the closest manufacturable material from the optimized material. A post processing step is also needed for the topology as the boundaries of the structure are not smooth.

The present method is only applicable to problems where the objective is to minimize the compliance. However, in an industrial context this is insufficient as other physical phenomena must be integrated in the optimization process (i.e., maximum displacement), in order to propose more robust and realistic solutions. However, as a result of current technological advances, especially in terms of the ever-increasing use of fiber-reinforced structures (and the corresponding increase in degrees of freedom) the proposed method opens up a wide range of very interesting perspectives.

7. Literature

[1] M. Bendsøe and O. Sigmund. *Topology Optimization Theory, Methods, and Applications*. German. Berlin, Heidelberg: Springer Berlin Heidelberg, 2004.

[2] L. Harzheim. *Strukturoptimierung: Grundlagen und Anwendungen*. ger. 2., überarbeitete und erweiterte Auflage. Edition Harri Deutsch. Haan - Gruiten: Verlag Europa - Lehrmittel - Nourney, Vollmer GmbH & Co. KG, 2014.

[3] A. Schumacher. *Optimierung mechanischer Strukturen*. de. Berlin, Heidelberg: Springer Berlin Heidelberg, 2013.

[4] G. Vanderplaats. "Structural optimization for statics, dynamics and beyond." en. In: *Journal of the Brazilian Society of Mechanical Sciences and Engineering* 28.3 (Sept. 2006), pp. 316–322.

[5] E. Lund. "Discrete Material and Thickness Optimization of laminated composite structures including failure criteria." en. In: *Structural and Multidisciplinary Optimization* 57.6 (June 2018), pp. 2357–2375.

[6] M. Bruyneel and C. Fleury. "Composite structures optimization using sequential convex programming." In: *Advances in Engineering Software* 33.7-10 (2002). ISBN: 0965-9978 Publisher: Elsevier, pp. 697–711.

[7] M. Kočvara, M. Stingl, and J. Zowe. "Free material optimization: recent progress." In: *Optimization* 57.1 (2008), pp. 79–100.

[8] K. Iqbal. *Fundamental Engineering Optimization Methods*. Englisch. bookboon.com, 2013.

[9] O. Sigmund. "A 99 line topology optimization code written in Matlab." en. In: *Structural and Multidisciplinary Optimization* 21.2 (Apr. 2001), pp. 120–127.

[10] W. Dorn. "Automatic design of optimal structures." In: *J. de Mecanique* 3 (1964), pp. 25–52.

[11] S. Bandaru and K. Deb. "Metaheuristic techniques." In: *Decision Sciences: Theory and Practice* (2016), pp. 693–750.

[12] A. Törn, M.M. Ali, and S. Viitanen. "Stochastic Global Optimization: Problem Classes and Solution Techniques." In: *Journal of Global Optimization* 14.4 (1999), pp. 437–447.

[13] C. Khompatraporn, J. Pintér, and Z. Zabinsky. "Comparative assessment of algorithms and software for global optimization." In: *Journal of global optimization* 31.4 (2005). ISBN: 0925-5001 Publisher: Springer, pp. 613–633.

[14] O. Sigmund. “On the usefulness of non-gradient approaches in topology optimization.” en. In: *Structural and Multidisciplinary Optimization* 43.5 (May 2011), pp. 589–596.

[15] O. Sigmund and J. Petersson. “Numerical instabilities in topology optimization: a survey on procedures dealing with checkerboards, mesh-dependencies and local minima.” In: *Structural optimization* 16.1 (1998), pp. 68–75.

[16] C. McGeoch. “Experimental analysis of algorithms.” In: *Notices of the AMS* 48.3 (2001), pp. 304–311.

[17] V. Beiranvand, W. Hare, and Y. Lucet. “Best practices for comparing optimization algorithms.” en. In: *Optimization and Engineering* 18.4 (Dec. 2017), pp. 815–848.

[18] R. Brent. *Algorithms for minimization without derivatives*. Courier Corporation, 2013.

[19] O. Begambre. “Performance assessment of modern heuristic algorithms used in structural optimization.” In: *Proceedings of the 10th World Congress on Computational Mechanics*. 2014, pp. 3146–3154.

[20] W. Zhang and C. Fleury. “A modification of convex approximation methods for structural optimization.” In: *Computers & Structures* 64.1-4 (1997), pp. 89–95.

[21] R. Fletcher and C. Reeves. “Function minimization by conjugate gradients.” In: *The computer journal* 7.2 (1964). ISBN: 0010-4620 Publisher: Oxford University Press, pp. 149–154.

[22] S. Ganguly and W.L. Neu. “Search direction improvement for gradient-based optimization problems.” Englisch. In: WIT Transactions on The Built Environment (2005).

[23] O. Dababneh, T. Kipouros, and J. Whidborne. “Application of an Efficient Gradient-Based Optimization Strategy for Aircraft Wing Structures.” en. In: *Aerospace* 5.1 (Jan. 2018), p. 3.

[24] M. Bruyneel, P. Duysinx, and C. Fleury. “A family of MMA approximations for structural optimization.” In: *Structural and Multidisciplinary Optimization* 24.4 (Oct. 2002), pp. 263–276.

[25] K. Svanberg. “The method of moving asymptotes—a new method for structural optimization.” In: *International journal for numerical methods in engineering* 24.2 (1987). ISBN: 0029-5981 Publisher: Wiley Online Library, pp. 359–373.

[26] M. Canonaco, U. Loher, V. Esslinger, and B. Weisse. “Structural Optimization Methods.” In: *WIT Transactions on The Built Environment* 31 (1970).

[27] G. Chiandussi, M. Codegone, and S. Ferrero. “Topology optimization with optimality criteria and transmissible loads.” en. In: *Computers & Mathematics with Applications* 57.5 (Mar. 2009), pp. 772–788.

[28] L. Yin and W. Yang. “Optimality criteria method for topology optimization under multiple constraints.” In: *Computers & Structures* 79.20-21 (2001), pp. 1839–1850.

[29] R. Kriechbaum. “Ein Verfahren zur Optimierung der Faserverläufe in Verbundwerkstoffen durch Minimierung der Schubspannungen nach Vorbildern der Natur.” PhD Thesis. Universität Karlsruhe (TH), Oct. 1994.

[30] T. Weise. “Global optimization algorithms-theory and application.” In: *Self-Published Thomas Weise* (2009).

[31] A. Gandomi, X. Yang, S. Talatahari, and A. Alavi. “Metaheuristic algorithms in modeling and optimization.” In: *Metaheuristic applications in structures and infrastructures* (2013), pp. 1–24.

[32] A. E. Charalampakis and G. C. Tsiatas. “Critical Evaluation of Metaheuristic Algorithms for Weight Minimization of Truss Structures. Front.” In: *Built Environ* 5 (2019), p. 113.

[33] G. Venter. “Review of optimization techniques.” In: *Encyclopedia of aerospace engineering* (2010).

[34] G. I. N. Rozvany. “A critical review of established methods of structural topology optimization.” en. In: *Structural and Multidisciplinary Optimization* 37.3 (Jan. 2009), pp. 217–237.

[35] M. Bendsøe. “Optimal shape design as a material distribution problem.” In: *Structural optimization* 1.4 (1989), pp. 193–202.

[36] O. Sigmund and K. Maute. “Topology optimization approaches: A comparative review.” en. In: *Structural and Multidisciplinary Optimization* 48.6 (Dec. 2013), pp. 1031–1055.

[37] O. Sigmund. “Topology optimization: a tool for the tailoring of structures and materials.” en. In: *Philosophical Transactions of the Royal Society of London. Series A: Mathematical, Physical and Engineering Sciences* 358.1765 (Jan. 2000). Ed. by J. M. T. Thompson, pp. 211–227.

[38] H. Eschenauer and N. Olhoff. “Topology optimization of continuum structures: a review.” In: *Appl. Mech. Rev.* 54.4 (2001). ISBN: 0003-6900, pp. 331–390.

[39] M. Bendsoe and N. Kikuchi. “Generating optimal topologies in structural design using a homogenization method.” In: (1988).

[40] M. Bendsøe and O. Sigmund. “Material interpolation schemes in topology optimization.” In: *Archive of applied mechanics* 69.9-10 (1999). ISBN: 0939-1533
Publisher: Springer, pp. 635–654.

[41] M. Stolpe and K. Svanberg. “An alternative interpolation scheme for minimum compliance topology optimization.” In: *Structural and Multidisciplinary Optimization* 22.2 (2001), pp. 116–124.

[42] G. Allaire and G. A. Francfort. “A numerical algorithm for topology and shape optimization.” In: *Topology design of structures*. Springer, 1993, pp. 239–248.

[43] Garret N. Vanderplaats. “An efficient feasible directions algorithm for design synthesis.” In: *AIAA journal* 22.11 (1984), pp. 1633–1640.

[44] K. Svanberg. “The method of moving asymptotes—a new method for structural optimization.” In: *International journal for numerical methods in engineering* 24.2 (1987), pp. 359–373.

[45] E. Andreassen, A. Clausen, M. Schevenels, Boyan S. Lazarov, and O. Sigmund. “Efficient topology optimization in MATLAB using 88 lines of code.” In: *Structural and Multidisciplinary Optimization* 43.1 (2011), pp. 1–16.

[46] V. Challis. “A discrete level-set topology optimization code written in Matlab.” en. In: *Structural and Multidisciplinary Optimization* 41.3 (Apr. 2010), pp. 453–464.

[47] M. Beckers. “Topology optimization using a dual method with discrete variables.” In: *Structural Optimization* 17.1 (1999). ISBN: 0934-4373 Publisher: Springer, pp. 14–24.

[48] M. Beckers. “Dual methods for discrete structural optimization problems.” In: *International Journal for Numerical Methods in Engineering* 48.12 (2000). ISBN: 0029-5981 Publisher: Wiley Online Library, pp. 1761–1784.

[49] Y. Xie and Grant P. Steven. “A simple evolutionary procedure for structural optimization.” In: *Computers & structures* 49.5 (1993), pp. 885–896.

[50] D. Nha Chu, Y. M. Xie, A. Hira, and G. P. Steven. “Evolutionary structural optimization for problems with stiffness constraints.” In: *Finite Elements in Analysis and Design* 21.4 (1996), pp. 239–251.

[51] X. Y. Yang, Y. M. Xie, G. P. Steven, and O. M. Querin. “Bidirectional evolutionary method for stiffness optimization.” In: *AIAA journal* 37.11 (1999), pp. 1483–1488.

[52] X. Huang and Y. Xie. “A further review of ESO type methods for topology optimization.” en. In: *Structural and Multidisciplinary Optimization* 41.5 (May 2010), pp. 671–683.

[53] L. Xia, Q. Xia, X. Huang, and Y. Xie. “Bi-directional Evolutionary Structural Optimization on Advanced Structures and Materials: A Comprehensive Review.” en. In: *Archives of Computational Methods in Engineering* 25.2 (Apr. 2018), pp. 437–478.

[54] O. M. Querin, G. P. Steven, and Y. M. Xie. “Evolutionary structural optimisation using an additive algorithm.” In: *Finite elements in analysis and design* 34.3-4 (2000), pp. 291–308.

[55] O. Querin, G. Steven, and Y. Xie. “Evolutionary structural optimisation (ESO) using a bidirectional algorithm.” In: *Engineering computations* (1998).

[56] M. Zhou and G. I. N. Rozvany. “On the validity of ESO type methods in topology optimization.” In: *Structural and Multidisciplinary Optimization* 21.1 (2001). ISBN: 1615-147X Publisher: Springer, pp. 80–83.

[57] E. Hinton and J. Sienz. “Fully stressed topological design of structures using an evolutionary procedure.” In: *Engineering Computations: Int J for Computer-Aided Engineering* 12.3 (1993), pp. 229–244.

[58] G. Rozvany and O. Querin. “Combining ESO with rigorous optimality criteria.” In: *International journal of vehicle design* 28.4 (2002), pp. 294–299.

[59] X. Huang and Y. M. Xie. “Bi-directional evolutionary topology optimization of continuum structures with one or multiple materials.” en. In: *Computational Mechanics* 43.3 (Feb. 2009), pp. 393–401.

[60] Z. Zuo, Y. Xie, and X. Huang. “Evolutionary topology optimization of structures with multiple displacement and frequency constraints.” In: *Advances in Structural Engineering* 15.2 (2012), pp. 359–372.

[61] X. Huang and M. Xie. *Evolutionary topology optimization of continuum structures: methods and applications*. John Wiley & Sons, 2010.

[62] V. Young, O. M. Querin, G. P. Steven, and Y. M. Xie. “3D and multiple load case bi-directional evolutionary structural optimization (BESO).” en. In: *Structural Optimization* 18.2-3 (Oct. 1999), pp. 183–192.

[63] L. Ambrosio and G. Buttazzo. “An optimal design problem with perimeter penalization.” In: *Calculus of variations and partial differential equations* 1.1 (1993). ISBN: 0944-2669 Publisher: Springer, pp. 55–69.

[64] Martin P. Bendsøe and O. Sigmund. *Optimization of structural topology, shape, and material*. Vol. 414. Springer, 1995.

[65] J. Petersson and O. Sigmund. “Slope constrained topology optimization.” In: *International Journal for Numerical Methods in Engineering* 41.8 (1998). ISBN: 0029-5981 Publisher: Wiley Online Library, pp. 1417–1434.

[66] B. Bourdin. “Filters in topology optimization.” In: *International journal for numerical methods in engineering* 50.9 (2001). ISBN: 0029-5981 Publisher: Wiley Online Library, pp. 2143–2158.

[67] O. Sigmund. “Design of material structures using topology optimization.” PhD thesis. Technical University of Denmark Lyngby, 1994.

[68] T. Poulsen. “Topology optimization in wavelet space.” In: *International Journal for Numerical Methods in Engineering* 53.3 (2002). ISBN: 0029-5981 Publisher: Wiley Online Library, pp. 567–582.

[69] B. Bourdin and A. Chambolle. “Design-dependent loads in topology optimization.” In: *ESAIM: Control, Optimisation and Calculus of Variations* 9 (2003). ISBN: 1292-8119 Publisher: EDP Sciences, pp. 19–48.

[70] G. Allaire. “Structural optimization using topological and shape sensitivity via a level set method.” In: *Control and cybernetics* 34.1 (2005), p. 59.

[71] O. Sigmund. “Morphology-based black and white filters for topology optimization.” en. In: *Structural and Multidisciplinary Optimization* 33.4-5 (Feb. 2007), pp. 401–424.

[72] P. Fernandes, J. Guedes, and H. Rodrigues. “Topology optimization of three - dimensional linear elastic structures with a constraint on “perimeter”.” In: *Computers & Structures* 73.6 (1999). ISBN: 0045-7949 Publisher: Elsevier, pp. 583–594.

[73] X. Y. Yang, Y. M. Xie, J. S. Liu, G. T. Parks, and P. J. Clarkson. “Perimeter control in the bidirectional evolutionary optimization method.” In: *Structural and Multidisciplinary Optimization* 24.6 (2002), pp. 430–440.

[74] Q. Li, G. P. Steven, and Y. M. Xie. “A simple checkerboard suppression algorithm for evolutionary structural optimization.” In: *Structural and Multidisciplinary Optimization* 22.3 (2001), pp. 230–239.

[75] X. Huang and Y.M. Xie. “Convergent and mesh-independent solutions for the bi- directional evolutionary structural optimization method.” en. In: *Finite Elements in Analysis and Design* 43.14 (Oct. 2007), pp. 1039–1049.

[76] A. Diaz and O. Sigmund. “Checkerboard patterns in layout optimization.” In: *Structural optimization* 10.1 (1995), pp. 40–45.

[77] H. Schürmann. *Konstruieren mit Faser-Kunststoff-Verbunden*. Vol. 2. Springer, 2005.

[78] C. Mattheck and D. Reuschel. “Design nach der Natur.” In: *Physik in unserer Zeit* 30.6 (1999). ISBN: 0031-9252 Publisher: Wiley Online Library, pp. 253–258.

[79] D. Kelly, C. Reidsema, and M. Lee. “An algorithm for defining load paths and a load bearing topology in finite element analysis.” In: *Engineering Computations* (2011). Publisher: Emerald Group Publishing Limited.

[80] G. Ibarra-Berastegi, C. A. Brebbia, and P. Zannetti, eds. *Development and application of computer techniques to environemental studies VIII*. Environmental studies v. 4. Meeting Name: International Conference on Development and Application of Computer Techniques to Environmental Studies. Southampton, UK ; Boston: WIT Press, 2000.

[81] D. Reuschel and C. Mattheck. “Optimization of fiber arrangement with CAIO (computer aided internal optimization) and application to tensile samples.” In: *WIT Transactions on The Built Environment* 40 (1999). ISBN: 1853126810 Publisher: WIT Press.

[82] H.C. Gea and J.H. Luo. “On the stress-based and strain-based methods for predicting optimal orientation of orthotropic materials.” en. In: *Structural and Multidisciplinary Optimization* 26.3-4 (Feb. 2004), pp. 229–234.

[83] H. Voelkl, M. Franz, D. Klein, and S. Wartzack. “Computer Aided Internal Optimisation (CAIO) method for fibre trajectory optimisation: A deep dive to enhance applicability.” en. In: *Design Science* 6 (2020), e4.

[84] D. Klein, C. Witzgall, and S. Wartzack. “A novel approach for the evaluation of composite suitability of lightweight structures at early design stages.” In: *DS 77: Proceedings of the DESIGN 2014 13th International Design Conference*. 2014.

[85] D. Klein, W. Malezki, and S. Wartzack. “Introduction of a computational approach for the design of composite structures at the early embodiment design stage.” In: *Proceedings of the 20th International Conference on Engineering Design (ICED15), Vol. 4: Design for X, 27.-30. Juli 2015, Mailand, 2015, S. 11-20.* July 2015, pp. 105–115.

[86] J. Stegmann and E. Lund. “Discrete material optimization of general composite shell structures.” en. In: *International Journal for Numerical Methods in Engineering* 62.14 (Apr. 2005), pp. 2009–2027.

[87] O. Sigmund. “On the design of compliant mechanisms using topology optimization.” In: *Journal of Structural Mechanics* 25.4 (1997), pp. 493–524.

[88] P. Pedersen. “On thickness and orientational design with orthotropic materials.” In: *Structural Optimization* 3.2 (1991). ISBN: 0934-4373 Publisher: Springer, pp. 69–78.

[89] J. P. Foldager, J. S. Hansen, and N. Olhoff. “Optimization of the buckling load for composite structures taking thermal effects into account.” In: *Structural and multidisciplinary optimization* 21.1 (2001). ISBN: 1615-147X Publisher: Springer, pp. 14–31.

[90] M. Miki and Y. Sugiyama. “Optimum design of laminated composite plates using lamination parameters.” In: *AIAA journal* 31.5 (1993). ISBN: 0001-1452, pp. 921–922.

[91] T. Nomura, Ercan M. Dede, T. Matsumori, and A. Kawamoto. “Simultaneous optimization of topology and orientation of anisotropic material using isoparametric projection method.” In: *Proceedings of the 11th World Congress on Structural and Multidisciplinary Optimization*. 2015, pp. 7–12.

[92] M. Stingl, M. Kočvara, and G. Leugering. “Free material optimization with fundamental eigenfrequency constraints.” In: *SIAM Journal on Optimization* 20.1 (2009), pp. 524–547.

[93] Z. Zuo and Y. Xie. “A simple and compact Python code for complex 3D topology optimization.” en. In: *Advances in Engineering Software* 85 (July 2015), pp. 1–11.

[94] D. Gross and T. Seelig. *Bruchmechanik: Mit einer Einführung in die Mikromechanik. 6., erw. Aufl*. Berlin: Springer Berlin and Springer Vieweg, 2016.

[95] H. Böhm. *A short introduction to basic aspects of continuum micromechanics*. ILSB-Arbeitsbericht 206 ILSB Report 207. Institute of Lightweight Design and Structural Biomechanics (ILSB) Vienna University of Technology, July 2020.

[96] T Mori and K Tanaka. “Average stress in matrix and average elastic energy of materials with misfitting inclusions.” en. In: *Acta Metallurgica* 21.5 (May 1973), pp. 571–574.

[97] O. Pierard, C. Friebel, and I. Doghri. “Mean-field homogenization of multi-phase thermo-elastic composites: a general framework and its validation.” In: *Composites Science and Technology* 64.10 (Aug. 2004), pp. 1587–1603.

[98] P Soden. “Lamina properties, lay-up configurations and loading conditions for a range of fibre-reinforced composite laminates.” In: *Composites Science and Technology* 58.7 (July 1998), pp. 1011–1022.

[99] C. Mattheck and I. Tesari. “Design in nature.” In: *WIT Transactions on Ecology and the Environment* 41 (2000). ISBN: 1853128198 Publisher: WIT Press.

[100] H. Völkl, D. Klein, M. Franz, and S. Wartzack. “An efficient bionic topology optimization method for transversely isotropic materials.” In: *Composite Structures* 204 (2018). ISBN: 0263-8223 Publisher: Elsevier, pp. 359–367.

Appendix

A. Python Codes

Listing A.1: Bisection algorithm for the update of the elemental design variables

```
def bisection_algorithm(alpha_i, x_i, tv):
    """
    Bisection algorithm to determine the threshold for elemental
    sensitivities for updating the design variables x_i

    Parameters
    ----------
    alpha_i: dict., filtered elemental sensitivities (key: int el. label)
    x_i:     dict., design variables of previous iteration
             (key: int el. label)
    tv:      scalar, target volume of the current iteration

    Returns
    -------
    x_i_new: dict. of the updated design variables (key: int el. label)
    """

    lo, hi = min(alpha_i.values()), max(alpha_i.values())

    while (hi - lo) / hi > 0.00001:
        th = (lo + hi) / 2.

        for key in x_i.keys():
            if alpha_i[key] > th:
                x_i_new[key] = 1.
            else:
                x_i_new[key] = 0.001

        if sum(x_i_new.values()) - tv > 0:
            lo = th
        else:
            hi = th

    return x_i_new
```

B. Further Results Single Loadcase

B.1. Comparison of Startdesigns

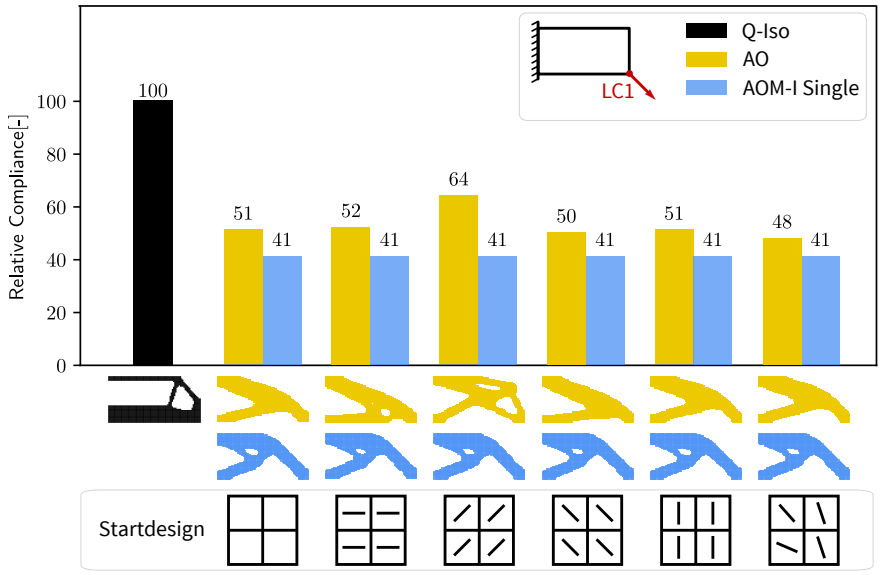

Figure B.1.: Comparison of influence of startdesigns on the compliance and final topologies of *Loadcase B* for the optimization methods *AO* and *AOM-I Single* ($m_{\text{size}} = 0.5\,\text{mm}$, $r_{\text{min}} = 3\,\text{mm}$, $ER = 0.01$)

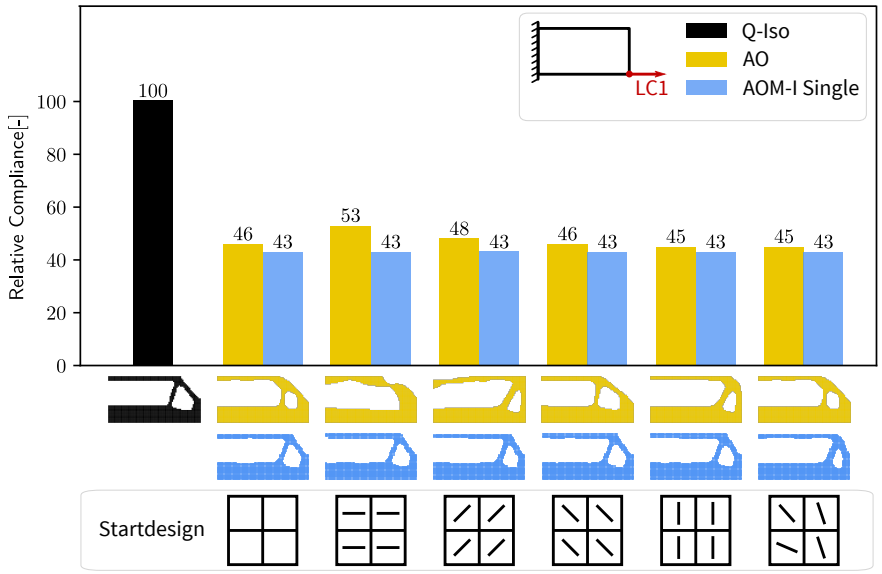

Figure B.2.: Comparison of influence of startdesigns on the compliance and final topologies of *Loadcase C* for the optimization methods *AO* and *AOM-I Single* ($m_{\text{size}} = 0.5\,\text{mm}$, $r_{\text{min}} = 3\,\text{mm}$, $ER = 0.01$)

B.2. Influence of Control Parameters

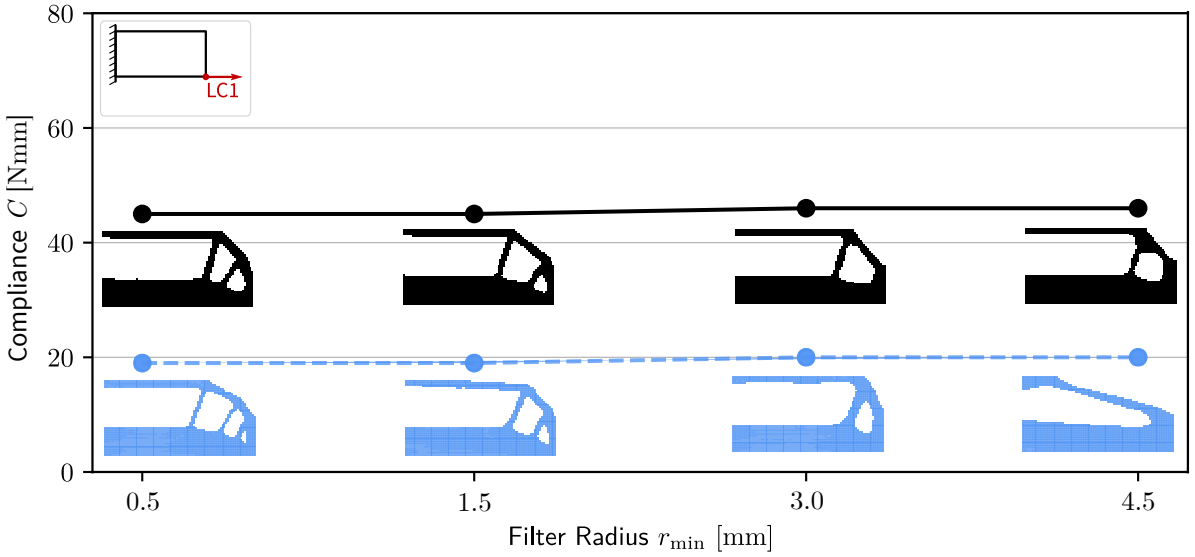

Figure B.3.: Influence of the scale parameter r_{min} on the compliance and final topologies of *Q-Iso* and *AOM-I Single* for *Loadcase C* ($m_{\text{size}} = 0.5\,\text{mm}$, $ER = 0.01$)

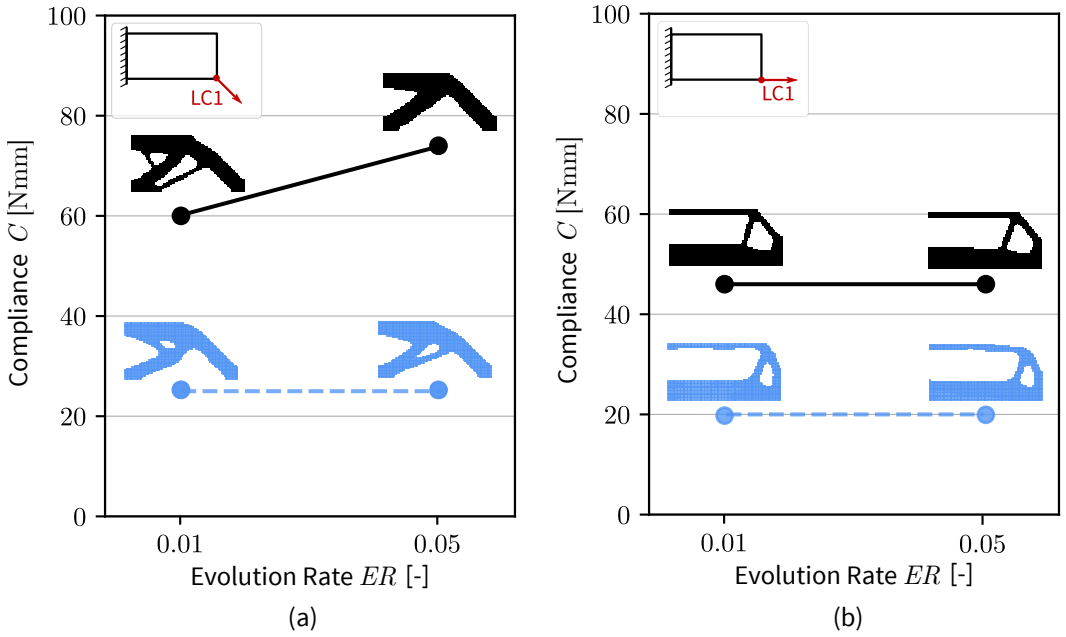

Figure B.4.: Influence of the volume evolution rate ER on the compliance and final topologies of *Q-Iso* and *AOM-I Single* for *Loadcase B* and *Loadcase C* ($m_{\text{size}} = 0.5\,\text{mm}$, $r_{\text{min}} = 3\text{mm}$)

B.3. Comparison of Optimization Methods

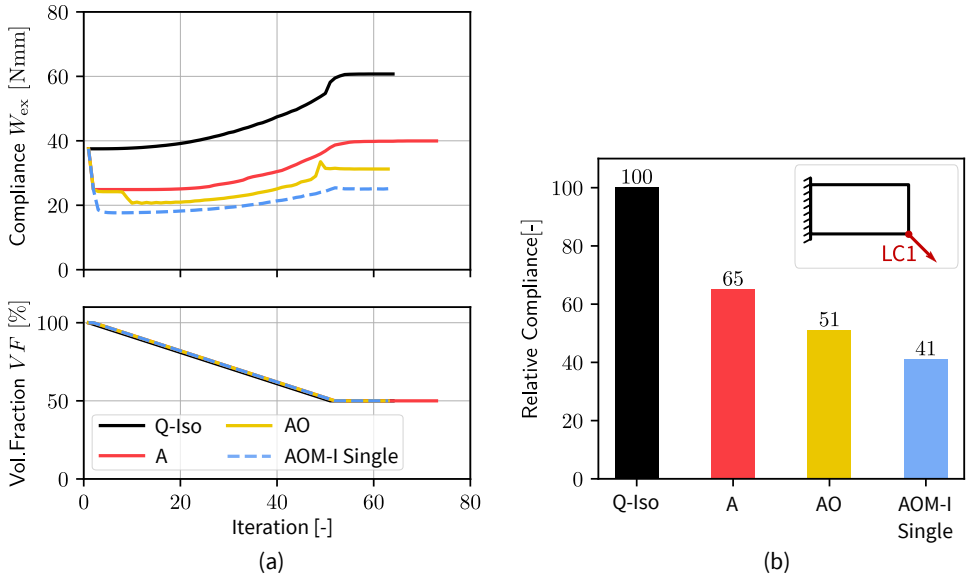

Figure B.5.: Comparison of compliance for optimization methods for *Loadcase B* ($m_{\text{size}} = 0.5\,\text{mm}$, $r_{\text{min}} = 3\,\text{mm}$, $ER = 0.01$). (a) Evolution histories of compliance and volume fraction, (b) Comparison of the relative compliance of the different optimization methods with regard to the compliance of the *Q-Iso* standard topology optimization

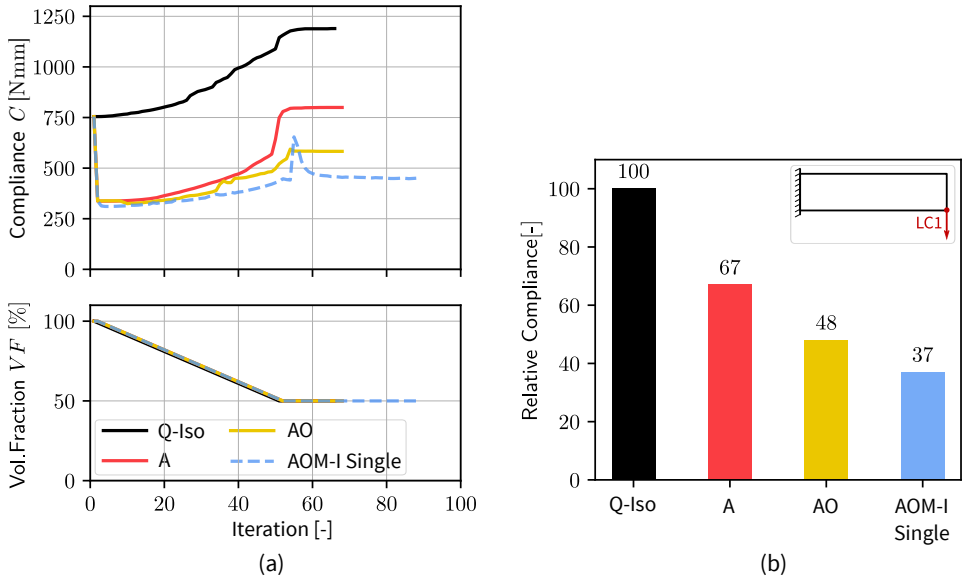

Figure B.6.: Comparison of compliance for optimization methods for *Loadcase A* (design domain $80\,\text{mm} \times 20\,\text{mm}$, $m_{\text{size}} = 0.5\,\text{mm}$, $r_{\text{min}} = 3\,\text{mm}$, $ER = 0.01$). (a) Evolution histories of compliance and volume fraction, (b) Comparison of the relative compliance of the different optimization methods with regard to the compliance of the *Q-Iso* standard topology optimization

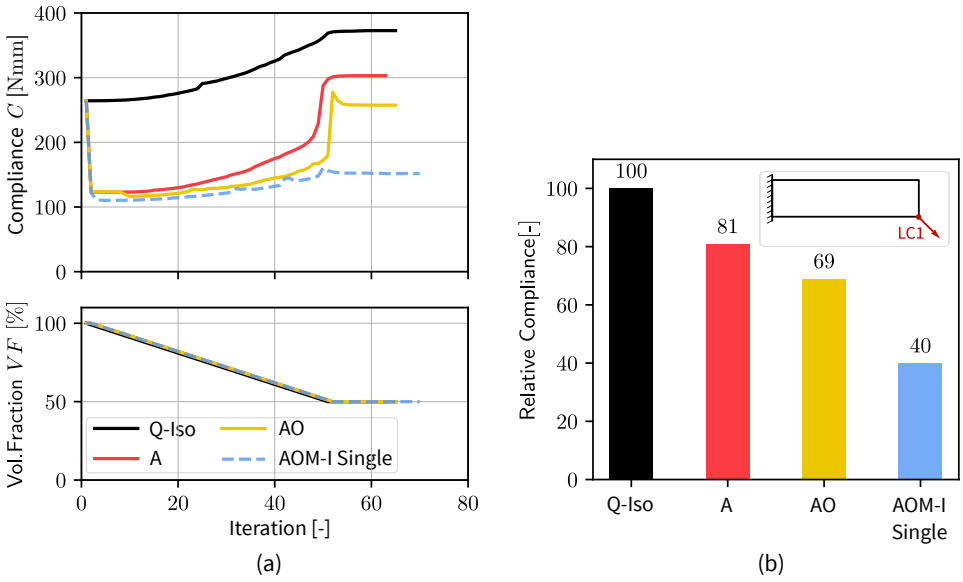

Figure B.7.: Comparison of compliance for optimization methods for *Loadcase B* (design domain $80\,\mathrm{mm} \times 20\,\mathrm{mm}$, $m_{\mathrm{size}} = 0.5\,\mathrm{mm}$, $r_{\mathrm{min}} = 3\,\mathrm{mm}$, $ER = 0.01$). (a) Evolution histories of compliance and volume fraction, (b) Comparison of the relative compliance of the different optimization methods with regard to the compliance of the *Q-Iso* standard topology optimization

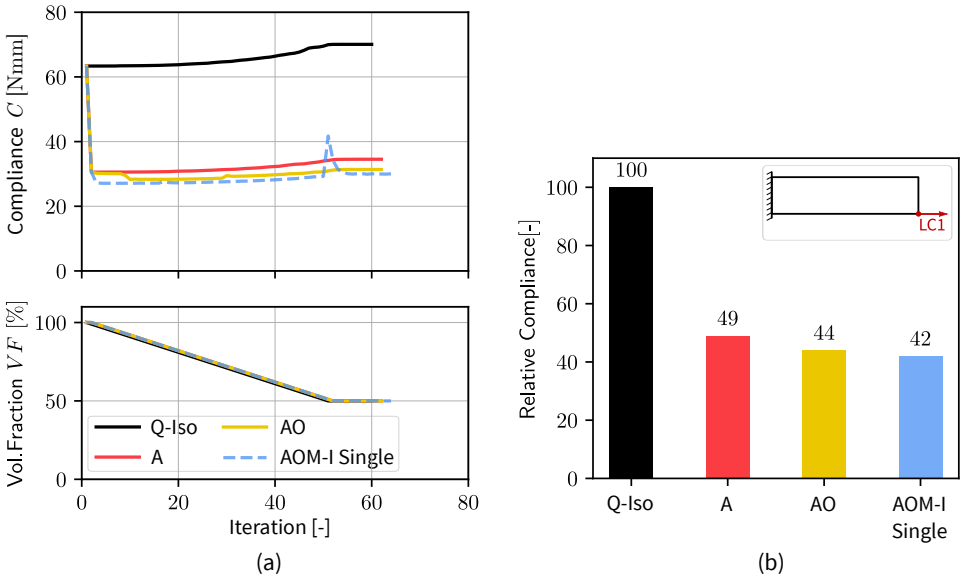

Figure B.8.: Comparison of compliance for optimization methods for *Loadcase C* (design domain $80\,\mathrm{mm} \times 20\,\mathrm{mm}$, $m_{\mathrm{size}} = 0.5\,\mathrm{mm}$, $r_{\mathrm{min}} = 3\,\mathrm{mm}$, $ER = 0.01$). (a) Evolution histories of compliance and volume fraction, (b) Comparison of the relative compliance of the different optimization methods with regard to the compliance of the *Q-Iso* standard topology optimization

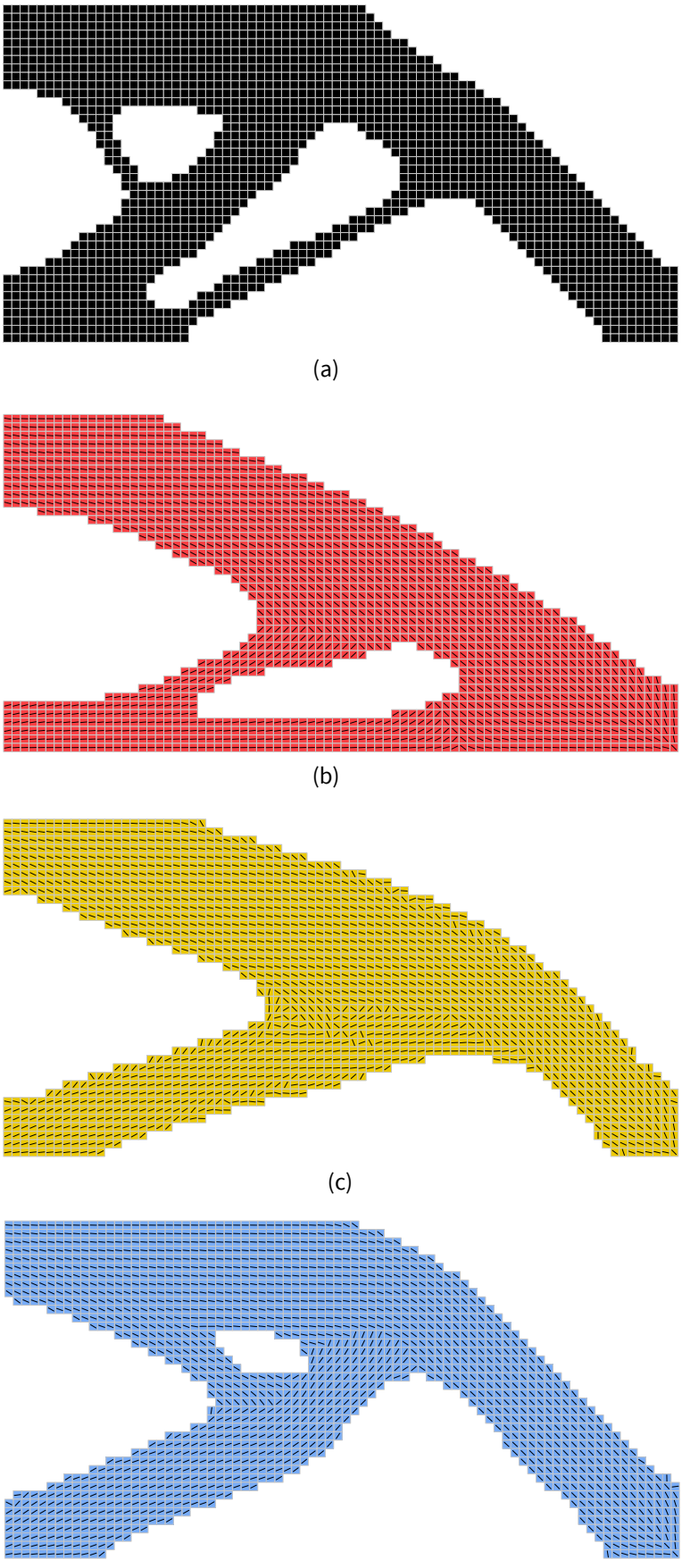

(a)

(b)

(c)

(d)

Figure B.9.: Comparison of the proposed final design topologies and material's 1-directions for *Loadcase B*

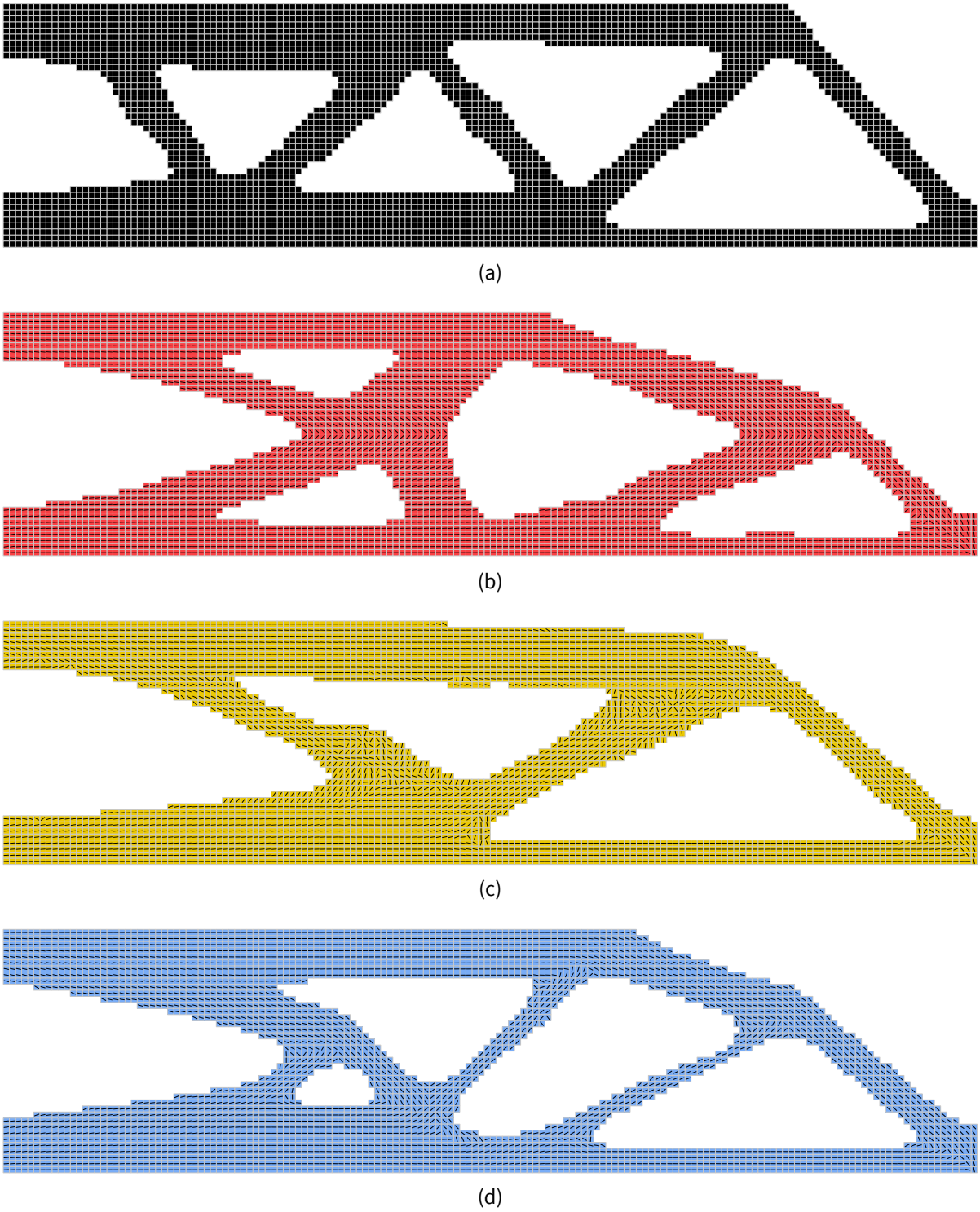

Figure B.10.: Comparison of the proposed final design topologies and material's 1-directions for *Loadcase A* for a design domain $80\,\mathrm{mm} \times 20\,\mathrm{mm}$

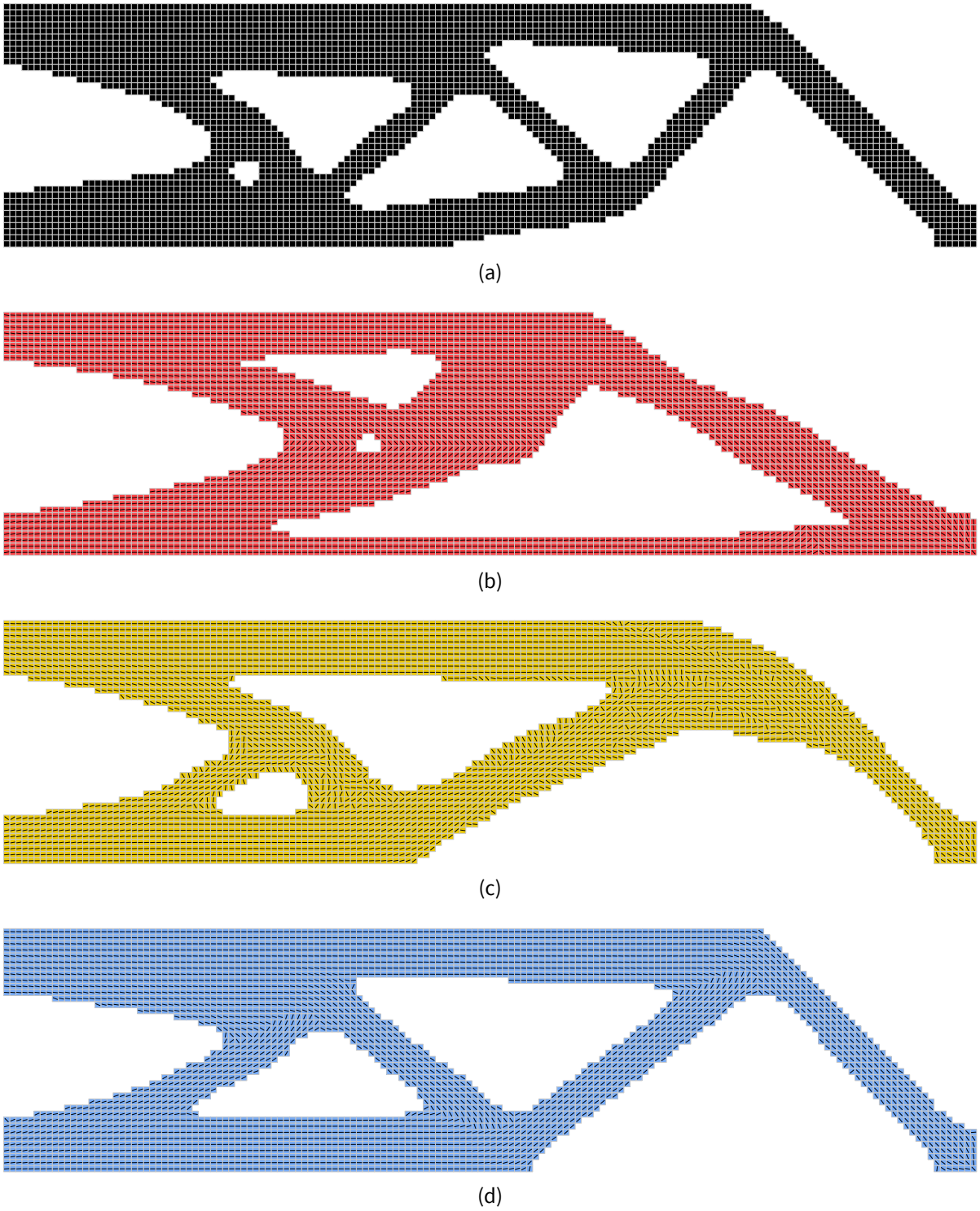

Figure B.11.: Comparison of the proposed final design topologies and material's 1-directions for *Loadcase B* for a design domain $80\,\mathrm{mm} \times 20\,\mathrm{mm}$

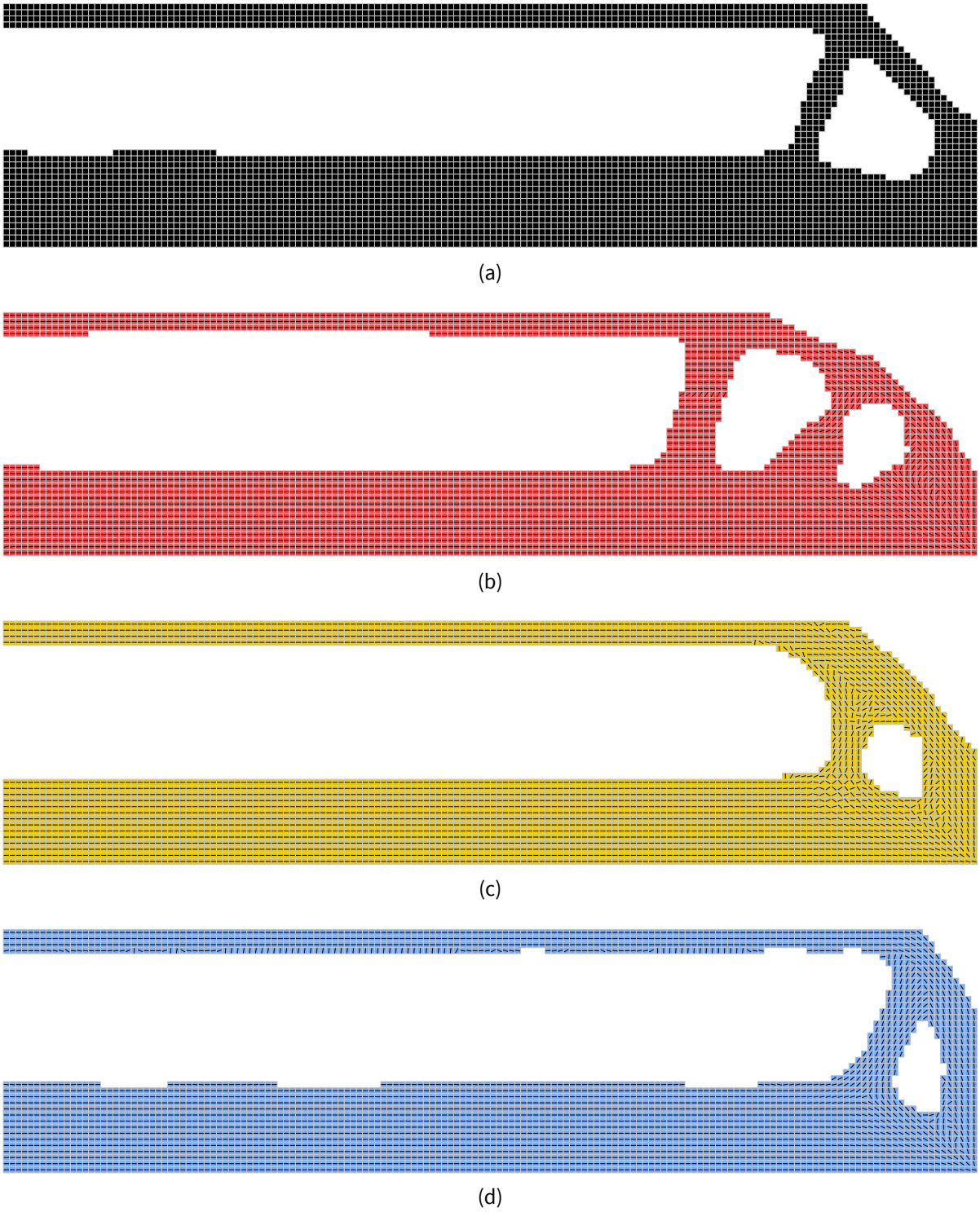

Figure B.12.: Comparison of the proposed final design topologies and material's 1-directions for *Loadcase C* for a design domain $80\,\mathrm{mm} \times 20\,\mathrm{mm}$

B.4. Sequential versus Simultaneous Optimization

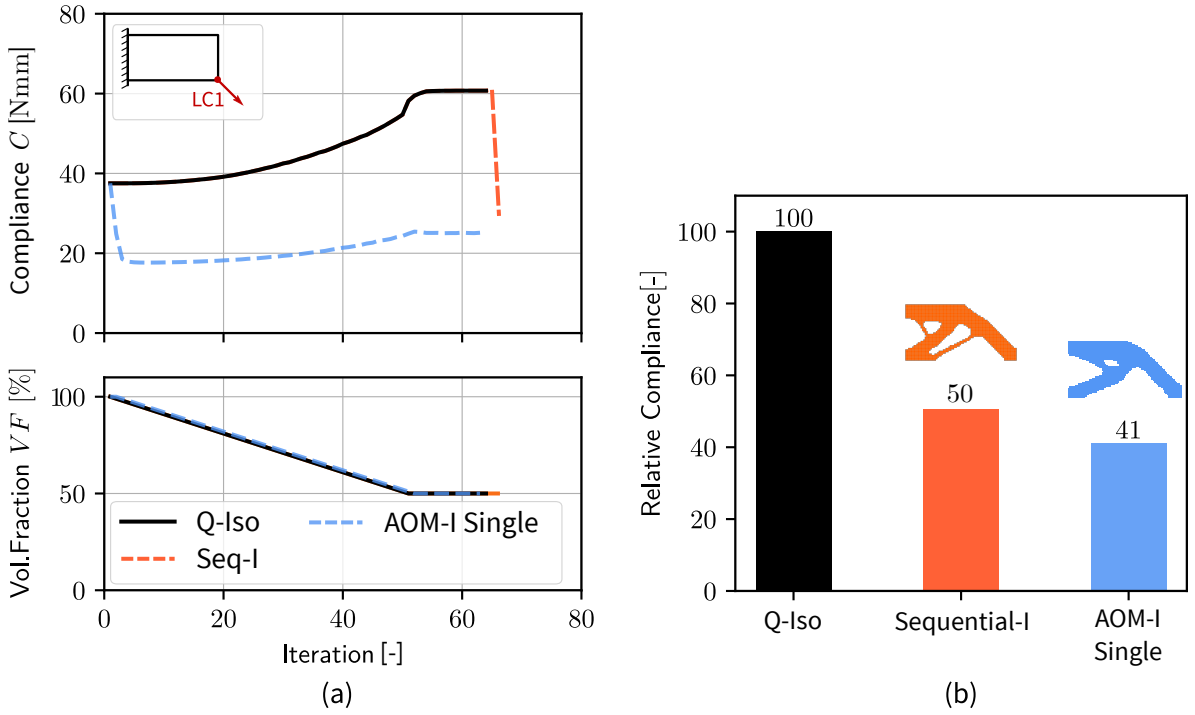

Figure B.13.: Comparison of sequential and simultaneous optimization for a cantilever beam with dimensions $40\,\mathrm{mm} \times 20\,\mathrm{mm}$ for *Loadcase B* ($m_{\mathrm{size}} = 0.5\,\mathrm{mm}$, $r_{\mathrm{min}} = 3\,\mathrm{mm}$, $ER = 0.01$)

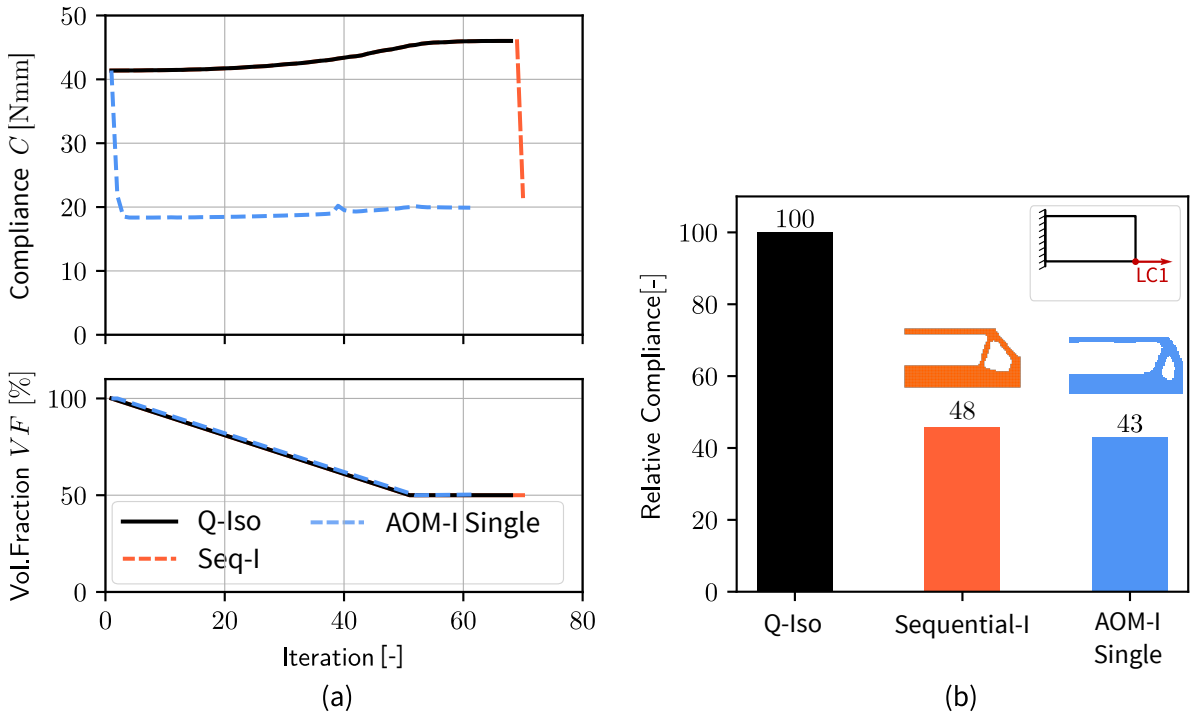

Figure B.14.: Comparison of sequential and simultaneous optimization for a cantilever beam with dimensions $40\,\mathrm{mm} \times 20\,\mathrm{mm}$ for *Loadcase C* ($m_{\mathrm{size}} = 0.5\,\mathrm{mm}$, $r_{\mathrm{min}} = 3\,\mathrm{mm}$, $ER = 0.01$)

C. Further Results Multiple Loadcases

C.1. Influence of Control Parameters

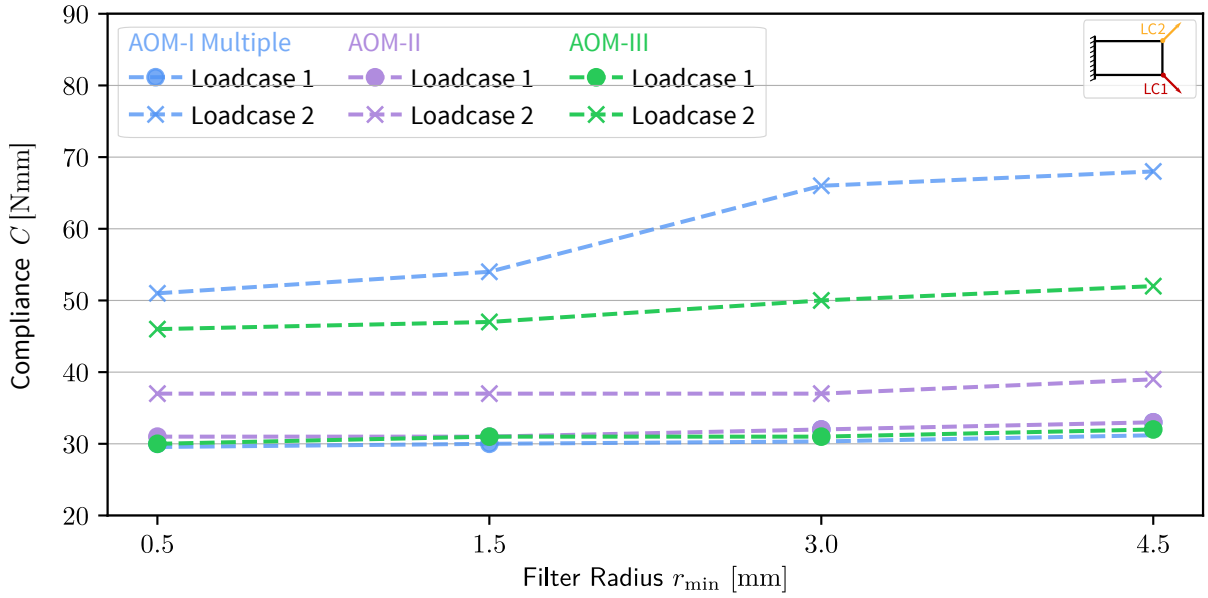

Figure C.1.: Influence of different values of the scale parameter $r_{\min}$ on the optimal compliance of *AOM-I Multiple*, *AOM-II*, and *AOM-III* for *Loadcase BB* ($m_{\text{size}} = 0.5\,\text{mm}$, $ER = 0.01$)

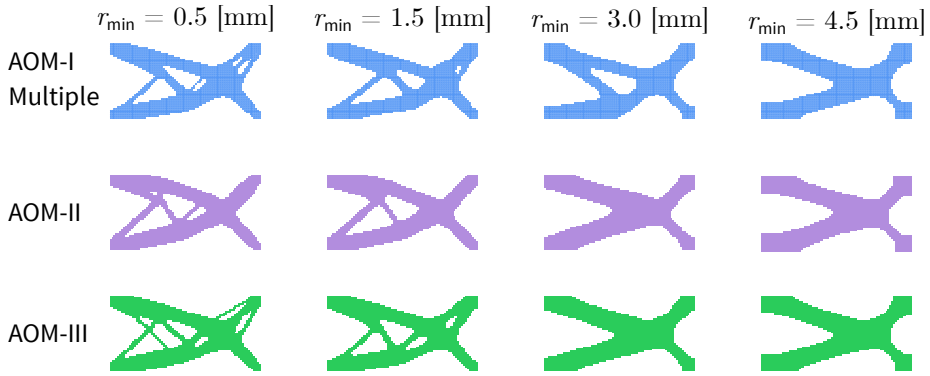

Figure C.2.: Influence of different values of the scale parameter $r_{\min}$ on the final topologies of *AOM-I Multiple*, *AOM-II*, and *AOM-III* for *Loadcase BB* ($m_{\text{size}} = 0.5\,\text{mm}$, $ER = 0.01$)

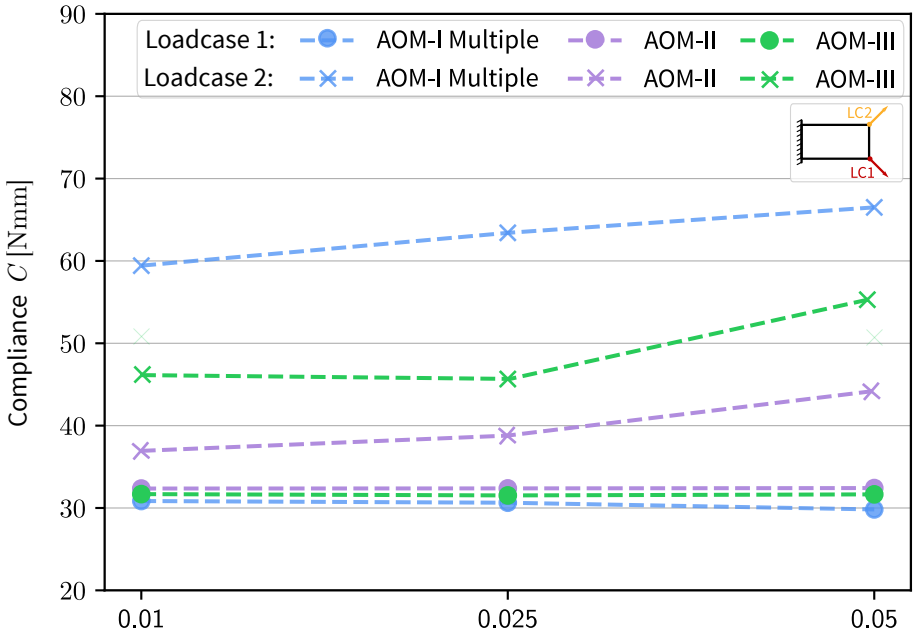

Figure C.3.: Comparison of the performance of *AOM-I Multiple*, *AOM-II*, and *AOM-III* for different evolution rates ER for *Loadcase BB* ($m_{\text{size}} = 0.5\,\text{mm}$, $r_{min} = 3\,\text{mm}$).

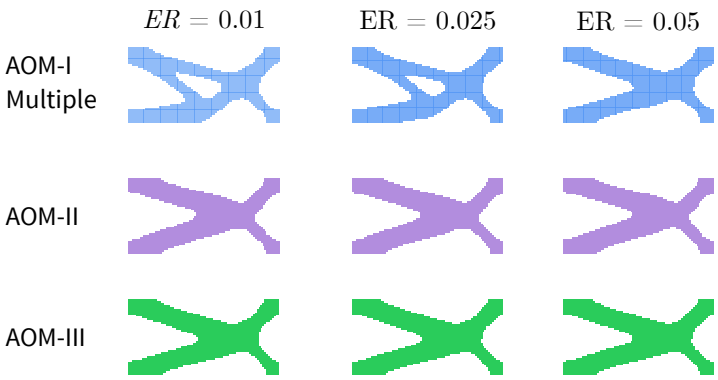

Figure C.4.: Comparison of the final topologies determined with *AOM-I Multiple*, *AOM-II*, and *AOM-III* for different evolution rates ER for *Loadcase BB* ($m_{\text{size}} = 0.5\,\text{mm}$, $r_{min} = 3\,\text{mm}$).

C.2. Comparison of Optimization Methods

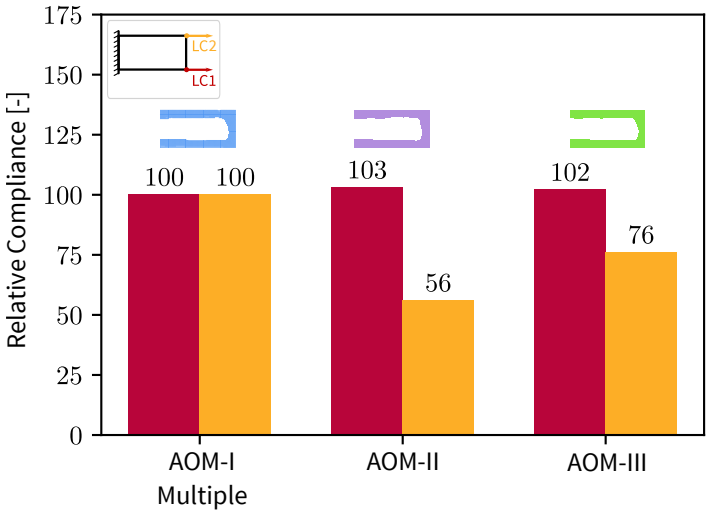

Figure C.5.: Illustration of the performance of *Loadcase 1* (Design Loadcase) and *Loadcase 2* optimized with *AOM-I Multiple*, *AOM-II*, and *AOM-III* for *Loadcase CC* where *AOM-I Multiple* serves as a reference. ($m_{\text{size}} = 0.5\,\text{mm}$, $r_{\text{min}} = 3\,\text{mm}$, $ER = 0.01$)

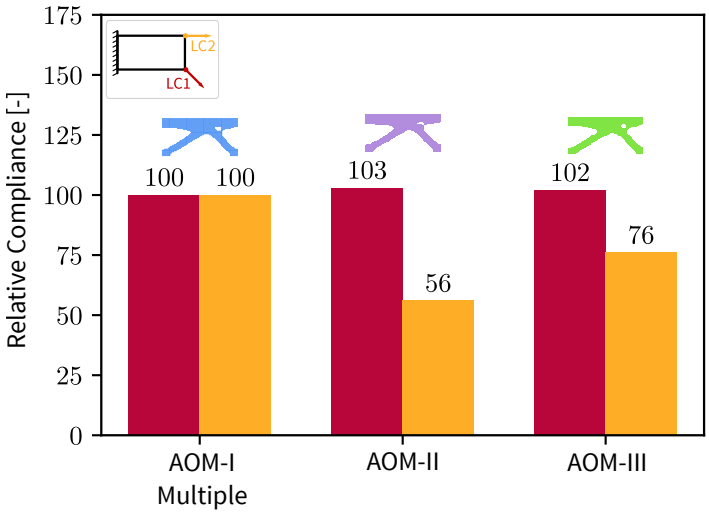

Figure C.6.: Illustration of the performance of *Loadcase 1* (Design Loadcase) and *Loadcase 2* optimized with *AOM-I Multiple*, *AOM-II*, and *AOM-III* for *Loadcase BC* where *AOM-I Multiple* serves as a reference. ($m_{\text{size}} = 0.5\,\text{mm}$, $r_{\text{min}} = 3\,\text{mm}$, $ER = 0.01$)

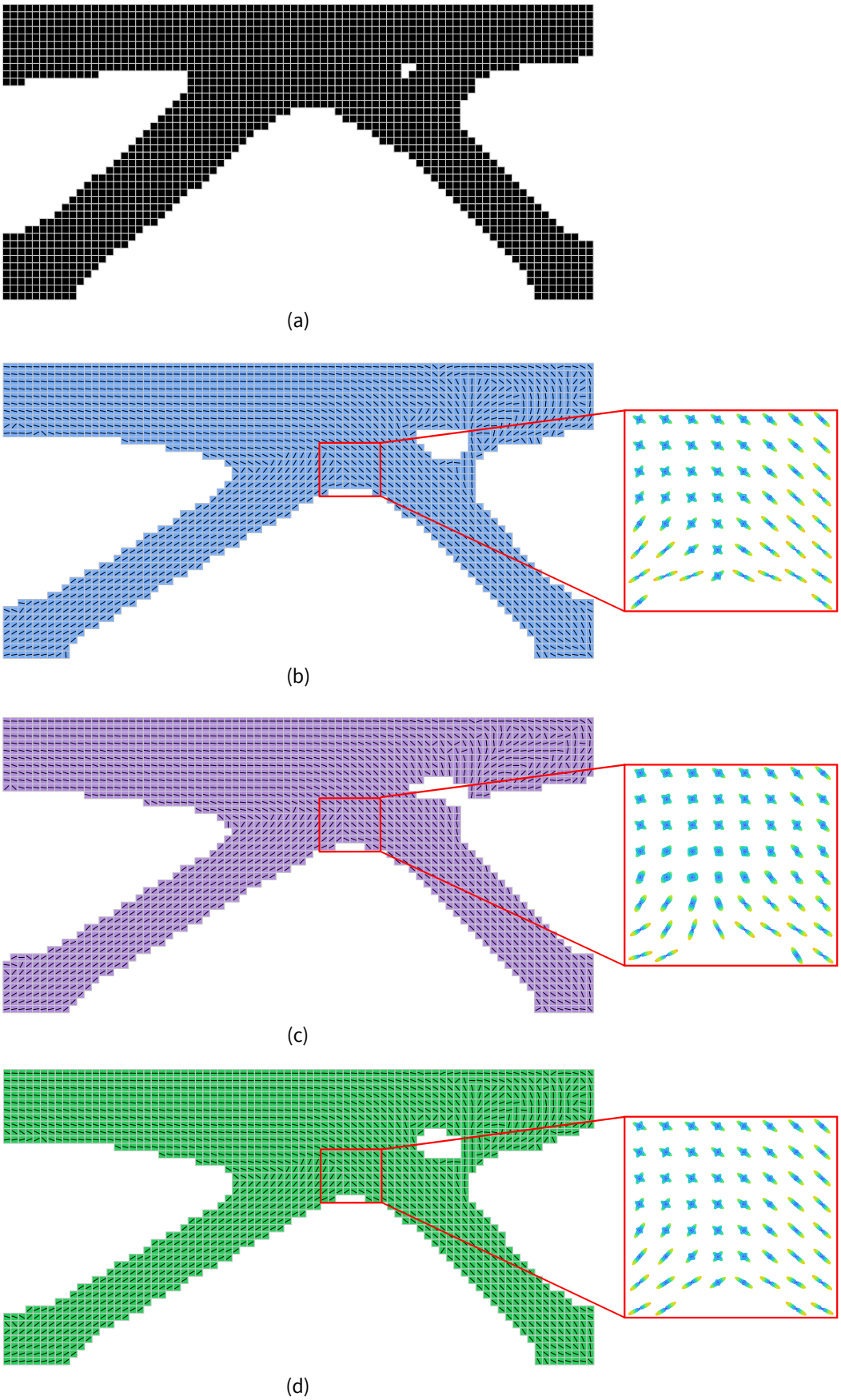

Figure C.7.: Illustration of final topologies, material 1-direction and stiffness tensor glyphs for selected regions of interest for *Loadcase BC* for the optimization methods (a) Q-Iso, (b) AOM-I Multiple, (c) AOM-II, (d) AOM-III ($m_{\text{size}} = 0.5\,\text{mm}$, $r_{\text{min}} = 3\,\text{mm}$, $ER = 0.01$).

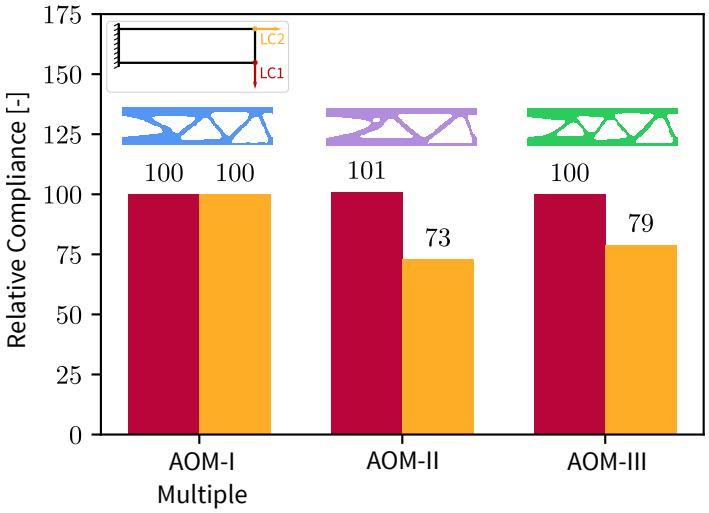

Figure C.8.: Illustration of the performance of *Loadcase 1* (Design Loadcase) and *Loadcase 2* optimized with *AOM-I Multiple*, *AOM-II*, and *AOM-III* for *Loadcase AC* where *AOM-I Multiple* serves as a reference. (design domain $80\,\mathrm{mm} \times 20\,\mathrm{mm}$, $m_{\mathrm{size}} = 0.5\,\mathrm{mm}$, $r_{\mathrm{min}} = 3\,\mathrm{mm}$, $ER = 0.01$)